

# CLUSTER OF EXCELLENCE QUANTUM UNIVERSE



# Spectator String Axions: Messages from the Early Universe

#### Dissertation

zur Erlangung des Doktorgrades an der Fakultät für Mathematik, Informatik und Naturwissenschaften Fachbereich Physik der Universität Hamburg

Vorgelegt Von

Margherita Putti

Hamburg

2025

### Declaration on oath

I hereby declare and affirm that this doctoral dissertation is my own work and that I have not used any aids and sources other than those indicated. If electronic resources based on generative artificial intelligence (gAI) were used in the course of writing this dissertation, I confirm that my own work was the main and value-adding contribution and that complete documentation of all resources used is available in accordance with good scientific practice. I am responsible for any erroneous or distorted content, incorrect references, violations of data protection and copyright law or plagiarism that may have been generated by the gAI.

Mary bente tut

Gutachter/innen der Dissertation:

Prof. Dr. Geraldine Servant Dr. Alexander Westphal

Zusammensetzung der Prüfungskommission:

Dr. Craig Lawrie Prof. Dr. Jochen Liske Prof. Dr. Geraldine Servant Prof. Dr. Timo Weigand Dr. Alexander Westphal

Vorsitzende/r der Prüfungskommission:

Prof. Dr. Jochen Liske

Datum der Disputation:

02.10.2025

Vorsitzender des Fach-Promotionsausschusses PHYSIK:

Prof. Dr. Wolfgang J.

Parak

Leiter des Fachbereichs PHYSIK:

Prof. Dr. Markus Drescher

Dekan der Fakultät MIN:

Prof. Dr.-Ing. Norbert Ritter

### Abstract

String theory compactifications generically predict the existence of a rich spectrum of axionlike fields, the so-called Axiverse, whose masses and couplings are determined by the geometry and flux structure of the compactification. In this thesis, we explore the cosmological and phenomenological implications of such axions, combining insights from both Type IIB orientifold and heterotic  $E_8 \times E_8$  Calabi-Yau compactifications.

We initiate the characterization of the generic structure of the heterotic axiverse, mapping the axion mass spectrum and the effective couplings of axions to gauge fields. This analysis reveals model-independent constraints on their role in solving the strong CP problem, contributing to dark matter, and mediating hidden-visible sector interactions.

We further investigate inflationary scenarios where spectator axions couple to hidden gauge sectors via Chern-Simons interactions, leading to distinctive multi-peak features in the scalar and tensor spectra. We study axion-gauge field models with transient fast-roll phases, showing how they can enhance spectral distortions while satisfying large-scale CMB bounds, and identifying the challenges of controlling such dynamics in non-Abelian scenarios. These models can produce a "gravitational-wave forest" spanning several decades in frequency, with the nHz band potentially explaining recent pulsar timing array signals. We analyze the complementary role of CMB spectral distortions in constraining the scalar sector, and identify the details of the string theory compactification that naturally realize the required couplings in the string landscape.

Finally, we examine non-perturbative dynamics in the early universe, focusing on axion production via parametric resonance during preheating in string inflation models. Kinetic couplings and moduli-dependent masses lead to generalized Mathieu equations, enabling efficient production of heavy axions that can overclose the universe unless inflationary parameters are suitably constrained.

Taken together, these results demonstrate how string theory provides a natural framework for embedding rich axion sectors, and how their cosmological dynamics offer unique observational windows, from gravitational waves to spectral distortions, into the high-energy physics of the early universe.

## Zusammenfassung

Die Kompaktifizierungen der Stringtheorie sagen im Allgemeinen die Existenz eines reichen Spektrums axionähnlicher Felder – des sogenannten Axiversums – voraus, deren Massen und Kopplungen durch die Geometrie und die Flussstruktur der Kompaktifizierung bestimmt werden. In dieser Arbeit untersuchen wir die kosmologischen und phänomenologischen Implikationen solcher Axionen und kombinieren Erkenntnisse sowohl aus Typ-IIB-Orientifolds als auch aus heterotischen  $E_8 \times E_8$ -Calabi-Yau-Kompaktifizierungen.

Wir beginnen mit der Charakterisierung der generischen Struktur des heterotischen Axiversums, indem wir das Axion-Massenspektrum sowie die effektiven Kopplungen der Axionen an Eichfelder abbilden. Diese Analyse liefert modellunabhängige Einschränkungen hinsichtlich ihrer Rolle bei der Lösung des starken CP-Problems, ihres Beitrags zur Dunklen Materie und ihrer Vermittlung von Wechselwirkungen zwischen sichtbarem und verborgenem Sektor.

Weiterhin untersuchen wir Inflationsszenarien, in denen Spektatoraxionen über Chern-Simons-Wechselwirkungen an verborgene Eichsektoren koppeln, was zu charakteristischen Mehrgipfelstrukturen in den Skalar- und Tensor spektren führt. Wir analysieren Axion-Eichfeld-Modelle mit transienten Fast-Roll-Phasen und zeigen, wie diese Spektralverzerrungen verstärken können, während gleichzeitig großskalige CMB-Beschränkungen eingehalten werden, und identifizieren die Herausforderungen bei der Kontrolle solcher Dynamiken in nichtabelschen Szenarien. Solche Modelle können einen "Gravitationswellenwald" erzeugen, der sich über mehrere Größenordnungen in der Frequenz erstreckt und im nHz-Bereich möglicherweise aktuelle Signale von Pulsartiming-Arrays erklären könnte. Wir analysieren die komplementäre Rolle von CMB-Spektralverzerrungen bei der Einschränkung des Skalarsektors und identifizieren die Details der Stringtheorie-Kompaktifizierung, die die erforderlichen Kopplungen im String-Landscape auf natürliche Weise realisieren.

Abschließend betrachten wir nichtperturbative Dynamiken im frühen Universum, wobei wir uns auf die Axionproduktion durch parametrische Resonanz während der Vorwärmephase in String-Inflationsmodellen konzentrieren. Kinetische Kopplungen und modulabhängige Massen führen zu verallgemeinerten Mathieu-Gleichungen, die eine effiziente Produktion schwerer Axionen ermöglichen, welche das Universum überdichten könnten, sofern die Inflationsparameter nicht entsprechend eingeschränkt werden. Zusammengefasst zeigen diese Ergebnisse, wie die Stringtheorie einen natürlichen Rahmen zur Einbettung reicher Axionsektoren bereitstellt und wie deren kosmologische Dynamik einzigartige Beobachtungsfenster, von Gravitationswellen bis zu Spektralverzerrungem, in die Hochenergiephysik des frühen Universums eröffnet.

## Acknowledgments

This thesis marks the culmination of my doctoral studies at the DESY Theory Group. It has been a long and rewarding journey, shaped above all by the people by my side. I take this opportunity to acknowledge and express my gratitude for their presence and support.

First and foremost, I thank my supervisors, Geraldine Servant and Alexander Westphal, for giving me this opportunity. Geraldine, I am sincerely grateful for your continuous support and advice. Throughout my years in Hamburg, you have been a steady and reassuring presence. Alexander, thank you for all you taught me, from string theory to creating plasma using a grape. With your enthusiasm and kindness, you showed me how to combine rigor with imagination, to trust my intuition while learning to test it, and above all, to enjoy the process. With you, research feels like an adventure.

I am deeply thankful to Jacob M. Leedom, whose collaboration has made me a far better researcher. Beyond your brilliance, your passion and humility have given me an example of integrity I hope to carry throughout my life. Thank you for teaching me to respect the time it takes to do things well, for your trust, and for the laughter.

My gratitude also goes to Nicole Righi, for being a wonderful academic "big sister", and an inspiration. I am also grateful to Marco Peloso, for supporting me throughout my academic life, and to my collaborators Nicola Bartolo, Sukannya Bhattacharya, Emanuela Dimastrogiovanni, and Matteo Fasiello.

A big thanks to the string-pheno group in Hamburg, for the lunches, the aperitivi, and the travels. Alessandro, Cesar and Timo, for making me feel welcome from the very beginning. Rafael, for all the useful, fun and random knowledge you shared. Mateo, for the best office. Thanks to Max, Lukas, Stefano, and Jeroen, to Lorenzo and Gonzalo, the "Spanish armada", for the laughs in Notkedam. Craig, thank you for all the fun and the advice, personal or scientific, but not for the Bitterol. Florent, for always lending an ear. And for the coffee, of course.

To all the friends and colleagues at DESY: thank you for the warmth, fun, and stimulating environment. In particular I would like to thank Carlo, Deniz, Alessio and Enrico. Special thanks also to Alessandro, for making our office the loudest one, Julian, Koschi, Henda, Aleksander, and Philip, for taking me in and showing me Hamburg. Thanks also to Hyungjin, Thomas, Bibushan, Simone, Andrea, Marco, Adriana, Felix, Yu, Xucheng, and Hyeonseok and the Italian PhDs, Martina, Enrico, Riccardo, Nabeen and Anna, for making the "Cosmorridor" a truly special environment. I am also grateful to Inna and Elizabeth for their invaluable help.

A special thanks to all the extraordinary friends I was fortunate to meet over these three years. Gabri e Barbara, *Garbrarbra*, per essere sempre pronti all'avventura; Lorenzo, per le innumerevoli volte in cui mi hai salvato la vita; Davide, per i meme; Alain, por tu contagioso entusiasmo. A Simone, che dietro la sua scontrosità in realtà è un patatone, per preoccuparsi anche nei momenti in cui non mi sopporta, e strapparmi sempre un sorriso. E a Sara, per la sua spontaneità e sincerità, per essere la mia complice, fin dal momento in cui abbiamo rubato quella stella. Avete reso questi anni più leggeri, più veri e infinitamente belli.

Un grazie speciale agli *amici di Mauro*, Chicco, Gabri, Tommi, Elena, Nenni, Checco, Gio, Ale, con cui questo percorso è iniziato, per i ricordi che abbiamo condiviso e per quelli che ancora ci aspettano. Alle amiche di sempre, Ele, Etta, Mare e Giuli, per essere una costante fonte di divertimento e di sostegno. Un grazie particolare alla Co e alla Pera, per riuscire a farmi sentire sempre al posto giusto, ovunque io sia. E alla Fra, che da quando eravamo bambine mi sta accanto, e continua a farlo ogni giorno.

Grazie a Tommaso, che ogni giorno sceglie di essere il mio migliore amico, riempiendo le mie giornate di leggerezza e sorrisi; grazie per essere la mia stabilità, e per tanto altro ancora.

Infine, un grazie speciale va alla mia famiglia, per celebrare sempre ogni mio traguardo, e per l'illimitato affetto. In particolare, alla Carli, per aver portato un po' di casa ad Amburgo (e per le cenette). Alle mie sorelle, che sanno spiegarmi la vita meglio di quanto io sappia spiegare la fisica. Gio, grazie per tenerci unite da sempre tra teatrini e degustazioni, per essere sempre pronta a difenderci, e per mostrarci che, quando ci metti il cuore, tutto riesce meglio. Eli, grazie per la tua profondità e ironia, per farmi vedere cose che a me sfuggono e mostrarmi sempre la strada; non posso che copiarti. Ai miei genitori, che mi hanno supportato sempre e insegnato tanto: Mami, grazie per farmi sempre trovare quello che mi serve, che sia il prosciutto cotto o un consiglio, e per essere sempre fiera di noi, incondizionatamente; Papi, grazie per avermi insegnato la bellezza di andare in fondo alle cose, per spingermi sempre a capire meglio. Tutto è iniziato con quel libro sul Chaos che mi hai regalato.

# Contents

1	Intr	roduction	1
<b>2</b>	Fou	andations of String Cosmology	7
	2.1	Early-Universe Cosmology	7
		2.1.1 The Need for Inflation	8
		2.1.2 Dynamics of Inflation	9
		2.1.3 Primordial Fluctuations	10
	2.2	Ingredients of the String Theory Framework	13
		2.2.1 String Theories	14
		2.2.2 Basics of compactification	16
		2.2.3 Branes and Fluxes	18
		2.2.4 Moduli Stabilization	20
	2.3	Inflationary Models in String Theory	22
			22
		2.3.2 Moduli Inflation	23
		2.3.3 Brane Inflation	23
		2.3.4 Modular Inflation	24
3	The	e String Axiverse	25
	3.1	The strong <i>CP</i> problem and the QCD axion	25
	3.2	Closed string axions	26
		3.2.1 The Axion Quality Problem in String Theory	27
	3.3	Type IIB axiverse	28
		3.3.1 Statistics of the IIB Axiverse	30
		3.3.2 Phenomenological roles of axions	30
	3.4	9	32
4	Het	terotic axiverse	35
	4.1	Review of the Heterotic String	36
			38
		4.1.2 The gauge group	39
		4.1.3 Heterotic EFT in 10D and 4D	42
		4.1.4 Heterotic axions in 4D	42
		4.1.5 Anomalies, Axions and Green-Schwarz	43
			45
	4.2	2 0	49
			49
		•	51
		4.2.3 Strong CP problem	53
			56
			62

10 Contents

		4.2.6 Three-Axion Summary	37
	4.3	Remarks	68
5	Spe	ctator Axions and Inflation 7	<b>7</b> 1
	5.1		73
		•	75
		-	78
	5.2	<u>.</u>	79
	J	*	32
		1 1	35
			38
			90
		· · · · · · · · · · · · · · · · · · ·	92
	5.3	• • • • • • • • • • • • • • • • • • • •	93
	5.4	1	99
	5.4	5.4.1 Primordial Power Spectra	
		5.4.2 Detectability of Gravitational Wave Signals	
	5.5	Remarks	
	5.5	Remarks	Ю
6	$\mathbf{Spe}$	ctator Sectors from the Landscape 10	7
	6.1	Spectator Sectors from D7-branes	)8
		6.1.1 States and Couplings	)8
		6.1.2 Axion Decay Constants	14
		6.1.3 Axion Masses	14
		6.1.4 From Strings to Spectators	17
	6.2	Constraints on Spectator Models in String Theory	18
	6.3	Type IIB MASA Models	22
	6.4	Remarks	27
7	Pos	t-Inflationary Dynamics	<b>t</b> 1
•	7.1	The Mathematics of Preheating	
	1.1	7.1.1 The Mathieu Equation and Preheating	
		7.1.2 The Hill Equation and Preheating	
		7.1.3 Cosmological Impact of Preheating	
	7.2	String axions and preheating	
	1.4	7.2.1 Structure & dynamics of the Hill equation for string axions	
		7.2.1 Structure & dynamics of the fini equation for string axions	
	7 9	Application: Fibre Inflation	
	7.3	7.3.1 Review of LVS & Fibre Inflation	
		G G	
		7.3.3 Preheating in Fibre Inflation	
		7.3.4 Constraints on Fibre Inflation	
	7.4	7.3.5 Influence of axion initial conditions	
	7.4	Remarks	)5
8	Con	nclusions	9
$\mathbf{A}$	Geo	ometry and String Conventions	′3
-	A.1	Geometry	_
	A.2	Cohomology	
	A.3	Topological invariants	
	A.4	Divisors	
	A.5	String Conventions	
	11.0		, U

Contents 11

		Type IIB Orientifolds	
	A.5.2	Worldvolume Theory of D7-branes and Induced Tadpoles	177
В	CY exam	ples	181
	B.0.1	Quintic Calabi-Yau	181
	B.0.2	Bi-cubic CICY	182
	B.0.3	CS couplings	183
$\mathbf{C}$	MASA Po	ower Spectra Calculations	185
	C.1 Tenso	r Perturbations	185
	C.2 Curva	ture Perturbations	186
	C.3 Backr	eaction and Perturbativity	187
D	Gravitatio	onal Chern-Simons Couplings in Type IIB Orientifolds	189
	D.1 Axion	Higgs coupling	190

<u>12</u> Contents

### Chapter 1

### Introduction

Big questions often have small beginnings, sometimes as small as a string.

The largest scales in the universe, galaxies, clusters, and the cosmic web, are shaped by physical processes that occurred at the tiniest length scales and at the highest energies in the earliest moments after the Big Bang. This connection between the largest and smallest is at the heart of modern theoretical physics: to understand the laws governing the phenomena we explore nature at increasingly fundamental layers. This has led us to smaller and smaller length scales, where the familiar picture of particles and forces gives way to more abstract, but more unified, frameworks.

And yet, there is a limit to how closely we can look. Probing smaller length scales requires ever higher energies, a principle that defines the domain of high-energy physics. Particle colliders like the LHC act as microscopes, smashing particles together at extremely high energies to break apart composite structures and reveal the fundamental ones. This endeavor has culminated in the development of the Standard Model of particle physics, a theory unifying three of the four fundamental forces, electromagnetism and the weak and strong interactions, into a consistent quantum theory through the symmetry group  $SU(3) \times SU(2) \times U(1)_Y$  and mediated by particles known as gauge bosons. The discovery of the Higgs boson confirmed the mechanism by which particles acquire mass and marked a major triumph for the SM [1–4].

Gravity, the fourth fundamental interaction, is conceptually different. Rather than being mediated by gauge bosons, it emerges from the geometry of spacetime itself. Formulated by Einstein in 1915, general relativity has withstood a century of experimental scrutiny and remains the accepted description of gravitational phenomena on large scales. However, attempts to incorporate gravity into a quantum framework, by treating it as mediated by a hypothetical graviton, leads to non-renormalizable divergent quantities. A consistent quantum theory of gravity at this level does not seem required or feasible.

General relativity also lays the foundation for cosmology, i.e., the study of the origin of the universe, its evolution, and its large-scale structure. The currently accepted cosmological model, known as  $\Lambda$ CDM, is remarkably successful in explaining a broad range of observations. It describes a Universe composed of roughly 5% ordinary matter, 25% cold dark matter (CDM), and 70% dark energy ( $\Lambda$ ), with dynamics governed by Einstein's equations. It accurately accounts for the primordial abundances of light elements, the structure of the cosmic microwave background (CMB), and the accelerated expansion of

the Universe. A crucial component of this model is inflation [5-7], a brief epoch of accelerated expansion in the early Universe, occurring around  $10^{-36}$  to  $10^{-32}$  seconds after the Big Bang. Inflation addresses several puzzles of the standard cosmological model, including the horizon, flatness, and monopole problems, and provides a mechanism for generating the primordial perturbations that seeded cosmic structure and ultimately the world we live in. These fluctuations, quantum in origin, were stretched to cosmic scales and are imprinted in the CMB anisotropies we observe today.

Despite their remarkable successes, both the Standard Model and the  $\Lambda$ CDM framework have significant shortcomings. The Standard Model fails to explain the origin of neutrino masses and the matter/antimatter asymmetry of the universe, and lacks a viable dark matter candidate.  $\Lambda$ CDM, while highly predictive, fails to account for the microscopic nature of inflation and the nature of dark energy and dark matter. These unresolved questions motivate the search for a more fundamental theory. Furthermore, the energy scales relevant during inflation are expected to be near the grand unification or Planck scale, regimes where all fundamental forces become comparable in strength and must be treated on equal footing. Therefore, gravity needs to be quantized similarly to the other three forces, motivating the need for a quantum theory of gravity.

Among the candidate frameworks, string theory stands out as one of the most promising. It replaces point particles with one-dimensional objects, the strings, whose different vibrational modes correspond to the spectrum of particles, including the graviton. It provides a consistent ultraviolet (UV) completion of gravity and unifies all known interactions within a single coherent theoretical structure. Moreover, string theory naturally incorporates many features of high-energy physics beyond the Standard Model: supersymmetry, extra dimensions, gauge unification, and mechanisms for symmetry breaking [8–12].

Yet theoretical consistency alone is not sufficient as physical theories must be tested. While particle accelerators such as the LHC have pushed the boundaries of terrestrial experiments, they remain far from the energy scales characteristic of quantum gravity. Indeed, colliders failed to observe supersymmetry, which was thought to be the smoking gun of string theory. This calls for exploring energies not reachable by colliders.

Cosmology offers a way forward. As the early universe is sensitive to extremely high energies, by observing the largest structures and oldest light in the cosmos we gain indirect access to the physics governing the smallest scales. Then, cosmological observables can be used to probe and drive theories that go well beyond known particle physics, an otherwise impossible task with current collider technologies. This fundamental idea underlies the field of string cosmology. String theory, as a candidate for a consistent ultraviolet completion of gravity, is expected to leave imprints on cosmological observables. Conversely, precision cosmology provides a window into aspects of string theory that may be otherwise inaccessible.

One of the most intriguing links between string theory and cosmology comes through axions. Axions are particles originally introduced as a consistent way to explain the strong CP (charge conjugation and parity) problem in quantum chromodynamics (QCD), i.e., the puzzling absence of CP violation in the strong interactions, despite it being allowed by the QCD Lagrangian. Peccei and Quinn proposed a mechanism introducing a new symmetry and a particle, the QCD axion, naturally cancelling the CP-violating term in QCD [13]. Beyond their original motivation, axions have emerged as promising candidates for dark matter. The QCD axion is produced non-thermally in the early universe via

the misalignment mechanism, potentially accounting for the observed cold dark matter abundance for decay constants in the appropriate range. More generally, theories beyond the Standard Model, especially string theory, predict the existence of axion-like particles (ALPs). These share the shift symmetry characteristic of the QCD axion, but not their energy scale, often spanning many orders of magnitude. In this thesis, we will refer to ALPs simply as axions.

String theory is formulated in spaces with dimension higher than the canonical four dimensional space-time. Axions arise naturally as lower dimensional fields upon compactification of the extra dimensions [14]. Their properties and their multiplicity are dictated by the topological data of the compactification and their dynamics are encoded in the effective four-dimensional action. The result is the so-called *string axiverse* [15–19], a landscape of axions with a broad spectrum of masses and decay constants. Many of these fields can remain light over cosmological timescales, making them viable candidates for dark matter or mediators of new forces. Others may have been active in the early universe, sourcing observables such as isocurvature fluctuations or gravitational waves.

Experimental detection of even a single axion would constitute undeniable evidence of new physics beyond the Standard Model. Observing more than one could point directly to the structure of extra dimensions, providing empirical support for the string theoretic origin of the Universe.

#### Outline

In this thesis we study the phenomenology of spectator string axions, by which we mean a light axion present during inflation whose energy density is subdominant to that of the inflaton, but which can nevertheless source scalar and tensor perturbations through derivative or Chern–Simons couplings.

We review the basics of string phenomenology in chapter 2, with a focus on the interconnection of string theory and cosmology. We emphasize inflation, where the relevant scales approach those investigated by string theory, and review the basics of string compactifications and their 4D phenomenology.

We then review the type IIB string axiverse in chapter 3. The axiverse has been extensively explored in type IIB settings, where many complexities, such as moduli stabilization, have been addressed (even if not fully resolved) [20].

In chapter 4 we investigate axion physics in heterotic string compactifications, focusing on the spectrum and couplings of both model-independent and model-dependent axions. Starting from the effective four-dimensional theory, we analyse the kinetic structure, Chern–Simons couplings, and non-perturbative potentials generated by gauge and stringy instantons, including gaugino condensation and worldsheet effects. We examine how axions acquire masses through these non-perturbative effects and under what conditions one linear combination remains sufficiently light and dominantly aligned with the QCD direction to solve the strong CP problem. Particular attention is given to the alignment of non-perturbative terms and the role of kinetic mixing, showing that successful axion phenomenology in string compactifications depends not only on the presence of instanton corrections, but also on their relative alignment in axion field space. These constraints impose non-trivial requirements on the geometry and gauge-bundle data of the compactification. We illustrate these features with explicit heterotic constructions on Calabi–Yau

manifolds with  $h^{1,1} = 1, 2$ . These examples highlight how decay-constant hierarchies and physical axion couplings can be engineered in principle, but also emphasize that achieving a light axion typically requires additional structure. Upon diagonalizing the mass and kinetic matrices, we extract the physical decay constants and recast the Chern–Simons couplings in the mass basis, identifying the surviving light states and their coupling structure. Altogether, our results show that the heterotic axiverse provides a compelling yet constrained setting for axion phenomenology: while multiple axions are generic, realizing light axions, particularly those able to solve the strong CP problem or play a cosmological role, is not automatic.

We next analyse spectator-axion inflation models in chapter 5, particularly those involving multiple axions coupled to Abelian gauge fields (MASA models). These scenarios offer a rich phenomenology of sourced scalar and tensor fluctuations, leading to localized features, peaks, in the power spectrum of primordial curvature perturbations and gravitational waves. Crucially, they predict a correlated *forest* of signals across scales, which can be probed by gravitational-wave observatories and cosmological surveys. We study the impact of axion-induced scalar and tensor fluctuations on the CMB, especially through spectral distortions. Our analysis reveals that in rolling-axion scenarios, scalar perturbations often dominate the spectral-distortion signal and can already be constrained by FIRAS data in certain parameter regimes. We provide explicit examples, including both U(1) and SU(2) axion—gauge models, demonstrating how localized features in the primordial spectra can shift distortions to observable scales. These results motivate a multi-channel approach, where gravitational-wave and spectral-distortion measurements work in tandem to constrain the underlying dynamics.

In chapter 6 we emphasize that, within string theory, realizing even a single visible spectator-axion sector requires satisfying non-trivial consistency conditions, such as avoiding Stückelberg masses, achieving sufficiently large Chern–Simons couplings (e.g. via D7-brane magnetic flux), and maintaining tadpole cancellation. Nevertheless, viable constructions exist, especially in setups where odd-sector axions from  $C_2$  survive as spectators, offering a concrete path to test string theory through cosmological observations.

Finally, in chapter 7 we turn to the non-perturbative dynamics of axions during and after inflation, focusing on particle production via parametric resonance in string-inspired inflationary models. Using a framework inspired by fibre inflation, we show that the exponential moduli dependence of axion masses leads to a modified version of resonance dynamics governed by the Whittaker–Hill equation. This alters the usual criteria for resonance and enhances the production of heavy axions, depending on the nature of their coupling (kinetic versus instanton-induced). We classify the cosmological implications into distinct regimes, including light relics contributing to dark radiation ( $\Delta N_{\rm eff}$ ), massive dark-matter candidates, and decay products that contribute to the matter content of the Universe. These findings highlight how even subleading stringy effects, such as worldsheet instantons, can control the viability of preheating and the production of cosmic axion backgrounds.

In the last chapter, chapter 8, we present our conclusions, highlight open questions (and those newly raised by our analysis), and propose research directions based on our findings.

#### List of publications

This thesis is based on results published in these papers which appeared in peer-reviewed journals:

- E. Dimastrogiovanni, M. Fasiello, J. Leedom, M. Putti, A. Westphal, *Gravitational Axiverse Spectroscopy: Seeing the Forest for the Axions*, JHEP **08** (2024) 072.
- M. Putti, S. Bhattacharya, N. Bartolo, M. Peloso, *CMB spectral distortions from enhanced primordial perturbations: the role of spectator axions*, JCAP **08** (2024) 016.
- J. Leedom, M. Putti, N. Righi, A. Westphal, *Preheating axions in string cosmology*, JHEP **04** (2025) 095.
- J. Leedom, M. Putti, A. Westphal, Towards a Heterotic Axiverse, arXiv:2509.03578.

### Chapter 2

# Foundations of String Cosmology

This chapter reviews the key cosmological motivations for inflation and outlines the core ingredients of string theory that will be relevant throughout this thesis. We begin with the standard cosmological framework and the case for inflation, then introduce the structure of string theory, including its compactifications, branes, and moduli. Finally, we sketch how these elements give rise to inflationary models.

### 2.1 Early-Universe Cosmology

To understand the interplay between string theory and cosmology, we begin by reviewing the key features of the standard cosmological model. In particular, we focus on the large-scale dynamics of the Universe, its expansion history, and the evolution of perturbations. In this section, we briefly review the standard cosmological model, focusing on the Friedmann-Lemaître-Robertson-Walker (FLRW) spacetime and its evolution under different matter contents. We then turn to the shortcomings of the hot Big Bang scenario, which are solved by a period of accelerated expansion known as inflation.

The evolution of our universe on large scales is successfully described by General Relativity coupled to a nearly homogeneous and isotropic fluid. The dynamics are governed by Einstein's field equations,

$$\mathcal{G}_{\mu\nu} = 8\pi G T_{\mu\nu} \,\,, \tag{2.1}$$

where  $\mathcal{G}_{\mu\nu} = R_{\mu\nu} - \frac{1}{2}Rg_{\mu\nu}$  is the Einstein tensor and  $T_{\mu\nu}$  the energy–momentum tensor.

Under the assumptions of spatial homogeneity and isotropy (cosmological principle), the most general spacetime metric is the Friedmann–Lemaître–Robertson–Walker (FLRW) metric:

$$ds^{2} = -dt^{2} + a^{2}(t) \left[ \frac{dr^{2}}{1 - kr^{2}} + r^{2}(d\theta^{2} + \sin^{2}\theta d\phi^{2}) \right],$$
 (2.2)

where a(t) is the scale factor and k denotes the spatial curvature. The corresponding Einstein equations reduce to the Friedmann equations:

$$H^{2} = \frac{8\pi G}{3}\rho - \frac{k}{a^{2}},$$

$$\frac{\ddot{a}}{a} = -\frac{4\pi G}{3}(\rho + 3p),$$
(2.3)

with  $H = \dot{a}/a$  the Hubble parameter, and  $\rho$ , p the total energy density and pressure, respectively.

The evolution of  $\rho$  is governed by the continuity equation,

$$\dot{\rho} + 3H(\rho + p) = 0 \tag{2.4}$$

which, under a constant equation of state  $p=w\rho$ , yields  $\rho\propto a^{-3(1+w)}$ . This leads to power-law behaviors for the scale factor:  $a(t)\propto t^{2/3}$  during matter domination (w=0) and  $a(t)\propto t^{1/2}$  during radiation domination (w=1/3). A cosmological constant (w=-1) leads to exponential expansion:  $a(t)\propto e^{Ht}$ .

The spatial curvature is conveniently parametrized by the density parameter  $\Omega \equiv \rho/\rho_c$ , where

$$\rho_c = \frac{3H^2}{8\pi G} \tag{2.5}$$

is the critical density for a flat universe. The Friedmann equation then reads

$$\Omega - 1 = \frac{k}{a^2 H^2} \tag{2.6}$$

so that  $\Omega=1$  corresponds to flat geometry, while  $\Omega>1$  or  $\Omega<1$  indicate closed or open universes, respectively. Observations [21] show that today's universe is spatially flat to high precision:  $\Omega_0=1.0007\pm0.0037$ .

#### 2.1.1 The Need for Inflation

While general relativity and the hot Big Bang model describe much of the Universe's history with remarkable precision, they do not explain the fine-tuning required for large-scale homogeneity and spatial flatness. These shortcomings are naturally resolved by a brief epoch of accelerated expansion, known as inflation. Here, we review the foundational motivations for inflation from both theoretical and observational perspectives.

#### Flatness problem.

The deviation of  $\Omega$  from 1 grows with time in decelerating universes, making the observed near-flatness today highly unnatural without extreme fine-tuning of the initial conditions. During accelerated expansion, however,  $\Omega \to 1$  dynamically. This makes inflation a compelling solution.

#### Horizon problem.

In standard cosmology, causally disconnected regions of the cosmic microwave background (CMB) appear to be in thermal equilibrium. The comoving particle horizon,

$$r_h(t) = \int_0^t \frac{dt'}{a(t')},$$
 (2.7)

is finite for  $a(t) \propto t^{\alpha}$  with  $\alpha < 1$  (i.e., w > -1/3), which characterizes both radiation and matter domination. This means many regions of the observable universe were never in causal contact.

Inflation, with  $\ddot{a} > 0$ , leads to a decreasing comoving Hubble radius  $r_H = (aH)^{-1}$ , allowing initially small, causally connected regions to grow and encompass the entire observable universe.

To solve the horizon problem, inflation must last long enough to stretch the initial causal patch to today's horizon size. This condition requires at least  $N \gtrsim 60~e$ -folds of expansion.

#### Monopole problem.

Grand Unified Theories generically predict heavy, stable relics such as magnetic monopoles, which are overproduced at high temperatures ( $T \sim 10^{16}$  GeV). These relics are not observed. Inflation solves this by diluting their number density to negligible levels and suppressing their regeneration if reheating occurs below the GUT scale.

#### 2.1.2 Dynamics of Inflation

Inflation is typically modeled as a quasi-de Sitter phase driven by a scalar field with a slowly varying potential. In this section, we review the dynamics of inflationary expansion, focusing on the background evolution of the inflaton and its associated slow-roll parameters. These concepts will be essential when we later discuss string-theoretic models of inflation driven by moduli or axions.

Acceleration requires  $\ddot{a} > 0$ , which from the second Friedmann equation implies

$$p < -\frac{1}{3}\rho \ . \tag{2.8}$$

This condition can be realized by a scalar field  $\varphi$ , the inflaton, whose equation of state satisfies w < -1/3 when its potential energy dominates over its kinetic energy. While many models have been proposed [22, 23], we restrict to single-field slow-roll inflation, which captures the essential physics of inflationary dynamics.

The action for a real scalar field minimally coupled to gravity is

$$S = \int d^4x \sqrt{-g} \left[ \frac{M_{\rm Pl}^2}{2} R + \frac{1}{2} g^{\mu\nu} \partial_{\mu} \varphi \partial_{\nu} \varphi - V(\varphi) \right] . \tag{2.9}$$

The corresponding energy-momentum tensor reads

$$T_{\mu\nu} = \partial_{\mu}\varphi \partial_{\nu}\varphi - g_{\mu\nu} \left( \frac{1}{2} \partial^{\lambda}\varphi \partial_{\lambda}\varphi + V(\varphi) \right) . \tag{2.10}$$

Assuming spatial homogeneity, the energy density and pressure are

$$\rho_{\varphi} = \frac{1}{2}\dot{\varphi}^2 + V(\varphi) , \qquad p_{\varphi} = \frac{1}{2}\dot{\varphi}^2 - V(\varphi) , \qquad (2.11)$$

and the equation of state becomes

$$w_{\varphi} = \frac{p_{\varphi}}{\rho_{\varphi}} = \frac{\frac{1}{2}\dot{\varphi}^2 - V}{\frac{1}{2}\dot{\varphi}^2 + V} < -\frac{1}{3} \quad \text{if } \dot{\varphi}^2 \ll V \ .$$
 (2.12)

The equation of motion for  $\varphi$  in a FLRW background is

$$\ddot{\varphi} + 3H\dot{\varphi} + V'(\varphi) = 0 , \qquad (2.13)$$

where  $()' \equiv \frac{\partial}{\partial \varphi}$ 

#### **Slow-Roll Approximation**

Inflation requires the potential to dominate the energy density and to vary slowly. This corresponds to the so-called slow-roll regime, characterized by the conditions

$$\dot{\varphi}^2 \ll V(\varphi) , \qquad \ddot{\varphi} \ll 3H\dot{\varphi} . \tag{2.14}$$

Under these approximations, the dynamics simplify to

$$\dot{\varphi} \simeq -\frac{V'}{3H} , \qquad H^2 \simeq \frac{8\pi G}{3} V(\varphi) .$$
 (2.15)

We define the slow-roll parameters

$$\varepsilon \equiv -\frac{\dot{H}}{H^2} \simeq \frac{1}{16\pi G} \left(\frac{V'}{V}\right)^2 ,$$
 (2.16)

$$\eta_H \equiv -\frac{\ddot{\varphi}}{H\dot{\varphi}} \simeq \eta_V - \varepsilon , \quad \text{with } \eta_V = \frac{V''}{3H^2} .$$
(2.17)

The slow-roll approximation holds as long as  $\varepsilon \ll 1$  and  $|\eta_H| \ll 1$ , and inflation ends when  $\varepsilon \simeq 1$ .

The number of e-folds of inflation between a given time t and the end of inflation is

$$N = \int_{t}^{t_{\rm end}} H \ dt \simeq 8\pi G \int_{\varphi_{\rm end}}^{\varphi} \frac{V}{V'} \ d\varphi \ , \tag{2.18}$$

and must satisfy  $N \gtrsim 60$  in order to solve the flatness and horizon problems.

#### 2.1.3 Primordial Fluctuations

Inflation not only solves horizon-scale problems but also provides a compelling origin for the primordial inhomogeneities that seeded cosmic structure. Quantum fluctuations of light fields during inflation are stretched to cosmological scales and imprinted as scalar and tensor perturbations. These fluctuations form the basis of the temperature anisotropies in the CMB and the large-scale structure observed today. Because they originated from quantum effects at high energies, their properties encode information about the early universe, and potentially about UV completions.

#### Scalar (Curvature) Perturbations

We begin by considering scalar perturbations in single-field inflation. Expanding the inflaton around its homogeneous background value,

$$\varphi(\vec{x},t) = \varphi_0(t) + \delta\varphi(\vec{x},t) , \qquad (2.19)$$

and linearizing the equation of motion in a flat FLRW background, we obtain:

$$\ddot{\delta\varphi} + 3H\dot{\delta\varphi} - \frac{\nabla^2 \delta\varphi}{a^2} = -V''(\varphi_0)\delta\varphi \ . \tag{2.20}$$

We promote  $\delta \varphi$  to a quantum field, expanded in Fourier modes:

$$\delta\hat{\varphi}(\tau, \vec{x}) = \frac{1}{(2\pi)^3} \int d^3k \left[ u_k(\tau) \,\hat{a}_k \, e^{i\vec{k}\cdot\vec{x}} + u_k^*(\tau) \,\hat{a}_k^{\dagger} \, e^{-i\vec{k}\cdot\vec{x}} \right] , \qquad (2.21)$$

where  $\tau$  is conformal time, and  $\hat{a}_k$ ,  $\hat{a}_k^{\dagger}$  are annihilation and creation operators satisfying the standard commutation relations. The vacuum state  $|0\rangle$  is defined by  $\hat{a}_k|0\rangle = 0$  for all k.

The mode functions  $u_k(\tau)$  obey the equation (where now the prime denotes the derivative with respect to conformal time)

$$u_k'' + 2\mathcal{H}u_k' + \left(k^2 + a^2 \frac{\partial^2 V}{\partial \varphi^2}(\varphi_0)\right) u_k = 0 , \qquad (2.22)$$

which in suitable gauges or variables (e.g., the Mukhanov–Sasaki variable) becomes simpler.

In curved spacetime, there is no unique notion of vacuum. However, for modes well inside the horizon  $(k \gg aH)$ , spacetime locally resembles flat Minkowski space. The equivalence principle then motivates choosing initial conditions for  $u_k$  such that

$$u_k(\tau) \to \frac{1}{\sqrt{2k}} e^{-ik\tau} \quad \text{as } -k\tau \to \infty ,$$
 (2.23)

which is known as the *Bunch-Davies vacuum*. This condition ensures that modes start as positive-frequency fluctuations deep inside the horizon.

The quantum fluctuations of the inflaton are described statistically. For a free scalar field, the two-point function in Fourier space is

$$\langle \delta \varphi_{\vec{k}} \, \delta \varphi_{\vec{k}'} \rangle = (2\pi)^3 \, \delta^3(\vec{k} + \vec{k}') \, P_{\delta \varphi}(k) \,, \tag{2.24}$$

where  $P_{\delta\varphi}(k) = |\delta\varphi_k|^2 = \frac{|u_k|^2}{a^2}$  is the power spectrum of inflaton fluctuations. The dimensionless power spectrum is defined as

$$\Delta_{\delta\varphi}^2(k) = \frac{k^3}{2\pi^2} P_{\delta\varphi}(k) , \qquad (2.25)$$

which represents the contribution to the variance per logarithmic interval in k.

To connect inflaton fluctuations to observables, we must consider gauge-invariant quantities. One such variable is the comoving curvature perturbation:

$$\zeta = \Psi + H \frac{\delta \varphi}{\dot{\varphi}} \,, \tag{2.26}$$

which remains constant on superhorizon scales for adiabatic perturbations. In the Newtonian (longitudinal) gauge, the perturbed FLRW metric reads

$$ds^{2} = a^{2}(\tau) \left[ -(1+2\Phi) d\tau^{2} + (1-2\Psi) \delta_{ij} dx^{i} dx^{j} \right], \qquad (2.27)$$

and in single-field inflation with no anisotropic stress, we have  $\Phi = \Psi$ .

Another useful expression for  $\zeta$  is in terms of the density on uniform density hypersurfaces:

$$\zeta = -\Phi - H \frac{\delta \rho}{\dot{\rho}} \ . \tag{2.28}$$

On superhorizon scales,  $\zeta$  is conserved, enabling us to relate the curvature perturbation at horizon exit during inflation to the energy density fluctuations at horizon re-entry:

$$\zeta|_{t_H^{(1)}(k)} = \zeta|_{t_H^{(2)}(k)} ,$$
 (2.29)

with

$$-H\frac{\delta\varphi}{\dot{\varphi}}\Big|_{t_{H}^{(1)}(k)} = \frac{1}{4} \frac{\delta\rho_{\gamma}}{\rho_{\gamma}}\Big|_{t_{H}^{(2)}(k)} , \qquad (2.30)$$

where the right-hand side corresponds to the temperature fluctuations observed in the CMB, since  $\rho_{\gamma} \propto T^4$ .

The power spectrum of the curvature perturbation is defined via:

$$\langle \zeta(\vec{k}) \zeta(\vec{k}') \rangle = (2\pi)^3 \delta^3(\vec{k} + \vec{k}') P_{\zeta}(k) , \qquad \Delta_{\zeta}^2(k) = \frac{k^3}{2\pi^2} P_{\zeta}(k) .$$
 (2.31)

During slow-roll inflation, one finds the approximate relation:

$$\Delta_{\zeta}^{2}(k) \simeq \left(\frac{H^{2}}{2\pi\dot{\varphi}}\right)^{2} \simeq \frac{1}{24\pi^{2}M_{\rm Pl}^{4}} \frac{V}{\varepsilon},$$
(2.32)

where  $\varepsilon = \frac{1}{2} M_{\rm Pl}^2 \left(\frac{V'}{V}\right)^2$  is the slow-roll parameter defined in the previous subsection. Observations of the CMB temperature anisotropies suggest  $\Delta_{\zeta}^2 \sim 2 \times 10^{-9}$ , fixing the overall scale of inflation.

Deviations from scale invariance are captured by the scalar spectral index:

$$n_s - 1 \equiv \frac{d \ln \Delta_{\zeta}^2}{d \ln k} = 2\eta_V - 6\varepsilon . \tag{2.33}$$

#### Tensor (Gravitational Wave) Perturbations

Tensor perturbations  $h_{ij}$  describe a stochastic background of primordial gravitational waves. The perturbed metric takes the form

$$ds^{2} = -dt^{2} + a^{2}(t)(\delta_{ij} + h_{ij})dx^{i}dx^{j}, \qquad (2.34)$$

with  $h_{ij}$  transverse and traceless.

These modes obey the wave equation

$$\ddot{h}_{ij} + 3H\dot{h}_{ij} - \frac{\nabla^2 h_{ij}}{a^2} = 0 , \qquad (2.35)$$

identical in form to a massless scalar field in an expanding background.

The tensor power spectrum sourced during slow roll inflation is

$$\Delta_T^2(k) = \frac{2}{\pi^2} \frac{H^2}{M_{\rm Pl}^2} \left(\frac{k}{aH}\right)^{-2\varepsilon} , \qquad (2.36)$$

with spectral tilt

$$n_T = \frac{d \ln \Delta_T^2}{d \ln k} = -2\varepsilon \ . \tag{2.37}$$

A detection of tensor modes would give a direct estimate of the Hubble scale during inflation,  $H \sim E_{\rm inf}^2/M_{\rm Pl}$ , and hence of the energy scale of inflation  $E_{\rm inf} = V^{1/4}$ .

Observational constraints on  $\Delta_T$  are often stated in terms of the tensor-to-scalar ratio:

$$r = \frac{\Delta_T^2}{\Delta_\zeta^2} = 16\varepsilon \ . \tag{2.38}$$

#### **Observational Constraints**

The scalar power spectrum is often parametrized as

$$P_{\zeta}(k) = A_s \left(\frac{k}{k_*}\right)^{n_s - 1} , \qquad (2.39)$$

with  $k_*$  a pivot scale. From Planck [21], the best-fit values are

$$A_s = (2.10 \pm 0.03) \times 10^{-9} ,$$
 (2.40)

$$n_s = 0.9649 \pm 0.0042$$
, (2.41)

indicating a nearly—but not exactly—scale-invariant spectrum. This deviation reflects the slow evolution of the inflaton potential during inflation.

The tensor-to-scalar ratio is constrained by BICEP/Keck [24] to be

$$r < 0.036 \quad (95\% \text{ C.L.}) \ . \tag{2.42}$$

These measurements provide stringent constraints on inflationary models and their embedding in high-energy frameworks. In particular, many string-theoretic models predict specific relations between r,  $n_s$ , and the inflationary energy scale.

#### **Beyond Vacuum Fluctuations**

The scalar and tensor perturbations discussed so far arise from vacuum fluctuations amplified by the background expansion. However, additional contributions can arise from field or metric couplings during inflation. These are referred to as *sourced perturbations*.

For instance, if the inflaton couples to a gauge field via a Chern-Simons term, the amplified vector field fluctuations can source additional scalar or tensor modes. These contributions are non-Gaussian and scale-dependent, and provide a promising observational signature for distinguishing between different high-energy models.

We will explore these effects in more detail in later chapters, particularly in the context of axion-like spectator fields coupled to gauge sectors.

### 2.2 Ingredients of the String Theory Framework

Cosmology and string theory address vastly different regimes: the former concerns the largest observable scales in the universe, while the latter focuses on the microscopic ingredients of quantum gravity. Yet, the early universe provides a unique setting in which these domains intersect. Inflation, in particular, is believed to have occurred at energy scales close to the GUT scale, and possibly even near the string scale. This makes inflationary observables valuable probes of Planck-scale physics.

From a bottom-up perspective, the inflationary paradigm is formulated as an effective field theory. However, the nature of the inflaton, the origin of its potential, and the mechanisms that ensure slow-roll conditions are all sensitive to UV physics. One prominent example is the so-called  $\eta$ -problem: Planck-suppressed corrections generically induce large contributions to the inflaton potential, spoiling the slow-roll conditions unless special symmetries or cancellations are invoked. This suggests that a consistent embedding of

inflation requires a UV-complete theory, and string theory offers the most well-developed candidate.

In the reverse direction, cosmological data can act as a filter on the vast landscape of string theory vacua. Requirements such as producing a viable inflationary phase, achieving successful reheating, and generating the correct spectrum of primordial perturbations while ensuring a stable four-dimensional vacuum, constrain the structure of allowed compactifications. String theory compactifications naturally give rise to numerous scalar fields (e.g. moduli and axions) which are promising candidates for key cosmological roles. These fields can drive inflation, constitute dark matter or dark radiation, and influence reheating or structure formation. Their abundance motivates a top-down approach to identifying distinctive dark sector signatures arising from string theory, and matching them to observables.

In this section, we introduce the essential ingredients of string theory relevant to cosmology. These include the structure of 10d string theories and their interrelations via dualities, the compactification of extra dimensions (typically on Calabi–Yau manifolds), and the emergence of branes, fluxes, and moduli fields. We then turn to mechanisms of moduli stabilization such as the KKLT and Large Volume Scenarios. We will use notation and concepts which are summarized in Appendix A.1

#### 2.2.1 String Theories

String theory proposes that the fundamental building blocks of nature are not point particles but one-dimensional extended objects: strings. As a string propagates through spacetime, it traces out a two-dimensional surface called worldsheet. The classical dynamics are governed by the Nambu-Goto action, proportional to the area of this surface A:

$$S = T \times A = -T \int d^2 \sigma \sqrt{-\det h_{\alpha\beta}}, \qquad (2.43)$$

where  $h_{\alpha\beta} = \partial_{\alpha} X^{\mu} \partial_{\beta} X^{\nu} \eta_{\mu\nu}$  is the induced metric on the worldsheet, The string tension T is given by

$$T = \frac{1}{2\pi\alpha'} = m_s^2 = \frac{1}{\ell_s^2} , \qquad (2.44)$$

where  $\ell_s$  is the string length and  $m_s$  the string scale. Although typically near the Planck scale,  $\ell_{\rm Pl} \sim 10^{-33}$  cm, it can be lower in specific compactifications.

Upon quantization, a closed string exhibits an infinite tower of excitations with masses spaced by the string scale:

$$\frac{M^2}{m_s^2} = -1, 0, 1, 2, \dots {2.45}$$

The lowest-lying massless modes include the graviton  $g_{\mu\nu}$ , an antisymmetric two-form  $b_{\mu\nu}$ , and the dilaton  $\phi$ , while the presence of a tachyon in the  $M^2 = -m_s^2$  state signals an instability in bosonic string theory. A consistent vacuum requires a supersymmetric extension to remove this instability and to ensure anomaly cancellation.

Introducing supersymmetry on the worldsheet leads to superstring theory, which is consistent only in ten spacetime dimensions. There are five of such theories:

- Type IIA: oriented closed strings, non-chiral;
- Type IIB: oriented closed strings, chiral;

- Type I: unoriented open and closed strings;
- Heterotic SO(32) and Heterotic  $E_8 \times E_8$ : hybrid constructions with closed strings whose left- and right-movers obey different constraints.

Although these theories were initially viewed as distinct, they are now known to be connected through a rich network of dualities:

- **T-duality** exchanges momentum and winding modes and relates Type IIA and Type IIB upon compactification;
- **S-duality** relates strong and weak coupling regimes (e.g., Type IIB is self-dual; Type I is S-dual to Heterotic SO(32));
- U-duality unifies T- and S-dualities in a broader non-perturbative framework.

These dualities reveal that the five superstring theories are perturbative expansions of a single underlying theory. In particular, the strong coupling limit of Type IIA gives rise to an emergent 11th dimension and a new theory, M-theory, which includes not only strings but also higher-dimensional extended objects like membranes and five-branes.

An important conceptual feature of string theory is that its coupling constants are dynamical: the string coupling  $g_s$  is determined by the expectation value of the dilaton field via

$$g_s = e^{\langle \phi \rangle} \ . \tag{2.46}$$

An equivalent formulation for the propagation of strings in curved spacetime, more convenient especially for quantization, is described by a two-dimensional sigma model with the Polyakov action:

$$S_{P} = -\frac{T}{2} \int d^{2}\sigma \sqrt{-\gamma} \gamma^{\alpha\beta} \partial_{\alpha} X^{\mu} \partial_{\beta} X^{\nu} \eta_{\mu\nu} =$$

$$= \frac{1}{4\pi\alpha'} \int d^{2}\sigma \sqrt{h} \left[ h^{\alpha\beta} \partial_{\alpha} X^{\mu} \partial_{\beta} X^{\nu} g_{\mu\nu}(X) + \varepsilon^{\alpha\beta} \partial_{\alpha} X^{\mu} \partial_{\beta} X^{\nu} B_{\mu\nu}(X) + \alpha' R^{(2)} \phi(X) \right], ,$$
(2.47)

where  $\gamma_{\alpha\beta}$  is an auxiliary worldsheet metric. Varying with respect to  $\gamma_{\alpha\beta}$  enforces that it equals the induced metric  $h_{\alpha\beta}$ , recovering the Nambu-Goto action. The Polyakov form is manifestly invariant under worldsheet diffeomorphisms and Weyl transformations, making it the standard starting point for covariant quantization.  $X^{\mu}$  describe the embedding into spacetime, and  $R^{(2)}$  is the worldsheet Ricci scalar. Perturbative expansions in the string coupling correspond to summing over worldsheet topologies: a genus-g surface contributes with weight  $g_s^{2g-2}$ .

Because coupling constants are set by scalar vevs, string theory naturally explores regimes where the effective field theory changes qualitatively due to strong coupling or geometric transitions. Dualities often allow such strongly coupled regions to be mapped to weakly coupled dual descriptions with different effective degrees of freedom. This interconnected web of dualities implies a deep unifying structure: all consistent string theories, and their M-theoretic extensions, are thought to describe different limits of a single underlying framework. Each compactification defines a point in this "string landscape," with low-energy physics governed by geometric data and background fields.

One of the most important features of string theory from a cosmological viewpoint is the existence of extra spatial dimensions. To obtain a four-dimensional effective theory, these must be compactified on a suitable internal manifold. The geometry and topology of the compact space, together with the inclusion of background fluxes, D-branes, and orientifold planes, determine the effective field content and interactions in four dimensions. Compactifications typically give rise to a large number of scalar fields that arise either from deformations of the compact geometry or from integrating higher-form gauge fields over internal cycles. These scalars are not arbitrary additions to the theory: they are unavoidable consequences of compactification and thus carry a predictive structure. Such fields are natural candidates for cosmological roles. Moduli and axions may drive inflation, act as dark matter or dark radiation, or source isocurvature perturbations. Because their properties are determined by the underlying compactification, studying them offers a rare opportunity for a top-down approach to cosmology.

#### 2.2.2 Basics of compactification

Let us now explain what we mean by the term compactification. String theory requires additional spatial dimensions for consistency: ten in superstring theory and eleven in M-theory. Yet, the observable universe is effectively four-dimensional at accessible energy scales. Reconciling this discrepancy leads to the concept of *compactification*, in which the extra dimensions are curled up into a compact internal manifold of small size and non-trivial geometry. This process yields an effective four-dimensional theory describing the light degrees of freedom at low energies.

In a compactified theory, fields originally defined in ten dimensions are expanded in eigenmodes on the internal space. The resulting four-dimensional spectrum includes an infinite tower of Kaluza–Klein excitations, but only the lightest modes, the zero modes, remain relevant below the compactification scale. These include the four-dimensional graviton and a number of massless scalar fields, or *moduli*, which encode the geometry of the compact space. The structure of the compactification manifold: its topology, metric, and the presence of background fluxes, determines the effective spectrum, interactions, and symmetries of the resulting 4D theory. Over the past decades, a rich landscape of compactifications has been uncovered, many of which feature ingredients of interest to cosmology, including scalar fields suitable for inflation, axion-like particles, and mechanisms for dark matter or dark radiation. Among these, due to their many computable features, Calabi–Yau compactifications have emerged as a particularly useful framework for connecting string theory to low-energy phenomenology.

#### Calabi-Yau Manifolds

To reduce ten-dimensional string theory to an effective four-dimensional theory, we seek solutions to the 10D equations of motion with a factorized spacetime geometry:

$$M_{10} = \mathcal{M}_{1.3} \times X_6 , \qquad (2.48)$$

where  $\mathcal{M}_{1,3}$  denotes 4D Minkowski space, and  $X_6$  is a compact internal manifold. Requiring a maximally symmetric 4D vacuum and satisfying the 10D vacuum Einstein equations  $R_{MN} = 0$  imposes Ricci-flatness on  $X_6$ .

A natural class of Ricci-flat manifolds is given by Calabi–Yau (CY) threefolds: compact, complex, Kähler manifolds of complex dimension three with vanishing first Chern class. Yau's theorem guarantees the existence of a Ricci-flat Kähler metric on such manifolds.

The decomposition of the Lorentz group under this factorization is  $SO(9,1) \to SO(3,1) \times SO(6)$ . Preserving supersymmetry in four dimensions requires the existence of a globally defined, nowhere-vanishing spinor on  $X_6$ . This condition restricts the holonomy of the internal manifold to  $SU(3) \subset SO(6)$ , a defining feature of CY threefolds.

This spinor structure implies the existence of two key geometric objects:

- A Kähler form J, a closed (1,1)-form that defines the Hermitian metric via  $g_{m\bar{n}} = \partial_m \bar{\partial}_{\bar{n}} K$ .
- A holomorphic (3,0)-form  $\Omega$ , unique up to rescaling, which satisfies  $h^{3,0}=1$  and is related to J via

$$J \wedge J \wedge J = \frac{3i}{4} \Omega \wedge \bar{\Omega} , \qquad J \wedge \Omega = 0 .$$
 (2.49)

Together, J and  $\Omega$  define the complex and symplectic structure of  $X_6$  and determine its moduli space.

#### Moduli and Metric Deformations.

Fluctuations of the internal metric  $g_{mn}$  that preserve Ricci-flatness correspond to massless scalar fields in 4D—moduli. These arise as zero modes of the Lichnerowicz operator:

$$\nabla^q \nabla_q \delta g_{mn} + 2R^q{}_m{}^r{}_n \delta g_{qr} = 0 . {2.50}$$

In a Kähler manifold, deformations decompose into:

- (1,1)-forms  $\delta g_{m\bar{n}} \in H^{1,1}(X) \to \mathbf{K\ddot{a}hler\ moduli};$
- (2,1)-forms  $\delta g_{\bar{m}\bar{n}} \in H^{2,1}(X) \to \mathbf{complex}$  structure moduli,

where  $H^{(1,1)}(X)$  and  $H^{(2,1)}$  are cohomology groups defined in Appendix A.2. These deformations are counted by the Hodge numbers  $h^{1,1}$  and  $h^{2,1}$ , which determine the dimension of the moduli space. The Hodge diamond symmetries (e.g.,  $h^{p,q} = h^{q,p}$ ,  $h^{i,j} = h^{D-i,D-j}$ ) imply only  $h^{1,1}$  and  $h^{2,1}$  are independent for a CY threefold. The Euler characteristic is then:

$$\chi(X) = 2(h^{1,1} - h^{2,1}) . (2.51)$$

#### Kähler Moduli

The Kähler form can be expanded in a basis of harmonic (1,1)-forms  $\{\omega_i\}$ :

$$J = t^i(x) \ \omega_i \ , \qquad t^i = \text{K\"{a}hler moduli} \ .$$
 (2.52)

The moduli  $t^i$  correspond to the volumes of 2-cycles. The volume of a 4-cycle  $\Sigma_4$  is given by

$$\tau_i = \frac{1}{2} \mathcal{K}_{ijk} t^j t^k \,, \tag{2.53}$$

where  $\mathcal{K}_{ijk} = \int_X \omega_i \wedge \omega_j \wedge \omega_k$  are the triple intersection numbers. The total volume is

$$\mathcal{V} = \frac{1}{6} \mathcal{K}_{ijk} t^i t^j t^k \,, \tag{2.54}$$

and must lie inside the Kähler cone to ensure positivity:

$$\int_{\Sigma_2} J > 0 , \quad \int_{\Sigma_4} J \wedge J > 0 , \quad \int_X J \wedge J \wedge J > 0 . \tag{2.55}$$

#### Complex Structure Moduli

Deformations of the complex structure change how holomorphic coordinates are defined. These are parametrized by  $z^a$  and can be expanded in a basis  $\{\alpha_a\} \subset H^{2,1}(X)$ :

$$\Omega_{kl}^{\bar{n}} \delta g_{\bar{m}\bar{n}} = z^a(\alpha_a)_{kl\bar{m}} . \tag{2.56}$$

The (3,0)-form  $\Omega$  depends holomorphically on  $z^a$ . One defines a symplectic basis of 3-forms  $(\alpha^a, \beta_b)$  dual to 3-cycles  $(\mathcal{A}^a, \mathcal{B}_b)$ :

$$\int_{X} \alpha^{a} \wedge \beta_{b} = \delta_{b}^{a} , \qquad (2.57)$$

and expands

$$\Omega = z^a \alpha_a - \mathcal{F}_a(z) \,\beta^a \,, \quad \mathcal{F}_a = \frac{\partial \mathcal{F}}{\partial z^a} \,.$$
 (2.58)

Here,  $\mathcal{F}(z)$  is the prepotential. The Kähler potential on the complex structure moduli space is

$$K_{cs} = -\ln\left(i\int_{X} \Omega \wedge \bar{\Omega}\right) = -\ln(i\bar{z}^{a}\mathcal{F}_{a} - iz^{a}\bar{\mathcal{F}}_{a}), \qquad (2.59)$$

and defines the metric  $g_{a\bar{b}} = \partial_a \partial_{\bar{b}} K_{cs}$ .

#### Moduli Space Geometry.

The moduli space locally factorizes as

$$\mathcal{M} = \mathcal{M}_{CS} \times \mathcal{M}_K \,, \tag{2.60}$$

where both are Kähler manifolds of dimensions  $h^{2,1}$  and  $h^{1,1}$  respectively. The Kähler moduli space metric reads

$$g_{ij} = \frac{3}{2\mathcal{K}} \int_{\mathcal{X}} \omega_i \wedge \star \omega_j = -\frac{3}{2} \left( \frac{\mathcal{K}_{ij}}{\mathcal{K}} - \frac{3}{2} \frac{\mathcal{K}_i \mathcal{K}_j}{\mathcal{K}^2} \right) , \qquad (2.61)$$

with 
$$K_i = \int_X \omega_i \wedge J \wedge J$$
 and  $K_{ij} = \int_X \omega_i \wedge \omega_j \wedge J$ .

Massless moduli are problematic: they mediate long-range forces and destabilize cosmology. Fifth-force constraints require  $m_{\phi} \gtrsim 10^{-3}$  eV, mandating mechanisms for moduli stabilization. As we will see, this is typically achieved by introducing background fluxes, branes, and non-perturbative effects, which generate potentials for the moduli fields. Stabilizing these moduli in a controlled way is a central task of string phenomenology and string cosmology alike.

#### 2.2.3 Branes and Fluxes

D-branes are dynamical extended objects in string theory on which open strings can end. A Dp-brane traces out a (p+1)-dimensional worldvolume in spacetime. Their inclusion as non-perturbative states was crucial for completing the web of string dualities [25], and their discovery marked a turning point in both formal and phenomenological developments in string theory [26].

From a phenomenological viewpoint, D-branes offer a natural setting to embed gauge theories within string theory. The endpoints of open strings attached to a D-brane carry gauge degrees of freedom, giving rise to a U(1) gauge field. When N D-branes coincide, the gauge symmetry is enhanced to U(N), and the low-energy dynamics is governed by a (p+1)-dimensional supersymmetric Yang-Mills theory. This enables D-branes to realize non-Abelian gauge sectors and chiral matter, making them key ingredients in string model building [27].

D-branes are electrically charged under the Ramond–Ramond (RR) sector and couple to RR (p+1)-form gauge potentials  $C_{p+1}$  via the Wess–Zumino term in the brane action:

$$S_{\rm CS} = \mu_p \int_{\Sigma_{p+1}} C \wedge e^{\mathcal{F}} , \qquad \mathcal{F} = B_2 + 2\pi \alpha' F , \qquad (2.62)$$

where C is the sum of all RR forms,  $B_2$  is the NS-NS 2-form, and F is the worldvolume gauge field strength. This coupling implies that D-branes act as sources for RR fluxes.

Global consistency of string compactifications requires cancellation of these RR charges—a condition known as tadpole cancellation. To achieve this, one must often include orientifold planes (O-planes): non-dynamical, negatively charged fixed loci under involutive symmetries of the theory. For example, O7-planes carry negative charge under  $C_8$  and must be compensated by D7-branes to ensure charge neutrality.

#### Fluxes.

String theories contain various higher-form gauge potentials, whose corresponding field strengths can be turned on as background fluxes. Similar consequences can be traced out in the different string theories, but let us focus on type IIB as it is the most useful example. Take  $C_{p+1}$ , with field strengths  $F_{p+2} = dC_{p+1}$ . These fluxes are quantized over internal cycles:

$$\int_{\Sigma_{p+2}} F_{p+2} = n \in \mathbb{Z} , \qquad \Sigma_{p+2} \in H_{p+2}(X, \mathbb{Z}) .$$
 (2.63)

Such fluxes are topological, analogous to magnetic monopole flux in Maxwell theory, and obey Dirac quantization. The NS-NS sector also includes a 2-form potential  $B_2$  whose 3-form field strength is

$$H_3 = dB_2 , \qquad S \supset \int d^{10}x \sqrt{-g} \left( R - \frac{1}{2 \cdot 3!} H_{MNP} H^{MNP} \right) .$$
 (2.64)

In compactifications, fluxes such as  $H_3$  and  $F_3$  can thread non-trivial 3-cycles in the internal manifold. Their combined contribution defines a complexified 3-form:

$$G_3 = F_3 - \tau H_3$$
,  $\tau = C_0 + ie^{-\phi}$ . (2.65)

Supersymmetric flux vacua require  $G_3$  to be imaginary self-dual (ISD) on the compact space:

$$\star_6 G_3 = iG_3$$
 , (2.66)

which implies that  $G_3$  must be of Hodge type (2,1) or (0,3). Only the (2,1) part preserves supersymmetry, while the (0,3) component leads to spontaneous supersymmetry breaking. The ISD condition also ensures that  $G_3$  contributes positively to the D3-brane charge.

#### Tadpole Cancellation and O-Planes.

The total D3-brane charge must vanish in a consistent compactification. This leads to the tadpole cancellation condition:

$$\frac{1}{(2\pi)^4 \alpha'^2} \int_X H_3 \wedge F_3 + N_{D3} - \frac{1}{4} N_{O3} = 0 , \qquad (2.67)$$

where  $N_{\rm D3}$  counts the number of localized D3-branes, and  $N_{\rm O3}$  is the number of orientifold O3-planes. Similar tadpole constraints arise for higher-dimensional branes such as D7-branes and O7-planes.

#### D-brane Dynamics and Moduli Dependence.

The low-energy dynamics of a Dp-brane is governed by two contributions:

$$S_{\text{DBI}} = -T_p \int_{\Sigma_{p+1}} d^{p+1} \xi \ e^{-\phi} \sqrt{-\det(g + B_2 + 2\pi\alpha' F)} \ , \tag{2.68}$$

$$S_{\rm CS} = \mu_p \int_{\Sigma_{p+1}} C \wedge e^{\mathcal{F}} . \tag{2.69}$$

The DBI action describes the kinetic terms and coupling to background fields, while the Chern–Simons term encodes the topological charge.

D-branes can also carry worldvolume fluxes, which affect the effective four-dimensional theory by modifying the definitions of Kähler and axionic moduli. These fluxes induce potentials for the moduli and contribute to supersymmetry breaking or stabilization. Moreover, open strings stretching between D-branes introduce additional light states, which correspond to position moduli or gauge fields, enriching the low-energy spectrum.

The inclusion of fluxes and branes plays a dual role in compactifications. On the one hand, they are needed to satisfy consistency conditions such as charge cancellation. On the other, they give rise to potentials for the moduli fields, thereby helping to stabilize previously flat directions in the effective theory. This is especially important in cosmological contexts, where runaway directions or massless scalars are phenomenologically problematic.

#### 2.2.4 Moduli Stabilization

As we have seen, string compactifications generically give rise to massless scalar fields known as *moduli*, associated with deformations of the compactification geometry and background fields. Although these moduli parametrize legitimate vacuum configurations from the higher-dimensional point of view, they must be stabilized to yield a viable four-dimensional effective theory. Unstabilized moduli can mediate long-range fifth forces, induce variations in physical couplings, or trigger runaway behaviour, all of which are in conflict with observations.

A central challenge in connecting string theory to particle physics and cosmology is thus the construction of vacua where all moduli are stabilized by controlled, computable potentials. This typically requires breaking the no-scale structure that emerges at leading order in many compactifications.

#### Flux-Induced Potentials.

One of the most robust mechanisms for moduli stabilization relies on background fluxes. In particular, Type IIB Calabi–Yau orientifolds allow for the inclusion of NS-NS and RR 3-form fluxes,  $H_3$  and  $F_3$ , which can thread internal 3-cycles. These combine into the complex 3-form

$$G_3 = F_3 - \tau H_3 , \qquad \tau = C_0 + ie^{-\phi} , \qquad (2.70)$$

where  $\tau$  is the axio-dilaton. As shown in [28], these fluxes generate a tree-level contribution to the four-dimensional  $\mathcal{N}=1$  superpotential, known as the Gukov–Vafa–Witten (GVW) superpotential [29]:

$$W_{\text{flux}} = \int_X G_3 \wedge \Omega \ . \tag{2.71}$$

This superpotential depends holomorphically on the complex structure moduli and  $\tau$ , and leads to their stabilization via the F-term conditions  $D_IW = 0$ .

The resulting scalar potential is of the standard  $\mathcal{N}=1$  supergravity form:

$$V = e^{K} \left( K^{I\bar{J}} D_{I} W D_{\bar{J}} \bar{W} - 3|W|^{2} \right) , \qquad (2.72)$$

where K is the Kähler potential, and  $D_IW = \partial_IW + (\partial_IK)W$  are the Kähler covariant derivatives. At tree level, the Kähler potential satisfies the no-scale identity

$$K^{i\bar{j}}\partial_i K \ \partial_{\bar{i}} K = 3 \ , \tag{2.73}$$

implying that the scalar potential is positive semi-definite and the Kähler moduli remain flat directions. Breaking this no-scale structure is necessary for full stabilization.

#### Non-Perturbative Stabilization: KKLT.

A well-studied mechanism to stabilize the Kähler moduli is the KKLT scenario [30]. In this setup, one adds non-perturbative contributions to the superpotential from effects such as D3-brane instantons or gaugino condensation on D7-branes wrapped on rigid 4-cycles:

$$W = W_0 + A e^{-aT} , (2.74)$$

where T denotes a Kähler modulus. The combination of the flux-induced  $W_0$  and the non-perturbative term stabilizes T in a supersymmetric AdS vacuum. This vacuum can be uplifted to a metastable de Sitter (dS) vacuum by including, for example, anti-D3-branes at warped throat tips.

#### The Large Volume Scenario (LVS).

An alternative approach is the Large Volume Scenario (LVS) [31], which uses perturbative  $\alpha'$  corrections to the Kähler potential along with non-perturbative terms in the superpotential. In this framework, one finds exponentially large compactification volumes:

$$V \sim \frac{A}{V^3} - \frac{B e^{-a\tau_s}}{V^2} + \frac{C e^{-2a\tau_s}}{V} ,$$
 (2.75)

where  $\mathcal{V}$  is the overall volume modulus, and  $\tau_s$  denotes a blow-up 4-cycle. This potential yields a non-supersymmetric AdS vacuum at large volume and can be uplifted to a dS vacuum with small positive cosmological constant. This is the stabilization mechanism we will adopt in the Type IIB examples throughout this thesis.

#### Open Challenges and Conceptual Issues.

Despite these advances, moduli stabilization remains one of the most delicate aspects of connecting string theory to low-energy physics. Non-perturbative effects like instantons or gaugino condensation depend sensitively on the detailed geometry and global brane embeddings, which are often only partially under control. The construction of metastable dS vacua remains controversial. In KKLT, the uplift via anti-D3-branes breaks supersymmetry explicitly, and concerns have been raised about their backreaction [32–34]. In LVS, uplift mechanisms often invoke ingredients—such as D-term potentials or non-SUSY branes—whose consistency in string theory is debated [35]. The swampland de Sitter conjecture [36–38] suggests that scalar potentials consistent with quantum gravity must satisfy a condition of the form  $|\nabla V|/V \ge c \sim \mathcal{O}(1)$  in asymptotic regions of moduli space, thereby disfavoring meta-stable dS vacua in such asymptotic regimes. While refinements and counterexamples have been proposed [39-41], the issue remains unsettled. Even when stabilized with large masses, moduli may decay late and interfere with Big Bang Nucleosynthesis or matter domination. This places constraints on the allowed parameter space. Full moduli stabilization typically breaks supersymmetry. However, the mechanism for SUSY breaking and its mediation to the visible sector are not universally understood and may involve sequestering or anomaly mediation scenarios. Most stabilization mechanisms assume static backgrounds, neglecting cosmological backreaction and time-dependent moduli evolution.

### 2.3 Inflationary Models in String Theory

While the *mechanism* of inflation is simple and effective, its *microphysical* origin remains elusive. Inflation is commonly modeled by the dynamics of one or more scalar fields, the inflaton, whose potential must be sufficiently flat to support slow-roll conditions over a sufficient number of e-folds. However, the required flatness of the inflaton potential makes it vulnerable to higher-dimensional operators suppressed by the Planck scale. This sensitivity suggests that inflation cannot be fully understood without reference to ultraviolet (UV) physics, in particular quantum gravity.

String theory provides a natural setting in which to study such UV completions of inflation. Indeed, it has been argued that consistency with quantum gravity imposes stringent constraints on low-energy scalar potentials, including those relevant for inflation [42]. Despite these challenges, several mechanisms for realizing inflation within string theory have been proposed. These include axion monodromy inflation [43–46], fibre inflation [47], and other constructions [48,49]. These scenarios typically arise only in specific corners of the string landscape, suggesting that the requirement of successful inflation may serve as a filter on viable compactifications.

In the following, we briefly review three main classes of string inflation models: axion inflation, moduli inflation, and brane inflation.

#### 2.3.1 Axion Inflation

Axion inflation refers to models in which the inflaton is an axion-like field, typically arising from the dimensional reduction of higher-form gauge potentials in string theory. Thanks to their approximate shift symmetry, axions are natural inflaton candidates: the symmetry protects the flatness of their potential against quantum corrections, helping to

maintain slow-roll conditions.

The simplest example is *natural inflation*, where the potential is given by

$$V(\phi) = \Lambda^4 \left( 1 - \cos\left(\frac{\phi}{f}\right) \right). \tag{2.76}$$

Successful natural inflation requires a super-Planckian decay constant,  $f > M_{\rm Pl}$ , which is difficult to achieve in well-controlled regions of string theory. This has motivated extensions such as axion monodromy inflation, in which the axion traverses multiple cycles of its fundamental domain due to a softly broken shift symmetry [43–45]. This leads to approximately linear or polynomial potentials over large field ranges, enabling large-field inflation without requiring a trans-Planckian decay constant.

Another proposal is *N-flation* [50], in which a large number of axions participate in inflation simultaneously. Collectively, their dynamics can support slow-roll inflation even when individual decay constants are sub-Planckian. This is natural in string theory, where compactifications on Calabi–Yau manifolds often yield many axions due to the abundance of internal cycles.

Axion inflation can imprint distinctive signatures in the cosmic microwave background (CMB), such as oscillatory features in the power spectrum, non-Gaussianities, and isocurvature perturbations. The latter are particularly interesting, as they can place strong observational constraints on models with light axions surviving after inflation.

#### 2.3.2 Moduli Inflation

In moduli inflation models, the inflaton is identified with a geometric modulus of the compactification, such as a Kähler, complex structure, or dilaton modulus. Since moduli fields are generically present in string compactifications, they are natural inflaton candidates. However, to realize inflation, their potential must exhibit an extended flat direction, which is not generic and typically arises only after subleading corrections are included.

The best-known examples are fibre and blow-up inflation models arising in the Large Volume Scenario (LVS) [47]. In these scenarios, the volume of a fibre or blow-up cycle plays the role of the inflaton. The inflationary potential emerges from subdominant effects, such as  $\alpha'$  corrections and string loop corrections, while the overall volume remains stabilized. These models are often characterized by small-field inflation and predict a low tensor-to-scalar ratio r, typically outside the reach of current experiments.

Because the inflaton is itself a modulus, ensuring consistent stabilization of the remaining moduli during inflation is challenging. If the evolution of the inflaton destabilizes the compactification or induces large kinetic mixing with other fields, the inflationary dynamics may fail or become unpredictable. Therefore, successful moduli inflation requires a hierarchy in the moduli masses such that the inflaton is light, while the others are sufficiently heavy and decoupled.

#### 2.3.3 Brane Inflation

Brane inflation refers to scenarios where the inflaton corresponds to the position of a D-brane moving in a compact internal space [51–53]. The potential energy driving inflation arises from interactions between the mobile brane and other ingredients in the compactification, such as antibranes, fluxes, or localized curvature.

A prototypical example is D3/D3 inflation, where a D3-brane moves toward an anti-D3-brane located at the bottom of a warped throat, such as the Klebanov–Strassler geometry. The attractive force between the branes drives inflation, and their annihilation at the end of inflation provides a natural reheating mechanism.

Warped throats play a crucial role by flattening the potential and suppressing higher-order corrections, thereby facilitating slow-roll inflation even over short brane displacements. In some variants, such as Dirac–Born–Infeld (DBI) inflation, the kinetic term becomes non-canonical, leading to characteristic non-Gaussian signatures.

Howewer, controlling the backreaction of moving branes on the compactification geometry is highly nontrivial, and preserving moduli stabilization during inflation requires tuning. These scenarios are also sensitive to initial conditions and often require careful engineering to ensure all constraints are satisfied.

#### 2.3.4 Modular Inflation

Modular inflation refers to inflationary scenarios where the inflaton is a modulus that transforms non-trivially under modular transformations. These include, for example, moduli fields in heterotic or Type IIB string compactifications that parameterize shapes of tori or orbifolds and transform under  $SL(2,\mathbb{Z})$  duality groups.

In these setups, the inflaton potential must respect (or softly break) the modular symmetry, leading to constraints on its functional form. For instance, the scalar potential is often built from modular forms, such as Dedekind eta functions or Eisenstein series, ensuring invariance under modular transformations. This approach can naturally suppress dangerous higher-dimensional operators and control the inflaton dynamics through symmetry considerations.

# Chapter 3

# The String Axiverse

Axions, by which we mean axion-like particles (ALPs), are among the most generic and phenomenologically relevant predictions of string theory [14]. They arise in vast numbers in typical compactifications and play a central role in modern discussions of dark matter, inflation, and the structure of the vacuum landscape. They originate as the zero modes from dimensional reduction of p-form fields [54], degrees of freedom of open strings attached to D-branes, and even as the lowest lying Kaluza-Klein states in extremely warped compactifications [55–57]. The number of axions in a compactification is tied to the topology of the compactification manifold via the Hodge numbers and can vary from a few to  $\mathcal{O}(10^2)$ , all the way to  $\mathcal{O}(10^5)$  in extreme cases [58,59]. This potentially huge number of axions is the basis for the so-called string axiverse [15–19]. The presence of multiple axions can significantly shape the dynamics of the early Universe, depending on their coupling to other fields in the EFT. More specifically, these axions tend to couple to hidden gauge sectors and gravity via Chern-Simons (CS) couplings.

## 3.1 The strong CP problem and the QCD axion

The original motivation for introducing axions in quantum field theory stems from the strong CP problem in Quantum Chromodynamics (QCD). The QCD Lagrangian admits a CP-violating term of the form

$$\mathcal{L}_{\theta} = \theta_{\text{QCD}} \frac{g_s^2}{32\pi^2} \operatorname{tr}(G_{\mu\nu} \tilde{G}^{\mu\nu}), \qquad (3.1)$$

where  $G_{\mu\nu}$  is the gluon field strength,  $\tilde{G}^{\mu\nu} = \frac{1}{2} \varepsilon^{\mu\nu\rho\sigma} G_{\rho\sigma}$  its dual, and  $\theta_{\rm QCD}$  a dimensionless parameter that quantifies CP violation in the strong sector. This term induces a nonzero electric dipole moment (EDM) for the neutron, which is tightly constrained by experiments. The current bound  $|d_n| < 1.8 \times 10^{-26} e$  cm translates into the extremely small limit  $|\theta_{\rm QCD}| \lesssim 10^{-10}$  [60], suggesting a fine-tuning problem.

This is puzzling from a theoretical standpoint, as there is no symmetry in the Standard Model that enforces  $\theta_{\rm QCD}=0$ . Moreover,  $\theta_{\rm QCD}$  receives contributions from the complex phase of the quark mass matrix, leading to the effective combination

$$\bar{\theta} = \theta_{\rm OCD} + \arg \det M_a$$
, (3.2)

where  $M_q$  is the quark mass matrix. The observed smallness of  $\bar{\theta}$  thus requires a cancellation between two unrelated terms, constituting the strong CP problem.

A compelling solution was proposed by Peccei and Quinn [13], who promoted  $\bar{\theta}$  to a dynamical field. By introducing a spontaneously broken global  $U(1)_{PQ}$  symmetry, an axion field  $\vartheta_a$  emerges as the pseudo–Nambu–Goldstone boson. Its coupling to the QCD topological term reads

$$\mathcal{L}_{PQ} \supset \frac{\vartheta_a}{f_a} \frac{g_s^2}{32\pi^2} \operatorname{tr}(G_{\mu\nu}\tilde{G}^{\mu\nu}), \qquad (3.3)$$

where  $f_a$  is the axion decay constant. Non-perturbative QCD effects generate a potential for  $\vartheta_a$  that dynamically minimizes the effective  $\bar{\theta}$  at zero:

$$V(\vartheta_a) \sim \Lambda_{\rm QCD}^4 \left( 1 - \cos \left( \frac{\vartheta_a}{f_a} + \bar{\theta} \right) \right) , \quad \Rightarrow \quad \langle \vartheta_a \rangle = -f_a \bar{\theta} .$$
 (3.4)

As a result, the axion field dynamically cancels the CP-violating term, thereby solving the strong CP problem.

Various realizations of the Peccei–Quinn mechanism exist, including the original Weinberg–Wilczek axion [61, 62], which is now experimentally excluded, and the so-called "invisible" axion models such as KSVZ [63, 64] and DFSZ [65, 66], which remain viable. These models typically predict  $f_a \gtrsim 10^9\,\mathrm{GeV}$  to evade astrophysical and laboratory constraints, implying a light and weakly coupled axion.

In string theory, axions often couple to  $tr(G \wedge G)$  terms, raising the possibility of realizing the QCD axion as one of the closed string axions [14,67]. However, constructing a viable stringy QCD axion is nontrivial. One must ensure that the axion couples dominantly to QCD, has a sufficiently high-quality potential (i.e., is not spoiled by other instanton effects), and possesses an appropriate decay constant. These requirements place strong constraints on the geometry, instanton spectrum, and gauge embedding of the Standard Model in the compactification [15, 19, 68].

## 3.2 Closed string axions

Axions are a generic and ubiquitous prediction of string theory, arising as the four-dimensional zero modes of higher-dimensional antisymmetric tensor fields present in the string spectrum. In particular, closed string axions descend from the dimensional reduction of bulk p-form fields, whose origins lie in the NS-NS and R-R sectors of the ten-dimensional supergravity theories that describe the low-energy limit of string theory.

Let us denote the ten-dimensional spacetime as  $\mathbb{R}^{1,3} \times X$ , where X is a compact six-dimensional manifold. A p-form field  $C_p$  propagating in ten dimensions can be expanded along a basis of harmonic p-forms on X. Each non-trivial p-cycle  $\Sigma_i^p$  supports a Kaluza-Klein (KK) zero mode:

$$\vartheta_i(x) = \int_{\Sigma_i^p} C_p \,, \tag{3.5}$$

giving rise to a four-dimensional pseudoscalar field  $\vartheta_i(x)$ . The number of such axions is topologically determined by the Betti numbers of the compactification manifold, specifically  $b_p(X)$ .

These axions inherit a continuous shift symmetry from the gauge invariance of the higher-dimensional p-form:

$$C_p \to C_p + d\Lambda_{p-1} \quad \Rightarrow \quad \vartheta_i \to \vartheta_i + \text{const.}$$
 (3.6)

This symmetry is broken by non-perturbative effects, such as Euclidean brane instantons or gaugino condensation, which generate periodic potentials of the form  $V(\vartheta_i) \sim \Lambda^4 \cos(\vartheta_i/f_i)$ , where  $f_i$  is the axion decay constant.

Importantly, closed string axions couple naturally to gauge fields and curvature via Chern-Simons (CS) terms, e.g.,

$$\mathcal{L}_{\text{CS}} \supset \frac{\vartheta}{f} \operatorname{tr}(F \wedge F) \quad \text{or} \quad \frac{\vartheta}{f} R \wedge R.$$
 (3.7)

These couplings originate from the dimensional reduction of Green–Schwarz terms and play a central role in anomaly cancellation. Anomalous U(1)s typically become massive via the Stückelberg mechanism, with the axion providing the longitudinal component.

Axions have been extensively studied in the context of Type IIB orientifold compactifications [17,19,56,57,69–72]. IIB models offer many advantages since moduli stabilization is relatively well-understood and concrete model-building tools like flux compactifications, KKLT, and the Large Volume Scenario are readily available. Direct couplings of IIB string axions were studed in [17,70] while spectator axions and their CS couplings were examined in [73]. Furthermore, the QCD axion in IIB and its potential quality problem were studied at length in [19]

#### 3.2.1 The Axion Quality Problem in String Theory

While the Peccei–Quinn mechanism elegantly solves the strong CP problem, its successful implementation requires the axion potential to be dominated by QCD instantons. However, in generic effective field theory (EFT) models, the axion is simply a pseudo–Nambu–Goldstone boson of a global  $U(1)_{PQ}$  symmetry, and global symmetries are expected to be explicitly broken by Planck-suppressed operators. This leads to the so-called axion quality problem [74–76].

Higher-dimensional operators of the form

$$\mathcal{L} \supset \frac{\phi^n}{M_{\text{Pl}}^{n-4}} + \text{h.c.}$$
 (3.8)

can break the Peccei–Quinn symmetry explicitly and generate additional contributions to the axion potential, schematically of the form

$$V_{\rm grav}(\vartheta_a) \sim \Lambda_{\rm grav}^4 \cos\left(\frac{\vartheta_a}{f_a} + \delta\right),$$
 (3.9)

where  $\Lambda_{\rm grav}$  depends on the dimension and coefficient of the operator. If  $\Lambda_{\rm grav} \gg \Lambda_{\rm QCD}$ , the axion will not relax  $\bar{\theta}$  to zero, and the strong CP problem remains unsolved. To satisfy  $|\bar{\theta}_{\rm eff}| \lesssim 10^{-10}$ , the gravitational corrections must be highly suppressed, implying that the PQ symmetry must be of extraordinarily high quality.

This is a serious issue in field-theoretic axion models, as there is no reason in generic EFTs to expect Planck-suppressed PQ-violating operators to be absent or suppressed to

the required level. While symmetry-based solutions exist — such as using discrete gauge symmetries, extra dimensions, or accidental symmetries — they often require significant model-building effort and tuning.

In contrast, string theory naturally provides axions with protected shift symmetries that descend from gauge symmetries of higher-dimensional p-form fields. These symmetries are exact at the perturbative level and can only be broken by specific non-perturbative effects, such as brane instantons or gaugino condensation. Crucially, these effects are exponentially suppressed and under detailed control in compactification scenarios. As a result, string axions are often associated with extremely high-quality PQ symmetries, where unwanted potential terms are naturally absent or strongly suppressed.

Moreover, in many string compactifications, the instanton zero-mode structure constrains which axions appear in the non-perturbative superpotential, effectively preventing dangerous contributions from arising. This feature has been explored in the context of the so-called "stringy QCD axion," where one closed-string axion couples dominantly to QCD and is shielded from other significant non-perturbative corrections [14, 19, 67, 68].

Therefore, while constructing a viable QCD axion in string theory still requires careful engineering — such as localizing the Standard Model on D-branes, aligning couplings, and stabilizing moduli — the *quality problem is much less severe* than in generic field-theoretic setups. This motivates the search for the QCD axion within the string axiverse and adds another layer of theoretical appeal to this framework.

## 3.3 Type IIB axiverse

Let us now focus on Type IIB string theory, one of the five consistent ten-dimensional superstring theories. Type IIB is a chiral theory with  $\mathcal{N}=2$  supersymmetry in ten dimensions and contains the following bosonic fields:

- The graviton  $q_{MN}$ ,
- The dilaton  $\phi$ ,
- The NS-NS 2-form  $B_2$ ,
- The R-R 0-form  $C_0$  (the axion),
- The R-R 2-form  $C_2$ ,
- The R-R 4-form  $C_4$ , with self-dual field strength  $F_5$ .

Here M, N = 0, ..., 9 are ten-dimensional indices. The axions of interest arise from the R-R sector, namely  $C_0$ ,  $C_2$ , and  $C_4$ , and from the NS-NS field  $B_2$ . Each of these fields can produce axionic zero modes in the four-dimensional theory upon compactification on a Calabi-Yau threefold X.

To connect with phenomenology, we are interested in  $\mathcal{N}=1$  supersymmetry in four dimensions. This requires breaking half of the original  $\mathcal{N}=2$  supersymmetry preserved by the Calabi-Yau compactification. The standard approach is to introduce an orientifold projection. In particular, compactifying Type IIB string theory on an orientifold of a Calabi-Yau threefold,  $X/\sigma$ , where  $\sigma$  is an involutive symmetry combined with worldsheet parity  $\Omega_p$ , leads to either O3- and O7-planes or O5- and O9-planes and preserves  $\mathcal{N}=1$  supersymmetry in four dimensions.

We work here with the O3/O7 case. The orientifold projection splits the cohomology of X into even and odd parts under  $\sigma$ :

$$H^{p,q}(X) = H^{p,q}_+(X) \oplus H^{p,q}_-(X)$$
. (3.10)

The fields survive the orientifold projection according to their transformation properties. The axionic fields that survive the projection come from the following expansions:

$$B_2 = b^{\alpha}(x)\,\omega_{\alpha}\,,\qquad \qquad \omega_{\alpha} \in H^2_{-}(X)\,,\tag{3.11}$$

$$C_2 = c^{\alpha}(x) \,\omega_{\alpha} \,, \qquad \qquad \omega_{\alpha} \in H^2_{-}(X) \,, \qquad (3.12)$$

$$C_4 = \rho^i(x)\,\tilde{\omega}_i \wedge \text{vol}_4\,, \qquad \qquad \tilde{\omega}_i \in H^4_+(X)\,, \qquad (3.13)$$

$$C_0 = \theta_0(x) \,, \tag{3.14}$$

where  $\alpha = 1, ..., h_{-}^{1,1}$  and  $i = 1, ..., h_{+}^{1,1}$ . The fields  $b^{\alpha}$ ,  $c^{\alpha}$ ,  $\rho^{i}$ , and  $\vartheta_{0}$  are four-dimensional pseudoscalars which enjoy continuous shift symmetries at the perturbative level:

$$\theta \to \theta + \text{const.}$$
 (3.15)

These originate from the ten-dimensional gauge redundancies of the p-form potentials and protect the axions from perturbative mass terms. At the same time, the number of axions is topologically controlled by the Hodge numbers of X, and in concrete setups can range from a handful to  $\mathcal{O}(10^2)$  or more.

These axions become dynamical fields in the four-dimensional effective theory and appear in the kinetic Lagrangian as

$$\mathcal{L} \supset \frac{1}{2} g_{ij} \partial_{\mu} \theta^{i} \partial^{\mu} \theta^{j} , \qquad (3.16)$$

where  $g_{ij}$  is the axion field space metric. This metric is derived from the Kähler potential K of the effective  $\mathcal{N}=1$  supergravity:

$$g_{ij} = 2 \frac{\partial^2 K}{\partial \theta^i \partial \bar{\theta}^j} \,. \tag{3.17}$$

Some of these axions may also participate in Stückelberg couplings with anomalous U(1) gauge bosons. These terms take the form  $(\partial_{\mu}\theta + MA_{\mu})^2$  and provide a mass to the gauge boson while removing one axionic degree of freedom from the low-energy spectrum. The remaining axions, orthogonal to the eaten directions, remain physical and may contribute to dark matter or inflationary dynamics.

To move to a physical basis, we diagonalize  $g_{ij}$  and define canonically normalized fields as

$$\theta_i^{\text{phys}} = \sqrt{\lambda_i} M_{\text{Pl}} \,\vartheta_i \,, \tag{3.18}$$

where  $\lambda_i$  are the eigenvalues of  $g_{ij}$  and  $\vartheta_i$  the corresponding eigenvectors. The decay constants then follow as

$$f_i = \frac{\sqrt{\lambda_i} M_{\rm Pl}}{a_i} \,, \tag{3.19}$$

with  $a_i$  the coefficient in the non-perturbative potential  $V(\vartheta_i) \sim \Lambda_i^4 \cos(a_i\vartheta_i)$ . These potentials are generated by non-perturbative effects such as Euclidean D3-brane (E3) instantons or gaugino condensation on D7-branes. E3 instantons wrap rigid, holomorphic four-cycles in the Calabi–Yau, while gaugino condensation arises on stacks of D7-branes

wrapping divisors supporting pure  $\mathcal{N}=1$  super Yang–Mills gauge theories. Both mechanisms break the continuous axionic shift symmetries down to discrete subgroups and generate periodic potentials for the corresponding axions. Specifically, for a non-perturbative contribution to be generated, the E3 instanton must satisfy certain zero-mode conditions. In particular, it must be rigid and O(1)-invariant under the orientifold projection, with no additional charged zero modes.

The dynamically generated scales  $\Lambda_i$  are exponentially sensitive to the moduli, typically scaling as

$$\Lambda_i^4 \sim e^{-S_{\text{inst}}} \sim \exp\left(-\frac{\text{Vol}(\Sigma)}{g_s}\right),$$
(3.20)

where  $\Sigma$  is the internal cycle wrapped by the instanton or brane stack.

In the simplest case, where the kinetic matrix is approximately diagonal and only a single instanton contributes, the periodicity of the canonically normalized field is directly related to the decay constant:

$$\vartheta_i^{\text{phys}} \to \vartheta_i^{\text{phys}} + 2\pi f_i \,.$$
 (3.21)

This structure—the presence of many light, weakly coupled pseudoscalars descending from compactification—is what defines the string axiverse. In the Type IIB context, the axions arise from the rich cohomological structure of the compactification manifold and couple via Chern-Simons terms to gauge fields and curvature. Their masses and couplings span a wide range of scales, depending on the stabilization mechanism and geometry. In large volume compactifications, for instance, the decay constants scale as

$$f \sim \frac{M_{\rm Pl}}{\mathcal{V}^{1/2}},\tag{3.22}$$

where  $\mathcal{V}$  is the (dimensionless) volume of the Calabi–Yau in string units. This setup generically leads to logarithmic hierarchies among axion masses and naturally predicts ultra-light fields, some of which may be cosmologically active today.

#### 3.3.1 Statistics of the IIB Axiverse.

Systematic scans of Calabi–Yau hypersurfaces in the Kreuzer–Skarke list reveal that the Hodge number  $h^{1,1}$  ranges from 1 up to 491 [77]. After the orientifold projection, this typically translates into hundreds of closed-string axions once the universal  $C_0$  mode is included [59]. Their masses are set by instanton actions that scale with the volumes of the wrapped cycles, and large ensembles show a quasi-log-flat spectrum spanning  $\mathcal{O}(10^{-33}\,\mathrm{eV}) \lesssim m_a \lesssim \mathcal{O}(10^{-10}\,\mathrm{eV})$  when  $h^{1,1} \gtrsim 25$  [18,78]. The axion field-space radius extracted from the kinetic matrix shrinks mildly with  $h^{1,1}$ , roughly as  $R \propto (h^{1,1})^{-1/2}$ , making trans-Planckian excursions statistically rare. More recent surveys of  $\sim 2 \times 10^5$  IIB orientifolds confirm this picture and uncover an additional trend: as  $h^{1,1}$  grows, the intersection matrices become sparse, which suppresses kinetic mixing and pushes photon/gluon couplings down to  $g_{a\gamma\gamma} \sim 10^{-4}/f_a$  for the bulk of the spectrum [79].

#### 3.3.2 Phenomenological roles of axions

The presence of many axions in string compactifications, combined with their light masses and weak couplings, makes them compelling candidates for a range of phenomena in early- and late-time cosmology. Their rich phenomenology stems from the underlying

shift symmetry, which protects them from perturbative mass terms and allows them to remain light, as well as from their coupling to gauge fields and gravity.

Dark matter. The most extensively studied role of axions is as dark matter candidates. When produced via the misalignment mechanism, ultra-light axions with masses in the range  $10^{-22} \text{ eV} \lesssim m_a \lesssim 10^{-18} \text{ eV}$  can form a type of fuzzy dark matter (FDM) [69,80,81], which suppresses structure formation below the corresponding de Broglie wavelength. Heavier axions in the  $\mu\text{eV}$  to meV range can behave as cold dark matter and are actively searched for via their coupling to photons in haloscope and helioscope experiments [82,83].

Inflation and dark energy. Axions have also been proposed as inflaton candidates in models such as natural inflation [84] and aligned or multi-axion inflation [85–89]. Their protected flat potentials and periodic structure make them ideal for large-field inflationary models, though realizing trans-Planckian field ranges in string theory remains challenging. On the other end of the energy spectrum, axions with extremely light masses  $m_a \sim H_0 \sim 10^{-33} \,\mathrm{eV}$  have been considered as quintessence fields driving cosmic acceleration [90,91].

Gravitational waves and spectral signatures. The axionic coupling to gauge fields and curvature tensors can lead to observable signatures in primordial perturbations. For instance, rolling axions coupled via  $\vartheta F \tilde{F}$  can produce gauge field quanta, which source scalar and tensor modes, leading to potentially detectable levels of non-Gaussianity or parity-violating gravitational waves [73, 86, 87, 92, 93]. Alternatively, axion decays in the post-inflationary era may leave imprints in the form of spectral distortions in the CMB [94, 95].

Early-universe dynamics and dark radiation. In the presence of many light axions, energy may be distributed among a large number of fields during reheating, potentially contributing to the effective number of relativistic species  $N_{\text{eff}}$ . This so-called dark radiation can be probed by precision cosmology and provides a constraint on the reheat temperature and axion couplings [96, 97].

Axion-photon and axion-gluon couplings. The low-energy interactions of axions with photons and gluons offer both phenomenological constraints and discovery channels. The QCD axion, originally introduced to solve the strong CP problem [13, 62], remains the most motivated single-field scenario. In string theory, realizing a high-quality QCD axion is nontrivial due to the ubiquity of additional couplings and instanton effects. Still, specific compactifications and alignment mechanisms can suppress unwanted terms and allow for viable solutions [19, 98].

In all these contexts, the string axiverse offers a framework that naturally accommodates a variety of axion masses and couplings. Their roles depend sensitively on the compactification geometry, moduli stabilization, and the cosmological history of the early Universe. Later in this thesis, we will explore some of these phenomenological directions in more detail within concrete string-motivated scenarios.

In summary, the string axiverse scenario, especially in the context of Type IIB orientifold compactifications, predicts a large number of axions with hierarchically distributed masses and decay constants. Geometry, moduli stabilization, and non-perturbative effects all play a role in the phenomenology of the string axiverse, with potential signatures ranging from

early Universe cosmology to astrophysical observations. In the next chapter, we will explore how specific axions from this landscape can play a role in concrete cosmological scenarios such as inflation, dark radiation, or the generation of gravitational waves.

## 3.4 Axions in heterotic string theory

Despite the powerful moduli stabilization techniques and computational control offered by Type IIB compactifications, one of their major limitations lies in the construction of realistic gauge sectors. The Type IIB spectrum lacks non-Abelian gauge fields at the perturbative level, requiring the introduction of localized sources such as D-branes to engineer viable particle physics. These ingredients, while effective, introduce additional model-building constraints and complications, especially when aiming for unification or detailed cosmological dynamics.

In contrast, heterotic string theories offer a compelling alternative. Both the  $E_8 \times E_8$  and SO(32) heterotic strings contain non-Abelian gauge groups in the ten-dimensional perturbative spectrum, allowing one to construct unified gauge theories and Standard Model–like spectra without the need for branes or localized defects. The compactification of the heterotic string on a Calabi–Yau threefold with a suitable gauge bundle can lead to four-dimensional  $\mathcal{N}=1$  supersymmetric models with chiral matter and GUT structures [99, 100].

Axions naturally arise in heterotic compactifications as well. They originate from the ten-dimensional NS-NS 2-form  $B_2$ , which gives rise to both:

- A model-independent axion, descending from the dual of the 4d two-form  $B_{\mu\nu}$  after dimensional reduction. This universal axion is present in all heterotic compactifications and couples to both the gauge and gravitational Chern–Simons terms via the Green–Schwarz mechanism.
- Model-dependent axions, associated with the internal components of  $B_2$  integrated over harmonic two-forms of the Calabi–Yau. Their number is controlled by the Hodge number  $h^{1,1}(X)$  and depends on the topology of the compactification manifold.

These axions enjoy perturbative shift symmetries inherited from the gauge symmetry of  $B_2$ , and can develop potentials via non-perturbative effects such as worldsheet instantons and gaugino condensation [101,102]. The universal axion plays a central role in anomaly cancellation through the Green–Schwarz mechanism and often mixes with other moduli through the Kähler potential.

Despite their attractive particle physics features, fully realistic and controlled cosmological scenarios in heterotic string theory, incorporating both moduli stabilization and inflation, remain underdeveloped. Many standard techniques from Type IIB, such as flux-induced superpotentials or large volume compactifications, are less straightforward to implement in the heterotic context due to the absence of RR fluxes and the restricted set of allowed background fields. Nevertheless, recent progress has opened new avenues. Vacuum stabilization using gaugino condensation and worldsheet instantons has been revisited in detail [103–105], including its implications for inflation and dark sectors.

While the heterotic axiverse is less explored than its Type IIB counterpart, early works have studied the possibility of realizing a QCD axion and the conditions for suppress-

ing Planck-suppressed PQ-violating operators [16, 106–109]. In particular, the model-independent axion was among the earliest candidates proposed to solve the strong CP problem in string theory. However, its decay constant is typically of order  $f_a \sim M_{\rm Pl}$  and its coupling to QCD is often too small to satisfy observational bounds. More refined constructions involving model-dependent axions have since been proposed to circumvent these issues.

More recently, work has begun to systematically explore the heterotic axiverse, including the structure of axion kinetic terms, their decay constants, and their couplings to gauge and gravitational sectors. The lack of warping and the absence of localized sources in heterotic models imply that kinetic mixings are generally significant, and alignment mechanisms may be required to obtain phenomenologically viable axions. This will be the subject of the following chapter.

# Chapter 4

# Heterotic axiverse

Despite the impressive tools available in type IIB compactifications, a major drawback of these models arise from realizing gauge theory sectors. As the type IIB perturbative spectrum lacks non-Abelian gauge theories, one must introduce non-perturbative objects such as D-branes that will furnish viable particle physics sectors. In contrast, heterotic string theories display the highly attractive feature of containing non-Abelian gauge fields even at the perturbative level, which facilitates the construction of GUTs and Standard Model-like spectra without the need for D-branes or localized sources. Axions also appear in heterotic compactifications, descending from the 10d NS-NS 2-form either as the universal, model-independent axion dual of the 4d 2-form or as model-dependent axions associated with the internal cohomology of the compactification manifold. However, a fully controlled cosmological setup, particularly one incorporating inflation and moduli stabilization, is still lacking in this framework. Recent progress, including mechanisms invoking NS-NS 3-form flux, gauge bundles, worldsheet instantons and gaugino condensation [105,110–117] as well as perturbative  $\alpha'$ , string loop, and non-perturbative corrections to the Kähler potential [118–122], suggests new possibilities for vacuum stabilization and cosmological model-building.

Despite the above attractive features, the heterotic sector of the axiverse is largely unexplored. Early studies of axions in heterotic theories focused on realizing the QCD axion and situations to avoid the quality problem [16, 106–109]. More recent works [123, 124] as well as a forthcoming work [125] study the realization of a QCD axion in heterotic CY compactifications from a linear combination of the universal 4D axion and the NS-NS 2-form axions of heterotic string theory, establishing that with very few limited exceptions such a heterotic QCD axion will acquire values in the  $g_{a\gamma\gamma} - m_a$ -plane above the so-called QCD axion line.

In this chapter, we will extend these studies and focus on the heterotic string axiverse and its discovery potential. In particular, we are interested in axions that couple to hidden gauge fields via CS couplings and may thereby produce gravitational waves during inflation, realizing the spectator axion mechanism. To that end, we characterize the generic structure of the axion mass spectrum and the effective couplings of heterotic axions beyond the QCD axion candidate to Abelian and non-Abelian gauge fields and discuss their implications for both cosmology and particle phenomenology. We also discuss the impact of generating non-perturbative potentials for the the non-QCD axions onto the CP quality problem of the QCD axion candidate.

GC	$v_1 \sim v_2$	Masses	CP	FDM
×	✓	$m_{\varphi_2}^2 \sim \Lambda_{\rm QCD}^4 \ll m_{\varphi_1}^2 , m_{\varphi_3}^2 \sim \Lambda_{\rm ws}^4$	✓	×
×	×	$m_{\varphi_1}^2 \sim \varepsilon \Lambda_{ m ws}^4 \ll m_{\varphi_2}^2 \sim \Lambda_{ m QCD}^4 \ll m_{\varphi_3}^2 \sim \Lambda_{ m ws}^4$	✓	<b>√</b>
<b>√</b>	✓	$m_{\varphi_2}^2 \sim \Lambda_{\rm gc}^4 \ll m_{\varphi_1}^2 , m_{\varphi_3}^2 \sim \Lambda_{\rm ws}^4$	×	×
<b>√</b>	×	$m_{\varphi_1}^2 \sim \Lambda_{\rm QCD}^4 \ll m_{\varphi_2}^2 \sim \Lambda_{\rm gc}^4 \ll m_{\varphi_3}^2 \sim \Lambda_{\rm ws}^4$	<b>(√)</b>	×

Table 4.1: Three-axion scenarios summarizing presence of gaugino condensation (GC), mass hierarchies, strong CP resolution, and dominant gauge couplings.

table 4.1 summarizes the upshot of our results: it combines the structure of the non-perturbative quantum effects providing the axion mass with the QCD instanton contribution and the constraints from maintaining CP quality as well as the rather strict upper bound on the compactification volume imposed by heterotic perturbativity. The resulting axion mass spectrum is quite different compared to the type IIB or M-theory axiverses - most of the 2-form axions here stay rather heavy, while typically the axion responsible for solving the QCD CP problem (if possible) is the lightest axion state with a mass scale proportional to  $\Lambda_{\rm QCD}^4$ . The only exception arises for fibred CY compactifications which break the hidden  $E_8$  gauge group completely via gauge bundle choice and/or Wilson lines, and with their two dominant Kähler moduli stabilized in a highly anisotropic regime. For this rather special case, a suppressed world-sheet instanton direction can arise providing a single fuzzy-dark matter (FDM) candidate among the heterotic string axions.

## 4.1 Review of the Heterotic String

Of the five perturbative superstring theories, weakly coupled heterotic string theory is particularly appealing from a phenomenological perspective as it naturally accommodates key features of the Standard Model within a consistent high-energy framework. Its gauge sector arises from either a ten-dimensional  $(E_8 \times E_8) \times \mathbb{Z}_2$  or  $\text{Spin}(32)/\mathbb{Z}_2^{-1}$  symmetry, allowing for grand unified theories (GUTs) and the embedding of realistic gauge groups after compactification. Compactifications on Calabi-Yau threefolds with suitable vector bundles can yield chiral spectra, which are essential for reproducing the observed particle content. From its discovery [128,129] there have been many works constructing a 4D low-energy EFT which matches the minimal supersymmetric standard model (MSSM) [130–134].

The heterotic worldsheet conformal field theory is built by combining left-moving modes of the 26-dimensional bosonic string with right-moving modes of the 10-dimensional superstring, in such a way that the resulting theory is consistent in ten spacetime dimensions. Concretely, the right-moving (antiholomorphic) sector describes ten-dimensional supersymmetric fields: spacetime bosons  $X^{\mu}(\bar{z})$  and their superpartners  $\psi^{\mu}(\bar{z})$  for  $\mu=0,\ldots,9$ . The left-moving (holomorphic) sector, instead, includes only the bosonic coordinates  $X^{\mu}(z)$ , and to fill the mismatch in central charges and ensure conformal invariance, one introduces an internal set of 16 extra left-moving degrees of freedom,  $\Xi^{I}(z)$ , where  $I=1,\ldots,16$ . One can write them as real fermionic coordinates, corresponding to 32 real left-moving worldsheet fermions, or as 16 complex fermions. Regardless of this choice,

<sup>&</sup>lt;sup>1</sup>Sometimes referred to as SemiSpin(32) [126, 127].

these are the fields which generate the gauge sector excitations of the heterotic string.

Modular invariance restricts the allowed choices for the compactification lattice of these internal degrees of freedom. The only even self-dual lattices in 16 Euclidean dimensions are the  $E_8 \times E_8$  and  $\mathrm{Spin}(32)/\mathbb{Z}_2$  lattices. These yield two consistent heterotic string theories, both living in D=10 dimensions: the  $E_8 \times E_8$  heterotic string, and the  $\mathrm{Spin}(32)/\mathbb{Z}_2$  heterotic string. Upon compactification to four dimensions, these internal gauge symmetries give rise to non-Abelian gauge groups and moduli.

To preserve  $\mathcal{N}=1$  supersymmetry in four dimensions, the compactification manifold is required to be a Calabi-Yau threefold: a compact Kähler manifold with vanishing first Chern class and SU(3) holonomy. This ensures the existence of a single covariantly constant spinor, which is necessary for a single unbroken 4D supersymmetry. In such compactifications, the ten-dimensional spacetime decomposes as

$$\mathbb{R}^{1,3} \times \mathrm{CY}_3 \,, \tag{4.1}$$

and the gauge bundle is chosen to satisfy the Hermitian Yang-Mills equations. Supersymmetry and anomaly cancellation constrain this bundle: its field strength F must obey  $F_{(0,2)} = F_{(2,0)} = 0$  and  $g^{i\bar{j}}F_{i\bar{j}} = 0$ , known as the DUY equations (Donaldson-Uhlenbeck-Yau) [135, 136], and the Bianchi identity for the NS-NS three-form H reads

$$dH = \frac{\alpha'}{4} \left( \operatorname{tr} R \wedge R - \operatorname{tr} F \wedge F \right) , \qquad (4.2)$$

requiring a non-trivial relation between geometry and gauge flux.

The simplest examples of CYs arise as hypersurfaces in toric varieties. One common construction is that of smooth hypersurfaces X in complex projective space  $\mathbb{CP}^{d+1}$  defined by the vanishing of a homogeneous polynomial of degree k=d+2. These are sections of the line bundle  $\mathcal{O}_{\mathbb{P}^{d+1}}(k)$ . For X to be Calabi-Yau, it must have trivial canonical bundle, even if the ambient toric variety does not. This ensures the existence of a globally defined holomorphic (d,0)-form  $\Omega$  which is equivalent to the demands of Ricci flatness and SU(3) holonomy.

The canonical bundle K is the line bundle of holomorphic top forms

$$\Omega_U(z_1,...,z_d)dz_1\wedge\cdots\wedge dz_d$$

on a patch U. On a smooth variety, K is trivial if and only if the first Chern class vanishes. For hypersurfaces, this can be verified using the adjunction formula. Consider X as a hypersurface in an ambient space A of dimension d. The tangent bundle  $T_A|_X$  splits as:

$$0 \to T_X \to T_A|_X \to N_X \to 0, \tag{4.3}$$

where  $N_X \cong \mathcal{O}_A(X)|_X$  is the normal bundle. The Chern classes satisfy:

$$c(T_X) = \frac{c(T_A)}{c(N_X)}. (4.4)$$

If the ambient space is  $\mathbb{CP}^{d+1}$ , each homogeneous coordinate  $z_i$  corresponds to a divisor H with line bundle  $\mathcal{O}(1)$ , so  $c(T_A) = (1+H)^{d+2}$ . A degree-k hypersurface corresponds to  $\mathcal{O}(k)$ , so:

$$c(T_X) = \frac{(1+H)^{d+2}}{1+kH} = (1+(d+2)H+\cdots)(1-kH+k^2H^2-\cdots). \tag{4.5}$$

We then find:

$$c_1(T_X) = (d+2-k)H. (4.6)$$

Requiring  $c_1 = 0$  gives k = d + 2, the Calabi-Yau condition.

#### 4.1.1 Gauged Linear Sigma Models (GLSMs)

The low energy effective worldsheet theory of the heterotic string compactified on a CY three-fold X is a nonlinear sigma model (NLSM) with  $\mathcal{N}=(0,2)$  supersymmetry, describing maps from the string worldsheet into the target space  $M^{1,3}\times X$  [137]. The internal geometry and gauge bundle data appear in the NLSM through the metric G, the 2-form gauge field B and couplings to worldsheet fermions. While physically relevant, the NLSM is strongly coupled in the UV, which makes it complicated to deal with. Therefore, we use gauged linear sigma models (GLSMs) as UV completions, which are 2d supersymmetric gauge theories that flow in the IR to NLSMs. For compactifications preserving  $\mathcal{N}=1$  supersymmetry in four dimensions, we need to look at  $\mathcal{N}=(0,2)$  GLSMs on the worldsheet. The field content includes the following multiplets:

- Chiral multiplets  $\Phi^i = (\phi^i, \psi^i_-)$  containing a complex scalar and a right-moving fermion.
- Vector multiplets V for each gauged Abelian symmetry  $(U(1)^m)$ , that contain gauge fields A, gauginos, and a complex scalar  $\sigma$ .
- Fermi multiplets  $\Lambda^{\alpha}=(\lambda^{\alpha},F^{\alpha})$  with a left-moving fermion and an auxiliary field F
- Twisted chiral multiplets that encode the gauge field strengths and couple to Fayet-Illiopoulos parameters and theta angles.

The  $\phi^i$  fields can be viewed as coordinates on  $\mathbb{C}^N$ . The scalar potential includes Fand D-terms, that impose moment map constraints that define a symplectic quotient  $\mathbb{C}^N/U(1)^m$ :

$$U(\phi, \sigma) = \sum_{I} \frac{1}{2e_{I}^{2}} D_{I}^{2} + \sum_{i} |F_{i}|^{2} + 2 \sum_{I} |\sigma_{I}|^{2} \sum_{i} Q_{i}^{I2} |\phi_{i}|^{2}, \tag{4.7}$$

with D- and F-terms given by:

$$D^{I} = \sum_{i} Q_{i}^{I} |\phi_{i}|^{2} - a^{I}, \quad F_{i}^{*} = \left. \frac{\partial W}{\partial \Phi_{i}} \right|_{\theta=0}. \tag{4.8}$$

The moduli space of the classical vacuum is then a toric variety, while adding a gauge-invariant transverse superpotential defines a hypersurface within the ambient space. To ensure that the resulting target space is a Calabi-Yau, the gauge charges  $Q^i$  must sum to 0:  $\sum_i Q^i = 0$ , guaranteeing that the first Chern class of the tangent bundle vanishes. This also enforces conformal invariance of the IR theory, in the absence of anomalies.

In  $\mathcal{N} = (0,2)$  theories, the Fermi multiplets are subject to chiratility constraints

$$\bar{\mathcal{D}}_{+}\Lambda^{\alpha} = \sum_{i} E_{i}^{\alpha}(\Phi)\Psi^{i}, \qquad (4.9)$$

where  $E_i^{\alpha}(\Phi)$  are holomorphic functions of the chiral superfields. These functions encode the geometry of a holomorphic vector bundle V over the CY, where the cohomology of

V is described by the surviving massless fermions (the ones that are not gauged away or become massive). These bundles usually are usually encoded in a so-called *monad* construction expressed as an exact sequence of holomorphic vector bundles [138, 139]:

$$0 \to \mathcal{O}^{\oplus p} \xrightarrow{M} \bigoplus_{\alpha} \mathcal{O}(Q^{\alpha}) \xrightarrow{N} \bigoplus_{m} \mathcal{O}(-q_{m}) \to 0.$$
 (4.10)

In the above equation,  $\mathcal{O}^{\oplus p}$  denotes a trivial bundle of tank p, corresponding to uncharged Fermi multiplets,  $\mathcal{O}(Q^{\alpha})$  and  $\mathcal{O}(-q^m)$  are direct sums of the line bundles over the CY characterized by integer charge vectors  $Q^{\alpha}$  and  $q^m$  under the GLSM gauge symmetries. The maps M and N encode the holomorphic data determined by the superpotential couplings and the chirality constraints.

The vector bundle defined this way reads as the cohomology of the complex:

$$V = \frac{\ker(N)}{\operatorname{Im}(M)}.$$
(4.11)

When p = 0 we have a minimal monad, and  $V = \ker(N)$ , while p > 0 allows for more general structures. This construction is used in heterotic compactifications to construct stable bundles. To ensure  $c_1(V) = 0$  (consistent with supersymmetry) we need to impose the condition

$$\sum_{\alpha} Q^{\alpha} = \sum_{m} q^{m} \,, \tag{4.12}$$

while to ensure that  $c_1(TX) = 0$  (CY condition), we require

$$\sum_{i} Q^{i} = 0. (4.13)$$

#### 4.1.2 The gauge group

For simplicity, we focus on the  $E_8 \times E_8$  heterotic string as the ten-dimensional gauge symmetry has the attractive feature of factorizing cleanly into two separate  $E_8$  sectors. Upon compactification, realistic gauge groups can be engineered by appropriately embedding the internal gauge bundle into one of the  $E_8$  factors. Specifically, one chooses a structure group  $G_1 \subset E_8$  for the internal bundle  $V_1$ , and the unbroken gauge symmetry in four-dimensions is given by the commutant of  $G_1$  in  $E_8$ 

$$E_8 \supset G_1 \times H_4 \tag{4.14}$$

where  $H_4$  is the visible 4d gauge group. The choice of structure group thus determines the visible gauge group [134], as well as the matter content, which is encoded in the decomposition of the adjoint representation of  $E_8$  under  $G_1 \times H_4$ , and the cohomology of the associated bundle-valued representation.

Typical embeddings used to get 4d gauge groups that resemble out universe are:

• SU(5) GUT:

Structure group:  $G_1 = SU(5)$ 

Commutant:  $H_4 = SU(5)$ 

This yields a grand unified theory with the usual  $10 \oplus \overline{5}$  matter content. Further breaking to the Standard Model can occur via Wilson lines.

• SO(10) GUT:

Structure group:  $G_1 = SU(4)$ 

Commutant:  $H_4 = SO(10)$ 

This setup has the advantage of allowing each SM generation to fit into a single **16** spinor of SO(10).

•  $E_6$ :

Structure group:  $G_1 = SU(3)$ 

Commutant:  $H_4 = E_6$ 

Here, the visible gauge group is large, which requires additional breaking mechanisms.

• Pati-Salam:

Structure group:  $G_1 = SU(4) \times SU(2)_R$ 

Commutant:  $H_4 = SU(2)_L \times SU(2)_R \times SU(4)$ 

These models unify quarks and leptons at an intermediate scale.

• Standard Model-like:

Structure group:  $G_1 = SU(3) \times SU(2) \times U(1)^n$  or more elaborate constructions.

Commutant:  $H_4 \supset SU(3)_c \times SU(2)_L \times U(1)_Y$ 

The low energy group resembles the SM group, though careful engineering (e.g., via fluxes or Wilson lines) is needed to obtain the correct spectrum and couplings.

The low-energy chiral spectrum is determined by decomposing the adjoint representation **248** of  $E_8$  under  $G_1 \times H_4$ , and computing the cohomology associated with the resulting bundle-valued representations.

To realize these constructions, we take a Calabi-Yau threefold X described by a complete intersection in a toric variety, with  $h^{1,1}=k$  independent Kähler parameters. A line bundle L on X is completely specified by its first Chern class  $c_1 \in H^2(X,\mathbb{Z})$ , which can be expanded in a basis  $\{\omega_i\}$  of  $H^2(X,\mathbb{Z})$ , as

$$c_1(L) = \sum_{i=1}^{h^{1,1}} n_i \omega_i, \qquad L = \mathcal{O}(n_1, \dots, n_k) = \mathcal{O}\left(\sum_{i=1}^{h^{1,1}} n_i \omega_i\right). \tag{4.15}$$

where  $n_i \in \mathbb{Z}$ . More general vector bundles can be constructed as cohomologies of complexes, as reviewed above. A vector bundle V of rank r can be defined via

$$0 \to \mathcal{O}^{\oplus p} \xrightarrow{M} \bigoplus_{\alpha=1}^{r_1} \mathcal{O}(n_i^{\alpha}) \xrightarrow{N} \bigoplus_{m=1}^{r_2} \mathcal{O}(m_i^m) \to 0.$$
 (4.16)

This defines the vector bundle V with rank  $\operatorname{rk}(V) = r_1 - r_2$ , as  $V = \frac{\operatorname{Ker}(N)}{\operatorname{Im}(M)}$  with  $p \geq 0$ . The total Chern class is given by:

$$c(V) = \prod_{\alpha,m} \frac{1 + \sum_{i} n_i^{\alpha} \omega_i}{1 + \sum_{i} m_i^{m} \omega_i}.$$
(4.17)

In particular, the first Chern class reads:

$$c_1(V) = \sum_{i=1}^{h^{1,1}} \left( \sum_{\alpha=1}^{r_1} n_i^{\alpha} - \sum_{m=1}^{r_2} m_i^m \right) \omega_i.$$
 (4.18)

For an SU(N) vector bundle, supersymmetry requires  $c_1(V) = 0$ . Given this setup, one can compute the massless spectrum by evaluating the cohomology groups associated to the bundle-valued representations.

**Bianchi identity** In addition, consistency of the string background imposes the Bianchi identity eq. (4.2), which relates the geometry of the compactification to the topology of the gauge bundle. Upon integration over compact 4-cycles in the Calabi–Yau, this identity translates into a topological condition involving second Chern classes [140]:

$$\sum_{i} c_2(V_i) = c_2(TX), \qquad (4.19)$$

for non-Abelian bundles. In models with Abelian bundles, the condition generalizes to:

$$\sum_{i=1}^{K} \operatorname{ch}_{2}(V_{n_{i}}) + \sum_{m=1}^{M} a_{m} c_{1}^{2}(L_{m}) = -c_{2}(T_{X}). \tag{4.20}$$

The constants  $a_m$  appearing in the Bianchi identity for Abelian bundles are not arbitrary: they are group-theoretic coefficients that depend on how the Abelian  $U(1)^m$  factors are embedded in the ten-dimensional gauge group. To determine them, we expand the internal gauge field in the Cartan subgroup of  $E_8$ , so that the embedding of each Abelian factor is specified by a charge operator  $Q_m \in \mathfrak{e}_8$ , and fields carry charges  $q_m \in \mathbb{Z}$  under this generator. The normalization of the trace is defined through

$$tr(F_m^2) = a_m c_1^2(L_m), (4.21)$$

where tr is the trace in the adjoint representation of  $E_8$ . The value of  $a_m$  is given by:

$$a_m = \frac{1}{4} \operatorname{Tr}_{\mathrm{adj}}(Q_m^2), \tag{4.22}$$

where the trace sums the squared charges of the adjoint representation. Alternatively, we can relate  $a_m$  to the level of embedding k of the U(1) into  $E_8$  by expressing the normalization in terms of the Kac-Moody level, as

$$a_m = \frac{k_m}{30} \,, \tag{4.23}$$

reflecting the standard trace identity in  $E_8$ :

$$\operatorname{tr}_{248}(T^a T^b) = k \delta^{ab} \,. \tag{4.24}$$

The Kac-Moody level  $k_m$  counts how the U(1) charges appear in the decomposition of the adjoint of  $E_8$  and determines the normalization of kinetic terms and anomaly coefficients.

**DUY equations** In addition to the topological constraints from the Bianchi identity, the D-term equations, derived from supersymmetry, impose the so called DUY conditions, which require that each slope-stable vector or line bundle has vanishing slope

$$\int_X J \wedge J \wedge c_1(V_{n_i}) = 0, \quad \int_X J \wedge J \wedge c_1(L_m) = 0, \tag{4.25}$$

with one-loop corrections when  $c_1(V) \neq 0$ . These constraints further restrict the allowed moduli, freezing some combinations of the Kähler moduli and the dilaton. The axions dual to those directions become longitudinal components of massive U(1) gauge bosons via the Green-Schwarz mechanism, and the effective theory retains only anomaly-free gauge symmetries.

#### 4.1.3 Heterotic EFT in 10D and 4D

Axions in heterotic string theory come from the Kalb-Ramond 2-form  $B_2$  [54]. The relevant part of the 10D heterotic action is

$$\mathcal{L}_{10D} = \frac{1}{2\kappa_{10}^2} \sqrt{-g}R - \frac{1}{4\kappa_{10}^2} H \wedge \star H - \frac{\alpha'}{8\kappa_{10}^2} \text{tr}(F \wedge \star F) 
= \frac{2\pi}{g_s^2 \ell_s^8} \sqrt{-g}R - \frac{2\pi}{g_s^2 \ell_s^4} \cdot \frac{1}{2} H \wedge \star H - \frac{1}{4(2\pi)g_s^2 \ell_s^6} F \wedge \star F,$$
(4.26)

where  $H = dB + \omega_{3L} - \omega_{3Y}$  and the trace refers to the adjoint of  $E_8 \times E_8$  or SO(32).

Compactifying to four dimensions and integrating over the internal manifold X with physical volume  $Vol(X) = \mathcal{V}\ell_s^6$  yields the effective action

$$S_{4D} \supset \frac{M_{\rm Pl}^2}{2} \int d^4x \sqrt{-g} R - \frac{1}{4g_{\rm YM}^2} \int d^4x \, F \wedge \star F - \frac{2\pi \mathcal{V}}{g_s^2 \ell_s^4} \int \frac{1}{2} H \wedge \star H \,,$$
 (4.27)

with the four dimensional parameters  $M_p^2 = 4\pi \frac{\mathrm{Vol}(X)}{g_s^2 \ell_s^8} = 4\pi \frac{\mathcal{V}}{g_s^2 \ell_s^2}$  and  $g_{YM}^2 = 4\pi \frac{g_s^2 \ell_s^6}{\mathrm{Vol}(X)} = 4\pi \frac{g_s^2}{\mathcal{V}}$ . Therefore, we can write  $\alpha_{YM} = g_{YM}^2/4\pi$  as

$$\alpha_{YM} = \frac{g_s^2}{\mathcal{V}}. (4.28)$$

If we allow for a non-standard embedding of the SM into the heterotic string at Kac-Moody level k > 1, then in general (see Witten for more)

$$\alpha_{GUT} = \frac{\alpha_{YM}}{k} = \frac{g_s^2}{k\mathcal{V}}.$$
 (4.29)

The string scale  $M_s = 1/\ell_s$  can be evaluated to be  $M_s = (k\alpha_G/4\pi)^{1/2}M_p$ , where  $\alpha_G$  is the strong coupling constant, such that if  $\alpha_G \sim 1/25$ , then  $M_s \sim M_p\sqrt{k}/18$  which is the usual perturbative heterotic string scale.

We emphasize here a direct consequence of the above relation between the 4D gauge coupling, the CY volume and the string coupling  $g_s$ . Namely, the restriction to perturbative heterotic string theory  $g_s \lesssim 1$  (implying the absence of e.g. M5-branes of heterotic M-theory) in combination with phenomenological requirement  $\alpha_{YM} \simeq 1/25$  of gauge coupling unification of the the MSSM gauge couplings into the  $E_8$  GUT structure implies a stringent upper bound on the compactification volume [117,141]

$$V \lesssim 20 - 30 \quad . \tag{4.30}$$

As we will see below, this crucially limits  $h^{1,1}$  if we demand that all 2-cycle volumes satisfy  $v^i \gtrsim 1$  to ensure control over the worldsheet instanton expansion. In highly anisotropic fibred CY compactifications, eq. (4.30) still places constraints by bounding the largest curve volume as  $v \lesssim 50$  (modulo the numerical values of the intersection numbers appearing in the volume form).

#### 4.1.4 Heterotic axions in 4D

Next, we discuss the top-down axion content of the theory. The heterotic string generically contains both: one model-independent axion a, which is the 4D dual of  $B_{\mu\nu}$  and universally present in all compactifications, and many model-dependent axions  $b_i$ , arising from

the internal components of the *B*-field, with  $i = 1, ..., h^{1,1}$ . The **model-independent** axion is defined via dualization as

$$a = 2\pi \int_{CY} B_6$$
, with  $dB_6 = \star dB_2$ , (4.31)

while model-dependent axions arise from expanding B in a basis of harmonic 2-forms  $\{\beta_i\}$ :

$$B = \frac{1}{2\pi} \sum_{i} b_i(x) \beta_i, \quad \text{with} \quad \int_{\Sigma_j} \beta_i = \delta_{ij}.$$
 (4.32)

We now analyze the couplings of these axions to gauge fields through the modified Bianchi identity for H. In four dimensions, we can enforce this identity by treating a as a Lagrange multiplier:

$$S \supset \int a \left( dH + \frac{1}{16\pi^2} (\operatorname{tr} R \wedge R - \operatorname{tr} F \wedge F) \right). \tag{4.33}$$

Integrating out H yields an effective action for a:

$$S(a) = \int d^4x \left[ -\frac{1}{2} f_a^2 (\partial a)^2 + \frac{a}{16\pi^2} (\operatorname{tr} F \wedge F - \operatorname{tr} R \wedge R) \right], \qquad (4.34)$$

where the axion decay constant is

$$f_a^2 = \frac{g_s^4}{2\pi \mathcal{V}} \,. \tag{4.35}$$

This reproduces the expected structure of an axion with a Chern-Simons coupling, where the coefficient is determined by the underlying string parameters and internal geometry.

The **model dependent axions** arise as the 0-form valued coefficients of the  $B_2$  expansion in the basis of harmonic 2-forms  $\{\beta_i\}$  as in eq. (4.32). The kinetic terms arise from dimensional reduction of the  $H \wedge \star H$  term in the 10D action. Defining the Kähler metric:

$$\gamma_{ij} = \int_{CY} \beta_i \wedge \star \beta_j \,, \tag{4.36}$$

the 4D kinetic action becomes:

$$S_{\rm kin} = -\frac{1}{2\pi g_s^2} \int d^4x \, \frac{1}{2} \gamma_{ij} \partial_\mu b_i \partial^\mu b_j \,. \tag{4.37}$$

These axions acquire couplings to gauge fields via the 10D Green-Schwarz anomaly cancellation mechanism [54, 140], as described in the following section.

#### 4.1.5 Anomalies, Axions and Green-Schwarz

In string theory, irreducible anomalies cancel due to group-theoretic identities, while factorizable (Abelian or mixed) anomalies cancel via a generalized Green-Schwarz mechanism that involves axionic couplings to Chern-Simons terms

$$S_{GS} = \frac{1}{48(2\pi)^5 \alpha'} \int B \wedge X_8 \,, \tag{4.38}$$

with

$$X_8 = \frac{1}{24} \operatorname{tr} F^4 - \frac{1}{7200} (\operatorname{tr} F^2)^2 - \frac{1}{240} (\operatorname{tr} F^2) (\operatorname{tr} F^2) + \frac{1}{8} \operatorname{tr} R^4 + \frac{1}{32} (\operatorname{tr} R^2)^2. \tag{4.39}$$

Using tadpole cancellation condition from the Bianchi Identity, separating the two gauge sectors, the action dimensionally reduced reads

$$S_{GS} = \frac{1}{64(2\pi)^{5}\alpha'} \int B \wedge (\operatorname{tr} F_{1}^{2}) \left( \operatorname{tr}_{1} \bar{F}^{2} - \frac{1}{2} \operatorname{tr} \bar{R}^{2} \right)$$

$$- \frac{1}{768(2\pi)^{5}\alpha'} \int B \wedge (\operatorname{tr} R^{2}) \left( \operatorname{tr} \bar{R}^{2} \right)$$

$$+ \frac{1}{48(2\pi)^{5}\alpha'} \int B \wedge \left[ \operatorname{tr}_{1} \left( F\bar{F} \right) \right]^{2}$$

$$+ \frac{1}{32(2\pi)^{5}\alpha'} \int B \wedge \operatorname{tr}_{1} \left( F\bar{F} \right) \left( \operatorname{tr}_{1} \bar{F}^{2} - \frac{1}{2} \operatorname{tr} \bar{R}^{2} \right) + (1 \leftrightarrow 2) ,$$

$$(4.40)$$

where the overlined quantities refer to the internal ones, while the others are the 4D ones. We are interested in the first line of the Green-Schwarz action eq. (4.40), which, after expanding the B-field in harmonic forms, gives us the Chern-Simons coupling for the model dependent axions [142],

$$-\frac{1}{2\pi^2 4!} \sum_{i} \int_{X} \beta_i \left[ -\frac{\operatorname{tr} R \wedge R}{2} + 2 \operatorname{tr}_1 F \wedge F - \operatorname{tr}_2 F \wedge F \right] \int b_i \frac{\operatorname{tr}_1 F \wedge F}{16\pi^2} + (1 \leftrightarrow 2) . \quad (4.41)$$

We make use of the Bianchi identity, eq. (4.2), whose integral over any compact 4-cycle in the internal manifold vanishes due to Stokes' theorem, assuming no boundaries or localized sources, to rewrite:

$$-\sum_{i} \int_{X} \beta_{i} \wedge \frac{1}{16\pi^{2}} \left( \operatorname{tr}_{1} F \wedge F - \frac{1}{2} \operatorname{tr} R \wedge R \right) \int b_{i} \left( \frac{\operatorname{tr}_{1} F \wedge F}{16\pi^{2}} - \frac{\operatorname{tr}_{2} F \wedge F}{16\pi^{2}} \right) . \quad (4.42)$$

The effective 4D CS couplings can be written as:

$$\mathcal{L}_{CS} = \sum_{i} \frac{n_i}{16\pi^2} b_i(x) \left( \operatorname{tr}_1 F \wedge F - \operatorname{tr}_2 F \wedge F \right) , \qquad (4.43)$$

where the coefficients  $n_i$  depend on the internal geometry and background fluxes through:

$$n_i = \int_X \beta_i \wedge \frac{1}{16\pi^2} \left( \operatorname{tr}_1 F \wedge F - \frac{1}{2} \operatorname{tr} R \wedge R \right) . \tag{4.44}$$

Diagonalizing the Kähler metric and canonically normalizing the axions as  $b_i \to \vartheta_i = f_i b_i$  with

$$f_i^2 = \frac{\gamma_i}{2\pi g_s^2} \,, (4.45)$$

we arrive at the Chern-Simons couplings:

$$\mathcal{L}_{CS} = \frac{1}{16\pi^2} \left( \frac{\vartheta_a}{f_a} + \sum_i \frac{n_i}{f_i} \vartheta_i \right) \operatorname{tr}_1 F \wedge F + \frac{1}{16\pi^2} \left( \frac{\vartheta_a}{f_a} - \sum_i \frac{n_i}{f_i} \vartheta_i \right) \operatorname{tr}_2 F \wedge F. \quad (4.46)$$

Canonically normalizing the gauge field  $F \to g_{YM} \times F$ , we find

$$\mathcal{L}_{CS} = \sum_{i} \frac{\lambda_{i}}{4f_{i}} \vartheta_{i} \left( \operatorname{tr}_{1} F \wedge F - \operatorname{tr}_{2} F \wedge F \right) , \qquad \lambda_{i} = \frac{n_{i} k \operatorname{Re}[f]}{2\pi^{2}} , \qquad (4.47)$$

where k is the current algebra level coming from the definition of the traces  ${\rm tr} F \wedge F = 2k{\bf tr} F \wedge F$ .

At tree level, the gauge kinetic function determined from the kinetic terms of F and the CS coupling with a is [143]

$$f = \frac{V}{4\pi g_s^2} + i \frac{a}{4\pi^2} \,. \tag{4.48}$$

However, at one-loop, different choices of internal gauge bundles V embedded into the first and second  $E_8$  factor yield distinct threshold corrections from the model dependent axion CS couplings. Since we expanded the  $B_2$  in a basis of harmonic two-forms  $\{\beta_i\}$  of the Calabi-Yau manifold as in eq. (4.32), we can do the same for the Kähler form:

$$J = 2\pi \sum_{i=1}^{h^{1,1}} v_i \,\beta_i \,, \tag{4.49}$$

then the  $b_i$ , as dimensionless axions with periodicity  $b_i \sim b_i + 2\pi$ , and the  $v_i$  are the volumes of the associated two-cycles, can be combined in the complexified Kähler moduli  $T_i$ :

$$T_i = v_i + ib_i. (4.50)$$

Then the one-loop corrected gauge kinetic function at large  $T^i$  is (see e.g. [111,144])

$$f = \frac{\mathcal{V}}{4\pi g_s^2} + i \frac{a}{4\pi^2} \pm \frac{1}{4\pi^2} \sum_i T^i n_i, \,\,(4.51)$$

where the  $\pm$  depends if we're looking at the visible or hidden gauge sector. Thus, the effective CS coupling reads:

$$\lambda_{i,visible} \equiv \lambda_{i,v} = k \frac{8n_i g_s^2}{(\mathcal{V}\pi + g_s^2 v_i n_i)},$$

$$\lambda_{i,hidden} \equiv \lambda_{i,h} = -k \frac{8n_i g_s^2}{(\mathcal{V}\pi - g_s^2 v_i n_i)}.$$

$$(4.52)$$

This way different couplings of the axions with the visible and with the dark sector can arise.

#### 4.1.6 Volume bound and axion multiplicity

To reproduce phenomenologically viable values for the unified gauge coupling as given in eq. (4.29), the Calabi–Yau volume in string units must satisfy

$$\mathcal{V} = \frac{1}{6} \kappa_{ijk} v^i v^j v^k \lesssim 20 \,, \tag{4.53}$$

where the  $v^i$  denote the Kähler parameters measuring volume of the 2-cycles in the internal manifold, and  $\kappa_{ijk}$  denote the triple intersection numbers. This volume bound can have different implications depending on the topology of the internal space.

In isotropic compactifications, where all 2-cycle volumes are of similar size  $v^i \sim v \lesssim 3$ , the number of non-vanishing intersection numbers grows as  $\sim \frac{1}{6}\mathcal{O}((h^{1,1})^3)$  [145]. Approximating  $\kappa_{ijk} \sim \mathcal{O}(1)$ , the volume constraint implies a bound on the combination of  $h^{1,1}$  and v

$$\mathcal{V} \simeq \frac{1}{36} (h^{1,1})^3 v^3 \lesssim 20.$$
 (4.54)

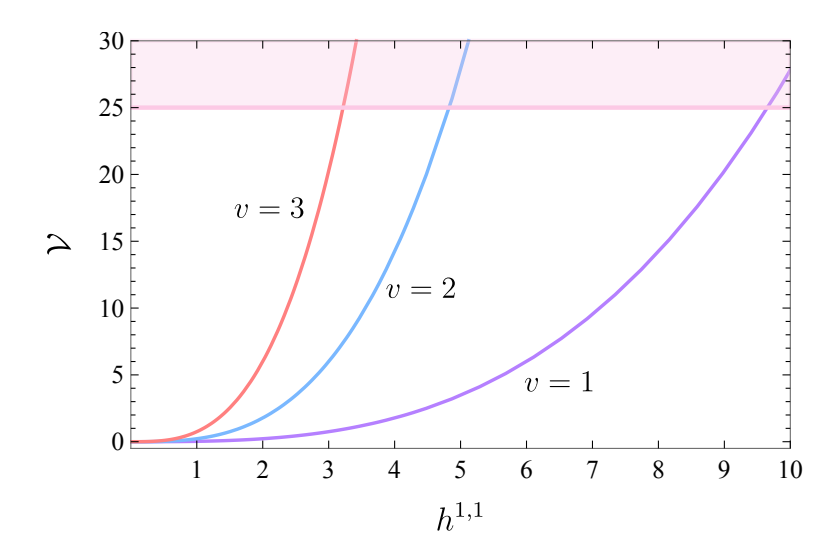


Figure 4.1: Volume bound for different values of the 2-cycle volume. The pink line shows the maximum allowed volume eq. (4.53).

This scaling arises because the triple intersection number is a rank-three totally symmetric tensor, which can have at most  $\binom{n+3-1}{3}$  independent number of components, where  $n=h^{1,1}$  is the dimension of the vector space n which the tensor is defined  $(H^{1,1})$ .

Suppression of non-perturbative corrections, which is equivalent to control of the instanton series, requires  $v^i \gtrsim \mathcal{O}(1)$ . This puts an upper bound on the number of sizable 2-cycles which we show in fig. 4.1. There can be at most 8 axions with  $v \sim 1$ , 4 axions if v = 2, and so on. Extrapolating this would bound the number of axions to be less than 1 for  $v \sim 8$ , however when we have  $\leq 2$  axions the combinatorial property that gives us the  $\frac{1}{6}$  scaling no longer applies as it comes to compensate the identical permutations. We note that these are loose bounds, as intersection numbers can be as large as  $\sim 10$ . Hence an isotropic heterotic compactification can support at most a handful of axions.

One might hope to evade this restriction in a highly anisotropic compactification, such as a "Swiss Cheese" Calabi-Yau with volume [146]

$$\mathcal{V} = \tau_b^{3/2} - \sum_s \tau_s^{3/2} \,, \tag{4.55}$$

where  $\tau_b$  denotes the volume of a large 4-cycle and the  $\tau_s$  are small blow-up cycles. Because the  $\tau_s$  appear with negative signs, taking  $\tau_b \approx \tau_s$  can keep the volume small while *individually* sending both  $\tau_b$  and  $\tau_s$  to large values. However, it seems unnatural to allow for this strategy to be unconstrained. We can provide several arguments suggesting that 4-cycle volumes cannot be arbitrarly large even if they keep the overall volume fixed. First, consider a compactification with  $h^{1,1}=2$ , with  $\tau_b=\kappa_{bbb}v_b^2$  and  $\tau_s=\kappa_{sss}v_s^2$ , such that the volume reads

$$\mathcal{V} = \left(\kappa_{bbb} \, v_b^3 - \kappa_{sss} \, v_s^3\right) \,, \tag{4.56}$$

Now impose the requirement  $\mathcal{V} \lesssim 20$ . If one tries to take both  $\tau_b$  and  $\tau_s$  parametrically large while keeping their difference small, which forces

$$v_b \simeq (\kappa_{sss}/\kappa_{bbb})^{1/3} v_s + \mathcal{O}\left(\frac{1}{3}\mathcal{V}v_s^{-2}\right) \to rv_s,$$
 (4.57)

i.e. the two Kähler parameters must approach each other with scaling given by the ratio  $r \equiv \left(\frac{\kappa_{sss}}{\kappa_{bbb}}\right)^{1/3}$ . We now define a divisor class

$$L = D_b - \lambda D_s$$
, with  $\lambda > 0$ . (4.58)

whose self intersection is  $L^3 = \kappa_{bbb} - \lambda \kappa_{sss} = 0$  if  $\lambda = \frac{1}{r}$ . Geometrically, this means that L lies on the boundary of the Kähler cone, as it is *nef* but not *ample*. In order words,  $L \cdot \mathcal{C} \geq 0$  for every effective curve  $\mathcal{C}$  but it does not lie in the interior of the cone since there will be one intersection with an effective curve that vanishes. By duality of the nef and the Mori cone, any nef divisor on the boundary must have zero intersection with some effective curve class: there exists an effective curve  $\mathcal{C}$  s.t.  $L \cdot \mathcal{C} = 0$ . (Indeed  $L^2$  is, intersecting two divisors which cuts out a holomorphic curve so basically  $L^2$  is dual to  $\mathcal{C}$ ).

Now take an effective curve C, with divisor intersections

$$a = D_b \cdot \mathcal{C} > 0, \qquad b = -D_s \cdot \mathcal{C} > 0 \qquad \lambda \equiv \frac{a}{b},$$
 (4.59)

which will have the volume

$$J \cdot \mathcal{C} = bv_s \left[ \lambda \frac{v_b}{v_s} - 1 \right] . \tag{4.60}$$

Therefore, in the limit eq. (4.57), the volume vanishes when  $\lambda = v_s/v_b \to 1/r$ .

This is the curve whose existance is guaranteed by  $L^3 = 0$ , as it shrinks to zero volume in the large two-cycle limit. The above illustrates that one cannot send both 4-cycle volumes to infinity with fixed overall volume without hitting a boundary of the Kähler cone where an effective curve collapses.

A similar argument can be made for more general swiss cheese structure manifolds. Such a swiss cheese CY may have an intersection number structure such that we have  $\tau_b = \kappa_{bij} v^i v^j = \kappa_{bbb} v_b^2 + \kappa_{bbs} v_b v_s + \kappa_{bss} v_s^2$ . In order to then rewrite the volume form in terms of  $\tau_b$  and  $\tau_s$  then one adds and subtracts an appropriate term  $cv_s^2$  to complete the squares in the volume form, such that in terms of  $\tau_b = (av_b + bv_s)^2$  and  $\tau_s = -cv_s^2$  the volume takes the swiss cheese form. The same result apply to this case, except that the linear relation between  $v_b$  and  $v_s$  gets modified

$$\mathcal{V} \sim (av_b + bv_s)^3 - cv_s^3 \sim \text{const}, \qquad v_b = v_s \frac{(c-b)}{a} + \mathcal{O}(\mathcal{V}v_s^{-2}).$$
 (4.61)

We now provide a simple explicit example illustrating this qualitatively. Consider the blow-up of  $\mathbb{P}^2$  at a point, with divisor basis  $\{H, E\}$ , where H denotes the pullback of the hyperplane class and E is the exceptional divisor: a (-1) curve satisfying  $E \cdot E = -1$ . Let the Kähler form be parametrized as

$$J = v_H H - v_E E, v_H, v_E > 0, (4.62)$$

ensuring positivity of volumes for all effective curves. An important effective curve class on this surface is

$$C = H - E, (4.63)$$

which corresponds to the proper transform of a line through the blown-up point. Although this class appears as a formal difference in the chosen basis, it is indeed an effective, rigid curve in the del Pezzo surface.

The volume of this curve is given by

$$Vol(\mathcal{C}) = J \cdot \mathcal{C} = (v_H H - v_E E) \cdot (H - E) = v_H - v_E. \tag{4.64}$$

This shows that  $\mathcal{C}$  becomes small as  $v_H \to v_E$  from above, and shrinks completely at the boundary  $v_H = v_E$  of the Kähler cone. While  $\mathcal{C}$  is a genuine effective curve class, its volume depends on the difference of two Kähler parameters.

Now take the case of multiple Kähler fields. Take  $\tau_b = \kappa_{bjk} v^j v^k$ , and  $\tau_{s_i} = \kappa_{s_ijk} v^j v^k$ , and take

$$\tau_b \sim \sum_i \tau_{s_i} \to \infty.$$
(4.65)

Implying

$$\kappa_{bjk}v^jv^k \sim \sum_i \kappa_{s_ijk}v^jv^k \quad . \tag{4.66}$$

This means that imposing the volume bound but keeping the four cycles big imposes one quadratic relation on the direction of growth of the 2-cycles: they must blow up proportionally with fixed ratios set by the intersection numbers.

The structure of the string loop corrections to the moduli Kähler potential provides another, and correlated, signal indicating a shrinking 2-cycle. Namely, sending 4-cycles to large volumes breaks down the EFT which comes from string loop corrections to the Kähler potential,  $\delta K^{(g_s)}$ , which behave as homogeneous functions of degree -2 in the 2-cycle volumes [147]. This implies that if one sends a Kähler modulus  $\tau \to \infty$  while keeping the overall volume  $\mathcal V$  fixed, the corresponding 2-cycle volume t also diverges, and hence  $\delta K^{(g_s)} \sim v/\mathcal V \sim \tau^{1/2}/\mathcal V$  grows without bound. Although the scalar potential exhibits an extended no-scale structure that ensures the cancellation of leading order contributions from such corrections when  $\delta K^{(g_s)}$  is of degree -2, the subleading contribution  $\delta V_2$  remains sensitive to their magnitude. Therefore, in this limit, the loop corrections to the scalar potential become large and the effective field theory breaks down.

#### A note on geometry and bundles

The structure of the gauge bundle in heterotic compactifications is intimately linked to the topology of the internal Calabi–Yau manifold, particularly its non-trivial cycles. For vector bundle V of rank n, the topological data is encoded in the chern classes  $c_i(V)$ . A holomorphic, stable in the sense of the slope, bundle, must satisfy the anomaly cancellation condition which related the second Chern class  $c_2(V)$  to that of the CY  $c_2(TX)$ . When talking about line bundles, we only need  $c_1(V) \in H^2(X) \sim$  divisors, counted by  $h^{1,1}$ . If  $h^{1,1}$  is small, the options for embedding the gauge bundle are limited and you can't construct too complicated bundles.

In many explicit constructions, especially those based on line bundles, the gauge bundle is written as a direct sum of line bundles over divisors:  $V = \bigoplus_i \mathcal{O}(D_i)$ . Here, each divisor  $D_i$  corresponds to an element of  $H^2(X)$ , whose dimension is counted by  $h^{1,1}$ . Thus, the number of available divisors directly limits the flexibility in defining such bundles. When  $h^{1,1}$  is small, the space of line bundle configurations is highly constrained, making it difficult to construct bundles that satisfy anomaly cancellation and supersymmetry. Conversely, a larger  $h^{1,1}$  provides more geometric freedom to define richer bundle topologies.

Therefore, while the rank of the bundle is not directly constrained by  $h^{1,1}$ , constructing more intricate gauge bundles typically requires a compactification geometry with a greater number of independent cycles.<sup>2</sup>

# 4.2 Heterotic axion EFT: CP problem & axion mass spectrum

#### 4.2.1 A short recap on heterotic moduli stabilization

Discussion of an axion EFT in string theory requires addressing moduli stabilization within a given class of string compactifications. The strategies employed in type IIB string theory for compactification on warped conformal CY orientifolds with 3-form fluxes and 7-branes is of no use for the  $E_8 \times E_8$  perturbative heterotic string. Namely, we cannot avail ourselves of the presence of an RR-sector 3-form flux  $F_3$  jointly with the NSNS 3-form flux  $H_3$  in order to produce a flux discretuum by which we can fix both the c.s. moduli and the axio-dilaton and at the same time fine-tuning the resulting flux superpotential  $W_0$  to be of small magnitude.

Heterotic moduli stabilization in CY compactifications (including their orbifold limits in CY moduli space) has to proceed from the effective action determined by a Kähler potential and superpotential:

$$K = -\ln(S + \bar{S}) - \ln \mathcal{V}(T_t, \bar{T}_i) - \ln \left( -i \int_X \Omega(z_a) \wedge \bar{\Omega}(\bar{z}_{\bar{a}}) \right) + \Delta K_{\text{non-/pert.}}$$

$$W = \int_X H_3 \wedge \Omega(z_a) + \sum_i A_i e^{-a_i f_i(S, T_j, z_b)} + \sum_n B_k e^{-2\pi T_k} .$$

$$(4.67)$$

Recalling the results of [105, 110–117], the first sum in W parametrizes non-perturbative effects from gaugino condensation driven by unbroken non-Abelian gauge group factors surviving from the hidden  $E_8$ -factor. The second sum describes the contribution from worldsheet instantons. The contributions from gaugino condensation depend on the Kähler and c.s. moduli through the 1-loop threshold corrections which for largish values of the  $T_i$  and  $z_a$  depend linearly on those moduli, but are e.g. for simple toroidal orbifold limits of CYs dictated by modular invariance to appear in the form of the logarithm of the Dedekind eta function [144].  $\Delta K_{\rm non-/pert.}$  in turn represents perturbative  $\alpha'$  and string loop as well as non-perturbative corrections to the Kähler potential [118–122].

In heterotic CY compactifications we can only use  $H_3$ -flux to fix the c.s. moduli. Its quantization produces either a VEV  $W_0 = |\langle \int H_3 \wedge \Omega \rangle| \gtrsim \mathcal{O}(1)$  in the case of standard integer-quantized 3-form flux  $H_3$ , or at best  $W_0 = |\langle \int H_3^{fract} \wedge \Omega \rangle| \gtrsim \mathcal{O}(0.1)$  in the case of  $H_3$ -flux due to the fractional CS term contribution e.g. from discrete Wilson lines [111].

In the absence of  $H_3$ -flux, generically a part of the c.s. moduli stabilization can happen at the SUSY Minkowski level ( $D_zW=W=0$ ) by turning on a non-trivial gauge bundle, already needed to break the visible  $E_8$  towards the SM gauge group, as part of the background fields of the compactification. The resulting unbroken subgroup of  $E_8 \times E_8$  typically contains anomalous U(1)-factors whose D-terms will have the structure

$$D = \frac{c}{S + \bar{S}} - q_C |C|^2 \tag{4.68}$$

<sup>&</sup>lt;sup>2</sup>We thank Fabian Ruehle for explaining the content of section 4.1.6 to us and for reminding us the existence of shrinking curves in anisotropic limits of CY compactifications.

where c denotes the coefficient of the field-dependent FI term and C are a summarily representation of the gauge bundle moduli which appear as SM gauge single chiral multiplets in the 4D EFT. Assume now that the dilaton S is stabilized at a non-zero VEV with Re  $\langle S \rangle \simeq 2$  consistent with MSSM gauge coupling unification (more on this below). Then, the D-term scalar potential from the anomalous U(1)-s' D-terms will now drive some bundle moduli to acquire non-zero VEVs. It was shown that the combined moduli space of the c.s. moduli and bundle moduli has a partial cross structure [104, 114, 148] following an observation in [149]. Hence, once the bundle moduli acquire non-zero VEVs from the D-terms, at least some of the c.s. moduli will be stabilized at zero VEV in turn. For certain CY manifold,s and in particular orbifolds, this mechanism can be sufficient to stabilize all of the c.s. moduli at the SUSY Minkowski level [104, 114, 117, 148].

A variant of this situation arises if the 4D EFT of the given heterotic CY or orbifold compactification possesses a higher-order discrete R-symmetry  $Z_N$  under which one the D-term chiral fields C is charged. In this case, the superpotential may contain R-invariant high-order monomial terms  $\Delta W \sim C^N$ . As C acquires a VEV of typical size  $|\langle C \rangle| \sim \sqrt{c/\text{Re}\langle S \rangle} \sim 0.1$ , this induces an effective  $W_0 \sim \langle C \rangle^N \sim 10^{-N}$  which can be as small as  $\mathcal{O}(10^{-10})$  for  $Z_N$  with N as large as 10 [115].

Next comes stabilizing the dilaton. Here, we can discriminate between two classes.

- GC There is gaugino condensation [150, 151] from unbroken non-Abelian gauge group factors surviving the breaking of the hidden  $E_8$ -factor [152, 153].
  - $W_0 \simeq 0.1$  from fractional CS-invariants. The hidden  $E_8$  now needs to remain unbroken, as only the Coxeter number of  $E_8$  is large enough to stabilize the dilaton against  $W_0$  in  $D_SW=0$  at  $\langle S\rangle\simeq 2$  required for gauge coupling unification [111,117].
  - $W_0 \ll 0.1$  from gauge bundle driven and D-term induced cs. moduli stabilization, producing high-order R-symmetry protected effectively constant terms in the superpotential. In this case, a lower-rank gauge group gaugino condensate surviving from the hidden  $E_8$  can stabilize S again near the phenomenologically desired value [115, 117].
  - $W_0 = 0$  after gauge bundle driven c.s. moduli stabilization. Dilaton stabilization via gaugino condensation now requires a racetrack (RT), i.e. two condensing non-Abelian gauge group factors surviving from breaking the hidden  $E_8$  [110, 154].
- noGC The hidden  $E_8$  gets completely broken by a combination of gauge bundle choice and additional Wilson lines to a surviving subgroup containing just several U(1)-factors. Gaugino condensation is now absent.
  - Dilaton stabilization has to proceed by a combination of perturbative and/or non-perturbative quantum corrections to the dilaton Kähler potential (such as the universally present 'Shenker-like' terms [118]) which may produce a generically SUSY breaking S-minimum [105,112].

Finally, stabilization of Kähler moduli needs to proceed along similar lines classified by the presence or absence of gaugino condensation and a possible constant contribution  $W_0$  to the superpotential.

GC Gaugino condensation occurs.

- Stabilization of the Kähler moduli can proceed either via the dependence of the gaugino condensate on compactification moduli through threshold corrections to the gauge kinetic function [144], or similar to the KKLT scenario, via worldsheet instanton corrections  $\Delta W_{ws} \sim e^{-2\pi T_i}$  balancing against  $W_0$  in the F-term condition  $D_{T_i}W = 0$ .
- Including the leading  $\alpha'$ -corrections to the volume moduli Kähler potential from 10D  $R^2$  and  $R^4$  curvature correction [119, 121, 122], we can engineer an  $\ell$ VS-scenario like stabilization scheme for the Kähler moduli on CY manifolds whose CY volume takes the Swiss-Cheese form [117]. Here, the  $\ell$  in  $\ell$ VS refers to the fact, that the total CY volume can at most be of  $\mathcal{O}(20...30)$  for perturbative  $(g_s < 1)$  heterotic string compactification which maintain MSSM gauge coupling unification, so the CY volume can at best be 'large-ish' but not Large.

noGC No gaugino condensation.

- Kähler moduli stabilization would now require at least one racetrack-like configuration of at two different worldsheet instantons for one volume modulus  $T_i$  generating a minimum for it with non-vanishing  $\Delta W_{\rm RT}(\langle T_i \rangle)$ . This part of the superpotential can now act as an effectively constant  $W_0$  against single worldsheet instantons for the remaining Kähler moduli to stabilize them similar to the KKLT scenario.
- Alternatively, if  $W_0 \neq 0$  one can stabilize the Kähler moduli perturbatively given sufficiently many string loop and/or  $\alpha'$ -corrections to the volume moduli Kähler potential.

#### 4.2.2 Sources of Axion Masses

Axions in heterotic string compactifications generally acquire masses via three non-perturbative mechanisms:

- 1. QCD instantons in the visible sector;
- 2. Hidden sector gaugino condensation;
- 3. Worldsheet instantons wrapping internal two-cycles.

Assuming the visible sector is embedded in the first  $E_8$ , the QCD anomaly induces an axion potential:

$$V_{\rm QCD} = -\Lambda_{\rm QCD}^4 \cos\left(\frac{\vartheta_a}{f_a} + \sum_i \frac{n_i}{f_i}\vartheta_i + \delta\right),\tag{4.69}$$

where  $\delta$  arises from the complex phase of the quark mass determinant. We assume a superpotential of the form

$$W = W_0 + W_{nn}, (4.70)$$

where  $W_0$  is a constant tree-level flux superpotential, and  $W_{np}$  is the contribution coming from either worldsheet instantons or some condensing gauge group.

If the second  $E_8$  contains a non-Abelian subgroup  $\mathcal{G}$  confining in the IR, gaugino condensation generates a superpotential in  $\mathcal{N}=1$  SUGRA:

$$W_{np} \sim \mathcal{A}e^{-\frac{8\pi^2}{c(\mathcal{G})}f_{\mathcal{G}}} \tag{4.71}$$

where  $f_{\mathcal{G}}$  and  $c(\mathcal{G})$  are the gauge kinetic function and the dual Coxeter number of  $\mathcal{G}$ , respectively. In heterotic compactifications, one typically has  $\text{Re}(f) \sim \mathcal{V}/(g_s^2)$ . For  $\mathcal{G} = SU(N)$ ,  $c(\mathcal{G}) = N$ , This leads to the potential:

$$V_{\rm gc} = -\Lambda_{\rm gc}^4 \cos\left(\frac{\vartheta_a}{f_a} - \sum_i \frac{n_i}{f_i} \vartheta_i\right),\tag{4.72}$$

with

$$\Lambda_{\rm gc}^4 = \mu^4 \exp\left(-\frac{2\pi}{N} \frac{\mathcal{V}}{g_s^2}\right). \tag{4.73}$$

Worldsheet instantons wrapping holomorphic two-cycles generate non-perturbative contributions to the superpotential of the form

$$W_{\rm np} = \mathcal{A} e^{-2\pi T} \tag{4.74}$$

where T = v + ib is the complexified Kähler modulus, with v the volume (in string units) of the wrapped cycle and b its associated axion. These contributions induce a scalar potential for axions of the general form

$$V_{\rm ws} = -\Lambda^4 \cos\left(\sum_i \frac{c_i \vartheta_i}{f_i}\right), \qquad \Lambda^4 \sim \mu^4 e^{-2\pi v}, \tag{4.75}$$

where the  $c_i$  are coefficients that depend on the specific instanton and its coupling to the axions. In the later sections we will restrict to the simplified case where each instanton only contributes to lifting one model dependent axion. The scale  $\mu^4$  depends on the compactification and moduli stabilization data. In supergravity, the potential typically includes cross-terms of the form  $V \sim e^K W_0 \mathcal{A} e^{-T}$ , so  $\mu^4$  often scales as  $W_0 \mathcal{A}$ . The flux superpotential  $W_0$  typically lies between  $10^{-13}$  and  $10^{-1} M_{\rm Pl}^3$ , depending on the compactification, tuning, and origin of  $W_0$ .

We now explore how these contributions determine the mass spectrum in two- and three-axion systems, and how they affect the coupling structure. We begin with a general framework for understanding the hierarchy and role of each contribution:

- 1. The QCD potential always contributes and generates a mass for the axion combination coupled to  $\operatorname{tr}_1 F \wedge F$ .
- 2. Gaugino condensation contributes when non-Abelian hidden sector gauge groups are present. If the hidden  $E_8$  is broken entirely to U(1) factors, this contribution is absent.
- 3. The internal Calabi-Yau volume  $\mathcal{V}$  controls both  $\alpha'$  corrections and gauge couplings. Realistic models require moderately large  $\mathcal{V}$  (e.g.,  $\mathcal{V} \sim \mathcal{O}(10-20)$ ), limiting the emergence of ultra-light axions.

#### 4.2.3 Strong CP problem

To address the Strong CP problem arising from the CP-violating term in the QCD Lagrangian,

$$\mathcal{L}_{\theta} = \frac{\theta_{\text{eff}}}{32\pi^2} \operatorname{tr}(G \wedge G), \qquad (4.76)$$

we invoke the Peccei–Quinn mechanism through a combination of axions that couple to the first  $E_8$ , which contains the visible-sector QCD gauge group. This specific linear combination of axions enters the QCD Chern-Simons term and therefore receives a potential from QCD instantons. The resulting potential dynamically minimizes the effective angle  $\theta_{\text{eff}}$ , driving it to zero. In this way, the axion field adjusts to cancel the CP-violating phase, providing a dynamical solution to the Strong CP problem.

It is important to emphasize, however, that the axion direction lifted by QCD instantons generally overlaps with those lifted by other non-perturbative effects, such as gaugino condensation or worldsheet instantons. These directions are not, in general, orthogonal in axion field space. To illustrate this, consider the following scalar potential:

$$V = -\Lambda_{\text{QCD}}^4 \cos\left(\frac{\vartheta_a}{f_a} + \sum_i n_i \frac{\vartheta_i}{f_i} + \delta\right) - \Lambda_{\text{gc}}^4 \cos\left(\frac{\vartheta_a}{f_a} - \sum_i n_i \frac{\vartheta_i}{f_i}\right) - \sum_{i=1}^{h^{1,1}} \Lambda_j^4 \cos\left(\sum_i c_i^{(j)} \frac{\vartheta_i}{f_i}\right),$$

$$(4.77)$$

where the scales  $\Lambda_{\rm QCD}$ ,  $\Lambda_{\rm gc}$ ,  $\Lambda_j$  are defined in the previous subsection, and the  $\vartheta_i$  denote model-dependent axions with decay constants  $f_i$ . In general, additional contributions from higher-order instanton effects, such as multi-instanton corrections, may also be present. These are typically suppressed by double exponentials and are therefore subleading compared to the single-instanton terms shown above. For the purposes of this analysis, we will neglect such higher-order corrections.

The theory described by eq. (4.77) contains  $N = h^{1,1} + 1$  axions and N + 1 leading terms in the potential. In the regime where  $\Lambda_{\rm QCD}$  is the smallest scale, all axion vacuum expectation values are already fixed by the larger contributions from gaugino condensation and worldsheet instantons. As a result, the QCD-induced term is no longer able to dynamically relax  $\theta_{\rm eff}$  to zero, and the Peccei–Quinn mechanism fails to solve the Strong CP problem.

Let us consider an isotropic compactification, where all worldsheet instanton contributions are of comparable magnitude, and the non-perturbative scales exhibit the hierarchy

$$\Lambda_{\rm ws}^4 \gg \Lambda_{\rm gc}^4 \gg \Lambda_{\rm QCD}^4$$
 (4.78)

In this setup, the worldsheet instanton potential  $V_{\rm ws}$  generically lifts  $N=h^{1,1}$  axion directions. The remaining axionic degree of freedom is then fixed by the gaugino condensation term. As a result, by the time the QCD contribution becomes relevant, all axion vacuum expectation values are already stabilized, leaving no freedom to dynamically minimize the effective angle  $\theta_{\rm eff} = \vartheta_a + \sum_i n_i \vartheta_i + \delta$ . In this case, the Strong CP problem is not solved dynamically, and the cancellation of  $\theta_{\rm eff}$  would require a fine-tuning of the axion vevs, which is no better than tuning the original  $\theta$  angle itself. The resolution lies in freeing one axion vev so that it remains unfixed until the QCD contribution becomes

dominant, allowing it to adjust and cancel the effective  $\theta$ -angle. To achieve this, we must ensure that only  $N=h^{1,1}$  axion directions are lifted by effects stronger than QCD, while one direction remains light enough to be fixed by the QCD potential. This requires at least one non-perturbative contribution, either from gaugino condensation or a worldsheet instanton, to be more suppressed than  $\Lambda_{\rm QCD}$ .

Before turning to explicit scenarios, let us comment on the constraints imposed by phenomenology. If the additional contribution is present but only slightly lighter than QCD, it can still interfere with the axion dynamics and shift the vev away from the CP-conserving minimum. To ensure that the Strong CP problem is reliably solved, the QCD contribution must dominate over any other source of explicit shift symmetry breaking for the axion. In particular, any subleading potential term must be suppressed relative to the QCD term by at least ten orders of magnitude, so that the induced shift in remains below current experimental bounds on the neutron electric dipole moment [14, 19, 75, 155]:  $\theta_{eff} \simeq \theta_{QCD} + \Delta \theta < 10^{-10}$ .

Let us now consider the case in which a hidden-sector non-Abelian gauge group undergoes gaugino condensation at a scale below  $\Lambda_{\rm QCD}$ . The associated contribution to the scalar potential takes the form

$$\Lambda_{\rm gc}^4 \sim W_0 M_s^3 e^{-\frac{2\pi}{N} \frac{\mathcal{V}}{g_s^2}} \ll 10^{-10} \times \Lambda_{\rm QCD}^4 \sim 10^{-85} M_{\rm pl}^4,$$
 (4.79)

where  $W_0$  is the flux superpotential,  $\mathcal{V} = \mathrm{Vol}(X)/\ell_s^6$  is the dimensionless Calabi-Yau volume in string units, and we take  $\Lambda_{\mathrm{QCD}}^4 \sim 10^{-75} M_{\mathrm{pl}}^4$ . Relating the string scale to the Planck scale via  $M_s \sim g_s \mathcal{V}^{-1/2} M_{\mathrm{pl}}$ , we can express the gaugino condensation scale entirely in Planck units as

$$\Lambda_{\rm gc}^4 \sim W_0 \, \frac{g_s^3}{\mathcal{V}^{3/2}} \, e^{-\frac{2\pi}{N} \frac{\mathcal{V}}{g_s^2}} \,.$$
(4.80)

Demanding  $\Lambda_{\rm gc}^4 \ll 10^{-85}$  imposes a stringent bound on the volume. Even taking optimistic values to minimize the contribution, such as  $W_0 \sim 10^{-13}$ ,  $g_s \sim 1$ , and a minimal confining group with N=2, one finds

$$\Lambda_{\rm gc}^4 \gtrsim 10^{-48} \gg 10^{-10} \Lambda_{\rm QCD}^4 \,,$$
 (4.81)

showing that gaugino condensation occurs at a scale vastly exceeding the QCD scale. As a result, any axion combination involved in this term will be stabilized well before the QCD potential becomes relevant. Thus, the axion vev is no longer free to adjust in response to the QCD contribution, and the Strong CP problem remains unsolved. The only viable resolution in this case is to ensure that the hidden-sector gauge group does not confine. This can be achieved by breaking it to its Cartan subgroup, leaving only Abelian U(1) factors, which do not undergo gaugino condensation and hence do not generate non-perturbative axion potentials.

Let us now consider the case here gaugino condensation occurs at a scale above QCD but the nearly free axion direction arises from a sufficiently low-scale worldsheet instanton contributing to the axion potential. Performing an analysis analogous to the gaugino condensation case, we find that the contribution takes the form

$$\Lambda_{\text{ws}}^4 \sim W_0 \frac{g_s^3}{\mathcal{V}^{2/3}} e^{-2\pi v} \ll 10^{-85} \qquad \iff v \gtrsim 25,$$
(4.82)

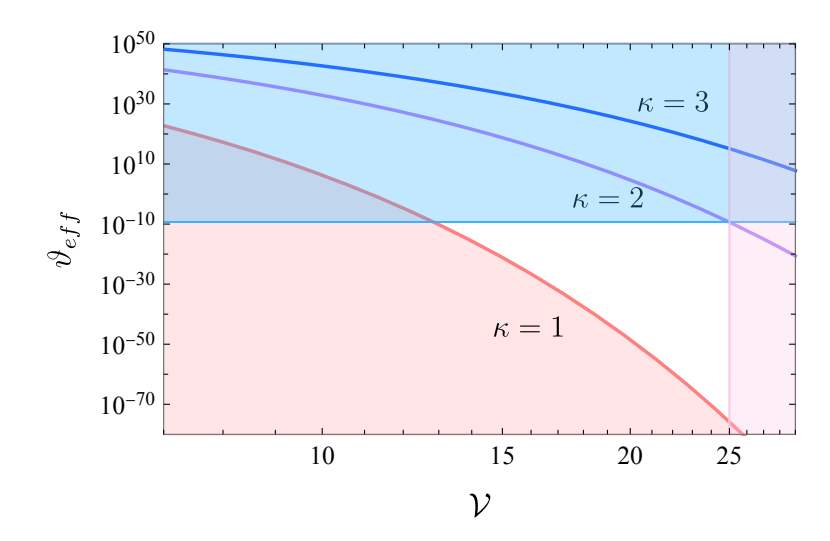


Figure 4.2: Effective  $\theta$  angle arising from the inclusion of worldsheet instanton contributions, plotted as a function of the overall volume. The shaded regions correspond to parameter values that are excluded. The red curve corresponds to  $\kappa=1$ , with the associated exclusion region determined by the bound in eq. (4.84); the purple and blue curves represent  $\kappa=2$  and  $\kappa=3$ , respectively. Higher values of the triple intersection number shift the curves upward, entering regions already excluded by observational and consistency constraints. The pink vertical line marks the upper bound on the volume,  $\mathcal{V}<25$ , while the light blue horizontal line corresponds to the observational upper limit on the effective  $\theta$  angle.

where v denotes the volume of the wrapped two-cycle in string units. Achieving such a large suppression requires  $v \gtrsim 25$ , which is only possible in highly anisotropic compactifications, specifically, when one two-cycle is significantly larger than the others and dominates the total volume. This situation can naturally arise in fibred Calabi-Yau compactifications, where the base cycle is large and the fibre cycles remain small (of order unity). We can translate this in a bound on the volume, and so the total volume  $\mathcal V$  is therefore bounded from both above and below. Since the 2-cycle volume v scales as

$$v = 2\frac{\mathcal{V}}{\kappa} < \frac{50}{\kappa},\tag{4.83}$$

we obtain the following constraint on the total volume:

$$\frac{25\kappa}{2} \le \mathcal{V} \le 25. \tag{4.84}$$

In fig. 4.2, we plot this angle as a function of  $\mathcal{V}$  for different values of the triple intersection number  $\kappa$ . Compactifications with  $\kappa > 2$  are already excluded by this analysis, as they would generate a  $\theta_{\text{eff}}$  exceeding observational bounds. While the plot explicitly shows the allowed region for  $\kappa = 1$ , we omit the forbidden region for  $\kappa = 2$  to avoid overshadowing the rest of the figure: in this case, the viable parameter space reduces essentially to a single point.

In the following subsections we will analyze the system in the simplest cases, when  $h^{1,1} = 1$  and  $h^{1,1} = 2$ , where there are respectively, two or three axions. The first case, the simplest, can be analytically solved, and we can find the CS couplings of the physical axions, whereas the three-axion case is more complicated and cannot be solved fully analytically. We then provide examples for both cases, specifying when the Strong CP

problem can be solved, when there can by a fuzzy dark matter axion candidate, and when the couplings between the hidden and the visible sector can be made different. We note that the examples we give are not complete models, as this would require more model building and case by case anlysis.

#### 4.2.4 Two-Axion System

We now consider a system of two axions: a model-independent axion  $\vartheta_a$  and a model-dependent axion  $\vartheta_1$ , with decay constants  $f_a$  and  $f_1$ , respectively.

Their kinetic terms and Chern-Simons couplings take the form:

$$\mathcal{L}_{kin} = \frac{1}{2} (\partial \vartheta_a)^2 + \frac{1}{2} (\partial \vartheta_1)^2, \tag{4.85}$$

$$\mathcal{L}_{CS} = \frac{1}{16\pi^2} \left( \frac{\vartheta_a}{f_a} + \frac{n_1}{f_1} \vartheta_1 \right) \operatorname{tr}_1 F \wedge F + \frac{1}{16\pi^2} \left( \frac{\vartheta_a}{f_a} - \frac{n_1}{f_1} \vartheta_1 \right) \operatorname{tr}_2 F \wedge F. \tag{4.86}$$

We consider two subcases: one where we only consider QCD and gaugino condensation contributing to the potential and one where we only consider QCD and worlsheet instantons. This is because we have two axions, and in order to align their vevs to solve the Strong CP problem we cannot have more than two contributions.

GC We first consider the case where gaugino condensation is present, and the world-sheet instanton contribution is so small it can be safely neglected. We note that this case is merely a toy model, as for  $h^{1,1} = 1$  we are by definition in an isotropic compactification, where all two-cycles have similar volume, and thus there cannot be one single large two-cycle, effectively suppressing the worldsheet instanton contribution. We also note that in the realistic setup, where the worldsheet instanton case cannot be neglected, and gaugino condensation happens, the strong CP problem cannot be solved. However, we still analyze this as it is an instructive case. This setup allows for a rotated field basis that diagonalizes the couplings:

$$\varphi_1 = \frac{1}{2}(\vartheta_a + \alpha\vartheta_1),\tag{4.87}$$

$$\varphi_2 = \frac{1}{2}(\vartheta_a - \alpha\vartheta_1),\tag{4.88}$$

with the field space 'squashing parameter'

$$\alpha = n_1 \frac{f_a}{f_1}.\tag{4.89}$$

In this rotated basis, the CS couplings become:

$$\mathcal{L}_{CS} = \frac{1}{8\pi^2 f_a} \left( \varphi_1 \operatorname{tr}_1 F \wedge F + \varphi_2 \operatorname{tr}_2 F \wedge F \right). \tag{4.90}$$

The kinetic terms contain cross-terms proportional to  $\alpha$ :

$$\mathcal{L}_{kin} = \frac{1}{2} \left( 1 + \frac{1}{\alpha^2} \right) \left[ (\partial \varphi_1)^2 + (\partial \varphi_2)^2 \right] + \left( 1 - \frac{1}{\alpha^2} \right) \partial \varphi_1 \partial \varphi_2. \tag{4.91}$$

For  $\alpha \approx 1$ , these can be approximately diagonalized and normalized by a rescaling  $\varphi_i \to \varphi_i \sqrt{\frac{1+\alpha^2}{\alpha^2}}$ .

In this limit, the visible and hidden sector couplings are aligned with orthogonal axion directions:  $\varphi_1$  couples to the visible sector (QCD), and  $\varphi_2$  to the hidden sector. The decay constants can be estimated as

$$f_a \sim \frac{1}{\sqrt{\mathcal{V}}}, \qquad f_1 \sim \frac{1}{v},$$
 (4.92)

and for  $n_1 \sim 2$ , we find  $\alpha \sim 1$ , rendering the basis approximately orthonormal. In the case where  $\alpha \neq 1$ , we need to rotate back to the original basis, but shift the decay constant of the model dependent axion in order to keep the axion periodicity:

$$\tilde{f}_1 = \frac{f_1}{\alpha}.\tag{4.93}$$

The Chern-Simons couplings in this basis then read as

$$\lambda_{\varphi_1,v} = k \frac{8n_i g_s^2}{\mathcal{V}\pi - g_s^2 v_i n_i},$$

$$\lambda_{\varphi_2,h} = -k \frac{8n_i g_s^2}{\mathcal{V}\pi - g_s^2 v_i n_i}.$$

$$(4.94)$$

**noGC** We now consider the case in which the hidden sector is broken to Abelian gauge groups only, so that no gaugino condensation occurs. In this case, axion masses arise solely from QCD instantons and worldsheet instantons. The relevant axion potentials are:

$$V_{\text{QCD}} = -\Lambda_{\text{QCD}}^4 \cos\left(\frac{\vartheta_a}{f_a} + \frac{n_1}{f_1}\vartheta_1 + \delta\right),\tag{4.95}$$

$$V_{\rm ws} = -\Lambda_{\rm ws}^4 \cos\left(\frac{\vartheta_1}{f_1}\right). \tag{4.96}$$

The QCD term breaks the shift symmetry along the direction

$$\varphi_{\text{QCD}} \propto f_1 \vartheta_a + n_1 f_a \vartheta_1,$$
 (4.97)

which we normalize to define an orthonormal basis:

$$\begin{pmatrix} \varphi_1 \\ \varphi_2 \end{pmatrix} = U \cdot \begin{pmatrix} \vartheta_a \\ \vartheta_1 \end{pmatrix}, \quad U = \frac{1}{\mathcal{F}} \begin{pmatrix} f_1 & n_1 f_a \\ -n_1 f_a & f_1 \end{pmatrix}, \quad \mathcal{F} = \sqrt{f_1^2 + n_1^2 f_a^2}. \tag{4.98}$$

Here,  $\varphi_1$  is the QCD axion, while  $\varphi_2$  is orthogonal and receives a dominant mass from worldsheet instantons. Expanding the potential to quadratic order, the mass eigenvalues are approximately:

$$m_{\varphi_1}^2 \simeq \frac{\Lambda_{\text{QCD}}^4}{f_a^2}, \qquad m_{\varphi_2}^2 \simeq \frac{n_1^2 \Lambda_{\text{QCD}}^4}{f_1^2} + \frac{\Lambda_{\text{ws}}^4}{f_1^2}.$$
 (4.99)

The anomaly coefficients and thus the CS couplings in the new basis become:

$$\frac{\vartheta_a}{f_a} + \frac{n_1 \vartheta_1}{f_1} = \frac{\mathcal{F}}{f_a f_1} \varphi_1, \tag{4.100}$$

$$\frac{\vartheta_a}{f_a} - \frac{n_1 \vartheta_1}{f_1} = \frac{f_1^2 - n_1^2 f_a^2}{f_a f_1 \mathcal{F}} \varphi_1 - \frac{2n_1}{\mathcal{F}} \varphi_2. \tag{4.101}$$

GC	Masses	CP	CS
×	$m_{\varphi_1}^2 \sim \Lambda_{\rm QCD}^4 \ll m_{\varphi_2}^2 \sim \Lambda_{\rm ws}^4$	<b>√</b>	$\lambda_{\varphi_1 1, v/h}, \lambda_{\varphi_2, h}$
<b>√</b>	$m_{\varphi_2}^2 \sim \Lambda_{ m gc}^4 \ll m_{\varphi_1}^2 \sim \Lambda_{ m ws}^4$	×	$\lambda_{\varphi_1,v},\lambda_{\varphi_2,h}$

Table 4.2: Two-axion scenarios summarizing presence of gaugino condensation (GC), mass hierarchies, and Strong CP resolution, and dominant gauge couplings.

This implies:

$$\mathcal{L}_{CS} = \frac{1}{16\pi^2} \left( \lambda_{\varphi_1, v} \frac{\varphi_1}{f_{\varphi_1}} \right) \operatorname{tr}_1 F \wedge F + \frac{1}{16\pi^2} \left( \lambda_{\varphi_1, h} \frac{\varphi_1}{f_{\varphi_1}} + \lambda_{\varphi_2, h} \frac{\varphi_2}{f_{\varphi_2}} \right) \operatorname{tr}_2 F \wedge F, \quad (4.102)$$

where the effective decay constants are defined by demanding that the total cosine argument of the worldsheet instanton potential is periodic under simultaneous shifts of  $\varphi_1$  and  $\varphi_2$ <sup>3</sup>

$$f_{\varphi_1} = \frac{f_a f_1}{\mathcal{F}},\tag{4.103}$$

$$f_{\varphi_2} = \frac{n_1 f_a^2}{\mathcal{F}}.\tag{4.104}$$

After canonical normalization, the CS couplings become:

$$\lambda_{\varphi_1,v} = k \cdot \frac{8n_1 g_s^2}{\mathcal{V}\pi + g_s^2 v n_1},\tag{4.105}$$

$$\lambda_{\varphi_1,h} = -k \cdot \frac{8n_1 g_s^2}{\mathcal{V}\pi - g_s^2 v n_1} \cdot \frac{f_1^2 - n_1^2 f_a^2}{f_1^2 + n_1^2 f_a^2},\tag{4.106}$$

$$\lambda_{\varphi_2,h} = +k \cdot \frac{16g_s^2 n_1^2 f_a^2}{(\mathcal{V}\pi - g_s^2 v n_1)(n_1^2 f_a^2 + f_1^2)}.$$
 (4.107)

These expressions determine how axions couple to the gauge sectors once gaugino condensation is absent and worldsheet effects dominate the hidden sector axion mass. The details of the two-axion system are summarized in table 4.2.

#### Illustrative example

Consider now the setup introduced in [14] where the CY is  $X = C \times Y$  where C is a Riemann surface with volume  $\mathcal{V}_C$  and Y a four-manifold with volume  $\mathcal{V}_Y$ . The integral therefore reduces to

$$-\frac{1}{16\pi^2} \int_C \beta \int_Y \left( \operatorname{tr}_1 F \wedge F - \frac{1}{2} \operatorname{tr} R \wedge R \right) \int_M b_C \frac{\operatorname{tr}_1 F \wedge F}{16\pi^2}$$
(4.108)

$$-\frac{1}{16\pi^2} \int_Y \left( \operatorname{tr}_1 F \wedge F - \frac{1}{2} \operatorname{tr} R \wedge R \right) \int_M b_C \frac{\operatorname{tr}_1 F \wedge F}{16\pi^2} \,. \tag{4.109}$$

where the last equality we used  $\int_C \beta = 1$ . Therefore, we need to evaluate the integer

$$n = \frac{1}{16\pi^2} \int_Y \left( \operatorname{tr}_1 F \wedge F - \frac{1}{2} \operatorname{tr} R \wedge R \right) . \tag{4.110}$$

The worldsheet contribution is  $\sim \cos(A\frac{\varphi_1}{f_{\varphi_1}} + B\varphi_2)$  where  $A = f_a^2 n_1/\mathcal{F}^2$  and  $B = \mathcal{F}^{-1}$ , such that  $f_{\varphi_2} = A/B$ 

Let us compute first the decay constant from the kinetic term: if we only have one axion, the only entry of the  $\gamma$  matrix reads:

$$\gamma = \int_X \beta \wedge \star \beta = \int_C \beta^2 d\text{Vol}_C \int_Y d\text{Vol}_Y = \mathcal{V}_C^{-1} \mathcal{V}_Y = \frac{\mathcal{V}}{\mathcal{V}_C^2}, \tag{4.111}$$

since  $\int_C \beta = \int_C \mathcal{V}_C^{-1} d\text{Vol}_C = 1$ . From the kinetic energy term, we find

$$f_b^2 = \frac{\gamma}{2\pi g_s^2} = \frac{\mathcal{V}}{2\pi g_s^2 \mathcal{V}_C^2} \,. \tag{4.112}$$

This setup is only a toy-model, however we can consider the case where the CY is a fibration with Y = K3 over  $C = \mathbb{CP}^1$ . This toy example cannot have  $h^{1,1} < 2$ , so to qualitively mimic scenarios with a single model-dependent axion, we will consider only the axion arising from the base. Let us now look at the CS couplings of that axion. The instanton numbers  $N_1$ ,  $N_2$  for the two factors of the  $E_8 \times E_8$  gauge bundle over Y, defined as

$$N = \frac{1}{16\pi^2} \int \operatorname{tr} F \wedge F \,, \tag{4.113}$$

are required to be  $N_1, N_2 \ge 0$  to satisfy SUSY constraints. The Bianchi identity requires  $N_1 + N_2 = 24$  since

$$\frac{1}{16\pi^2} \int_{K3} (\operatorname{tr} R \wedge R - \operatorname{tr} F \wedge F) = \chi(K3) - \frac{1}{16\pi^2} \int_{K3} \operatorname{tr} F \wedge F = 24 - \frac{1}{16\pi^2} \int_{K3} \operatorname{tr} F \wedge F = 0,$$
(4.114)

where  $\chi(K3) = 24$  is the Euler's characteristic. Thus, from eq. (4.110),

$$n = N_1 - \frac{1}{2}\chi(K3) = N_1 - 12 \quad \to |n| \le 12.$$
 (4.115)

Let us now consider the two different cases: the absence of worldsheet instantons or the absence of gaugino condensation. In the absence of worldsheet instantons, the value for the mixing parameter reads eq. (4.87)

$$\alpha = n \frac{6g_s^2}{v^2} \sim 0.1 \,, \tag{4.116}$$

Therefore, we need to go back to the canonical basis  $\vartheta$ , with decay constants  $f_a$  and  $f_1/n_1$ , where the CS couplings read eq. (4.52), which, if taking  $n=12,\ v\sim 3$ , and  $g_s\sim 0.7$ , become  $\lambda_v\sim 0.5,\ \lambda_h\sim 1.1$ .

In the case of absence of gaugino condensation instead, we go to the mass basis  $\varphi$ , defined in eq. (4.98), where, taking the same values as before, the CS couplings read  $\lambda_{1,v} \sim 0.5$ ,  $\lambda_{1,h} \sim -0.47$ ,  $\lambda_{2,h} \sim 0.03$ .

#### **Example: Quintic**

To illustrate the general mechanism, we consider a more concrete example based on the quintic Calabi-Yau threefold  $\mathbb{CP}^4[5]$  with  $h^{1,1} = 1$ . We define a two-axion model with one model-independent axion  $\vartheta_a$  and one model-dependent axion  $\vartheta_1$ .

The quintic is reviewed in Appendix B.0.1. The triple intersection number reads  $\kappa_{111} = 5$ , such that that the internal volume is given by

$$\mathcal{V} = \frac{1}{6}\kappa_{111}v^3 = \frac{5}{6}v^3,\tag{4.117}$$

where v is the volume of the single 2-cycle. The decay constants are estimated as

$$f_a = \frac{g_s}{\sqrt{2\pi\mathcal{V}}} = \sqrt{\frac{3}{5}} \cdot \frac{g_s}{\sqrt{\pi v^3}},\tag{4.118}$$

$$f_1 = \frac{v}{\sqrt{2\pi}q_s}.\tag{4.119}$$

Let us now compute the Chern class of the Calabi-Yau, denoting H as the hypersurface corresponding to the single divisor of the quintic:

$$c(T_X) = c(T_A)/c(N_X) = \frac{(1+H)^5}{(1+5H)} = = 1 + 10H^2 + \dots$$
 (4.120)

Therefore  $c_1(T_X) = 0$ , consistently with the CY condition, and  $c_2(T_X) = 10H^2$ .

Following [156] we consider the gauge bundle  $W = V_1 + V_2 + L$ , where  $V_1, V_2$  are SU(4) gauge bundles and L is a line bundle.  $V_1$  and L are embedded in the hidden  $E_8$  whereas  $V_2$  is in the visible one. The bundle  $V_1$  is defined via the cohomology of the short exact sequence, known here as a monad,

$$0 \longrightarrow \mathcal{O}|_{X} \xrightarrow{M} \mathcal{O}(1)^{\oplus 5} \oplus \mathcal{O}(3) \xrightarrow{N} \mathcal{O}(8) \longrightarrow 0, \tag{4.121}$$

where  $\mathcal{O}(1)^{\oplus 5} = \mathcal{O}(1) \oplus \cdots \oplus \mathcal{O}(1)$ . The bundle is then

$$V = \frac{\ker(N)}{\operatorname{Im}(M)}.$$
(4.122)

Its rank is

$$\operatorname{rk}(V) = \operatorname{rk}(\mathcal{O}(1)^{\oplus 5} \oplus \mathcal{O}(3)) - \operatorname{rk}(\mathcal{O}|_X) - \operatorname{rk}(\mathcal{O}(8)) = 4, \tag{4.123}$$

confirming that it is an SU(4) gauge bundle.

The total Chern class is

$$c(V) = \frac{c(\mathcal{O}(1)^{\oplus 5} \oplus \mathcal{O}(3))}{c(\mathcal{O}|_X) c(\mathcal{O}(8))} = \frac{(1+H)^5(1+3H)}{(1+8H)}$$
$$= (1+H)^5(1+3H)(1-8H+64H^2+\dots)$$
$$= 1+25H^2+\dots$$
 (4.124)

so that  $c_2(V) = 25H^2$ . We can now compute the topological CS coupling:

$$n_{1} = \int_{X} \beta \wedge \frac{1}{16\pi^{2}} \left[ \operatorname{tr}_{1}(\overline{F} \wedge \overline{F}) - \frac{1}{2} \operatorname{tr}(\overline{R} \wedge \overline{R}) \right]$$

$$= \int_{X} \beta \wedge \left[ c_{2}(V_{1}) - \frac{1}{2} c_{2}(TX) \right]$$

$$= \left( 25 - \frac{1}{2} \cdot 10 \right) \int_{X} \beta \wedge H^{2}$$

$$= 20 \int_{Y} \beta \wedge H^{2}.$$

$$(4.125)$$

Since  $PD[\beta] = \Pi_4$  is a 4-cycle and  $h^{1,1}(X) = 1$ , every 4-cycle is homologous to H, so  $[\Pi_4] = m[H]$ . With the normalization  $\int_{\Sigma} \beta = 1$ , we set m = 1, hence

$$n_1 = 20 H^3 = 20 \times 5 = 100.$$
 (4.126)

This is the Chern-Simons coefficient coupling the axion to the gauge sector.

GC The squashing parameter defined in eq. (4.87) becomes:

$$\alpha = n \cdot g_s^2 \cdot \frac{6}{5v^2}.\tag{4.127}$$

To remain within the perturbative regime  $V \lesssim 20$ , we bound  $v \lesssim 2.5$ , leading to

$$\alpha \gtrsim 40g_s^2 \gtrsim 20$$
 for  $g_s \sim 0.7$ . (4.128)

This implies large kinetic mixing:

$$\mathcal{L}_{kin} = \frac{1}{2} (\partial \varphi_1)^2 + \frac{1}{2} (\partial \varphi_2)^2 + \partial \varphi_1 \partial \varphi_2. \tag{4.129}$$

We then rotate to the mass basis

$$\chi_1 = \varphi_1 + \varphi_2 = \vartheta_a, \qquad \chi_2 = \varphi_1 - \varphi_2 = \alpha \vartheta_1, \tag{4.130}$$

with decay constants

$$f_{\chi_1} = f_a, \qquad f_{\chi_2} = \frac{f_1}{\alpha},$$
 (4.131)

effectively lowering the model dependent axion decay constant by a factor of  $\alpha$ . The Chern-Simons couplings in this basis are

$$\lambda_{\chi_1,v} = -\lambda_{\chi_2,v} = 8ng_s^2 \cdot \left(\frac{1}{\frac{5\pi v^3}{6} + g_s^2 vn}\right),\tag{4.132}$$

$$\lambda_{\chi_1,h} = -\lambda_{\chi_2,h} = -8ng_s^2 \cdot \left(\frac{1}{\frac{5\pi v^3}{6} - g_s^2 vn}\right). \tag{4.133}$$

For example, taking plausible values v = 3, n = 100, and  $g_s = 0.7$  gives

$$\lambda_{\chi_1,v} \approx 1.8, \qquad \lambda_{\chi_1,h} \approx -5.2,$$

$$(4.134)$$

showing a visible/hidden hierarchy induced by the large anomaly coefficient.

**noGC** Let us now consider the possibility of no gaugino condensation. In this case there will be one axion only coupled to the dark sector, and one coupled to both dark and visible sector. The CS couplings are defined in eq. (4.105). In this case, by taking k = 1 and  $g_s = 0.7$ , we can also estimate the decay constants as

$$f_a = \frac{g_s}{\sqrt{2\pi V}} = \sqrt{\frac{3}{5}} \frac{g_s}{\sqrt{\pi v^3}}, \qquad f_1 = \frac{v}{\sqrt{2\pi}g_s}$$
 (4.135)

The Chern-Simons coupling read

$$\lambda_{\varphi_1,v} \sim 1.8, \quad \lambda_{\varphi_1,h} \sim -0.1, \quad \lambda_{\varphi_2,h} \sim -4.7.$$
 (4.136)

One axion is coupled only to the hidden sector, whereas the first one is coupled to both sectors but mainly to the visible one.

#### 4.2.5Three-Axion System

We now extend our setup to include three axions: two model-dependent axions  $\vartheta_1, \vartheta_2$ and one model-independent axion  $\theta_a$ , with respective decay constants  $f_1$ ,  $f_2$ , and  $f_a$ . The Chern-Simons couplings take the form:

$$\mathcal{L}_{CS} = \frac{1}{16\pi^2} \left( \frac{\vartheta_a}{f_a} + \frac{n_1}{f_1} \vartheta_1 + \frac{n_2}{f_2} \vartheta_2 \right) \operatorname{tr}_1 F \wedge F + \frac{1}{16\pi^2} \left( \frac{\vartheta_a}{f_a} - \frac{n_1}{f_1} \vartheta_1 - \frac{n_2}{f_2} \vartheta_2 \right) \operatorname{tr}_2 F \wedge F.$$
(4.137)

The resulting potential receives contributions from QCD, gaugino condensation, and worldsheet instantons:

$$V_{\text{mass}} = -\Lambda_{\text{QCD}}^4 \cos\left(\frac{\vartheta_a}{f_a} + \frac{n_1}{f_1}\vartheta_1 + \frac{n_2}{f_2}\vartheta_2 + \delta\right) - \Lambda_{\text{gc}}^4 \cos\left(\frac{\vartheta_a}{f_a} - \frac{n_1}{f_1}\vartheta_1 - \frac{n_2}{f_2}\vartheta_2\right) - \Lambda_{\text{ws},1}^4 \cos\left(\frac{\vartheta_1}{f_1}\right) - \Lambda_{\text{ws},2}^4 \cos\left(\frac{\vartheta_2}{f_2}\right).$$

$$(4.138)$$

Expanding the potential to second order gives the mass matrix:

$$\begin{pmatrix}
\frac{\Lambda_{\rm gc}^4 + \Lambda_{\rm QCD}^4}{f_a^2} & \frac{n_1(\Lambda_{\rm QCD}^4 - \Lambda_{\rm gc}^4)}{f_a f_1} & \frac{n_2(\Lambda_{\rm QCD}^4 - \Lambda_{\rm gc}^4)}{f_a f_2} \\
\frac{n_1(\Lambda_{\rm QCD}^4 - \Lambda_{\rm gc}^4)}{f_a f_1} & \frac{n_1^2(\Lambda_{\rm QCD}^4 + \Lambda_{\rm gc}^4) + \Lambda_{\rm ws,1}^4}{f_1^2} & \frac{n_1 n_2(\Lambda_{\rm QCD}^4 + \Lambda_{\rm gc}^4)}{f_1 f_2} \\
\frac{n_2(\Lambda_{\rm QCD}^4 - \Lambda_{\rm gc}^4)}{f_a f_2} & \frac{n_1 n_2(\Lambda_{\rm QCD}^4 + \Lambda_{\rm gc}^4)}{f_1 f_2} & \frac{n_2^2(\Lambda_{\rm QCD}^4 + \Lambda_{\rm gc}^4) + \Lambda_{\rm ws,2}^4}{f_2^2}
\end{pmatrix}.$$
(4.139)

We now analyze this system in different limiting cases.

**noGC** - **Isotropic** We begin with the case where gaugino condensation is absent, and the axion potential receives contributions only from QCD and worldsheet instantons. In isotropic compactifications with  $v \sim \mathcal{V}^{1/2} \sim 3$ , the worldsheet instanton contribution can dominate: even if  $W_0 \sim 10^{-13} M_{Pl}$ ,

$$\Lambda_{\rm ws}^4 \sim 10^{-22} M_{\rm Pl}^4 \gg \Lambda_{\rm QCD}^4 \sim 10^{-75} M_{\rm Pl}^4.$$
 (4.140)

Assuming  $\Lambda_{\rm ws,1} \approx \Lambda_{\rm ws,2} \gg \Lambda_{\rm QCD}$ , and  $f_1 \sim f_2$ , one axion (aligned with QCD) which is mostly  $\vartheta_a$  remains light, while the other two become heavy.

The mass basis  $\varphi$  in this case will be the original  $\vartheta$  one, at first order, where the light axion will be mainly  $\vartheta_a$  while the model dependent axions will get contributions mainly from worldsheet instantons:

$$\frac{\varphi_1}{f_{\varphi_1}} = \frac{\vartheta_a}{f_a}, \qquad m_{\varphi_1}^2 \simeq \frac{\Lambda_{\text{QCD}}^4}{f_a^2}, \qquad (4.141)$$

$$\frac{\varphi_2}{f_{\varphi_2}} = \frac{\vartheta_1}{f_1}, \qquad m_{\varphi_2}^2 = \frac{\Lambda_{\text{ws}}^4}{f_1^2}, \qquad (4.142)$$

$$\frac{\varphi_3}{f_{\varphi_3}} = \frac{\vartheta_2}{f_2}, \qquad m_{\varphi_3}^2 = \frac{\Lambda_{\text{ws}}^4}{f_1^2}. \qquad (4.143)$$

$$\frac{\varphi_2}{f_{\varphi_2}} = \frac{\vartheta_1}{f_1}, \qquad m_{\varphi_2}^2 = \frac{\Lambda_{\text{ws}}^4}{f_1^2},$$
 (4.142)

$$\frac{\varphi_3}{f_{\varphi_3}} = \frac{\vartheta_2}{f_2}, \qquad m_{\varphi_3}^2 = \frac{\Lambda_{\text{ws}}^4}{f_1^2}.$$
 (4.143)

All axions couple to both visible and hidden sectors, and the CS couplings can be evaluated by separating the contribution from the

$$\lambda_{\varphi_i, \text{hv}} = \pm \tilde{\lambda}_{\varphi_i} \cdot \frac{\pm 8n_i k g_s^2}{\pi \mathcal{V} \pm g_s^2 v_i n_i},\tag{4.144}$$

with leading-order expressions for the  $\tilde{\lambda}_{\varphi_i} \sim 1$ . In the absence of gaugino condensation, one QCD axion is light, while the others may be much heavier, especially in isotropic compactifications.

**noGC** - Anisotropic In anisotropic compactifications, one worldsheet instanton term can be exponentially suppressed, allowing a second axion to remain light. In this regime, we obtain a light axion  $\varphi_1$  orthogonal to the heavier combinations lifted by dominant worldsheet effects. Taking  $v \sim 30$  and small remaining cycles, we can still ensure

$$\mathcal{V} = \frac{1}{6} \kappa_{ijk} v^i v^j v^k < 25, \tag{4.145}$$

so that only one worldsheet instanton is suppressed. We model this by setting

$$\Lambda_{\text{ws }2}^4 = \varepsilon \Lambda_{\text{ws }1}^4, \quad \text{with } \varepsilon \ll 1,$$
(4.146)

with small  $\varepsilon$  parameter. The axion mass basis is:

$$\varphi_{1} = \frac{\vartheta_{2}}{f_{2}} - \frac{n_{2}\vartheta_{a}}{f_{2}},$$

$$\varphi_{2} = \frac{f_{2}^{2}\vartheta_{a} + \vartheta_{2}n_{2}f_{a}^{2}}{n_{2}f_{a}^{2}f_{2}},$$

$$\varphi_{3} = \frac{\vartheta_{2}}{f_{2}} + \frac{\frac{\vartheta_{1}(n_{2}^{2}f_{a}^{2} + f_{2}^{2})(n_{1}^{2}\Lambda_{\text{gc}}^{4} - \Lambda_{\text{ws},1}^{4})}{f_{2}n_{1}f_{a}^{2}\Lambda_{\text{ws},1}^{4}} - \frac{f_{2}\vartheta_{a}}{f_{a}^{2}} + \frac{f_{2}\vartheta_{1}\left(\frac{\Lambda_{\text{ws},1}^{4}}{\Lambda_{\text{gc}}^{4}} + n_{1}^{2}\right)}{f_{1}^{2}n_{1}}}{f_{2}n_{1}},$$

$$(4.147)$$

with masses

$$m_{\varphi_1}^2 = \frac{\varepsilon \Lambda_{\text{ws},1}^4}{n_2^2 f_a^2 + f_2^2},$$

$$m_{\varphi_2}^2 = \Lambda_{\text{QCD}}^4 \left( \frac{1}{f_a^2} + \frac{n_2^2}{f_2^2} \right),$$

$$m_{\varphi_3}^2 = \frac{\Lambda_{\text{ws},1}^4}{f_1^2}.$$
(4.148)

Thus, the axion  $\varphi_1$  becomes ultra-light,  $\varphi_2$  is at the QCD scale, and  $\varphi_3$  is heavy. This hierarchy is only achievable in anisotropic scenarios. The CS couplings again take the form eq. (4.144) and the leading  $\tilde{\lambda}_{\varphi_i}$  are given by a combination of the decay constants and the  $n_i$ . We report them in Appendix B.0.3 as they are lengthy and their functional form is not instructive. In anisotropic compactifications, therefore, an ultralight axion with visible couplings can arise in the absence of gaugino condensation.

**GC** - **Isotropic** When gaugino condensation is present, its associated scale typically dominates over QCD and may compete with worldsheet instantons depending on the compactification and the rank of the condensing gauge group. We first consider the isotropic limit. The scale of gaugino condensation is given by

$$\Lambda_{\rm gc}^4 \sim \mu^4 e^{-\frac{2\pi}{Ng^2} \mathcal{V}}.$$
(4.149)

Assuming similar  $\mu$  for  $V_{\rm gc}$  and  $V_{\rm ws}$ , the hierarchy becomes in the isotropic case:

$$\Lambda_{\text{ws}}^4 \equiv \Lambda_{\text{ws},1}^4 \simeq \Lambda_{\text{ws},2}^4 \gg \Lambda_{\text{oc}}^4 \gg \Lambda_{\text{OCD}}^4. \tag{4.150}$$

As a result, no axion remains at the QCD scale, and observable axions are generically heavy. The axion mass basis is:

$$\varphi_{1} = -\frac{\vartheta_{2}}{f_{2}} - \frac{\vartheta_{1}n_{2}}{f_{1}n_{1}},$$

$$\varphi_{2} = \frac{\vartheta_{a}\left(f_{a}^{2}\left(\frac{\Lambda_{\text{ws}}^{4}}{\Lambda_{\text{gc}}^{4}} + n_{1}^{2} + n_{2}^{2}\right) - f_{1}^{2}\right)}{f_{1}n_{2}f_{a}^{2}} + \frac{\vartheta_{2}}{f_{2}} + \frac{\vartheta_{1}n_{1}}{f_{1}n_{2}},$$

$$\varphi_{3} = \frac{\vartheta_{2}}{f_{2}} + \frac{\vartheta_{1}n_{2}}{f_{1}n_{1}},$$
(4.151)

with masses

$$m_{\varphi_1}^2 = \frac{\Lambda_{\text{ws}}^4}{f_1^2},$$

$$m_{\varphi_2}^2 = \Lambda_{\text{gc}}^4 \frac{1}{f_a^2},$$

$$m_{\varphi_3}^2 = \frac{n_1^2 \Lambda_{\text{gc}}^4 + n_2^2 \Lambda_{\text{gc}}^4 + \Lambda_{\text{ws}}^4}{f_1^2}.$$
(4.152)

**GC** - **Anisotropic** In this regime, one worldsheet instanton is exponentially suppressed, allowing one axion to remain light (at the QCD axion mass scale) despite the presence of gaugino condensation.

$$\Lambda_{\text{ws},1}^4 \gg \Lambda_{\text{gc}}^4 \gg \Lambda_{\text{QCD}}^4 \gg \Lambda_{\text{ws},2}$$
 (4.153)

$$\varphi_{1} = \frac{\vartheta_{2}}{f_{2}} + \frac{\vartheta_{a}n_{2}}{f_{2}},$$

$$\varphi_{2} = -\frac{f_{2}^{2}\vartheta_{a} - \vartheta_{2}n_{2}f_{a}^{2}}{n_{2}f_{a}^{2}f_{2}},$$

$$\varphi_{3} = \frac{\vartheta_{2}}{f_{2}} + \frac{\frac{\vartheta_{1}(n_{2}^{2}f_{a}^{2} + f_{2}^{2})(n_{1}^{2}\Lambda_{gc}^{4} - \Lambda_{ws,1}^{4})}{f_{2}n_{1}f_{a}^{2}\Lambda_{ws,1}^{4}} - \frac{f_{2}\vartheta_{a}}{f_{a}^{2}} + \frac{f_{2}\vartheta_{1}\left(\frac{\Lambda_{ws,1}^{4}}{\Lambda_{gc}^{4}} + n_{1}^{2}\right)}{f_{1}^{2}n_{1}}}{n_{2}},$$

$$(4.154)$$

with masses

$$m_{\varphi_1}^2 = \frac{4n_2^2 \Lambda_{\text{QCD}}^4}{n_2^2 f_a^2 + f_2^2},$$

$$m_{\varphi_2}^2 = \Lambda_{\text{gc}}^4 \left(\frac{1}{f_a^2} + \frac{n_2^2}{f_2^2}\right),$$

$$m_{\varphi_3}^2 = \frac{n_1^2 \Lambda_{\text{gc}}^4 + \Lambda_{\text{ws},1}^4}{f_1^2}.$$
(4.155)

#### Example: Bi-cubic CICY

Let us consider the bi-cubic CICY defined as a degree-(3,3) hypersurface  $\mathbb{P}^2 \times \mathbb{P}^2$  with Hodge numbers  $(h^{1,1},h^{2,1})=(2,83)$ .

$$\begin{array}{c|c}
\mathbb{P}^2 & 3 \\
\mathbb{P}^2 & 3
\end{array},$$
(4.156)

Its Chern class and intersection numbers are computed in Appendix B.0.2 Following [157], we consider a vector bundle V defined as

$$0 \to V \to \mathcal{O}(1,0)^{\oplus 3} \oplus \mathcal{O}(0,1)^{\oplus 3} \to \mathcal{O}(1,1) \oplus \mathcal{O}(2,2) \to 0 \tag{4.157}$$

which gives a bundle with structure group G = SU(4), such that in 4D the gauge group is a SO(10) GUT, which reproduces an MSSM-like spectrum after a suitable Wilson line breaks the  $SO(10) \rightarrow SU(3) \times SU(2) \times U(1)_Y \times U(1)_{B-L}$ . In the original example in order to satisfy anomaly cancellation they considered M5-branes, such that the hidden sector bundle  $\tilde{V}$  could remain trivial. If  $c_2(TX) - c_2(V)$  is an effective class on the CY, then the anomaly and the effectiveness conditions are automatically satisfied for a trivial hidden bundle and a five brane class  $W = c_2(TX) - c_2(V)$  [139], as the actual anomaly cancellation condition reads

$$c_2(TX) - c_2(V) - c_2(\tilde{V}) = [W],$$
 (4.158)

where [W] in an effective five-brane class. However, we are interested in the hidden gauge sector, and therefore we chose a non-Abelian vector bundle with structure group SU(N) in the hidden sector, such that the resulting 4D gauge group is its commutant inside  $E_8$ . Using the basis of divisors  $H_1$ ,  $H_2$  corresponding to the two  $\mathbb{P}^2$  factors, the second Chern class of the tangent bundle reads

$$c(TX) = \frac{(1+H_1)^3(1+H_2)^3}{(1+3H_1+3H_2)} \qquad c_2(TX) = 3H_1^2 + 3H_2^2 + 9H_1H_2, \tag{4.159}$$

while the second Chern class of the monad bundle reads

$$c(V) = \frac{(1+H_1)^3(1+H_2)^3}{(1+H_1+H_2)(1+2H_1+2H_2)} \qquad c_2(V) = H_1^2 + H_2^2 + 5H_1H_2. \tag{4.160}$$

To satisfy the anomaly cancellation condition, taking [W] = 0, we need

$$c_2(\tilde{V}) = 2H_1^2 + 2H_2^2 + 4H_1H_2 \qquad c_1(\tilde{V}) = 0.$$
 (4.161)

Take

$$0 \longrightarrow \tilde{V} \longrightarrow \bigoplus_{i}^{r+s} \mathcal{O}(a_i, b_i) \xrightarrow{f} \bigoplus_{i=1}^{s} \mathcal{O}(c_j, d_j) \longrightarrow 0$$
 (4.162)

and ask to satisfy the conditions eq. (4.161). This translates into

$$\sum_{i} a_{i} = \sum_{j} c_{j} \qquad \sum_{i} b_{i} = \sum_{j} d_{j},$$

$$\sum_{i} \frac{1}{2} \left( a_{i}^{2} H_{1}^{2} + 2a_{i}b_{i}H_{1}H_{2} + b_{i}^{2}H_{2}^{2} \right) = \sum_{j} \frac{1}{2} \left( c_{j}^{2} H_{1}^{2} + 2c_{j}d_{j}H_{1}H_{2} + d_{j}^{2}H_{2}^{2} \right).$$

$$(4.163)$$

One example of monad construction that satisfies this is

$$0 \longrightarrow \tilde{V} \longrightarrow \mathcal{O}(1,0)^{\oplus 6} \oplus \mathcal{O}(0,1)^{\oplus 4} \xrightarrow{f} \mathcal{O}(2,0)^{\oplus 2} \oplus \mathcal{O}(1,2)^{\oplus 2} \longrightarrow 0 \tag{4.164}$$

which is a rank 6 gauge bundle giving an SU(2) hidden gauge sector in 4D. This can be further broke down to abelian U(1)s via Wilson lines. The tree level DUY equation is satisfied, as  $c_1(V) = 0$ . The bundle's stability is assured if any subsheaf  $\mathcal{F} \in V$  with  $0 < \text{rk}(\mathcal{F}) < \text{rk}(V)$  has  $\mu(\mathcal{F}) < \mu(V) = 0$ . Therefore, one would need to check that for every subsheaf the slope is negative. One way to ensure this is to check that  $H^0(X, V) = 0$ , which would be sufficient [139].

Another possibility is instead to have the line bundle  $\mathcal{L} = \mathcal{O}(2,2)$ , for which the second Chern character reads  $\operatorname{ch}_2(\mathcal{L}) = \frac{1}{2}c_1^2 = \frac{1}{2}\left(2H_1 + 2H_2\right)^2$ . This would result in a 4D gauge group that looks like  $E_7 \times U(1)$ , where the U(1) would be anomalous as it is there also in the structure group, and thus becomes massive by eating one of the two model dependent axions. This will always happen when there is a line bundle in the structure group. In this case we are effectively back to the two-axion scenario, with

$$n_1 = n_2 = \int H_1\left(c_2(V) - \frac{1}{2}c_2(TX)\right) = 3.$$
 (4.165)

#### Example: CICY with U(4) Bundle

Let us take a U(4) bundle on the CICY studied in [156]

$$\begin{array}{c|c}
\mathbb{P}^3 & 4 \\
\mathbb{P}^1 & 2
\end{array},$$
(4.166)

which has  $h^{1,1} = 2$  and  $h^{2,1} = 86$ . Calling  $\eta_1$  the 2-form defined on  $\mathbb{P}_3$  and  $\eta_2$  the two-form defined on  $\mathbb{P}_1$ , the Stanley-Reissner ideal, which contains those coordinates that cannot be set to zero simultaneously (or equivalently, those divisors which do not intersect) can be read from the D-terms to be

$$SR = \{\eta_1^4, \eta_2^2\}. \tag{4.167}$$

The intersection form reads

$$I_3 = 2\eta_1^3 + 4\eta_1^2 \eta_2. (4.168)$$

Therefore, there exist 2 possible 4-forms on the CY:

$$\{\eta_1^2, \eta_1 \eta_2\}$$
. (4.169)

The Chern classes can be computed via

$$c(TX) = \frac{(1+\eta_1)^2(1+\eta_2^2)}{(1+4\eta_1+2\eta_2)} = \dots = 1+6\eta_1^2+8\eta_1\eta_2+\dots$$
 (4.170)

The second Chern class can be read from the equation above to be  $c_2(TX) = 6\eta_1^2 + 8\eta_1\eta_2$ . The gauge bundle chosen to reproduce the SM-like sector in the first  $E_8$  reads

$$W = V \oplus L^{-1} \tag{4.171}$$

where the line bundle is taken to be  $L = \mathcal{O}(-2, 2)$  and the U(4) bundle V is defined via

$$0 \to V \to \mathcal{O}(1,0)^{\oplus 2} \oplus \mathcal{O}(0,1)^{\oplus 2} \oplus \mathcal{O}(1,1)^{\oplus 2} \Big|_{CY} \xrightarrow{f} \mathcal{O}(4,1) \oplus \mathcal{O}(2,1) \Big|_{CY} \to 0 \quad (4.172)$$

such that it satisfies the tadpole condition

$$c_2(V) - c_1^2(L) = c_2(TX),$$
 (4.173)

and the map f is chosen to not degenerate at any point. One can indeed check that

$$c(V) = \frac{(1+\eta_1)^2(1+\eta_2^2)(1+\eta_1+\eta_2)^2}{(1+4\eta_1+\eta_2)(1+2\eta_1+\eta_2)},$$
(4.174)

such that

$$c_2(V) = \eta_2^2 + 10\eta_1^2 = 10\eta_1^2, (4.175)$$

since  $\eta_2^2 = 0$  as for the SR. Taking the two axions defined as the dimensional reduction of the  $B_2$  as

$$B = b_1 \eta_1 + b_2 \eta_2 \,, \tag{4.176}$$

we can compute the  $n_i$  as

$$n_{1} = \int \eta_{1} \wedge \left( c_{2}(V) - c_{1}^{2}(L) - \frac{1}{2}c_{2}(TX) \right) = \int \eta_{1} \wedge \left( \frac{1}{2}c_{2}(TX) \right)$$

$$= 3 \int \eta_{1}^{3} + 4 \int \eta_{1}^{2}\eta_{2} = 6 + 16 = 22$$

$$n_{2} = \int \eta_{2} \wedge \left( \frac{1}{2}c_{2}(TX) \right) = 3 \int \eta_{1}^{2}\eta_{2} = 6.$$

$$(4.177)$$

Since W was taken such that there is no gauge bundle embedded in the hidden sector, the 4D gauge group remains  $E_8$ .

**noGC** To arrive at cases where the hidden  $E_8$  is fully broken down to just U(1)-factors, we may need to turn on non-trivial Wilson lines if the gauge bundle is insufficient to do the full breaking on its own. Getting such Wilson lines requires the CY to have a non-trivial first homotopy group. Besides a very small number directly existing within known sets of CYs such as the CICYs, such CY manifolds can be obtained by modding out a freely acting discrete involution from an original CY possessing the required discrete symmetry [158–160].

Given that we only have two non vanishing intersection numbers,  $\kappa_{111}$  and  $\kappa_{112}$ , we find that the volume reads

$$\mathcal{V} = \frac{1}{6} \left( 2v_1^3 + 4v_1^2 v_2 \right) . \tag{4.178}$$

In this case, let us look at the possible CS couplings. In the isotropic case, we take  $v_1 \sim v_2 \sim 3$ , we find that the CS couplings read

$$\lambda_{\varphi_1,v} \sim 2.5 \,, \quad \lambda_{\varphi_2,v} \sim 1.2 \,, \quad \lambda_{\varphi_3,v} \sim -0.02$$

$$\lambda_{\varphi_1,h} \sim 1.4 \,, \quad \lambda_{\varphi_2,h} \sim 0.7 \,, \quad \lambda_{\varphi_3,v} \sim 0.01$$
(4.179)

In this example it is difficult to construct an anisotropic case: knowing the intersection numbers from the expression of the volume, we see that if we take the limiting case  $v_1 \sim 1$ , in order to maintain the volume smaller than  $\sim 20$ , we have to take at most  $v_2 \sim 5$ . In this case we find

$$\lambda_{\varphi_1,v} \sim 8.2 \,, \quad \lambda_{\varphi_2,v} \sim 6.1 \,, \quad \lambda_{\varphi_3,v} \sim 0.5$$

$$\lambda_{\varphi_1,h} \sim 29.4 \,, \quad \lambda_{\varphi_2,h} \sim 40.1 \,, \quad \lambda_{\varphi_3,h} \sim -2.4 \,.$$
(4.180)

### 4.2.6 Three-Axion Summary

Let us summarize our findings by recalling that  $\varepsilon$  is a small parameter used in the anisotropic case relating the two worldsheet instanton scales, and the hierarchy:

$$\Lambda_{\rm ws}^4 \gg \Lambda_{\rm gc}^4 \gg \Lambda_{\rm QCD}^4 \gg \varepsilon \Lambda_{\rm ws}^4$$
. (4.181)

$$\begin{array}{|c|c|c|c|}\hline {\bf noGC} & {\bf Isotropic} & {\bf FDM} & & {\bf noGC} & {\bf Anisotropic} & {\bf FDM} \\ \hline \\ m_{\varphi}^2 = \begin{pmatrix} \frac{\Lambda_{\rm ws}^4}{f_1^2} \\ \frac{\Lambda_{\rm QCD}^4}{f_a^2} \\ \frac{\Lambda_{\rm ws}^4}{f_1^2} \end{pmatrix} & \times & m_{\varphi}^2 = \begin{pmatrix} \varepsilon \frac{\Lambda_{\rm ws}^4}{n_2^2 f_a^2 + f_2^2} \\ \Lambda_{\rm QCD}^4 \left( \frac{1}{f_a^2} + \frac{n_2^2}{f_2^2} \right) \\ \frac{\Lambda_{\rm ws}^4}{f_1^2} \end{pmatrix} & \checkmark \\ \hline \\ {\bf GC} & {\bf Isotropic} & {\bf FDM} & {\bf GC} & {\bf Anisotropic} & {\bf FDM} \\ \hline \\ m_{\varphi}^2 = \begin{pmatrix} \frac{\Lambda_{\rm ws}}{f_1^2} \\ \frac{\Lambda_{\rm gc}^4}{f_1^2} \\ \frac{\Lambda_{\rm gc}^4}{f_1^2} \end{pmatrix} & \times & m_{\varphi}^2 = \begin{pmatrix} \frac{4n_2^2 \Lambda_{\rm QCD}^4}{n_2^2 f_a^2 + f_2^2} \\ \Lambda_{\rm gc}^4 \left( \frac{1}{f_a^2} + \frac{n_2^2}{f_2^2} \right) \\ \frac{n_1^2 \Lambda_{\rm gc}^4 + \Lambda_{\rm ws}^4}{f_1^2} \end{pmatrix} & \times & \\ \end{array}$$

Table 4.3: Summary of Mass Matrices in Different Regimes. The last column refers to the possibility of having a fuzzy dark matter candidate. This is available only in the  $\boxed{\text{noGC}}$  anisotropic case, where the FDM candidate aligns with  $\varphi_1$ .

We find that a fuzzy dark matter candidate can arise only in the <u>noGC</u> anisotropic configuration. In all other setups, the hierarchy of the contirbutions to the scalar potential prevents the presence of an extremely light axion.

Our analysis covered both two- and three-axion systems. A compactification with larger  $h^{1,1}$ , and thus a greater number of axions, would proceed analogously, so higher- $h^{1,1}$  cases are not discussed here as they would not be illustrative. The general conclusion is that at least one potential term must be absent (as in the  $\boxed{\text{noGC}}$  case) or strongly suppressed (as in the anisotropic case) to address the Strong CP problem. Achieving a fuzzy dark matter candidate requires both the absence of gaugino condensation and the presence of a highly suppressed worldsheet instanton, which requires a fibred CY.

The relevant physical description is given in the mass basis, where the Chern–Simons couplings become nontrivial combinations of the decay constants and topological quantities. In certain compactifications, it is possible to achieve a clean separation between couplings to the visible and hidden sectors. In special cases, some couplings vanish entirely, allowing for axions that interact exclusively with one of the two sectors. Such configurations must, however, be examined on a case-by-case basis.

### 4.3 Remarks

We have investigated axion physics in Calabi-Yau compactifications of the heterotic string, with a focus on the mass spectrum and couplings of both the model-independent and model-dependent axions. Starting from the effective four-dimensional theory, we analyzed the kinetic structure, Chern-Simons couplings, and non-perturbative potentials generated by gauge and stringy instantons, including gaugino condensation and world-sheet effects. We examined how axions acquire masses through these non-perturbative effects and under what conditions one linear combination remains sufficiently light and

4.3. Remarks 69

dominantly aligned with the QCD direction to solve the strong CP problem. Particular attention was given to the alignment of non-perturbative terms and the role of kinetic mixing, showing that successful axion phenomenology in string compactifications depends not only on the presence of instanton corrections, but also on their relative alignment in axion field space. These constraints impose nontrivial requirements on the geometry and gauge bundle data of the compactification. We illustrated these features with explicit heterotic construction on Calabi-Yau manifolds with  $h^{1,1}=1,2$ . These example highlight how decay constant hierarchies and physical axion couplings can be engineered in principle, but also emphasizes that achieving a light axion typically requires some work. Upon diagonalizing the mass and kinetic matrices, we extracted the physical decay constants and recast the Chern–Simons couplings in the mass basis, identifying the surviving light states and their coupling structure.

Altogether, our results show that the heterotic axiverse provides a compelling and highly constrained setting for axion phenomenology. While the presence of multiple axions is generic, realizing light axions, particularly those that can solve the strong CP problem or play a role in cosmology, is not automatic. This observation has important implications for the landscape of viable string models with axionic dark matter or observable axion couplings.

## Chapter 5

# Spectator Axions and Inflation

Axions coupled to gauge fields via CS couplings are common in string theory. At a generic point in the string Landscape viable for cosmology, one could expect the EFT to contain an inflationary sector and a spectator sector consisting of multiple axions and their hidden gauge theories. Such scenarios are multi-spectator generalizations of the rolling axion models of [161, 162] and of spectator chromonatural inflation (SCNI) models [93, 163], themselves related to natural inflation [84, 86, 87, 164–174]. We will refer to such models as Multiple Abelian Spectator Axion (MASA) and Multiple non-Abelian Spectator Axion (MASA) inflationary models, depending on the nature of the hidden gauge groups.

During inflation, spectator axions roll down their potential and, as a result of the CS couplings, dissipate into hidden gauge bosons. The enhanced gauge quanta can then source significant gravitational waves and, depending on the specific setup, scalar fluctuations. Among the most interesting features that ensue is a large chiral GW spectrum, which may also exhibit a blue or bump-like structure. Multi-spectator models support a rich peak structure for the gravitational wave signal, giving rise to what we call a "gravitational wave forest". What makes this class of models particularly compelling is the realistic prospect of testing significant portions of their parameter space via upcoming cosmological probes. Chirality of the GWs may be put to the test at CMB scales [176,177] as well as at interferometers [177–180]. We emphasize that this specific feature, which can be traced back to the parity breaking CS term (including the gravitational CS [181–183]), is a very distinctive signature of this class of models<sup>2</sup>. Large GW non-Gaussianities [184–187] are yet another testable feature of such scenarios. In the case of Abelian gauge sectors the sourcing mechanism for scalar curvature and tensor perturbations, the former being mediated by the axion field, are analogous. This makes for peaked scalar and GW spectra, a possibility that has been investigated also in the context of primordial black holes as a dark matter candidate [188, 189].

Thus, a potentially generic signature of inflationary models descending from string theory is a gravitational wave forest from a plethora of spectator axions during inflation. Observations of the corresponding peak-like structure in the GW spectrum would shed light on the number of axions in the EFT as well as their properties – thus constituting

<sup>&</sup>lt;sup>1</sup>This term was used in [175] for gravitational waves from the axiverse, where a different mechanism was in play with respect to the one we shall employ here.

<sup>&</sup>lt;sup>2</sup>One should add, vis-à-vis birefringence, that at CMB scales low multiples are more effective at constraining primordial chirality [176].

a form of gravitational spectroscopy of the axiverse. As there is no guarantee in string constructions that additional axions beyond the QCD axion will couple to the Standard Model<sup>3</sup>, gravitational wave signals may represent one of the very few observables to test the axiverse. For other discussions on observing the axiverse, see [17,192–202]. Note that an axion-driven GW forest can have two sources. One is comprised of the spectators we are discussing here. The second arises from the inflationary sector itself if it occurs in several shortly interrupted epochs [174] of slow-roll axion inflation [86,87].

In general the salient features of the spectator models GW signal depend heavily on the specifics of the gauge group, the axion initial conditions and mass, and the strength of the axion-gauge coupling. The latter is particularly relevant. As axions enjoy a (perturbative) continuous shift symmetry, they couple to gauge fields via the usual Chern-Simons terms with a coupling we denote by  $\lambda$  (see eq. (5.1) below). To get a sizable GW signal, one requires that  $\lambda \simeq \mathcal{O}(10)$ , or larger still, in the non-Abelian case. Superficially this appears to be an innocuous demand, but in truth it is non-trivial and challenging to realize from a UV perspective [203, 204]. The fundamental challenge is that  $\lambda \propto m\alpha$ , where m is some integer and  $\alpha$  is the fine-structure constant of the hidden gauge group coupled to the spectator axion. For non-Abelian spectators, the models in the literature require small values of  $\alpha$ , and so attaining  $\lambda \gtrsim 10$  requires a large integer m. The primary difficulty of UV embeddings of SCNI models lies in realizing a sufficiently large m. In contrast, spectator axions coupled to Abelian gauge fields do not self-interact, one can take larger values of  $\alpha$  and thereby reduce the demand on the integer m. That is not to say that Abelian spectators are without constraints - attempts to boost the Chern-Simons coupling can result in issues such as the descent of Landau poles. We will revisit constraints on both Abelian and non-Abelian spectator models.

If one wishes to make deeper connections between spectator models and the string axiverse, one must explore how to realize spectator sectors within string compactifications. For SCNI models, this task was considered in [205, 206]. The axionic portion of the spectator sector can arise from dimensional reduction of p-forms in the 10d string theories. The gauge sector of spectator models depends greatly on which corner of the string landscape one works in. We will largely focus on type IIB string theory compactified on orientifolded Calabi-Yau (CY) manifolds with quantized 3-form fluxes, D7-branes and O7-orientifold planes. In this setting, 4d axions arise as KK zero modes of the 4-form  $C_4$  and 2-form  $C_2$  gauge fields. As mentioned above, the number of axions is governed by the number of compact n-dimensional sub-manifolds (n-cycles) of the 6d CY manifold chosen, as well as the structure of the orientifold projection: some number of 4-form axions are always present, while 2-form axions arise from a non-trivial 'projection-odd' sector of the orientifold action. Gauge sectors are realized by the worldvolume theory of D7-branes wrapping 4-cycle submanifolds of the CY and permeating our 4d spacetime. The two types of closed string axions differ in the way they couple to the D7-brane worldvolume gauge fields via Chern-Simons terms: the 4-form axions intrinsincally couple to the worldvolume theory, while 2-form axions only acquire such a coupling in the presence of a particular type of quantized magnetic flux on the D7-brane. The "intrinsic" size of these CS couplings turns out to be too small to generate GW signals detectable with current or planned experiments. However, both CS couplings increase linearly with the number of times the D7-brane stack "wraps" a 4-cycle, and the 2-form axion CS

<sup>&</sup>lt;sup>3</sup>Although such a coupling can be induced if the axiverse solves the QCD axion quality problem via the mechanism in [190, 191].

coupling in addition increases with the amount of magnetic flux on the stack. A non-trivial obstacle to realizing Abelian spectator sectors in this construction is the presence of Stückelberg couplings between axions and U(1) gauge bosons, which cause the Abelian gauge boson and axion degrees of freedom to combine into that of a massive spin-1 boson. This is a generic issue for 2-form axions, whose Stückelberg couplings arise geometrically. In contrast, 4-form axions acquire Stückelberg couplings only in the presence of certain magnetic fluxes. Under certain assumptions on the topology of the CY compactification manifold, both Stückelberg couplings can be avoided.

### 5.1 Spectator mechanism

The study of axion-like particles in inflationary physics has a rich history, with the natural inflation model [84] being perhaps the most well-known example. Coupling the axion with a gauge sector is the next logical step given that the symmetries of the theory are preserved and the great interest and motivation in exploring the inflationary particle content. The simplest realization is that of coupling the axion-inflaton to U(1) vector fields [165] via a Chern-Simons term, thereby effectively flattening the potential without resorting to a trans-Planckian axion decay constant<sup>4</sup>. The multi-field nature of these models and the parity violation originating from the CS term makes for an interesting inflationary phenomenology with very distinct, testable, signatures: from the non-trivial spectral shape of scalar and tensor degrees of freedom to chiral gravitational waves, from large non-Gaussianities to primordial black holes.

The interest in exploring the broader class of axion - gauge fields models together with the formidable power of cosmological probes to constrain our models has led to a flurry of (on-going) research activity. Relaxing the requirement that the axion be the inflaton opens up new intriguing directions. Spectator axions make these models more malleable in terms, for example, of the scales at which their key signatures are most pronounced. For specific models, the spectator nature of the axion is dictated by the need to overcome the possible tensions with CMB observations. The Lagrangian encompassing the case of spectator axions reads

$$\mathcal{L} \supset \mathcal{L}_{\inf} + \mathcal{L}_{S},$$

$$\mathcal{L}_{\inf} = -\frac{1}{2} (\partial \varphi)^{2} - V_{\inf}(\varphi),$$

$$\mathcal{L}_{S} = -\frac{1}{4} F_{a\mu\nu} F^{a\mu\nu} - \frac{1}{2} (\partial \vartheta)^{2} - V_{S}(\vartheta) - \frac{\lambda}{4f} \vartheta F_{a\mu\nu} \tilde{F}^{a\mu\nu}.$$
(5.1)

In the above expressions we have defined  $V_{\rm inf}(\varphi)$  and  $V_S(\vartheta)$  as the inflaton  $\varphi$  potential and the spectator axion  $\vartheta$  one, respectively. The spectator gauge boson is coupled to the axion via a Chern-Simons coupling term with  $\widetilde{F}^{a\mu\nu} = \frac{1}{2\sqrt{-g}} \varepsilon^{\mu\nu\rho\sigma} F^a_{\rho\sigma}$  and f the axion decay constant. The Chern-Simons coupling typically takes the form of

$$\lambda = \mathfrak{q} \, \frac{\alpha}{\pi} \,, \tag{5.2}$$

where  $\alpha = \frac{g^2}{4\pi}$  is the fine structure constant with g the gauge coupling and  $\mathfrak{q}$  is a constant that varies from model to model. Both Abelian [161, 162, 188, 208, 209] and non-Abelian [93, 177, 184–186, 210–212] gauge fields have been considered in the literature.

<sup>&</sup>lt;sup>4</sup>The latter is hard to implement in string theory constructions [14, 207].

A key compelling feature of the above spectator models lies in their gravitational wave signature. In single-field slow-roll inflation, the gravitational waves are vacuum modes of the metric that are amplified through the inflationary expansion. A slightly red-tilted GW spectrum ensues, with the planned BBO experiment [213] as the only probe which may be able to detect such a signal. Multi-field scenarios can support a much richer GW spectrum but it remains non-trivial to realize mechanisms for which the tensor modes can be significant: any source of GWs must produce curvature perturbations through an unavoidable gravitational coupling to the inflaton field. The sourced perturbations generally obey a non-Gaussian statistics so that the existing strong limits on non-Gaussianity of the primordial perturbations force the sourced scalar modes to be subdominant at large scales. This necessarily limits the strength of the sourcing mechanism and its signal. As we shall see, axion - gauge field models and in particular spectator models are able to evade these constraints while providing detectable signals.

The dynamics common to all<sup>5</sup> models goes as follows. The axion rolls down its relatively steep potential. Its coupling to the gauge sector acts as friction and excites the gauge modes. Due to the parity breaking nature of the CS term, the solution for the left and right-handed polarization of the (vector or tensor) gauge quanta have a different equation of motion, one of them being temporarily amplified. This amplification is transmitted on to scalar curvature fluctuation and gravitational waves, with the details depending on the specific model. The sourced gravitational wave spectrum is chiral and is typically blue in the case of an axion-inflaton whilst bump-like features<sup>6</sup> are possible for a spectator axion. These features make such models attractive from both the experimental and theoretical standpoint, as they may evade potential constraints from quantum gravity [42].

Models where the axion acts as the inflaton and is driven by the standard cosine potential are naturally much more constrained. This is true for the Abelian case, whilst observational constraints directly rule out [214, 215] the well known chromo-natural (CNI) model [170], at least in its simplest realization. There are manifold ways to render axiongauge field models viable while preserving their tantalizing GW signatures. One may consider a different potential or remain completely agnostic as to the nature of the potential altogether. Another possibility is spontaneous symmetry breaking of the gauge symmetry [216]. Yet another natural step is to ask the axion(s) to be a spectator field and let another field be the inflaton [93, 163, 208]. This, as may be expected, relaxes the constraints on the axion dynamics: it is true that GW signatures remain tied to the axion rolling-down its potential, but it is now the slow-roll of another field along another potential that is directly related to observables such as the scalar spectral index  $n_s$ . Advocating a spectator axion pays off in the case of an SU(2) gauge sector: the spectator model of [93], SCNI, has a viable cosmology. This comes at a not insignificant cost from the top-down perspective: the required values of the Chern-Simons coupling  $\lambda$  are  $\lambda \sim \mathcal{O}(10^2)$  when  $\alpha \sim \mathcal{O}(10^{-12})$ , and this gives an unnaturally high integer q in eq. (5.2). This has been argued to be problematic for embedding the models in an ultraviolet completion, at least for some model-building techniques [203, 204]. The same issues are not in place for Abelian models.

As we shall see below, in both Abelian and non-Abelian models with spectator axions, the latter are typically taken to be heavy, such that their energy density washes away

<sup>&</sup>lt;sup>5</sup>By that we mean here models where the the inflaton is (not) an axion and models whose gauge sector is (non)-Abelian. These features apply to all the four possible combinations.

<sup>&</sup>lt;sup>6</sup>The latter are of particular interests vis-à-vis primordial black holes.

after they reach their minimum, and the curvature perturbations can be identified with that of the inflaton. However, in general, inflationary constructions can accommodate both heavy and light axions, fully in accordance with the expectations of the axiverse.

In the following, we will first study these models considering one spectator axion, and then generalize to multiple spectators. The non-Abelian spectator model of [93] will not generally, in the weak backreaction regime (see [217] for strong backreaction<sup>7</sup>), exhibit distinctive peaks in the GW spectrum but a rather broad profile. This is due to the constraining power of stability and consistency conditions [95] the model ought to satisfy. When generalizing to multiple spectator sectors, we find it convenient to focus on the Abelian case (MASA) given that this configuration shows distinctive peak-like structures whose detection is less taxing on the values of the Chern-Simons couplings.

#### 5.1.1 Inflation with Abelian Spectators

We first consider the Abelian models of [162, 208]: these are described by Eq. (5.1), the trace over the gauge sector being trivial in this case. The inflaton potential  $V_{\inf}(\varphi)$  is assumed to be sufficiently flat to grant a nearly constant Hubble rate H. A simple cosine potential characterizes the spectator axion,

$$V_S(\vartheta) = \frac{\Lambda^4}{2} \left[ \cos \left( \frac{\vartheta}{f} \right) + 1 \right] , \qquad (5.3)$$

with f the axion decay constant, and the mass of the axion being  $m_{\vartheta}^2 = \frac{\Lambda^4}{2f^2} ^8$ , where in the slow roll regime  $\eta_V \equiv M_P^2 |V''/V| \propto m_{\vartheta}^2 \simeq \frac{\Lambda^4}{2f^2} \cos(\vartheta/f)$ . Such a periodic potential is relatively steep, so much so that it has been necessary to postulate a trans-Planckian decay constant to avoid the tension between natural inflation [84,164] and CMB data, until recent observations [21,24] ruled out the model altogether. An efficient mechanism to effectively flatten the potential is to couple the axion to a gauge sector via a Chern-Simons term: the rolling axion "dissipates" energy into the gauge sector. Even if the axion plays merely a spectator role, the following dynamics is still in play: the rolling field excites gauge quanta that are non-linearly coupled to tensor modes thus engendering an intriguing GW phenomenology. By virtue of its spectator nature<sup>9</sup>, the axion does not directly provide a significant contribution to scalar curvature perturbations. It is nevertheless gravitationally coupled to the inflaton field: the axion will then mediate an interaction between gauge fields and the inflaton, thus sourcing the curvature fluctuation  $\zeta$ .

If the curvature of its potential is tuned to be  $\mathcal{O}(H)$  during inflation, the axion rolls from (nearly) the maximum at  $\vartheta = 0$  down to (nearly) the minimum of the potential at  $\vartheta = \pi f$  in a few e-folds, of the order of  $\mathcal{O}(H^2/m^2)$ . The slow roll solution to the  $\vartheta$  equation of motion derived from eq. (5.1) is [162]

$$\vartheta = 2f \arctan(e^{\delta H(t-t_*)}),$$

$$\dot{\vartheta} = \frac{fH\delta}{\cosh(\delta H(t-t_*))},$$
(5.4)

<sup>&</sup>lt;sup>7</sup>There also exists a rich literature on strong backreaction in Abelian models, see e.g. [218–224].

<sup>&</sup>lt;sup>8</sup>In Sec. ?? we will be using  $\mu^4 \equiv \frac{\Lambda^4}{2}$  for consistency with conventional notation in string theory.

<sup>&</sup>lt;sup>9</sup>Strictly speaking one ought to also require that its energy density becomes negligible by the end of inflation or, at least, that it stays sub-leading. This is in contradistinction, for example, to the well-know curvaton scenario [225].

with  $\delta \equiv \frac{\Lambda^4}{6H^2f^2}$  and  $t_*$  the moment when  $\frac{\vartheta}{f} = \frac{\pi}{2}$ , corresponding to the time when the axion is at its maximal velocity. The resulting power spectra will show a peak in the vicinity<sup>10</sup> of  $k = k_*$  [162], which can be deduced from the previous equation in terms of the initial conditions

$$k_* = k_{in} \tan \left(\frac{\vartheta_{in}}{2f}\right)^{-1/\delta} , \qquad (5.5)$$

where we identify  $k_{in} \simeq \frac{1}{3} \times 10^{-4} \mathrm{Mpc^{-1}}$  as the CMB scale, and  $\vartheta_{in}$  is the initial condition given to the axion. In order for slow roll to hold, we require

$$\frac{\ddot{\vartheta}}{3H\dot{\vartheta}} = -\frac{\delta}{3}\tanh(\delta H(t - t_*)) \ll 1 \to \delta \ll 3.$$
 (5.6)

It turns out to be very useful to define, for both Abelian and non Abelian models, the parameter

$$\xi \equiv \frac{\lambda \dot{\vartheta}}{2Hf} \,. \tag{5.7}$$

In the Abelian case one finds  $\xi_* = \lambda \frac{\delta}{2}$ , which is independent of the axion decay constant f.

During its brief roll, the axion sources gauge fields, with an amplitude that is exponentially proportional to the parameter  $\xi \equiv \frac{\lambda \dot{\phi}}{2fH}$ . In the following, we denote with  $\xi_*$  the maximum value attained by  $\xi$  while the roll of the axion is fastest, which occurs when  $\vartheta \simeq \frac{\pi}{2} f$  (the small time variation of H can be disregarded for these considerations). The highly amplified gauge fields source perturbations of the axion (via inverse decay) as well as inflaton perturbations and gravitational waves (through gravitational interaction)

$$\delta A + \delta A \to \delta \vartheta , \delta \phi, h_{\lambda} ,$$
 (5.8)

where  $\lambda=\pm$  denotes the two circular GW polarizations. In turn, the axion perturbations can "convert" into inflaton perturbations through their linear coupling due to gravity (which arises while the two fields are both rolling). Due to its significant mass during inflation, the energy density in the axion rapidly dilutes away after the field has reached the minimum, so that the primordial scalar density perturbations  $\zeta$  in this model can be identified with the inflaton perturbations (more precisely, we work in spatially flat gauge, in which  $\zeta=-\frac{H}{\dot{\phi}}\,\delta\phi$ ). The choice of a decoupled axion and inflaton potential guarantees a minimum amount of production of the primordial scalar perturbations, which was one of the motivations of [162] for constructing this model.

The scalar and tensor perturbations sourced by the gauge field add up incoherently to the standard vacuum modes (those amplified by the inflationary expansion), so that the total scalar and tensor power spectra, namely

$$P_{\zeta}(k)\delta^{(3)}(\vec{k}+\vec{k'}) \equiv \frac{k^3}{2\pi^2} \langle \zeta(\vec{k})\zeta(\vec{k'}) \rangle , \qquad (5.9)$$

(and analogously for  $h_{\pm}$ ) are obtained from the sum of the vacuum and sourced contributions

$$P_i(k) = P_i^{(0)}(k) + P_i^{(1)}(k) , i = \zeta, h_+, h_-.$$
 (5.10)

<sup>&</sup>lt;sup>10</sup>A more accurate estimate would amount to  $k_{\text{peak}} = \mathcal{O}(\text{a few}) \times k_*$ .

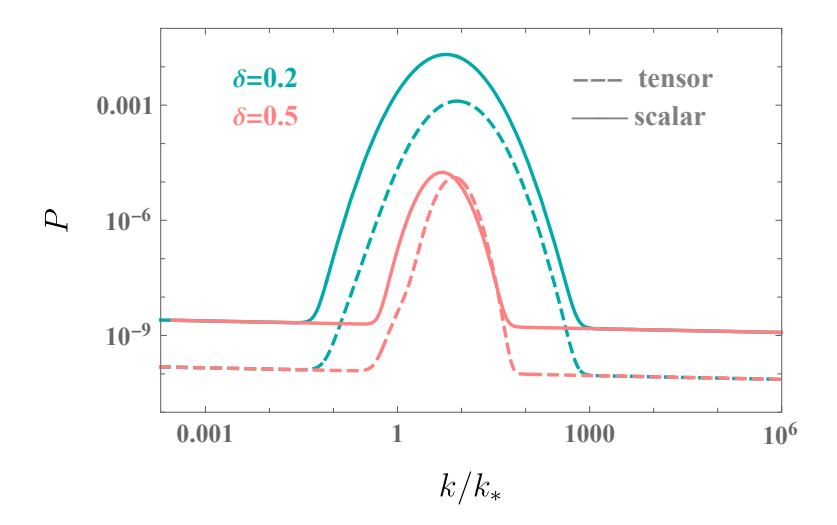


Figure 5.1: Scalar (solid blue line) and tensor (dashed pink line) power spectra produced in the model in which an axion, coupled to a U(1) gauge field, experiences a momentary phase of significant roll during inflation. The results are shown for  $\xi_* = 4.56$  (the peak value of the parameter that controls the gauge field production) and  $\delta = 0.2$  (the inverse of this parameter is approximately the number of e-folds during which the axion roll is significant). The wavenumber  $k_*$  is a model parameter.

We employ the standard parametrization of the scalar vacuum power spectrum:

$$P_{\zeta}^{(0)} = A_s \left(\frac{k}{k_0}\right)^{n_s - 1},\tag{5.11}$$

and we assume that the axion is still (nearly) at rest when the CMB modes were produced, so that the CMB data are directly mapped only to the vacuum signal. We then take  $A_s = e^{3.047} \times 10^{-10}$ ,  $n_s = 0.9665$  at the Planck pivot scale  $k_0 = 0.05\,\mathrm{Mpc}^{-1}$ , according to the central values given in Table 2 of [226]. We also take  $\varepsilon = 0.002$  for the slow roll parameter  $\varepsilon \equiv \frac{M_{\mathrm{Pl}}^2}{2} \left(\frac{1}{V} \frac{dV}{d\phi}\right)^2$  (where  $M_{\mathrm{Pl}}$  is the reduced Planck mass), which saturates the current bound  $r = 16\varepsilon \lesssim 0.03$  on the tensor-to-scalar ratio [227, 228]. For simplicity, we also take this ratio to be scale independent,

$$P_T^{(0)} = r \times P_C^{(0)}, \tag{5.12}$$

at all (comoving) wavenumbers k. Relaxing this assumption (that is immediately done for any specific choice of the inflationary potential, given the two different dependences of the scalar and tensor tilt on the slow-roll paramters) has no consequence on our results, since in slow-roll inflation the vacuum tensor modes are too small to generate appreciable SDs.

The rolling of the axion that takes place after the CMB modes have been produced leads to a bump in the scalar and tensor power spectra at scales smaller than the CMB ones, that can be parametrized as [162]

$$P_{\zeta}^{(1)}(k) = \left[\varepsilon P_{\zeta}^{(0)}(k)\right]^{2} f_{2,\zeta} , P_{T}^{(1)}(k) = \left[\varepsilon P_{\zeta}^{(0)}(k)\right]^{2} (f_{2,+} + f_{2,-}) , \qquad (5.13)$$

where the dimensionless functions  $f_{2,j}$  are well fitted by [162]

$$f_{2,j} \simeq f_{2,j}^c \left[ \xi_*, \delta \right] \exp \left[ -\frac{1}{2\sigma_{2,j}^2 \left[ \xi_*, \delta \right]} \ln^2 \left( \frac{k}{k_* x_{2,j}^c \left[ \xi_*, \delta \right]} \right) \right] , \quad j = \zeta, h_+, h_-.$$
 (5.14)

The three functions  $f_{2,j}^c$ ,  $\sigma_{2,j}^2$ ,  $x_{2,j}^c$  control, respectively, the height, the width, and the location of the bump. Ref. [162] provided an analytic fit for the dependence of these functions on  $\xi_*$ , for the two specific values  $\delta=0.2, 0.5$ . The quantity  $k_*$  in eq. (5.14) is the comoving wavenumber of the modes that exit the horizon while the axion roll is the fastest. As  $x_{2,j}^c$  is an order one quantity, this is parametrically the scale at which the sourced modes have maximum amplitude. The scale  $k_*$  is a free parameter of the model, which we vary in the following analysis of the SDs produced by the scalar and tensor modes.

Having defined some of the key background quantities, we can briefly discuss the axion mass. Very light axions are certainly possible in the string theory context<sup>11</sup> with ultralight axions having a mass that can be as low as  $m_{\vartheta} \sim 10^{-12}\,\mathrm{eV}$ . However, in the context of this work we shall deal with much heavier axions. This higher mass range arises from conditions we impose on the roll duration of the axion, in particular from requiring that the rolling last (i) more than a few e-folds and (ii) (indicatively) less than 60 e-folds. The lower bound holds on account of stringent CMB bounds on scalar and tensor spectra: longer rolling ensures the peak of the signal is at smaller, less constrained, scales. Conversely, the upper bound guarantees that the most interesting phenomenology takes place during the last sixty e-folds of inflation. Upon recalling that the axion rolls for about  $\Delta N \sim 6H^2/m_{\vartheta}^2$  e-folds, we ought to require that

$$m_{\vartheta} \gtrsim \frac{H}{\sqrt{10}} \,, \tag{5.15}$$

thus identifying a minimum value for the axion mass in terms of the proxy inflationary scale H and highlighting the difficulty in fitting a light axion within these setups.

#### 5.1.2 Inflation with non-Abelian Spectators

The Lagrangian in eq. (5.1) includes non-Abelian scenarios such as the model in [93], with the proviso that this time the trace goes over gauge indices. We focus on the SU(2) case given the rich literature on this model (see e.g. [229]) and the fact that the key features of its dynamics and observables are shared by a much larger class of theories [230]. The axion potential is the same as in Eq. (5.3), but without the overall 1/2 factor, removed in order to conform to the existing literature. One may choose the vector field vacuum expectation value (vev) components as  $\langle A_0^a(t) \rangle = 0$  and  $\langle A_i^a(t) \rangle = \delta_i^a a(t) Q(t)$ . Contrary to the Abelian case, the SU(2) setup can accommodate an isotropic background solution upon identifying the gauge and rotation indices [231]. It turns out the isotropic one is an attractor solution [232], further motivating our starting out already in FLRW. The background quantity  $\xi$  is defined according to Eq. (5.7) and it is convenient to introduce also

<sup>&</sup>lt;sup>11</sup>Axion masses arise from instanton-like non-perturbative potentials that break the continuous symmetry down to a discrete one. In QFT, maintaining this shift symmetry to a high order in perturbation theory requires explicit imposition, as there is no inherent reason for it to naturally hold. Higher-order operators could therefore potentially disrupt the symmetry and contribute to the axion mass. In contrast, in string theory, closed string axions originate from the compactification of higher-dimensional p-form gauge potentials. These axions inherit their shift symmetry from the 10d gauge symmetry of the p-form fields, resulting in an exact shift symmetry to all orders in perturbation theory. This exact symmetry prevents any higher-order operator from spoiling it, making the existence of light axions more naturally explained if they are string axions.

$$m_Q \equiv g \frac{Q(t)}{H} \,, \tag{5.16}$$

directly associated with the gauge field vev. The two parameters are identical in the large  $m_Q$  limit<sup>12</sup>. Examination of the perturbations at the linear level shows that this model is unstable for  $m_Q < \sqrt{2}$  [214].

One of the polarizations of the gauge tensor perturbations is amplified and sources GWs. By solving the background equations of motion in slow roll dynamics for Q(t) and  $\vartheta(t)$ , one can find a good approximation for  $m_Q$  that reads

$$m_Q \propto \frac{V_{S,\vartheta}(\vartheta)^{1/3}}{H^{4/3}} = \frac{m_\vartheta^{2/3} f^{1/3}}{H^{4/3}} \sin^{1/3} \left(\frac{\vartheta}{f}\right) ,$$
 (5.17)

where  $m_{\vartheta}^2 \equiv \Lambda^4/f^2$  is the axion mass. Given the instability for  $m_Q < \sqrt{2}$ , we can lower the axion mass only as long as the opposite of this inequality holds. One simple possibility is to lower the value of H, which has been the subject of a thorough investigation in [233]. It turns out one may indeed lower the Hubble rate by many orders of magnitude without trespassing into the strong backreaction regime. This is done by simultaneously acting on g. On the other hand, if we also require that the GW signal be detectable by upcoming experiments we are forced to tie the value of H to that of  $m_Q$  (for a fixed r, the smaller is H the larger becomes  $m_Q$ ). Given how the power spectra scale with the two quantities, when exploring larger and larger  $m_Q$  values one soon hits e.g. PBH bounds [234], which implies that  $m_Q$  is limited from above (and, correspondingly, H from below). It follows that plausible detectability confines us to a large  $H \gtrsim 10^{10}$  GeV and therefore (via Eq. (5.17)) to a relatively heavy spectator mass.

## 5.2 Spectral Distortions

Since the measurements taken by COBE/FIRAS [235] in the 1990s, the Cosmic Microwave Background (CMB) radiation is a remarkable example of a nearly perfect blackbody spectrum at the temperature  $T_0 = (2.726 \pm 0.001)K$  today [236], representing a cornerstone in modern cosmology. This striking agreement arises from the thermal equilibrium between matter and radiation during the early stages of the universe. However, as the universe evolves, various mechanisms come into play, potentially leading to modifications in the CMB frequency spectrum. The thermalization process of the CMB in the early universe has been extensively studied. In the early stages (redshift  $z \ge 2 \times 10^6$ ), a blackbody spectrum is maintained through ongoing processes, such as Compton scattering, Bremsstrahlung, and double Compton scattering. As the universe expands, these interactions become less efficient, allowing for deviations from the blackbody spectrum. These deviations, known as CMB spectral distortions (SDs), are induced by energy injections occurring at epochs with  $z \leq 10^6$ , and therefore represent a yet unexplored new window into both the early and the late universe physics. A guaranteed mechanism of early SDs, predicted by the standard  $\Lambda$ CDM cosmological model, is that due to the so called Silk-damping effect [237]. Additionally, there are other numerous processes, occurring at a variety of redshifts, known to potentially disturb the thermal distribution, including reionization and structure formation [238], energy injection from annihilating or decaying

<sup>&</sup>lt;sup>12</sup>For completeness we should add that in the strong backrection regime there exists a different attractor solution [217] that does not satisfy this identity.

particles [239], the presence of small-scale primordial magnetic fields [240], and cosmic strings [241], among others. These diverse mechanisms provide intriguing avenues to investigate and understand the origins of SDs as signatures of new physics. Also, spatial anisotropies of CMB SDs (and their cross-correlations with CMB temperature and polarization fields) provide further ways to exploit SDs as a valuable observable to have a new insight into both early and late time physics (including, but not limited to primordial non-Gaussianity), see, e.g., [242–254].

CMB distortions are classified into two main types based on the epoch of the energy release:  $\mu$ -type and y-type distortions. The  $\mu$ -distortion exhibits a frequency dependent chemical potential, and it is generated after the decoupling of the double Compton scattering ( $z \sim 10^6$ ), while the Compton scattering is still active, guaranteeing kinetic equilibrium. Conversely, the y distortion is produced as the Compton scattering is no longer efficient in maintaining this equilibrium ( $z \sim 10^5$ ). Measurement of these CMB distortions provides a powerful tool for investigating the thermal history of the Universe. The most precise measurement of the CMB spectrum to date is provided by COBE/FIRAS, which constrained the distortions to  $\mu \leq 9 \times 10^{-5}$  and  $y \leq 1.5 \times 10^{-5}$  at a 95% C.L. [255]. A later analysis by [256] improved the  $\mu$ -distortion constraint to  $\mu \leq 4.7 \times 10^{-5}$  at a 95% C.L., thanks to an improved component separation and Bayesian analysis approach. The last decade has witnessed an intense ongoing discussion regarding potential future missions (PIXIE [257], PRISM [258], COSMO [259], BISOU [260]) that could detect  $\mu$ - and y-distortions down to the  $10^{-9} - 10^{-8}$  range [94, 261].

Interestingly, CMB spectral distortion observations would let us venture into much smaller scales than those available by CMB anisotropy measurements, which range from our horizon scale  $k \simeq 2 \times 10^{-4} \ \mathrm{Mpc^{-1}}$  to  $k \simeq 0.2 \ \mathrm{Mpc^{-1}}$ . Indeed, any scalar fluctuation in the CMB temperature will be erased by Silk damping around the dissipation scale  $k_D$ , which, for  $z \simeq 2 \times 10^6$ , is of the order  $k_D \simeq 2 \times 10^4 \ \mathrm{Mpc^{-1}} \gg 0.2 \ \mathrm{Mpc^{-1}}$  [237]. Even in conventional cosmology (for example, even without assuming entropy injection from some long-lived species), entropy release associated to cosmological perturbations produced during inflation and that re-enter the horizon at  $z < \mathcal{O}\left(10^6\right)$ , generates distortion. Under assumption of (approximate) scale invariance of primordial perturbations, a curvature power spectrum of  $P_{\zeta} \sim 2 \times 10^{-9}$  guarantees a signal of  $\mu, y \sim 10^{-8}$ , that could be a target for Voyage 2050 [94]. Moreover, improving on the experimental results can play a vital role in constraining various inflationary models that involve a breaking of scale invariance after CMB scales, leading to enhanced power at smaller scales than the CMB.

Inflation, however, gives rise not only to scalar modes, but also to tensor modes (Gravitational Waves, GWs). Recent detections of GWs by the ground-based LIGO [262], Virgo [263], and KAGRA [264] (LVK) observatories, as well as evidence from the pulsar timing arrays (PTA) [265, 266], have expanded the field of GWs, leading to significant advancements in theory and observation. With the advent of new experiments, from PTA to astrometry [267], from laser interferometer space antennas (LISA) [268] to new ground based detectors (such as Einstein Telescope [269] and Cosmic explorer [270]) we are entering an era of unprecedented opportunities to explore the cosmos through gravitational wave signals. It has been shown that CMB SDs can also play a part in the observation of GWs [271,272]. Indeed, tensor modes can generate SDs at their horizon re-entry, just like scalar modes. The effect of this contribution to SDs has been quantified in [271]. The authors of [273] investigated the spectral distortions from tensor and scalar fluctuations arising in post-inflationary scenarios that lead to production of GWs, finding that the

contribution from the tensor modes were highly suppressed with respect to the scalar ones

We study the SDs from scalar and tensor modes in a specific context, namely in inflation models where rolling axions are coupled to gauge fields as explained above. This includes one of the scenarios considered in previous works by [272], that focused on the tensor-induced SDs. As we show below, our results agree with [272]. In addition to the generation of tensor modes leading to CMB distortions in these models, we also investigate the generation of scalar modes leading to CMB distortions. The latter effect is generally present, as we have seen that scalar modes are generated gravitationally, along with tensor modes. In fact, these models produce a significantly higher scalar signal as compared to the tensor one, making it qualitatively inevitable and in need of quantitative assessment. The production of scalar modes gives a higher hope for a detection of SDs or a possibility to constrain these model, compared to relying only on tensor-induced SDs. The issue of scalar production that limits the detectable signatures of tensor production has been a long-standing concern in various mechanisms that generate additional tensor modes beyond the standard quantum-vacuum tensor fluctuations. For instance, models designed to enhance the tensor-to-scalar ratio  $r = \frac{P_T}{P_\zeta}$  at CMB scales by generating an additional contribution of gravitational waves also unavoidably produce scalar modes. This not only affects the denominator of the ratio, but also can encounter strong bounds from the non-Gaussian character of the sourced scalar modes [208, 274]. Moreover, the production of observable GWs, as might be detected by future missions like LISA or the LVK collaboration, encounters a delicate trade-off: if too many fields are involved in generating the GWs, the excessive energy injection can lead to the formation of primordial black holes (PBHs) at undesired levels [275, 276]. As such, careful considerations of both scalar and tensor modes are essential, as their coexistence necessitates a comprehensive evaluation of their mutual effects on cosmological observables.

Firstly, we explore the U(1) model designed [162] to maximize the relative production of tensor versus scalar modes. By avoiding any direct coupling in the potential, the two sectors are coupled only by the unavoidable gravitational interactions. Although this can result in an increased tensor signal, while suppressing to a minimum level the production of scalar modes, we find that the tensor contribution to SDs is still significantly smaller than the scalar one. Therefore, isolating and probing the much subdominant tensor contribution to SDs is extremely challenging. Next, we turn our attention to the SU(2)version of this model, introduced in [93], and already discussed in [272] as a concrete model for SDs from tensor modes. The linearized study of the primordial perturbations leads to the conclusion that the production of additional tensor modes in this model can be significantly greater than that of additional scalars. This is due to the existence of an unstable gauge field mode, that experiences significant growth while the axion is rolling, and that couples linearly to GWs but not to the curvature perturbation  $\zeta$ . However, the unstable gauge mode sources a significant amount of scalar perturbations nonlinearly [161]. We find that also in this model the SDs generated by tensor modes are much smaller than those due to the nonlinearly produced scalar perturbations. We also find that generating a localized signal in the primordial tensor and scalar perturbations in the SU(2) model is more challenging than in the U(1) case. <sup>13</sup> This is due to additional

<sup>&</sup>lt;sup>13</sup>This can only be seen from evolving the background equations for the model (with parameters appropriately chosen so to generate a roll of the axion only for a limited amount of e-folds during inflation), and not from the parametrization of the peaked signal adopted in some literature [177].

interactions present in the SU(2) case, that make it more difficult to keep the gauge field/axion sector in a 'dormant' phase, so to obtain a fast axion roll at some specific desired time. We present a possible way out to this problem, by relating the onset of the fast axion roll to a sudden change of the coupling between the axion and the gauge fields.

#### 5.2.1 Spectral distortions from primordial perturbations

Photons in the early universe have the Bose-Einstein distribution function

$$f(x) = B(x) \equiv \frac{1}{e^x - 1} , \quad x \equiv \frac{p}{T} , \qquad (5.18)$$

where p is the physical momentum of the photons and T their temperature. The expansion of the universe modifies this distribution function through a rescaling of the temperature T, so that the primordial photons retain this blackbody spectrum in absence of interactions. Such interactions, and, in general, energy transfers to or from the photon field will cause a distortion of this spectrum [239,277–279]. To linear order in the parameters  $\Delta T/T$ ,  $\mu$ , y, the modifications are typically of the form <sup>14</sup>

$$\Delta f(x) = \frac{\Delta T}{T} G(x) + \mu M(x) + y Y(x) . \qquad (5.19)$$

Only the last two terms in this expression represent a distortion of a blackbody distribution. The first term,

$$G(x) \equiv -x \frac{\partial B(x)}{\partial x} = \frac{x e^x}{(e^x - 1)^2}, \qquad (5.20)$$

represents instead a change of temperature of the photon distribution without altering its blackbody shape. This is the only modification introduced by any entropy injection that occured at early redshifts,  $z \gtrsim z_{\rm dc} \equiv 2 \times 10^6$  [239,279], when processes that change the number (double Compton and bremsstrahlung) and energy (Compton scattering) of photons requilibrate the distortion into a new blackbody spectrum with a modified temperature. Below this redshift, and up to approximately the redshift  $z \equiv z_{\mu y} = 6 \times 10^4$  [239, 285], double Compton and bremsstrahlung processes progressively go out of equilibrium, while Compton scattering is still active and guarantees kinetic equilibrium. Any entropy release then results in both a change of temperature and of chemical potential of the photon distribution, with the latter effect given by

$$M(x) \equiv -G(x)\left(\frac{1}{x} - 0.4561\right). \tag{5.21}$$

For an entropy injection below this redshift, and up to recombination ( $z = z_{\rm rec} \simeq 1100$ ), Compton scatterings of the photons with the electrons (assumed to have a Maxwellian phase-space distribution) take place with a progressively decreased efficiency, giving rise to a so called Compton y-distortion, with shape

$$Y(x) \equiv G(x) \left( x \frac{e^x + 1}{e^x - 1} - 4 \right) . \tag{5.22}$$

To linear order, an entropy release  $\dot{Q}$  (where Q(z) is the energy density injected at the redshift z in the thermal bath, and dot denotes derivative with respect to time) produces

<sup>&</sup>lt;sup>14</sup>We refer the readers to ref. [280] for a pedagogical derivation of the expressions reported here. For a more detailed study of modifications beyond the modelization in eq. (5.19) see for instance refs. [281–284].

distortions that can be parametrized as

$$\mu = 1.4 \int_0^\infty \tilde{\mathcal{J}}_{\mu}(z) \frac{d(Q/\rho_{\gamma})}{dz} dz , \quad y = \frac{1}{4} \int_0^\infty \tilde{\mathcal{J}}_{y}(z) \frac{d(Q/\rho_{\gamma})}{dz} dz , \qquad (5.23)$$

where  $\rho_{\gamma}$  is the energy density of the thermal distribution (without the injection) and the two visibility functions  $\tilde{\mathcal{J}}_{\mu,y}$  account for the particle physics processes that we have summarized above.

The visibility functions have been studied with increasing accuracy in the literature, see for instance the discussion in ref. [286]. The simplest approach is to take two square top hat functions evaluating to 1 in the redshift intervals  $z_{\mu y} < z < z_{\rm dc}$  (for the  $\mu$ -distortion) and  $z_{\rm rec} < z < z_{\mu y}$  (for the y-distortion) and to 0 outside these intervals. Improvements have been obtained by noting that the efficiency does not abruptly vanish at  $z_{\rm dc}$  [239, 278, 279, 287], which can be accounted for by a  ${\rm e}^{-(z/z_{\rm dc})^{5/2}}$  factor, and by considering the fact that the transition between  $\mu$ - and y-distortions is not abrupt at  $z_{\mu y}$ . We employ the analytic approximation [285]

$$y \simeq \frac{1}{4} \int_{z_{\text{rec}}}^{\infty} dz' e^{-(z'/z_{dc})^{5/2}} \frac{d(Q/\rho_{\gamma})}{dz'} \mathcal{J}_{y}(z') \quad , \quad \mu \simeq 1.4 \int_{z_{\text{rec}}}^{\infty} dz' e^{-(z'/z_{dc})^{5/2}} \frac{d(Q/\rho_{\gamma})}{dz'} \mathcal{J}_{\mu}(z') ,$$
(5.24)

with

$$\mathcal{J}_{y}(z) \simeq \left(1 + \left[\frac{1+z}{z_{\mu y}}\right]^{2.58}\right)^{-1} , \quad \mathcal{J}_{\mu}(z) \simeq 1 - \mathcal{J}_{y}(z) .$$
 (5.25)

Let us discuss the entropy injections of interest for our work. A guaranteed source of distortions is from the energy release due to the Silk-damping [237] of primordial small-scale perturbations after their horizon re-entry [288–291]. This gives rise to CMB SDs that are directly related to the shape and amplitude of the primordial scalar power spectrum  $P_{\zeta}$ . Defining the latter as in eq. (5.9), <sup>15</sup> the injection of energy from the scalar modes can be approximated as [285] (see also refs. [238, 280, 294])

$$\frac{d(Q/\rho_{\gamma})}{dz}\bigg|_{\zeta} \simeq -3.25 \int d\ln k \, P_{\zeta}(k) \sin^2(kr_s) \, \partial_z \, e^{-2k^2/k_D^2} , \qquad (5.26)$$

where, assuming radiation domination, the sound horizon is  $r_s \simeq c_s \, \eta \simeq 2.7 \times 10^5 \, (1+z)^{-1}$ , while the damping scale is  $k_D \simeq 4.0 \times 10^{-6} \, (1+z)^{3/2} \, \mathrm{Mpc}^{-1}$ . <sup>16</sup>

Combining eqs. (5.23) and (5.26), it is customary to write the distortions as

$$\mu_{\zeta} = \int_{k_{\min}}^{\infty} d\ln k \, P_{\zeta}(k) \, W_{\mu}^{\zeta}(k) \quad , \quad y_{\zeta} = \int_{k_{\min}}^{\infty} d\ln k \, P_{\zeta}(k) \, W_{\zeta}^{y}(k) \quad , \tag{5.27}$$

with  $k_{\rm min} \simeq 1 \,{\rm Mpc}^{-1}$ . We show the scalar window functions obtained in this way with solid lines in Figure 5.2. <sup>17</sup>

<sup>&</sup>lt;sup>15</sup>This definition corresponds to the one of ref. [292] times a  $\frac{k^3}{2\pi^2}$  factor. In our notation, a scale-invariant power spectrum corresponds to a constant  $P_{\zeta}$ . The same applies to the tensor power spectrum that we consider below. We only consider the effect of an adiabatic primordial perturbation. Ref. [293] studied the distortions due to scalar isocurvature modes.

<sup>&</sup>lt;sup>16</sup>In writing the numerical coefficient of eq. (5.26) and the following relations for the heating rates and window functions taken from the literature we set the fractional contribution of neutrinos to the energy density of relativistic species to  $R_{\nu} \equiv \rho_{\nu}/(\rho_{\gamma} + \rho_{\nu}) \simeq 0.41$ .

<sup>&</sup>lt;sup>17</sup>Analytic approximations for the scalar window functions can be found in Ref. [293].

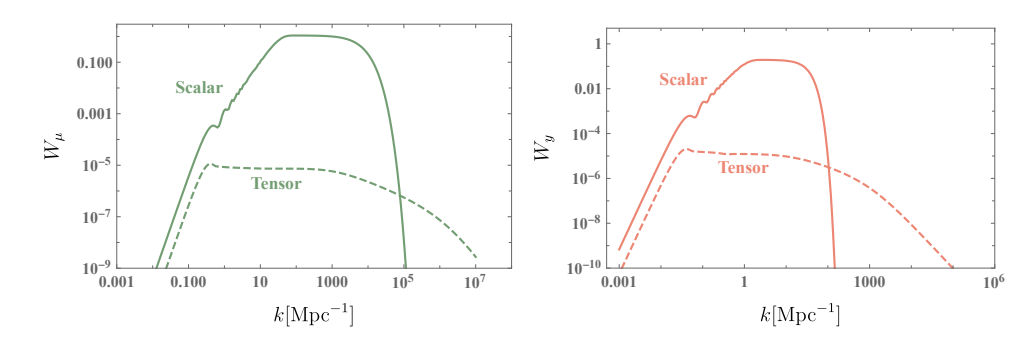


Figure 5.2: Window functions for (left)  $\mu$ - and (right) y-distortions. They encode the effect of primordial modes on the distortions as in eq. (5.27). The solid (respectively, dashed) line corresponds to the scalar (respectively, tensor) window function.

Primordial tensor modes can also source CMB distortions [295]. Contrary to scalar modes, they create a local quadrupole anisotropy without the need of photon diffusion. Scatterings between photons and electrons in presence of this anisotropy then cause nearly scale independent dissipation [271,295], giving rise to the distortions. Ref. [271] provided analytical relations for the heating rate from tensors and for the resulting distortions. The heating rate can be expressed as

$$\frac{d(Q/\rho_{\gamma})}{dt}\Big|_{T} \simeq \frac{4H^{2}}{45\dot{\tau}} \int_{0}^{\infty} d\ln k \, P_{T}(k) \, \mathcal{T}_{\theta}\left(\frac{k}{a\dot{\tau}}\right) \mathcal{T}_{h}(k\eta) \, e^{-\Gamma_{\gamma}\eta} \,, \tag{5.28}$$

where  $\dot{\tau} = \sigma_T N_e = 4.4 \times 10^{-21} (1+z)^3 \text{ s}^{-1}$  is the Thomson scattering rate,  $\eta$  is conformal time, and a is the scale factor. In this relation,  $P_T(k)$  is the tensor power spectrum (summed over the two polarizations), defined analogously to eq. (5.9). The gravitational wave transfer function [296]

$$\mathcal{T}_h(x) \simeq 2 \left\{ \sum_{n=0, even}^{6} a_n [nj_n(x) - xj_{n+1}(x)] \right\}^2,$$
 (5.29)

(where the  $j_n$  are the spherical Bessel functions, and  $a_0 = 1$ ,  $a_2 = 0.243807$ ,  $a_4 = 5.28424 \times 10^{-2}$ ,  $a_6 = 6.13545 \times 10^{-3}$ ) accounts for the damping due to neutrino free streaming [297, 298], while the rate  $\Gamma_{\gamma}$  accounts for the damping due to photons, and  $\Gamma_{\gamma} \eta \simeq 5.9 \, a$  as derived in eq. (D.6) of [271]. Finally, the photon transfer function encodes how the distortion is produced by the tensor mode, and it can be approximated by [271]

$$\mathcal{T}_{\theta}(x) \simeq \frac{1 + 4.48x + 91x^2}{1 + 4.64x + 90.2x^2 + 100x^3 + 55.0x^4}.$$
 (5.30)

From these expressions, we can express the distortions analogously to eq. (5.27), namely

$$\mu_T = \int_0^\infty d\ln k \, P_T(k) \, W_\mu^T(k) \, , \, y_T = \int_0^\infty d\ln k \, P_T(k) \, W_T^y(k) \, , \qquad (5.31)$$

in terms of the tensor power spectrum and the tensor window functions

$$W_y^T \simeq \int dz \frac{1}{(1+z)} \frac{H}{45\dot{\tau}} \mathcal{T}_h(k\eta) \, \mathcal{T}_\theta \left(\frac{k}{\tau'}\right) e^{-\Gamma_\gamma \eta} \, \mathcal{J}_t(z) ,$$

$$W_\mu^T \simeq \int dz \, e^{-\left(\frac{z}{z_{dc}}\right)^{\frac{5}{2}}} \frac{1}{(1+z)} \frac{5.6H}{45\dot{\tau}} \mathcal{T}_h(k\eta) \, \mathcal{T}_\theta \left(\frac{k}{\tau'}\right) e^{-\Gamma_\gamma \eta} \, \mathcal{J}_\mu(z) . \tag{5.32}$$

that we show with dashed lines in fig. 5.2.

The comparison between the tensor and scalar window functions shown in this figure allows for the following observation: while the scalar window functions are significantly greater than the tensor ones at large scales, the tensor window functions become greater than the scalar ones at smaller scales, approximately at  $k \gtrsim 7.5 \times 10^4 \; \mathrm{Mpc^{-1}}$ for  $\mu$ -distortions and at  $k \gtrsim 10^2 \; {\rm Mpc^{-1}}$  for y-distortions. This phenomenon aligns with expectations, considering that the scalar window function starts to decrease around the diffusion scale due to Silk damping effects. In contrast, as already mentioned, tensor modes directly induce a quadrupole anisotropy, and a consequent CMB distortion, without relying on photon diffusion. Accordingly, the damping process for tensor modes is significantly less scale-dependent, as the figure shows. When comparing the effects of scalar vs. tensor modes it is also important to recall that the window functions multiply the primordial scalar and tensor power spectra, and that tensor modes are typically produced with a significantly lower amplitude than scalars in vanilla slow-roll inflation. Therefore, in hope to have a visible distortion from tensors (which is not overshadowed by that from scalars), one needs to resort to specific inflationary models that can generate enhanced tensor perturbations at the scales relevant for the distortions [272]. In the following, we consider one class of models that have been proposed in the literature for this purpose, namely enhanced tensor perturbations from gauge fields amplified by a rolling axion during inflation. In addition to the existing literature, we consider also the effect of scalars that are also unavoidably produced by the gauge fields.

### **5.2.2 SD** from U(1)

Here, we study the application for SDs of the analogous (and earlier) model of [162],  $^{18}$  in which the rolling spectator axion is coupled to a U(1) gauge field.

We begin this analysis with the scalar and tensor heating rate, shown in fig. 5.4. We plot the heating rates (obtained after integration over k) as a function of  $k_*$  for various relevant redshifts. We observe that, the greater the redshift, the greater is the value  $k_*$  at which the heating rate is maximum. This is due to the fact that modes mostly contribute to the heating when they re-enter the horizon, and that the comoving horizon is smaller in the past (hence, greater  $k = (aH)^{-1}$ ). We also observe that, at any given redshift, the scalar heating rate strongly decreases at scales that are smaller than the diffusion scale  $k_D(z)$  at that redshift. A similar effect is not found for the tensor heating rate, which shows a plateau that extends for a greater range of wavenumbers. This agrees with the large-k behaviour of the window functions shown in fig. 5.2 and with the discussion we had after eq. (5.32). We also observe that the heating rate caused by tensor modes decreases at high redshifts. On the contrary, the heating rate due to scalars reaches a similar maximum level across the three redshifts examined. Since  $\mu$ -distortions occur at higher redshifts compared to y-distortions, the diminishing effect of tensor heating at high redshifts implies that the ratio between the peak amplitudes of  $\mu$ - and y-distortions is smaller for tensor contributions compared to scalar contributions, as Figure 5.5 shows.

We note that the CMB data already constrain part of the parameter space by placing strong bounds on the strength of the curvature power spectrum up to  $k_* \sim 5 \text{ Mpc}^{-1}$ . fig. 5.3 shows the maximum value of  $\xi_*$  as a function of  $k_*$  that satisfies the  $2\sigma$  bound

<sup>&</sup>lt;sup>18</sup>SDs in this model were considered in association to primordial scalar perturbations that can result in primordial black hole dark matter [188].

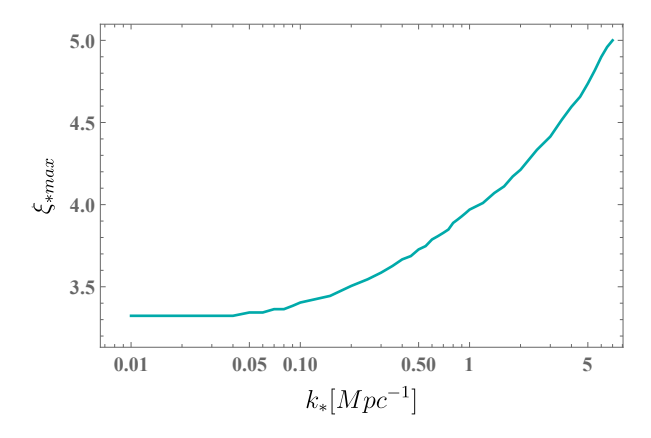


Figure 5.3: Maximum allowed value of  $\xi_*$  as a function of  $k_*$ . Parameters above the curve result in a sourced power spectrum that exceeds the one inferred from CMB [21].

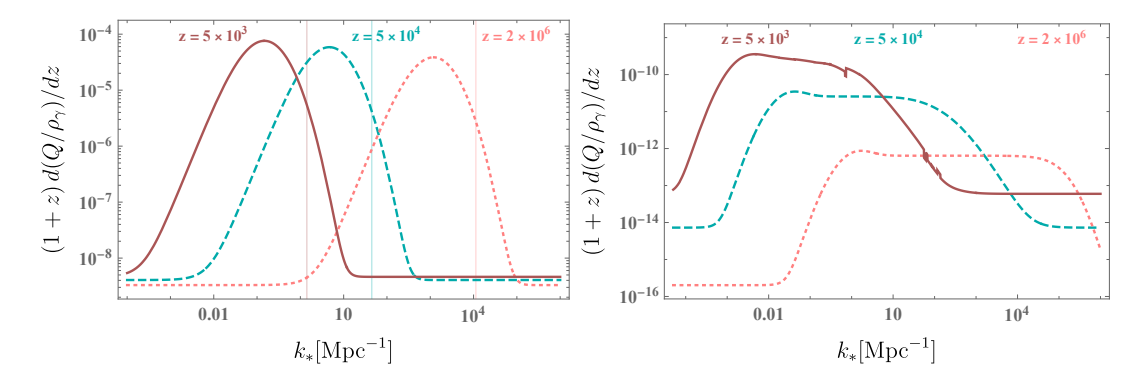


Figure 5.4: Left (respectively, right) panel: scalar heating rate (5.26) (respectively, tensor heating rate (5.28)) due to the primordial perturbations produced in the Abelian model and shown in Figure 5.1. The rates are shown as a function of  $k_*$  (which is the comoving momentum, of the modes that leave the horizon when the evolution of the axion is fastest). In each panel, the curves, from left to right, show the heating rates at three increasing redshift:  $z = 5 \times 10^3$  (solid line),  $z = 5 \times 10^4$  (dashed line), and  $z = 2 \times 10^6$  (dotted line). In the left panel the thin vertical lines correspond to the damping wavenumber  $k_D(z)$  for each redshift, beyond which the distortions from scalar modes are reduced.

reported in Figure 20 (bottom panel) of Ref. [21]. We note that the limit loosens (greater values of  $\xi_*$  are allowed) for progressively increasing  $k_*$ , as this corresponds to progressively smaller scales (eventually becoming smaller than the scales probed by the CMB). This limit excludes the left portion of fig. 5.5, which is shaded in the Figure.

We begin this analysis with the scalar and tensor heating rate, shown in fig. 5.4. We plot the heating rates (obtained after integration over k) as a function of  $k_*$  for various relevant redshifts. We observe that, the greater the redshift, the greater is the value  $k_*$  at which the heating rate is maximum. This is due to the fact that modes mostly contribute to the heating when they re-enter the horizon, and that the comoving horizon is smaller in the past (hence, greater  $k = (aH)^{-1}$ ). We also observe that, at any given redshift, the scalar heating rate strongly decreases at scales that are smaller than the diffusion scale  $k_D(z)$  at that redshift. A similar effect is not found for the tensor heating rate, which shows a plateau that extends for a greater range of wavenumbers. This agrees with the large-k behaviour of the window functions shown in fig. 5.2 and with the discussion

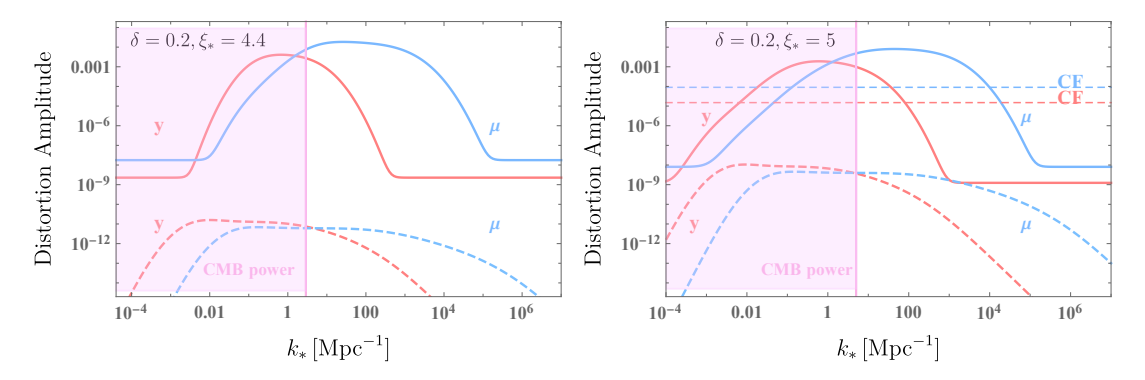


Figure 5.5: Solid (respectively, dashed) lines: SDs from the scalar (respectively, tensor) perturbations produced by the model (??) and shown in fig. 5.1. The distortions are shown as a function of the parameter  $k_*$ , which controls the wavenumber at which the perturbations are peaked. The horizontal lines correspond to the current bounds from COBE/FIRAS [235]. The two panels correspond to different values of the parameter  $\xi_*$ , that controls the amplitude of the sourced perturbations. The shaded region in the left part of the two panels show the parameters that result in a sourced power spectrum that exceeds that inferred from the CMB (see the previous figure). The flat tails at small and large  $k_*$  are due to the vacuum modes and the choice of parameters discussed above eq. (5.12).

we had after eq. (5.32). We also observe that the heating rate caused by tensor modes decreases at high redshifts. On the contrary, the heating rate due to scalars reaches a similar maximum level across the three redshifts examined. Since  $\mu$ -distortions occur at higher redshifts compared to y-distortions, the diminishing effect of tensor heating at high redshifts implies that the ratio between the peak amplitudes of  $\mu$ - and y-distortions is smaller for tensor contributions compared to scalar contributions, as Figure 5.5 shows.

We note that the CMB data already constrain part of the parameter space by placing strong bounds on the strength of the curvature power spectrum up to  $k_* \sim 5 \text{ Mpc}^{-1}$ . fig. 5.3 shows the maximum value of  $\xi_*$  as a function of  $k_*$  that satisfies the  $2\sigma$  bound reported in Figure 20 (bottom panel) of Ref. [21]. We note that the limit loosens (greater values of  $\xi_*$  are allowed) for progressively increasing  $k_*$ , as this corresponds to progressively smaller scales (eventually becoming smaller than the scales probed by the CMB). This limit excludes the left portion of fig. 5.5, which is shaded in the Figure.

Finally, in support of our earlier claim that computing only the tensor contribution would significantly underestimate the CMB distortions from this mechanism, we observe that the scalar heating rate reaches values that are much greater than the tensor ones. This is also in agreement with the window functions shown in fig. 5.2 and with the fact that the tensor modes produced by this mechanism are smaller than the scalar ones. <sup>19</sup>

The SDs for this specific model are shown in fig. 5.5. <sup>20</sup> In agreement with the above discussions and results, we observe that indeed the distortions due to tensor modes produced in this model are much smaller than the scalar-induced ones. We also observe the

<sup>&</sup>lt;sup>19</sup>Although we do no perform a full parameter search for the model, we do not expect to obtain tensor modes of many orders of magnitude greater than the scalar ones, so to compensate the hierarchy in the scalar vs. tensor window functions shown in fig. 5.2, due to the fact that the gauge field is coupled with comparable (gravitational) magnitude to both sectors.

<sup>&</sup>lt;sup>20</sup>We stress that fig. 5.4 and fig. 5.5 are not spectra, but they show the heating rates and the distortions after integration over k. The horizontal axis  $k_*$  is the comoving momentum at which the spectra of the primordial perturbations are peaked.

relative size between the maximum value attained by the  $\mu$ - vs. y-distortions is greater for the scalar contribution than for the tensor one, in agreement with what discussed in the context of the previous figure. Finally, we note that, after the peak, the tensor contributions have a milder decrease with  $k_*$  than the scalar ones, and so they reach the baseline minimum value (due to the nearly scale invariant vacuum modes) at greater values of  $k_*$ . This is also something that we already discussed above.

In conclusion, the model can result in significant CMB distortions. As already discussed, the amplitude of the signal is exponentially proportional to the parameter  $\xi_*$ . The left panel of fig. 5.5 corresponds to a value of  $\xi_*$  that is compatible with the present limits for all choices of  $k_*$ . The right panel shows instead the results for the maximum estimated value of  $\xi$  that is compatible with perturbativity (in this case the range  $6 \times 10^{-3} \mathrm{Mpc^{-1}} \lesssim k_* \lesssim 10^4 \mathrm{Mpc^{-1}}$  is already excluded by COBE/FIRAS). We stress that in all cases, the distortions produced in this model are strongly dominated by the primordial scalar modes.

#### 5.2.3 SD from non-Abelian

Let us now move our attention to the model of ref. [93], which is essentially an analogous version of the model of the previous section, with the U(1) field replaced by an SU(2) multiplet.

The model is governed by the action

$$\mathcal{L} = -\frac{1}{2}(\partial\phi)^2 - V(\phi) - U(\vartheta) - \frac{1}{2}(\partial\vartheta)^2 - \frac{1}{4}F^a_{\mu\nu}F^{a\mu\nu} + \frac{\lambda\vartheta}{4f}F^a_{\mu\nu}\tilde{F}^{a\mu\nu}, \qquad (5.33)$$

where  $\phi$  is the inflaton and  $\vartheta$  is the spectator axion, coupled to the SU(2) field of field strength

$$F_{\mu\nu}^{a} = \partial_{\mu}A_{\nu}^{a} - \partial_{\nu}A_{\mu}^{a} + gf^{abc}A_{\mu}^{b}A_{\nu}^{c} , \qquad (5.34)$$

where g is the gauge coupling constant and  $f^{abc}$  are the structure constants of the SU(2) algebra. As in the previous model, the inflaton and the axion-gauge sector are decoupled (apart from gravity), and therefore the inflaton and axion have the separate potentials  $V(\phi)$  and  $U(\vartheta)$ , respectively. The SU(2) triplet has vacuum expectation values (vevs) [170]

$$A_0^a = 0, A_i^a = \delta_i^a a(t) Q(t), (5.35)$$

which allows for a statistically isotropic phenomenology.

One component of the SU(2) multiplet is strongly amplified due the rolling of the axion, similar to the instability of the U(1) field studied in the previous section. The instability is controlled by the combination

$$m_Q \equiv \frac{gQ(t)}{H_{\rm inf}} \,, \tag{5.36}$$

which plays an analogous role to the parameter  $\xi$  introduced in the U(1) case. Indeed, it can be shown that  $m_Q \simeq \xi$  in the  $m_Q \gg 1$  limit, see eq. (5.44) below.

Differently from the U(1) case, the amplified SU(2) component is linearly coupled to one GW polarization, due to the vevs (5.35). Therefore, the latter is significantly sourced already at the linearized level, with the power spectrum [93]

$$P_{\text{GW,sourced}}(k) = \frac{\varepsilon_B H^2}{\pi^2 M_{\text{Pl}}^2} \mathcal{F}^2(m_Q), \qquad (5.37)$$

where  $\varepsilon_B \equiv \frac{g^2 Q^4}{M_{\rm Pl}^2 H_{\rm inf}^2} = \frac{m_Q^4 H_{\rm inf}^2}{g^2 M_{\rm Pl}^2}$  is a parameter that roughly indicates the energy fraction of the SU(2) gauge fields. The function  $\mathcal{F}(m_Q)$  was evaluated in Ref. [93], and reported in their eqs. (3.6)-(3.9). This is the expression that we use in our computations. Ref. [177] obtained a much simpler approximate fitting function:

$$\mathcal{F}(m_Q) \simeq \exp\left[2.4308 \, m_Q - 0.0218 \, m_Q^2 - 0.0064 \, m_Q^3 - 0.86\right] , \ 3 \le m_Q \le 7 .$$
 (5.38)

As in the U(1) model, also the scalar perturbations need to be computed to provide the phenomenology of the model. The power spectrum of the linear modes is given by (see Appendix F of [299] for a derivation)

$$P_{\zeta}^{(0)} \simeq \frac{H^2}{8\pi^2 M_p^2} \frac{\varepsilon_{\phi}}{(\varepsilon_{\phi} + \varepsilon_B)^2} \simeq P_{\zeta, \text{CMB}} \cdot \frac{\varepsilon_{\phi}^2}{(\varepsilon_{\phi} + \varepsilon_B)^2}, \tag{5.39}$$

where  $\varepsilon_{\phi} \equiv \frac{\dot{\phi}^2}{2H^2M_{\rm Pl}^2}$  is the standard slow-roll parameter associated with the motion of the inflaton. As in the previous section, we consider a model characterized by negligible axion roll when CMB perturbations are produced, and therefore standard vacuum signals at CMB scales, which justifies the last expression in eq. (5.39), where  $P_{\zeta,\rm CMB}$  is the power observed at CMB scales, with the amplitude  $A_s$  reported in the previous section. We employ the results of Ref. [299], which, in addition to the scalar perturbations from linear theory, also computed the scalar perturbations sourced at nonlinear order by two amplified gauge modes. The power spectrum of these sourced scalar modes is approximately given by

$$P_{\zeta,\text{sourced}} \simeq 1.1 P_{\zeta,\text{CMB}}^2 \frac{\varepsilon_{\phi}^4}{(\varepsilon_B + \varepsilon_{\phi})^2} N_k^2 m_Q^{11} e^{7m_Q} , \quad 2.5 \lesssim m_Q \lesssim 4 , \quad (5.40)$$

where  $N_k$  is the number of inflationary e-folds during which the axion rolls.

While Ref. [93] studied this model in a regime in which the axion rolls continuously all throughout inflation, Ref. [177] was interested in the case in which the axion moves significantly for only a few e-folds during inflation, analogous to the model considered in the previous section. <sup>21</sup> Ref. [177] did not study a concrete dynamical evolution for the axion in a specific model. They considered the typical cosine axion potential and Taylor expanded the evolution of the axion about the time  $t_*$  when it is at the steepest part of the potential, and therefore  $\dot{\vartheta}(t = t_*) \equiv \dot{\vartheta}_*$  is maximum,

$$\vartheta(t) = \frac{\pi}{2} f + \dot{\vartheta}_* (t - t_*) + O\left((t - t_*)^2\right) . \tag{5.41}$$

Then, inserting this expansion in eqs. (5.37) and (5.38), they obtained an analytically approximate expansion for the top of the bump of the tensor modes produced while the axion is rolling.

<sup>&</sup>lt;sup>21</sup>The implementation of [177] was then employed by [272] as a model for SDs from tensors, which is the main motivation for this section. Strictly speaking, the relations (5.37) and (5.38) used in these two works for the tensor signal, as well as the relation (5.40) for the source scalars were obtained for constant  $m_Q$ , and then evaluated for a time varying  $m_Q$  in Refs. [177,272] (specifically, for any wavenumber k, the relations (5.37) and (5.38) are evaluated at the time at which that mode left the horizon). As our goal is to compare the results of [272] for the case in which also the scalar modes are considered, we employ in this work the same methodology used in Refs. [177,272]. However, we caution that the relations. (5.37), (5.38) and (5.40) can only be considered as approximations in the case in which  $m_Q$  varies too quickly.

As we study in the next subsection, realizing such a bump in the SU(2) case is more difficult than in the U(1) model considered in the previous section. This cannot be seen from the analytical approximation (5.41) that only describes the evolution around the moment of fastest roll, but it emerges from the study of the full dynamical background equations in concrete models. We discuss this difficulty in the next subsection, where we outline a possible construction that can indeed produce a fast roll of the axion restricted to the scales that are relevant for the CMB distortions.

### 5.2.4 Background evolution for localized peaks beyond the CMB scales

Let us study the background evolution for the model (5.33). Concerning the dominant inflaton sector, we consider for definiteness the so called  $\alpha$ -attractor potential

$$V = V_0 \tanh\left(\frac{\phi}{\sqrt{6\alpha}M_{\rm Pl}}\right),\tag{5.42}$$

which has the advantage of providing a nearly constant H during inflation, and of admitting an analytic solution for the evolution of the inflaton and of the expansion rate (in the limit of negligible energy in the axion/gauge sector that we are considering), see e.g. Ref. [300]. For definiteness, we choose  $V_0 = 1 \times 10^{-9} M_{\rm Pl}^4$ ,  $\alpha = 1$ , and  $\phi_{\rm in} = 6.24 M_{\rm Pl}$  (leading to 60 e-folds of inflation). Other inflaton potentials might have been considered without affecting our results.

The background evolution of the axion/gauge sector is instead controlled by

$$\ddot{\vartheta} + 3H\dot{\vartheta} + \frac{dU}{d\vartheta} = -\frac{3g\lambda}{f}Q^2\left(\dot{Q} + HQ\right) ,$$

$$\ddot{Q} + 3H\dot{Q} + \left(\dot{H} + 2H^2\right)Q + 2g^2Q^3 = \frac{g\lambda}{f}\dot{\vartheta}Q^2 .$$

$$(5.43)$$

In the limit of constant or adiabatically evolving Q, and provided the parameters satisfy  $3f^2H^2 \ll g^2\lambda^2Q^4$  and  $\lambda^2Q^2 \gg 2f^2$ , these equations are approximately solved by [93,170]

$$Q \simeq \left(-\frac{f}{3g\lambda H}\frac{dU}{d\vartheta}\right)^{1/3} , \frac{\lambda\dot{\vartheta}}{2fH} \simeq m_Q + \frac{1}{m_Q} .$$
 (5.44)

We are not interested in a solution with constant Q, as we want to obtain a peaked signal. As shown in fig. 5.2, the tensor window function can dominate over the scalar one at relatively smaller scales. Consequently, an ideal scenario for obtaining visible distortion from tensor modes involves tailoring the model to produce a peak in  $m_Q$  at these relatively small scales, effectively minimizing the scalar contribution.

The tensor (as well as the scalar) signal is generated by the gauge fields, whose amplification is directly linked to the velocity of the axion. For the cosine potential, using the relations (5.44) in the  $m_Q \gg 1$  limit, we can estimate the value of  $m_Q$  at the peak

$$m_{Q,\text{peak}} \sim \left(\frac{g^2 \Lambda^4}{3\lambda H^4}\right)^{1/3} ,$$
 (5.45)

as well as the width of the peak (namely, the number of e-folds for which the axion rolls)

$$\Delta N_{\rm peak} \sim H \, \Delta t \sim H \, \frac{\Delta \vartheta}{\dot{\vartheta}} \sim \frac{\pi}{2} \frac{\lambda}{m_Q} \sim {\rm O}(2) \times \left(\frac{\lambda \, H}{\sqrt{g} \, \Lambda}\right)^{4/3} \,.$$
 (5.46)

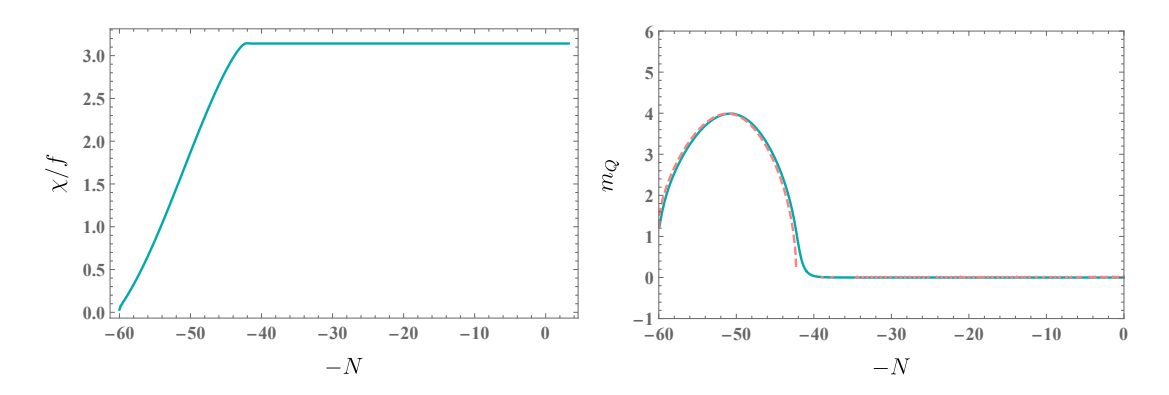


Figure 5.6: Evolution of the axion  $\vartheta$  (left panel) and of the combination  $m_Q$  (right panel) in the SU(2) case for the values of parameters indicated in the main text. Continuous blue lines show the exact numerical solution. The dashed red line in the right panel is based on the approximation of eq. (5.44), and it presents gaps after the peak since this approximation results in an imaginary Q whenever  $\vartheta > \pi f$  (where the approximation is invalid).

The order two factor in the last expression comes from the numerical factors and from the fact that we have estimated  $m_Q$  at its maximum (at  $\vartheta = \frac{\pi}{2}f$ ), while in fact  $m_Q$  is smaller at the beginning and at the end of the peak. For definiteness, we choose  $g = 5.5 \times 10^{-3}$ ,  $\lambda = 40$ ,  $f = 9 \times 10^{-3} M_{\rm Pl}$ ,  $\Lambda = 2.3 \times 10^{-3} M_{\rm Pl}$ , and  $\vartheta_{\rm in} = 10^{-2} \pi f$ . This leads to  $\Delta N_{\rm peak} \sim 10$  in the estimate (5.46), and it ensures that the conditions leading to (5.44) are satisfied.

In fig. 5.6 we show the evolution of the axion and of the parameter  $m_Q$  (5.36) for this choice of parameters. As mentioned, we start from  $\vartheta_{\rm in} = 10^{-2}\pi\,f$ , and the initial conditions for  $\dot{\vartheta}$  and Q are then set according to (5.44), while  $\dot{Q}_{\rm in} = 0$ ). This results in a bump of  $\dot{\vartheta}$ , and hence of  $m_Q$  (and a consequent peak in the primordial scalar and tensor perturbations) right at the start of the evolution, as obtained from an exact numerical integration of eqs. (5.43), shown by a continuous blue line in the figure. At the beginning of the evolution and all throughout the bump the approximation (5.44), indicated by a dashed red line, is well satisfied.

We notice that the bump of particle production occurs when  $\vartheta = \frac{\pi}{2} f$ , and the axion roll is fastest. As mentioned, we wish to delay the moment at which this takes place, so to have the bump at scales smaller than the CMB one. Achieving this in the U(1) model is rather simple, as it only requires taking the initial value of the axion sufficiently close to the maximum of the potential, where the potential is flat and therefore the classical value of  $\dot{\vartheta}$  can be made arbitrarily small. This is no longer the case now, due to the nonvanishing right hand side in the first of eqs. (5.43). We performed an evolution of the system for  $\vartheta_{\rm in} = 10^{-4} \pi f$  (without changing the other parameters) obtaining a qualitatively similar evolution to the one shown in fig. 5.6, with no delay of the onset of the peak. Further decreasing the initial value of  $\vartheta_{\rm in}$  breaks the conditions reported before eq. (5.44).

Eqs. (5.45) and (5.46) suggest an alternative, and more successful, route to attempt to delay the onset of the peak. We note that the height and the duration of the peak are, respectively, decreasing and increasing as  $\lambda$  increases. If therefore  $\lambda$  is decreased for an intermediate stage during inflation, a higher and narrower peak in  $m_Q$  can be obtained during this stage, on the top of a slowly evolving baseline (that in turn corresponds to the much smaller and wider peak that occurs while  $\lambda$  is large). This is visible in the

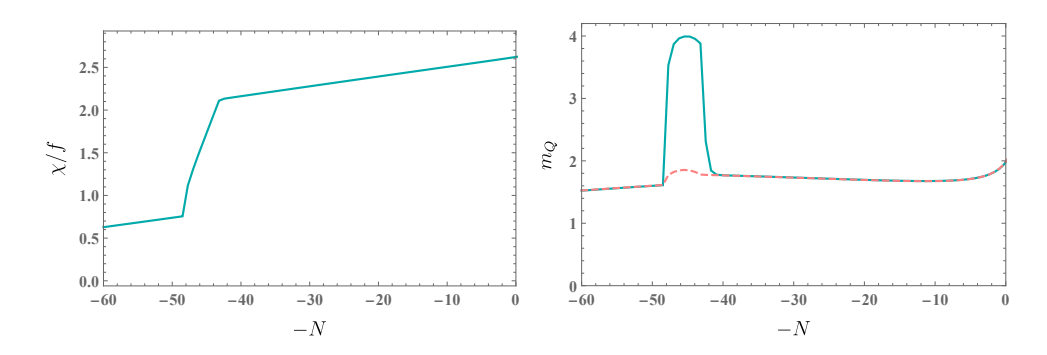


Figure 5.7: Evolution of the axion  $\vartheta$  (left panel) and of the combination  $m_Q$  (right panel). As compared to the previous figure,  $\lambda$  is decreased by a factor of 10 in the interval  $48 \gtrsim N \gtrsim 43$ , resulting in peak in  $m_Q$  during this stage. The red-dashed curve in the right panel is based on the approximations (5.44), which are invalid at the peak.

evolution shown in fig. 5.7, where  $\lambda$  is initially (at  $\vartheta_{\rm in} = \frac{\pi}{5}f$ ) taken to be  $\lambda = 400$ , and it is suddenly decreased by a factor of 5 between  $N \simeq 48$  and  $N \simeq 43$  e-folds before the end of inflation (more precisely, the evolution in the figure corresponds to N = 48.3 and N = 43.1). We are implicitly assuming that the value of  $\lambda$  is controlled by some other field, that experiences a sudden transition at the beginning and the end of this stage (presenting a complete model is beyond the scope of this work).

This successfully delays the onset of the main peak. We note that, for the sole purpose of delaying the peak it is not necessary that  $\lambda$  grows back to relatively large values after the peak. However, if this does not occur,  $m_Q$  rapidly decreases after the peak, becoming smaller than  $\sqrt{2}$ . When this happens, the system of scalar perturbations in this model has a strong instability in the sub-horizon regime [214]. The evolution shown in fig. 5.7 is exempt from this problem.

We note that the dashed red line in the right panel of fig. 5.7 departs from the solid blue curve during the peak, indicating the approximation (5.44) is invalid during this stage. These relations are therefore not used in the computation of the scalar and tensor modes, to which we turn next.

#### 5.2.5 Spectral Distortions for a localized peak in the SU(2) model

Let us now compute the primordial scalar and tensor modes produced in the model. We consider the background evolution shown in fig. 5.7. We then evaluate the spectrum of the scalar modes from the sum of eqs. (5.39) and (5.40) and the spectrum of the tensor modes from the sum of the vacuum term  $P_T^{(0)} = \frac{2}{\pi^2} \frac{H^2}{M_{\rm Pl}^2}$  and of eq. (5.37). The resulting spectra are shown in the left panel of fig. 5.8. We observe that in this case one can obtain a tensor power spectrum of comparable or greater amplitude than the scalar power spectrum. Inserting the scalar spectrum in eq. (5.27) we then obtain the peak values of the CMB distortions  $y_{\zeta} \simeq 3.1 \times 10^{-7}$  and  $\mu_{\zeta} \simeq 2.7 \times 10^{-6}$ . Inserting the tensor spectrum in eq. (5.31) we instead obtain  $y_T \simeq 3.8 \times 10^{-11}$  and  $\mu_T \simeq 3.3 \times 10^{-11}$ . We note that the scalar contribution strongly dominates the distortions, due to their much greater window function, despite the parameters of the model resulting in scalar and tensor modes of comparable power at the peak.

To shift the position of the peak, we simply change the value of the number of e-folds N

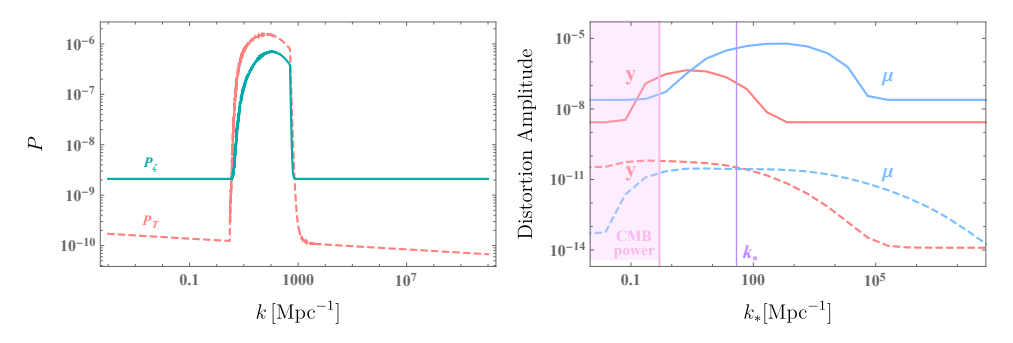


Figure 5.8: Left panel: scalar (solid line) and tensor (dashed line) power spectrum produced in the model (5.33) for the background evolution shown in the previous figure. Right panel: SDs from the scalar (solid lines) and tensor (dashed lines) modes. The distortions are shown as a function of the parameter  $k_*$ , which controls the wavenumber at which the perturbations are peaked. This is varied by shifting the position of the peak shown in the left panel, as explained in the text. The vertical line in the right panel corresponds to the value of  $k_*$  obtained for the evolution leading to the spectra shown on the left panel. The shaded region on the left portion of the panel is excluded since it leads to an induced scalar power in excess to what inferred from the CMB.

at which the decrease of  $\lambda$  takes place (we keep the duration of the stage of low  $\lambda$  fixed), while all the other parameters are unchanged. We then compute the primordial scalar and tensor modes produced also in these cases, and the corresponding CMB distortions. This allows us to plot in the right panel of fig. 5.8 the distortions as a function of the scale of the peak  $k_*$ .

We note that the scalar contribution dominates the distortions for all values of  $k_*$ . The distortions obtained in this model are slightly smaller than those shown in fig. 5.5 in the U(1) case. To increase the distortions generated by this model requires increasing  $m_Q$  to values for which the fitting formula (5.40) is no longer valid. Given the functional dependence of the tensor and scalar signal on  $m_Q$ , and the fact that the nonlinear scalar production involves more unstable modes than the linear tensor one we do not expect that increasing  $m_Q$  would lead to a drastic increase of the ratio between the tensor and scalar sourced modes.

Similar to the U(1) case, the parameter space at relatively small  $k_*$  visible in fig. 5.8 is excluded as it produces a scalar power spectrum in excess to that inferred by the CMB data. The limit shown in the figure has been computed identically to what done in the previous section for the Abelian case.

## 5.3 A Multitude of Spectators & Their Power Spectra

The previous two subsections featured only a single spectator axion coupled to a gauge sector. As argued above, a natural expectation from string compactifications is the existence of a whole axiverse, with the surfeit of axions that it entails. This serves as a strong motivation to extend the above axion gauge field constructions to allow for multiple axionic (and gauge) spectators<sup>22</sup>. Of course, there are plentiful possibilities, including those where the spectator gauge group is a semi-simple sum of both non-Abelian and Abelian

<sup>&</sup>lt;sup>22</sup>See [301] for a related discussion regarding CNI models.

groups. The class of theories we will explore stems from generalizing eq. (5.1) as follows

$$\mathcal{L} \supset \mathcal{L}_{\inf} + \sum_{i} \mathcal{L}_{S_{i}},$$

$$\mathcal{L}_{\inf} = -\frac{1}{2} (\partial \varphi)^{2} - V_{\inf}(\varphi),$$

$$\mathcal{L}_{S_{i}} = -\frac{1}{4} F_{ia\mu\nu} F_{i}^{a\mu\nu} - \frac{1}{2} (\partial \vartheta_{i})^{2} - V_{S_{i}}(\vartheta_{i}) - \frac{\lambda_{i}}{4 f_{i}} \vartheta_{i} F_{ia\mu\nu} \tilde{F}_{i}^{a\mu\nu},$$

$$(5.47)$$

where  $\vartheta_i$  and  $F_i^a$  are the spectator axions and gauge field strengths, respectively, with  $i=1,...,N_S$ . We have also defined the Chern-Simons couplings  $\lambda_i$ , the axion decay constants  $f_i$ , and the scalar potentials  $V_{S_i}(\vartheta_i)$ , the explicit form of the latter being that of Eq. (5.3). For the sake of simplicity, we will focus here on the Abelian case. Note that we are not pursuing the possibility of a direct coupling between the inflaton and the spectators. We are also neglecting mixing between axions and/or gauge fields from different spectator sectors. Such possibilities are of course permitted and can be included to further enrich the landscape of MASA models.

We shall now study the gravitational wave spectrum of MASA models. First, let us revisit the gravitational waves generated in the single spectator case.

When  $\vartheta$  is rolling,  $\dot{\vartheta} \neq 0$  and gauge fields are produced via

$$\delta\vartheta \to \delta A + \delta A$$
, (5.48)

then, in turn, gauge perturbations source scalar and tensor perturbations via

$$\delta A + \delta A \to \delta \phi \text{ (via } \delta \theta) 
\delta A + \delta A \to \delta h_{\lambda}.$$
(5.49)

The interaction between the gauge field and the inflaton is purely gravitational so that the direct channel  $\delta A + \delta A \to \delta \phi$  is negligible. By assumption,  $\vartheta$  in this model has an energy density much smaller than that of the inflaton and thus we can identify the scalar curvature perturbation  $\zeta$  with the perturbation of the inflaton. A linear coupling of gravitational nature however still remains between the perturbations of  $\vartheta$  and of  $\phi$  as long as  $\dot{\vartheta} \neq 0$ , which leads to the partial conversion  $\delta \vartheta \to \delta \phi$ . Feynman diagrams in Figs.5.9 & 5.10 help in identifying the interactions involved.



Figure 5.9: Left: the pictorial representation of the (quadratic) interaction between  $\delta\phi$  (black propagator) and  $\delta\vartheta$  (blue). Center: the cubic interaction between  $\delta\vartheta$  and the gauge field quanta  $A_{\mu}$  (dashed line) Right: the cubic interaction between tensor modes (wiggly propagator) and the gauge field quanta.

The power spectrum of curvature perturbations  $\zeta$  is defined as

$$P_{\zeta}(k)\delta^{(3)}(\vec{k}+\vec{k'}) := \frac{k^3}{2\pi^2} \langle \zeta(\vec{k})\zeta(\vec{k'}) \rangle,$$
 (5.50)



Figure 5.10: Left: the sourced scalar power spectrum mediated by  $\delta\vartheta$ . The fluctuation of the inflaton  $\phi$  are linearly related to  $\zeta$ . Right: the sourced tensor power spectrum. One may use the in-in formalism to calculate these observables. However, in what follows we employ the equally valid Green's function method.

and analogously for  $h_{\pm}$  (where + and - denote the two gravitational wave polarizations). The power spectra receive contributions from vacuum fluctuations (superscript "vac") and the sources (superscript "src"), i.e.:

$$P_i(k) = P_i^{\text{vac}}(k) + P_i^{\text{src}}(k) \quad , i = \zeta, h_+, h_- .$$
 (5.51)

The vacuum power spectrum is parametrized as

$$P_{\zeta}^{\text{vac}} = A_s \left(\frac{k}{k_0}\right)^{ns-1} , \qquad (5.52)$$

and the tensor to scalar ration r is defined as

$$r \equiv P_T^{\text{total}}/P_\zeta^{\text{total}}$$
 (5.53)

Let us specialize our discussion of eq. (5.47) to the case with  $N_S = 2$ . For both axions we take  $\dot{\vartheta}_i \neq 0$  and the slow roll solutions will be analogous to the case with one spectator sector

$$\vartheta_{i} = 2f_{i} \arctan(e^{\delta_{i}H(t-t_{*})})$$

$$\dot{\vartheta}_{i} = \frac{f_{i}H\delta_{i}}{\cosh(\delta_{i}H(t-t_{*}^{i})},$$
(5.54)

with  $\delta_i = \frac{\Lambda_i^4}{6H^2f_i^2}$  and  $t_*^i$  is again the moment when  $\vartheta_i = \frac{\pi f}{2}$ . The validity of the slow-roll approximation requires

$$\frac{\ddot{\vartheta}_i}{3H\dot{\vartheta}_i} = -\frac{\delta_i}{3}\tanh(\delta_i H(t - t_*^i)) \ll 1 \to \delta_i \ll 3.$$
 (5.55)

As before, we define

$$\xi_i = \frac{\lambda_i \dot{\vartheta}_i}{2H f_i} = \frac{\xi_*^i}{\cosh(\delta_i H(t - t_*^i))} = \frac{2\xi_*^i}{\left(\frac{a}{a_*^i}\right)^{\delta_i} + \left(\frac{a_*^i}{a}\right)^{\delta_i}}, \tag{5.56}$$

with 
$$\xi_*^i = \frac{\lambda_i \dot{\vartheta}_*^i}{2Hf_i} = \frac{\lambda_i \delta_i}{2}$$
.

#### **Tensor Perturbations**

Let us move on to tensor perturbations. The amplification w.r.t. the vacuum comes from the standard kinetic term of the gauge fields in eq. (5.47). Indeed, the Chern-Simons term does not contain the metric tensor directly as the indices of  $\tilde{F}$  are raised with the antisymmetric tensor  $\varepsilon^{\mu\nu\rho\sigma}$ . Naturally, the CS coupling is still crucial in light of its effect on gauge fields at the level of their wavefunction. Following e.g. [162], we employ the Coulomb gauge and perform the mode expansion

$$\hat{A}_{m}^{i}(\tau, \vec{x}) = \int \frac{d^{3}k}{(2\pi)^{3/2}} e^{i\vec{k}\cdot\vec{x}} \hat{A}_{m}^{i}(\tau, \vec{k}) =$$

$$= \sum_{\lambda = +} \int \frac{d^{3}k}{(2\pi)^{3/2}} \left[ \varepsilon_{m}^{(\lambda)}(\vec{k}) A_{\lambda}^{i}(\tau, \vec{k}) \hat{a}_{\lambda}^{i}(\vec{k}) e^{i\vec{k}\cdot\vec{x}} + \text{ h.c. } \right],$$
(5.57)

where i=1,2 refers to the spectators while m is the space index. In a spatially flat, inflating, Universe with Hubble parameter H and scale factor  $a(\tau)=-1/(H\tau)$ , the mode functions satisfy (for both l=1,2)

$$A_{\pm}^{i''} + \left(k^2 \pm \frac{4k\xi_*^i}{\tau \left[ (\tau/\tau_*^i)^{\delta_i} + (\tau_*^i/\tau)^{\delta_i} \right]} \right) A_{\pm}^i = 0 , \qquad (5.58)$$

where the prime indicates a derivative with respect to the conformal time  $\tau$ . Taking  $\xi_* \geq 0$ , only the positive helicity mode is amplified. Dropping the index l for the moment, we can solve eq. (5.58) using the WKB approximation:

$$A_{+}(\tau,k) \simeq \left[\frac{-\tau}{8k\xi(\tau)}\right]^{1/4} \tilde{A}(\tau,k),$$

$$A'_{+}(\tau,k) \simeq \left[\frac{k\xi(\tau)}{-2\tau}\right]^{1/4} \tilde{A}(\tau,k),$$
(5.59)

where

$$\tilde{A}(\tau, k) \equiv N\left[\xi_*, x_*, \delta\right] \exp\left[-\frac{4\xi_*^{1/2}}{1+\delta} \left(\frac{\tau}{\tau_*}\right)^{\delta/2} (-k\tau)^{1/2}\right], \tag{5.60}$$

with N a time-independent normalization factor. The electric and magnetic field can be defined as

$$\hat{E}_m \equiv -\frac{1}{a^2}\hat{A}'_m, \quad \hat{B}_m \equiv \frac{1}{a^2}\varepsilon_{mnp}\partial_n\hat{A}_p.$$
 (5.61)

The mode expansion for the transverse, traceless tensor perturbations of the metric  $\hat{h}_{mn}$  defined in chapter C reads

$$\hat{h}_{mn}(\tau, \vec{k}) = \frac{2}{M_p \, a(\tau)} \int \frac{d^3k}{(2\pi)^{3/2}} e^{i\vec{k}\cdot\vec{x}} \sum_{\lambda = +, -} \Pi^*_{mn,\lambda}(\hat{k}) \hat{Q}_{\lambda}(\tau, \vec{k}) , \qquad (5.62)$$

with  $\Pi_{mn,\lambda}^*(\hat{k}) = \varepsilon_m^{(\pm)}(\hat{k}) \, \varepsilon_n^{(\pm)}(\hat{k})$  the polarization operators. The tensor modes equation of motion reads

$$\left(\frac{\partial^2}{\partial \tau^2} + k^2 - \frac{2}{\tau^2}\right) \hat{Q}_{\lambda}(\vec{k}, \tau) = \hat{S}_{\lambda}^1(\tau, \vec{k}) + \hat{S}_{\lambda}^2(\tau, \vec{k}), \tag{5.63}$$

where

$$\hat{S}^{i}_{\lambda}(\tau, \vec{k}) \equiv -\frac{a^{3}}{M_{p}} \Pi_{mn,\lambda}(\hat{k}) \int \frac{d^{3}x}{(2\pi)^{3/2}} e^{-i\vec{k}\cdot\vec{x}} \left[ \left( \hat{E}_{m}\hat{E}_{n} + \hat{B}_{m}\hat{B}_{n} \right)^{i} \right],$$
 (5.64)

and where we have re-introduced the spectator label l. The sourcing explicit in Eq. (5.64) is the one represented<sup>23</sup> in the right panel of Fig. 5.10. Decomposing the solution into homogeneous and sourced parts, the vacuum mode is given by

$$\hat{Q}_{\lambda}^{\text{vac}}(\vec{k}) = h_{\lambda}(\tau, k)\hat{a}_{\lambda}(\vec{k}) + h_{\lambda}^{*}(\tau, k)\hat{a}_{\lambda}^{\dagger}(-\vec{k}),$$

$$h_{\lambda}(\tau, k) = \frac{e^{-ik\tau}}{\sqrt{2k}} \left(1 - \frac{i}{k\tau}\right).$$
(5.65)

The inhomogeneous solution is given by the source terms

$$\hat{Q}_{\lambda}^{\rm src}(\tau, \vec{k}) = \int^{\tau} d\tau' G_k(\tau, \tau') \left[ \hat{S}_{\lambda}^1(\tau, \vec{k}) + \hat{S}_{\lambda}^2(\tau, \vec{k}) \right], \qquad (5.66)$$

where the Green's function is defined in chapter C. The power spectrum  $\mathcal{P}$  is defined as

$$\mathcal{P}_{\lambda}(k)\delta_{\lambda\lambda'}\delta^{(3)}\left(\vec{k}+\vec{k'}\right) = \frac{k^3}{2\pi^2} \left\langle \hat{h}_{\lambda}(\vec{k})\hat{h}_{\lambda'}(\vec{k'}) \right\rangle. \tag{5.67}$$

Given that in our case the two source terms are to a good approximation uncorrelated, one may compute the two corresponding inhomogeneous solutions separately and sum them to obtain the resulting spectrum. The calculation of the sourced scalar spectrum is a bit more involved in that the inflaton is only gravitationally coupled to the axion. As a result, the effect of the gauge quanta on the scalar curvature  $\zeta$  is mediated by the field  $\vartheta$ .

#### **Scalar Perturbations**

We take the spatially flat gauge, such that the scalar sector of the metric can be written solving for the non dynamical variables  $\varphi$ , B as:

$$ds^{2} = a^{2}(\tau)\left[-(1+2\varphi)d\tau^{2} + 2\partial_{i}Bdx^{i}d\tau + \delta_{ij}dx^{i}dx^{k}\right]. \tag{5.68}$$

The remaining physical modes can be decomposed as

$$\hat{\phi}(x,\tau) = \phi(\tau) + \int \frac{d^3k}{(2\pi)^{3/2}} e^{-\vec{k}\cdot\vec{x}} \frac{\hat{Q}_{\phi}(\vec{k})}{a(\tau)} 
\hat{\vartheta}_i(x,\tau) = \vartheta_i(\tau) + \int \frac{d^3k}{(2\pi)^{3/2}} e^{-\vec{k}\cdot\vec{x}} \frac{\hat{Q}_{\vartheta_i}(\vec{k})}{a(\tau)} .$$
(5.69)

We can then rewrite $^{24}$  the action of eq. (5.47) paired with the Einstein-Hilbert action as

$$S = S_{\text{free}} + S_{\text{int}}^{1} + S_{\text{int}}^{2}$$

$$S_{\text{free}} \left[ \hat{Q}_{i} \right] = \frac{1}{2} \int d\tau d^{3}k \left[ \hat{Q}_{i}^{\prime\dagger} \hat{Q}_{i}^{\prime} - \hat{Q}_{i}^{\dagger} \left( k^{2} \delta_{ij} + \tilde{M}_{ij}^{2} \right) \hat{Q}_{j} \right]$$

$$S_{\text{int}}^{i} = - \int d^{4}x \sqrt{-g} \, \lambda_{i} \frac{\vartheta_{i}}{4f_{i}} F_{\mu\nu}^{i} \tilde{F}^{l\mu\nu} = \int d^{4}x a^{4} \lambda_{i} \frac{\vartheta_{i}}{f_{i}} \mathbf{E}_{i} \cdot \mathbf{B}_{i} ,$$

$$(5.70)$$

where we have defined  $(\hat{Q}_1, \hat{Q}_2, \hat{Q}_3) \equiv (\hat{Q}_{\phi}, \hat{Q}_{\vartheta_1}, \hat{Q}_{\vartheta_2})$  and  $(\phi_1, \phi_2, \phi_3) \equiv (\phi, \vartheta_1, \vartheta_2)$ . The electric  $\mathbf{E}_i$  and magnetic  $\mathbf{B}_i$  field vectors are those of eq. (5.61) and one finds

$$\tilde{M}_{ij}^{2} \equiv -\frac{a''}{a}\delta_{ij} + a^{2}V_{,ij} + \left(3 - \frac{\phi'_{l}\phi'_{l}}{2M_{p}^{2}}\frac{a^{2}}{a'^{2}}\right)\frac{\phi'_{i}\phi'_{j}}{M_{p}^{2}} + \frac{a^{3}}{M_{p}^{2}a'}\left(\phi'_{i}V_{,j} + \phi'_{j}V_{,i}\right),$$
(5.71)

<sup>&</sup>lt;sup>23</sup>There is one such diagram for each value run by the spectator label "l".

<sup>&</sup>lt;sup>24</sup>Note that we are omitting the kinetic term of gauge fields as these do not play a key role in sourcing scalars.

with  $V_{,i} \equiv \partial V/\partial \phi_i$ . Introducing slow-roll parameters for each of the fields  $\phi_i$  as in chapter C, we obtain, to leading order, the following equations of motion

$$\left(\frac{\partial}{\partial \tau^2} + k^2 - \frac{2}{\tau^2}\right) \hat{Q}_{\phi} \simeq \frac{6}{\tau^2} \sqrt{\varepsilon_{\phi} \varepsilon_{\vartheta_1}} \hat{Q}_{\vartheta_1} + \frac{6}{\tau^2} \sqrt{\varepsilon_{\phi} \varepsilon_{\vartheta_2}} \hat{Q}_{\vartheta_2}, 
\left(\frac{\partial}{\partial \tau^2} + k^2 - \frac{2}{\tau^2}\right) \hat{Q}_{\vartheta_i} \simeq \lambda_i \frac{a^3}{f_i} \int \frac{d^3 x}{(2\pi)^{3/2}} e^{-i\vec{k}\cdot\vec{x}} \mathbf{E}_i \cdot \mathbf{B}_i \equiv \hat{S}_{\vartheta_i}(\tau, \vec{k}).$$
(5.72)

Considering the dominant terms in the mass matrix and in the equations leads us to the two independent equations of motion for the axions. Given that we assume that the two axions' energy densities will vanish after CMB, in the spatially flat gauge the scalar curvature perturbation are given just by the perturbations of the inflaton,

$$\hat{\zeta}(\tau, \vec{k}) \simeq -\frac{H}{\dot{\phi}} \hat{\delta\phi}(\tau, \vec{k}) = \frac{H\tau}{\sqrt{2\varepsilon_{\phi}} M_{pl}} \hat{Q}_{\phi}(\tau, \vec{k}). \tag{5.73}$$

It turns out to be convenient to write the solution as

$$\hat{Q}_{\phi} = \hat{Q}_{\phi}^{\text{vac}} + \hat{Q}_{\phi}^{\text{src}}, \qquad (5.74)$$

where  $\hat{Q}_{\phi}^{\text{vac}}$  is the homogeneous solution to the inflaton equation of motion and  $\hat{Q}_{\phi}^{\text{src}}$  is the particular solution. Expanding the homogeneous solution operator as

$$\hat{Q}_{\phi}^{\text{vac}}(\tau, \vec{k}) = Q_{\phi}^{\text{vac}}(\tau, k)a(\vec{k}) + Q_{\phi}^{*\,\text{vac}}(\tau, k)a^{\dagger}(-\vec{k}), \qquad (5.75)$$

and imposing Bunch-Davis initial conditions, we find

$$Q_{\phi}^{\text{vac}}(\tau, k) = \frac{e^{-ik\tau}}{\sqrt{2k}} \left( 1 - \frac{i}{k\tau} \right) . \tag{5.76}$$

The particular solution is found, using the retarded Green's function from chapter C, to be given by

$$\hat{Q}_{\phi}^{\text{src}} = 6\sqrt{\varepsilon_{\phi}} \int d\tau' G_{k}(\tau, \tau') 
\left(\frac{\sqrt{\varepsilon_{\vartheta_{1}}}}{\tau'^{2}} \int d\tau'' G_{k}(\tau', \tau'') \hat{S}_{\vartheta_{1}}(\tau'', \vec{k}) + \frac{\sqrt{\varepsilon_{\vartheta_{2}}}}{\tau'^{2}} \int d\tau'' G_{k}(\tau', \tau'') \hat{S}_{\vartheta_{2}}(\tau'', \vec{k})\right).$$
(5.77)

The corresponding solution for the curvature perturbation is

$$\hat{\zeta}^{\text{src}} = \frac{3\sqrt{2}H\tau}{M_{nl}} \int d\tau' G_k \left( \frac{\sqrt{\varepsilon_{\vartheta_1}}}{\tau'^2} \int d\tau'' G_k \hat{S}_{\vartheta_1} + \frac{\sqrt{\varepsilon_{\vartheta_2}}}{\tau'^2} \int d\tau'' G_k \hat{S}_{\vartheta_2} \right) , \qquad (5.78)$$

where the source functions  $\hat{S}_{\vartheta_i}(\tau, \vec{k})$  are defined in eq. (5.72). The standard definition of the power spectrum is

$$P_{\zeta}(k)\delta^{(3)}(\vec{k}+\vec{k}') = \frac{k^3}{2\pi^2}\langle \zeta(k)\zeta(k')\rangle.$$
 (5.79)

Much like for the tensor power spectrum, the sourcing is such that the scalar power spectrum is also additive, so that we can write

$$P_{\zeta} = P_{\zeta}^{\text{vac}} + \sum_{i=1}^{N} P_{\zeta}^{i \text{ src}},$$

$$P_{GW} = P_{GW}^{\text{vac}} + \sum_{i=1}^{N} P_{GW}^{i \text{ src}}.$$

$$(5.80)$$

#### Axion and Gauge Field Mixing

In the next section we will rely on the notion that both (i) the coupling between different axions and (ii) the coupling between different gauge sectors are only gravitational and can therefore be disregarded. The coupling comes with a slow-roll suppression in the scalar sector (see e.g. Eq. (5.72)) and turns out to be negligible also in the case of gauge fields mixing.

One may intuitively arrive at the latter conclusion as follows. First of all, in the Abelian case any coupling between gauge sectors starts out at the level of the cubic Lagrangian, so we are already in the realm of loop corrections. Secondly, the CS terms is not directly involved given that the field strengths are not contracted through the metric. In solving the constraint equation no one gauge sector plays a leading role with respect to the other one(s). It follows that neglecting mixing across sectors is tantamount to neglecting the sub-leading gauge self-interactions as routinely done in models with only one gauge sector.

In neglecting the mixing between the different axions extra care needs to be exerted. The leading contribution to the  $\delta\vartheta_i$  power spectra comes from the non-linear interaction with the gauge fields  $A_{\mu}^{(i)}$ , where "i" is the index that runs through the various axion sectors, and is schematically proportional to  $\lambda_i^2$ . If we want to probe the contribution of another  $A_{\mu}^{(j\neq i)}$  gauge sector to the power spectrum of a given field  $\delta\vartheta_i$ , we need the mediation of the field  $\delta\vartheta_j$ . The price to pay is, as mentioned, a suppression<sup>25</sup> of order  $\varepsilon^2$ . The  $\delta\vartheta_j$ -mediated contribution to the  $\delta\vartheta_i$  power spectrum will have to then be compared to the contribution due directly to the  $A_{\mu}^i$  sector. In other words we have  $\lambda_i^2 \leftrightarrow \varepsilon^2 \lambda_j^2$ . So long as there is not a significant hierarchy in place for the values of the coupling constants  $\lambda_k$ , one can safely neglect the contribution coming from mixing the axion and gauge sectors.

# 5.4 Detecting the Spectator Axiverse

In the previous sections, we introduced MASA models and explored their gravitational wave spectrum. A key point is that the lack of direct mixing between axions implies that the total gravitational wave spectrum is, to a good approximation, a superposition of the spectrum from each spectator axion. This raises interesting possibilities for signals arising from MASA models, namely multiple peaks and signal boosting.

Specific initial conditions and parameter choices lead to different features in the power spectra. For example, if we examine axions with comparable initial conditions and parameter values, the resulting power spectra will lead to an amplified signal strength within a specific range of scales. In principle, the number of spectator sectors  $N_S$  can then serve as another handle for signal enhancement, independent of values of the Chern-Simons couplings. However, the crucial question is whether such a scenario is plausible or if it is too finely tuned to be regarded as compelling and relevant for cosmological model building. In fact, when considering random initial conditions and parameters, we can expect to observe a mix of signals at distinct wavelengths, some of which may exhibit greater enhancements than others. These enhanced signals could arise from scenarios involving stronger Chern-Simons couplings or the stacking described above.

<sup>&</sup>lt;sup>25</sup>Note that here  $\varepsilon^2$  is a placeholder for a suppression of the order of slow-roll parameters and is to be understood, conservatively, as satisfying  $\varepsilon < 10^{-2}$ .

Once the number of e-folds for which the axion "i" rolls is fixed, the amplitude of the peaks in the power spectra will primarily depend on the Chern-Simons coupling parameter  $\lambda_i$ , which is encoded in  $\xi_*^i$ . The signal strength depends exponentially on  $\lambda_i$  whilst in contrast the stacking of axions, although capable of boosting the signal, is approximately only linear. Given a sufficient number of axions the outcome for the signal becomes essentially stochastic thus motivating the use of statistical methods in this context, akin to [302] for multi-field inflation.

#### 5.4.1 Primordial Power Spectra

As we showed above in eq. (5.5), the position of the peak of the GW signal  $(k_*)$  is set by the initial phase of the axion,  $\vartheta_{in}/f$ , and the number of e-folds during which it rolls,  $1/\delta$ . Further analysis (see Fig. 5.11) shows the existence of a preferred range in  $k_*$  corresponding to a higher degeneracy in the initial conditions. This is the most favorable domain for axion stacking.

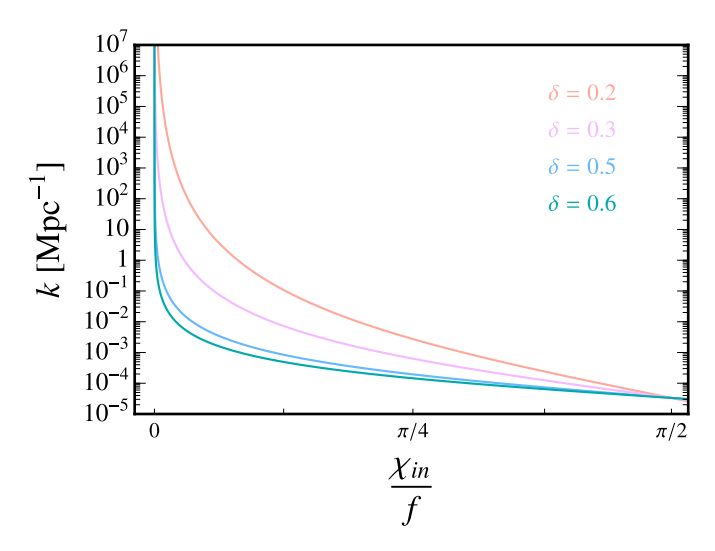


Figure 5.11:  $k_*$  as a function of the initial axion phase, for each choice of  $\delta$  considered: red for  $\delta = 0.2$ , pink for  $\delta = 0.3$ , blue for  $\delta = 0.5$  and turquoise for  $\delta = 0.6$ .  $k_*$  peaks for small values of  $\vartheta_{in}/f$ . The domain with the lowest absolute value of the slope is the most favorable to stacking.

The power spectra can be parameterized through [162, 303]

$$P_{\zeta}^{\text{src}}(k) = \left[\varepsilon P_{\zeta}^{\text{vac}}(k)\right]^{2} f_{2,\zeta} \quad , \quad P_{T}^{\text{src}}(k) = \left[\varepsilon P_{\zeta}^{\text{vac}}(k)\right]^{2} (f_{2,+} + f_{2,-}) \quad , \tag{5.81}$$

An analytic fit for the dependence of these functions on  $\xi_*$  was described in [162], for the two given values  $\delta=0.2,\,0.5$ . We compute these functions for  $\delta=0.3$  and  $\delta=0.6$  (tables 5.1 and 5.2).

We also compute the second order scalar induced gravitational waves, given by:

$$P_T^{\text{ind}}(k) = 1.4 \int_0^\infty dv \int_{|1-v|}^{1+v} du \frac{\mathcal{T}(u,v)}{u^2 v^2} P_{\zeta}(vk) P_{\zeta}(uk)$$
 (5.82)

where the transfer function  $\mathcal{T}(u,v)$  is standard (see e.g. [304]). The total GW power spectrum then amounts to the sum of the following contributions:

$$P_T(k) = P_T^{\text{vac}}(k) + P_T^{\text{src}}(k) + P_T^{\text{ind}}(k)$$
. (5.83)

$\{2,i\}$	$\ln \left  f_{2,i}^c  ight  \simeq$	$x_{2,ij}^c \simeq$	$\sigma_{2,i} \simeq$
$\{2,\zeta\}$	$-4.926 + 9.339\xi_* + 0.0839\xi_*^2$	$-28.747 + 12.37\xi_* - 1.0989\xi_*^2$	$-3.584 + 1.633\xi_* - 0.155\xi_*^2$
$\{2, +\}$	$-4.516 + 8.882\xi_* + 0.108\xi_*^2$	$-1.324 + 1.619\xi_* - 0.041\xi_*^2$	$1.242 - 0.227\xi_* + 0.017\xi_*^2$
$\{2, -\}$	$-9.515 + 8.781\xi_* + 0.115\xi_*^2$	$-0.279 + 0.526\xi_* - 0.009\xi_*^2$	$1.081 - 0.135\xi_* + 0.010\xi_*^2$

Table 5.1:  $\xi_*$  dependence of the functions appearing in eq. (5.14), for  $\delta = 0.3$ .

$\{2,i\}$	$\ln \left  f_{2,i}^c  ight  \simeq$	$x_{2,ij}^c \simeq$	$\sigma_{2,i} \simeq$
$\{2,\zeta\}$	$-8.819 + 9.662\xi_* - 0.076\xi_*^2$	$0.434 + 0.962\xi_* - 0.020\xi_*^2$	$0.969 - 0.180\xi_* + 0.015\xi_*^2$
$\{2, +\}$	$-0.759 + 7.005\xi_* + 0.118\xi_*^2$	$-0.216 + 1.096\xi_* + 0.006\xi_*^2$	$0.670 - 0.085\xi_* + 0.005\xi_*^2$
$\{2, -\}$	$-6.010 + 6.743\xi_* + 0.136\xi_*^2$	$0.536 + 0.214\xi_* + 0.025\xi_*^2$	$0.414 + 0.058\xi_* - 0.006\xi_*^2$

Table 5.2:  $\xi_*$  dependence of the functions appearing in eq. (5.14), for  $\delta = 0.6$ .

When it comes to axion masses in the Axiverse the expectation is that these are homogeneously distributed on a log scale [15]. However, in the present context we are to negotiate with two additional constraints. We randomly draw  $\delta$ , which is related to the axion mass through  $\delta = \frac{m_{\vartheta}^2}{6H^2}$ . Assuming that the inflationary scale does not vary more than three orders of magnitude,  $\delta$  no longer follows the logarithmic distribution. The aforementioned constraints stem from, on the one hand, operating in the slow-roll regime, which enforces  $\delta \ll 3$  (see Eq. (5.6)). As we shall see below, avoiding PBH overproduction also requires  $\delta \gtrsim 0.2$ . Given the rather limited interval of allowed values, we draw them from a flat distribution.

By performing random draws of the parameters,  $\xi_* \in [2.5, 5]$ ,  $\delta \in \{0.2, 0.3, 0.5, 0.6\}$ , and  $x_{in} \equiv \vartheta_{in}/f \in [0, \pi/4]$ , we can generate the signal corresponding to specific numbers of spectator sectors in fig. 5.12. For the sake of simplicity, we randomly draw using flat distributions. In fig. 5.12 one can notice how, as the number of axions increases, non-regular patterns on and between the peaks become more visible as a result of the sum and stacking of the signals from multiple spectators.

We report here the predictions for the average distortions arising from the dissipation of curvature perturbations in the cases illustrated in fig. 5.12. One obtains the following values:

$$\mu = 2.7 \times 10^{-7}$$
,  $y = 2.3 \times 10^{-9}$  for  $N_s = 5$  spectators,  
 $\mu = 1.5 \times 10^{-5}$ ,  $y = 1.2 \times 10^{-4}$  for  $N_s = 10$  spectators,  
 $\mu = 1.2 \times 10^{-3}$ ,  $y = 3.2 \times 10^{-9}$  for  $N_s = 50$  spectators. (5.84)

Notice that there are striking differences in the results for spectral distortions corresponding to the different profiles of Fig. 4. This is entirely due to the fact that, besides the changes in the number of spectator fields, in order to generate the three profiles we have drawn different values for both the parameters  $\vartheta_{\rm in}$  and  $\lambda$ . The first quantity controls the position of the peak(s) whilst the height of the peak(s) is very sensitive to the value of  $\lambda$ . The  $N_s=10$  and  $N_s=50$  scenarios are at odds with existing constraints. This shows how spectral distortion constraints have the ability to limit the allowed range for the Chern-Simons coupling, in conjunction with the number of axions in the model, whenever the signal reaches its peak within the spectral distortions window. An exhaustive analysis of these constraints would involve accounting for the interplay of several elements of the theory, including the number of axions, their initial conditions, and parameters in the

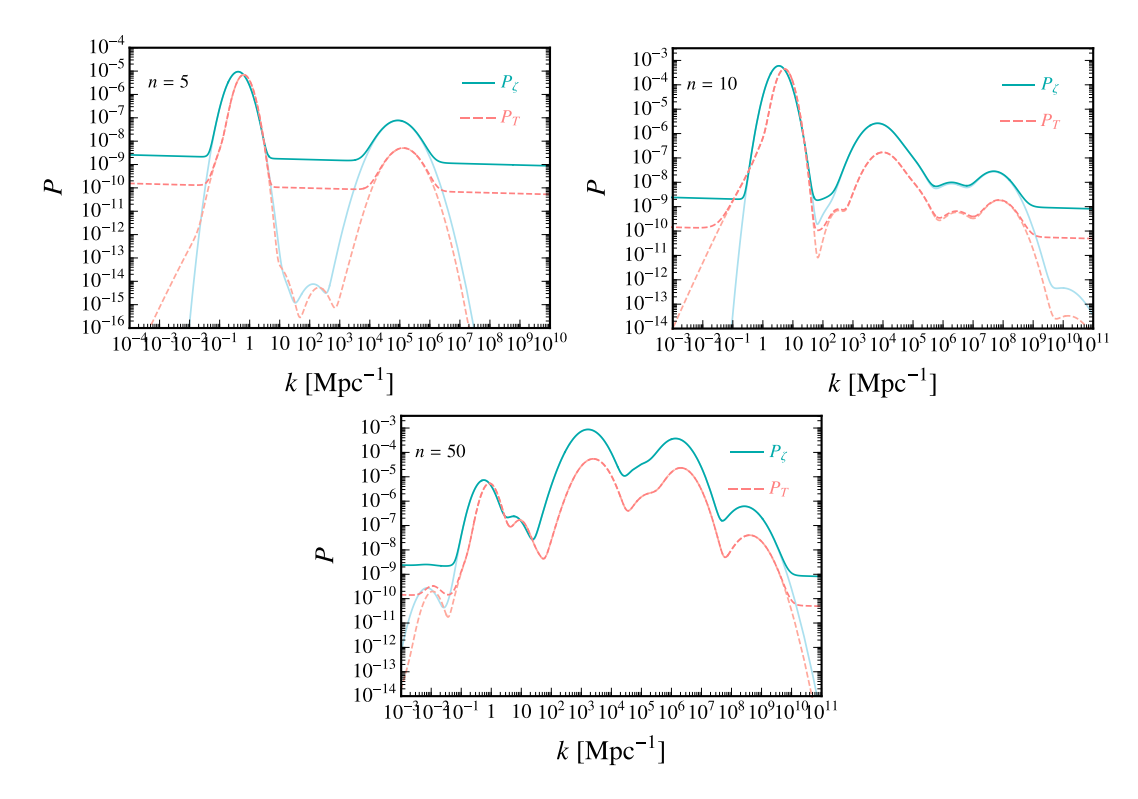


Figure 5.12: Typical power spectra for a number of spectator sectors n=5, 10, 50. Continuous turquoise lines indicate the total curvature power spectrum, while dashed pink lines show the total  $P_T$ . Light pink and light turquoise lines mark the sourced contributions alone, without the vacuum term. The values for  $\delta$ ,  $\xi_*$  and  $\vartheta_{in}/f$  have been drawn randomly as described in the text. One can notice that not all the spectator sectors contribute in a significant way: some will indeed have a Chern-Simons coupling such that the sourced signal is weaker than its vacuum counterpart.

potential. Undertaking such an exhaustive analysis goes beyond the scope of the present paper and is deferred to future work. Our goal here is rather to underscore the necessity of taking spectral distortion into account when investigating predictions of the axiverse, both as a constraining factor and as a signature itself.

#### 5.4.2 Detectability of Gravitational Wave Signals

In this section, we will investigate the conditions on the model parameters that ensue from requiring a GW signal be at the level of the recent PTA observations of a stochastic background [266, 305, 306], or above the sensitivity limits of planned interferometers.

Let us begin at PTA scales and consider for simplicity the scenario with one spectator sector. We present in table 5.3 a representative sample parameters set that delivers a GW signal with a strength comparable to the one observed, corresponding to a primordial power spectrum of order  $P_T \sim 10^{-3}$  <sup>26</sup>.

Here  $\mathfrak{q}$  is related to the Chern-Simons coupling via  $\lambda = \mathfrak{q}\alpha/\pi$ , with the fine structure constant taken to be  $\alpha = 0.1$ . For every chosen value of  $\delta$  and for a given target value of

<sup>&</sup>lt;sup>26</sup>We verified that the chosen parameters fall within the constraints posed by working in a regime of (i) weak backreaction for the spectator fields, and of (ii) perturbative control for the theory. See Appendix C.3 for details.

δ	$\vartheta_{in} \simeq$	$\xi_* \simeq$	$\lambda \simeq$	$\mathfrak{q}\simeq$
0.2	$1.9 \times 10^{-2}$	5	50	1570
0.3	$1.9 \times 10^{-3}$	5.2	35	1089
0.5	$1.8 \times 10^{-5}$	5.5	22	691
0.6	$1.8 \times 10^{-5}$	5.9	20	617

Table 5.3: Set of parameters used to reproduce, for each given  $\delta$ , the PTA signal in single-spectator MASA models.

 $P_T$ , a value of  $\xi_*$  will follow (and, from there, a value for  $\lambda$ ). Given the relation  $\xi_* = \lambda \delta/2$ , higher values of  $\delta$  require a lower  $\lambda$  to reach a given amplitude of the signal. One can construct, keeping the power spectrum amplitude fixed and interpolating the parameters found above, an approximate relation between the duration of the rolling for the axion, encoded in  $\delta$ , and the parameter  $\lambda$ , finding:

$$\lambda = 90.2 - 246.3\delta + 216.7\delta^2 \,, \tag{5.85}$$

a description valid for  $\delta$  values ranging between 0.2 and 0.6.

The scalar and tensor power spectra corresponding to the benchmark values in table 5.3 are plotted in fig. 5.13. The plots show that smaller values of  $\delta$  correspond to increasingly high values of  $P_{\zeta}$  and to a lower value of the tensor-to-scalar ratio  $(r = P_T/P_{\zeta})$ . We note that a change in  $\delta$  affects the scalar fluctuations more strongly than the tensor fluctuations. This can be easily understood as follows: by increasing  $\delta$  one is decreasing the time during which  $\vartheta$  rolls, thus lowering the amplitude of the produced signal as well its width (the smaller  $\Delta N \sim 1/\delta$ , the fewer the modes that exited the horizon while  $\dot{\vartheta}$  was non negligible). Inflaton perturbations are sourced by the  $\delta\vartheta$  modes only while  $\dot{\vartheta} \neq 0$ , therefore a decrease of  $\Delta N$  affects the sourced scalar modes more than the tensor modes because it decreases both the number of modes that are sourced, and the time interval during which the  $\delta\vartheta$  modes can be converted into inflaton perturbations.

We find that, for the set value of  $P_T$ ,  $P_{\zeta}$  is slightly above the PBH bound in the  $\delta = 0.2$  case, while larger values of  $\delta$  are viable. The left tail of the peak falls within SDs scales, producing a  $\mu$  distortion of order  $10^{-8}$ , possibly at reach for future probes.

The range considered for  $\delta$  (and, as a result, for  $\xi_*$ ,  $\lambda$  and  $\mathfrak{q}$ ) corresponds to the extent of parameter space supporting a signal compatible with PTA observations: we are working under the condition  $\delta \ll 3$  (hence the chosen maximum,  $\delta \lesssim 0.6$ ), while values of  $\delta \lesssim 0.2$  are ruled out by constraints on  $P_\zeta$ . A value of  $\mathfrak{q}$  of order  $10^2-10^3$  (see Table 5.3) is therefore a prerequisite for a signal compatible with PTA observations. The authors of [203] discussed the UV embedding of spectator-axion models pointing out that the previously defined  $\mathfrak{q}$  (as opposed to  $\lambda$ ) should be the parameter of choice in that context. We will address the feasibility of a  $\mathfrak{q}$  of the order of  $10^2-10^3$  in the next sections, where we compute the restrictions on  $\lambda$  and  $\mathfrak{q}$  from UV embeddings. The scalar-induced second order GWs encoded in  $P_T^{ind}$  are visible on the left tail of the spectrum in Fig. 5.13. Fig. 5.13 shows how the profile of SIGW is broader around the peak as compared to the other contributions to the GW signal. The SIGW signal is also asymmetric around the peak skewing towards lower frequencies (the domain immediately to the left of the peak). One may get a glimpse of such effects in the total GW power spectrum by inspecting the first peak of Fig. 5.12 where these features are somewhat discernible in the  $\mathfrak{n}=5$  and  $\mathfrak{n}=10$  cases, while they are not visible for  $\mathfrak{n}=50$ .

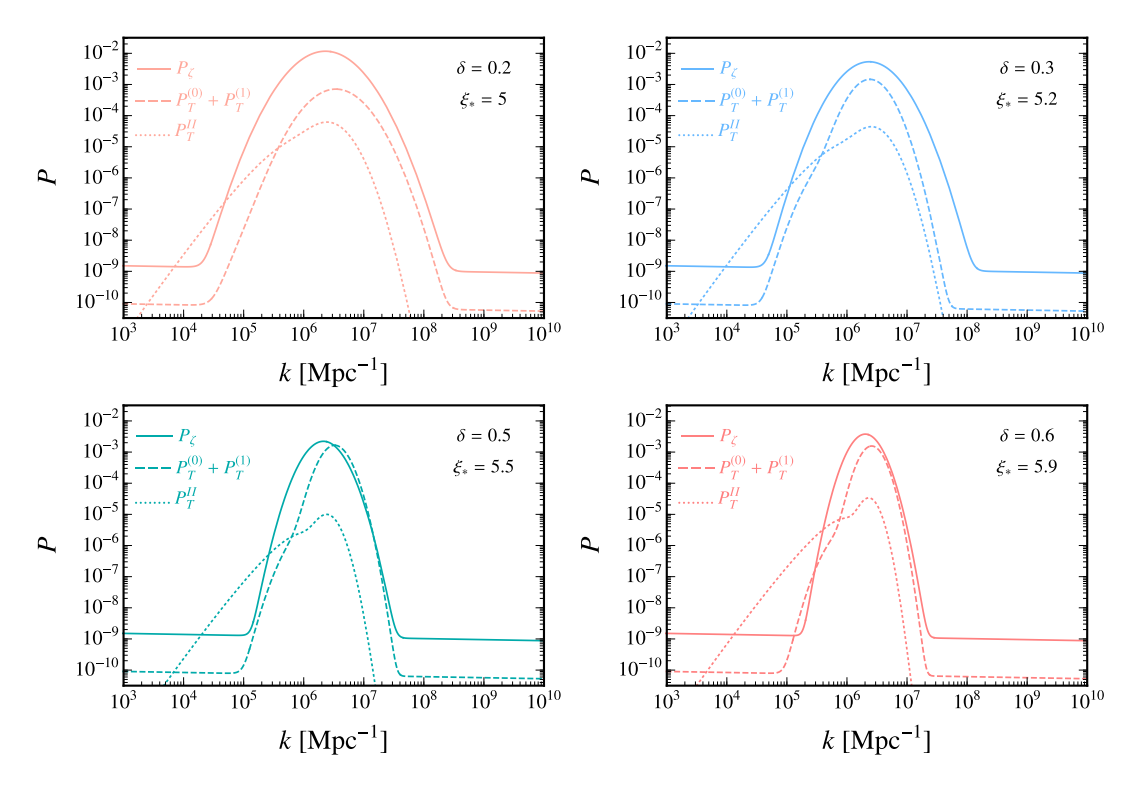


Figure 5.13: Curvature perturbation (solid line) and GW (dashed line) power spectra for  $\delta = 0.2$  (top left),  $\delta = 0.3$  (top right),  $\delta = 0.5$  (bottom left) and  $\delta = 0.6$  (bottom right). The dotted line corresponds to the induced gravitational waves computed in eq. (5.82)

Let us now discuss what would be the requirements on the model parameters for the signal to be visible by GW detectors at smaller scales.

We provide in fig. 5.14 the values of  $\lambda$  that are needed, for fixed  $\delta=0.5$ , in order for the signal to reach the sensitivity limits of a number of experiments. These values have been derived under the simplifying assumption of one spectator sector (or, which is effectively equivalent, of one spectator sector whose signal dominates over those from other sectors). One can notice how strongly sensitive the signal is to  $\lambda$ : a small change in this parameter can produce a dramatic change in the spectrum amplitude. As an example, for  $\delta=0.5$ , at LISA scales  $(10^{10}-10^{13}{\rm Mpc}^{-1})$  one requires  $\xi_*\gtrsim 4$ , so  $\lambda\gtrsim 16$  and  $\mathfrak{q}\sim 6\times 10^2$ , to reach the minimum detectable amplitude of  $P_T\sim 10^{-9}$ . The BBO sensitivity limit (matched up by  $P_T\sim 10^{-13}$  around scales of  $k\sim 10^{13}{\rm Mpc}^{-1}$ ) would require  $\xi_*\sim 3.1$ , corresponding to  $\lambda\sim 12.4$  and  $\mathfrak{q}\sim 4\times 10^2$ . It is also worth stressing that from the argument offered in Sec. 5.4.1, a  $k_*$  at interferometer scales may not be favoured if parameters are drawn randomly and assuming, as we did, a flat distribution.

As we will elaborate further in the following sections, when embedding these models in string theory, one would like to lower the required CS coupling in order to broaden, as much as possible, the parameter space. To this aim, one can exploit the stacking of the signals: assigning multiple axions initial conditions and parameters in such a way as to have similar  $k_*$  leads to peaks at similar scales which then add up. The simplest possibility is to have spectators with similar parameters and initial conditions. As an example, for a detectable signal by BBO with  $\delta = 0.5$  and one axion, the required CS coupling is  $\lambda \sim 12.4$ . On the other hand, incorporating ten spectator axions with comparable initial

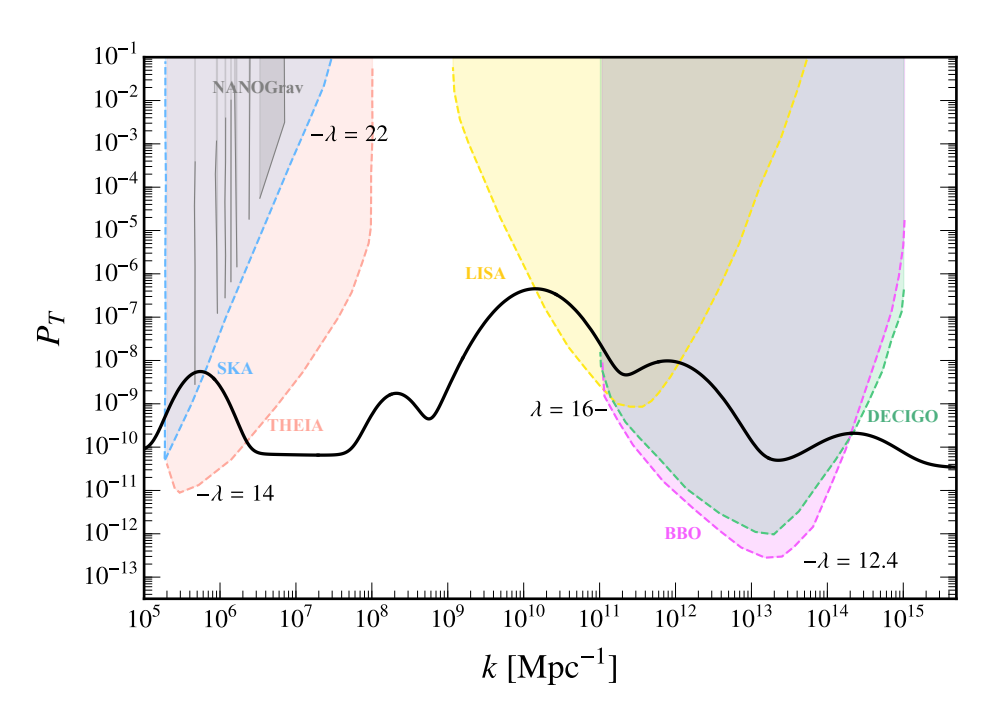


Figure 5.14: Sensitivity and observations of stochastic GW backgrounds of current and future detectors, such as LISA [307], SKA [308], THEIA [309], BBO [310] and DECIGO [311]. Next to the sensitivity curves we show the values of  $\lambda$  necessary for the signal in our model to reach those amplitudes when  $\delta = 0.5$ . The black curve shows what a typical signal may look like for n = 10 spectator sectors with  $\xi_* \in [3.5, 5]$ .

conditions reduces the necessary CS coupling to  $\lambda \sim 11.4$ . While stacking undeniably helps reduce the required CS coupling for signal observation, it introduces the need for rather specific initial conditions. In the absence of a precise distribution of initial conditions, one may question the naturalness of requiring ten different axions with identical initial field values. Moreover, requiring ten distinct axions with a CS coupling significantly greater than one might prove to be more challenging than having a single axions with a slightly higher CS coupling.

The general feature of any "stringy" inflationary model is the presence of axions, or more precisely ALPs, that can couple to dark U(1) sectors through CS coupling. The number of these axions and their precise properties depend on the model and the compactification considered. However, regardless of the specifics of the UV properties, one can arrive at a general feature: the presence of a gravitational wave forest. Indeed, the natural end point of the above discussion is to expect GWs signals and curvature perturbation peaks throughout the whole frequency spectrum. We refrain from giving a specific shape of the signal as this depends on the number of axions, the CS coupling, and the amount of e-folds for which the axions roll. Instead, we want to emphasize that we expect to find a gravitational wave forest by searching for GWs and  $\zeta$ -peaks at different scales. However, it is essential to acknowledge a significant challenge posed by our analysis. To detect this signal today, a sufficiently large Chern-Simons coupling value is required. This observation raises valid concerns from the perspective of UV physics, as it complicates the integration of these models into a coherent UV framework. We will address these questions in the following chapter.

#### 5.5 Remarks

Inflationary models with spectator axions are an interesting framework for primordial cosmology, potentially allowing for observable signals from sectors that are highly sequestered from the Standard Model. In the context of string theory, a natural expectation is that the spectators may consist of multiple axions coupled to gauge fields. With this motivation, in the present paper we have extended the typical spectator models to account for multiple such fields, proposing the study of what we refer to as "Multiple (non-)Abelian Spectator Axion" inflationary models. Our primary objective has been to investigate the cosmological predictions from these models, exploring also their viability in string constructions and their connection to the axiverse. In this respect, models with Abelian gauge groups (MASA models) appear easier to realize in controlled string settings with respect to their non-Abelian (MnASA) counterpart.

Our analysis, focused on the Abelian case, reveals distinct signatures in both the curvature and GWs power spectra, manifesting as multiple peaks at different scales. We stress that our considerations and finding do not necessarily apply to scenarios involving axions coupled to multiple gauge fields, or to cases where Abelian gauge fields interact via kinetic mixing. There is some indication that the former scenario may be rather rare in the type IIB landscape [70], while the latter may be entirely absent or quite suppressed [312].

The many possibilities granted by the choice of initial conditions, the number of spectators and their couplings chart an intriguing map of cosmological signatures, with multi-peaked spectra of varying width, amplitude, and position. Such map includes the possibility of a primordial GW signal at PTA scales, fully compatible [313] with the recently detected stochastic background in the nHz range and satisfying both perturbativity and backreaction constraints. Naturally, the presence of multiple spectator sectors has much more to offer: a gravitational wave forest which is ripe for the testing via existing as well as forthcoming GW probes. The sourcing mechanism for scalar and tensor fluctuations is analogous: the gauge fields non-linearly source both two-point functions. As a result, there is a scalar counterpart to the GW forest which, as we show, can be tested and constrained via CMB anisotropies, spectral distortions, and PBH bounds, depending on the scales involved. Scalar fluctuations also serve as a non-linear source of gravitational waves, something that provides a rather unique fingerprint that can potentially differentiate MASA models from other inflationary scenarios.

# Chapter 6

# Spectator Sectors from the Landscape

In the preceding chapter, we have described MASA inflationary models and their experimental signatures. To tie these observables to the string axiverse, we must discuss embeddings of spectator models within string theory. In this section we consider this task, as well as the constraints on such embeddings and their implications for observable signals.

Since MASA models are Abelian variations of the SCNI model, we first review previous attempts to embed this model in a UV framework. Inclusion at the level of  $\mathcal{N}=1$  supergravity was discussed in [314]. Constructions within type IIB orientifold compactifications were pursued in [205, 206]. In particular, [206] sought to embed SCNI models in a Large Volume Scenario (LVS) [31] with the inflaton itself as either a blow-up mode that realizes Kähler inflation or the fibre modulus in fibre inflation [47]. The non-Abelian spectator sector is realized by a stack of magnetized D7-branes with an axion arising from dimensional reduction of the 2-form gauge potential  $C_2$ .

In the following we will mimic and extend this construction. We will largely focus on realizing Abelian spectator sectors due to their distinctive signals discussed above. However, we shall start broadly and attempt a categorization and analysis of axionic spectator candidates and constructions to realize the gauge theory of the spectator sector.

Before proceeding into the details of string models, it is worth considering to what extent one should expect to be able to embed models with large Chern-Simons couplings into string theory. As briefly discussed above, there have been several arguments restricting possibilities to realize large Chern-Simons couplings [203, 204]. To motivate the difficulty, recall that in the typical quantum field theory perspective of the QCD axion, the Chern-Simons coupling to electromagnetism has a coefficient  $\lambda \propto \text{Tr}(Q_{PQ}Q_{EM}^2)\alpha_{EM}$ , where the trace runs over the charged fermions in the EFT. Naively, a large CS coupling can then be realized by one of the following strategies: a). large Peccei-Quinn charges  $Q_{PQ}$ , b). large electromagnetic charges  $Q_{EM}$ , or c). a large number of fermions. These latter two options are problematic since the charged fermions also contribute to the self-energy of the photon and a large number of fermions or large charges will bring down the scale of the QED Landau pole [315]. The issue with large PQ charges is more subtle, but involves the exponential suppression of fermion masses – see the appendix of [315] for further

discussion.

However, this is not to say that it is impossible to increase CS couplings beyond naive expectations. With the strategies above, one may obtain an  $\mathcal{O}(10-10^2)$  enhancement. From the QFT perspective, several other model-building strategies have been utilized to boost CS couplings, mostly in the context of the electromagnetic coupling of the QCD axion [315–318] and ultralight axion dark matter [319]. Such strategies involve models with (i) kinetic mixing of axions [320], (ii) KNP alignment [88] or clockworking [321–323], and (iii) introduction of a discrete symmetry [324].

While these mechanisms can indeed enhance the CS coupling of an axion to gauge fields, they typically induce unpleasant side effects into the EFT, akin to the descent of the Landau pole. Discrete symmetries introduce many new degrees of freedom, leading to a non-trivial cosmological history. Kinetic mixing appears unrestricted apart from the necessary inclusion of an additional light axion in the EFT, but it remains unclear if sufficient mixing can be realized in a string construction [315]. However, we will address this mechanism below. In the context of spectator models, [203, 204] argue that EFT restrictions and cosmological observations completely rule out the possibility of utilizing clockwork to realize SCNI models.

Given the above arguments restricting the possibilities of realizing large CS couplings in QFT, and therefore spectator models with observable signals, we may wonder if string theory somehow evades these arguments. Such a statement would be surprising given that the ongoing swampland program posits broad restrictions on EFTs coupled to gravity<sup>1</sup>. Indeed, in alignment with the swampland paradigm, we will find that methods to realize MASA/MnASA models in string theory are extremely restricted.

# 6.1 Spectator Sectors from D7-branes

#### 6.1.1 States and Couplings

We will consider 4d effective field theories obtained by compactifying 10d type IIB string theory on a 6d space  $\widetilde{X}_3$ . To maintain  $\mathcal{N}=1$  supersymmetry, we take  $\widetilde{X}_3$  to be an orientifold defined via the action of a holomorphic involution on a Calabi-Yau 3-fold  $X_3$ . Below the string scale, the theory is described by a supergravity effective field theory. This EFT contains moduli fields and, in the presence of Dp-branes, gauge sectors. While we will not be concerned with realizing the particle physics of our Universe, we assume that there exists some stack of branes that contain the Standard Model or some suitable unified gauge theory extension (for review, see [329]).

We are primarily interested in the axionic content of the EFT. From dimensional reduction of the higher-form gauge potentials  $C_4$ ,  $C_2$ , and  $B_2$ , the EFT inherits the "even axions"  $\rho_{\alpha}$  as well as the "odd-axions"  $c^a$ , and  $b^a$ . The span of the indices is determined by the topology of the orientifold via the Hodge numbers as  $\alpha = 1, ..., h_+^{1,1}$  and  $a = 1, ..., h_-^{1,1}$ . For more details, see section A.5. There is also the  $C_0$ -axion that descends from the 10d 0-form. These axions are organized in  $\mathcal{N} = 1$  chiral supermultiplets with scalar

<sup>&</sup>lt;sup>1</sup>For reviews, see [325–328].

components [330, 331]

$$S = C_0 + ie^{-\phi},$$

$$G^a = c^a - Sb^a,$$

$$T_{\alpha} = \tau_{\alpha} + i\left(\rho_{\alpha} - \frac{1}{2}\kappa_{\alpha bc}c^bb^c\right) + \frac{i}{2(S - \bar{S})}\kappa_{\alpha bc}G^b(G^c - \bar{G}^c)$$

$$= \tau_{\alpha} + i(\rho_{\alpha} - \kappa_{\alpha bc}c^bb^c) + \frac{i}{2}S\kappa_{\alpha bc}b^bb^c.$$
(6.1)

Here we have introduced the dilaton  $\phi$  as well as the real scalars  $\tau_{\alpha}$ . The dilaton vev determines the string coupling  $g_s = \langle e^{\phi} \rangle$  while  $\langle \tau_{\alpha} \rangle$  are the volumes of 4-dimensional submanifolds (4-cycles)  $\widetilde{\Pi}_{\alpha}$  in  $\widetilde{X}_3$ . In addition to the above axion content, there are also open string axions arising from the worlvolume theory of branes, but we will not be concerned with these.

The  $\{\rho_{\alpha}, c^a, b^a\}$  fields are candidates for the axionic content of the spectator sector, but they must couple to gauge fields via a Chern-Simons coupling to furnish examples of the MASA models described in the previous sections of this paper. As in [205, 206], we can realize the gauge theory portion of the spectator sector by wrapping  $N_{\rm D7}$  D7-branes on a divisor  $\widetilde{\mathcal{D}}$  of  $\widetilde{X}_3^2$ . The worldvolume theory of such a stack contains a gauge theory with a unitary, orthogonal, or symplectic gauge group. The particular group realized by the brane stack depends on further details of the compactification.

The action of the 4d EFT descends from dimensional reduction (and orientifold projection) of the Dirac-Born-Infeld (DBI) and Chern-Simons actions of the D7-branes as well as the 10d bulk type IIB action. It has the schematic form

$$S_{EFT} \supset S_{moduli} + S_{axions} + S_{gauge} + S_{potential}$$
 (6.2)

Here  $S_{moduli}$ ,  $S_{axions}$ , and  $S_{gauge}$  correspond to contributions to the EFT action from moduli, axions, and the D7-brane stack worldvolume gauge theory, respectively. In particular,  $S_{moduli}$  contains the kinetic terms of the  $\tau_{\alpha}$  whereas  $S_{axions}$  contains the kinetic terms for the axions  $\rho_{\alpha}$ ,  $c^{a}$ , and  $b^{a}$ . We will discuss the contributions to the scalar potential of the EFT, encoded in  $S_{potential}$ , in a subsequent section. For the worldvolume gauge theory, we have

$$S_{gauge} \supset \int d^4x \sqrt{-g} \left[ -\frac{1}{4} \text{Re}[f_{\widetilde{\mathcal{D}}}] F_{\mu\nu}^A F^{A\mu\nu} - \frac{1}{4} \text{Im}[f_{\widetilde{\mathcal{D}}}] F_{\mu\nu}^A \widetilde{F}^{A\mu\nu} \right], \tag{6.3}$$

where  $F_{\mu\nu}^A$  are the gauge fields arising from the D7-brane stack. The holomorphic gauge kinetic function  $f_{\widetilde{D}}$  depends on the chiral superfields, and so the worldvolume gauge theory coupling and fine structure constant are determined by moduli vevs as

$$g_{\widetilde{\mathcal{D}}}^{-2} = \langle \operatorname{Re}[f_{\widetilde{\mathcal{D}}}] \rangle \qquad \alpha_{\widetilde{\mathcal{D}}} = \frac{g_{\widetilde{\mathcal{D}}}^2}{4\pi} \,.$$
 (6.4)

In the absence of magnetic flux, the tree-level gauge kinetic function is determined by the fields in eq. (6.1) as

$$f_{\widetilde{\mathcal{D}}}^{(1)} = \frac{\omega^{\alpha}}{2\pi} T_{\alpha} \,, \tag{6.5}$$

<sup>&</sup>lt;sup>2</sup>A divisor  $\widetilde{\mathcal{D}}$  is a formal sum of 4-cycles  $\widetilde{\Pi}_{\alpha}$  in  $\widetilde{X}_3$  whose coefficients are the wrapping numbers of the branes. For more formal details, see section A.5.

where  $w^{\alpha}$  corresponds to the wrapping number of the D7-brane stack on the divisor  $\widetilde{\mathcal{D}}$  in  $\widetilde{X}_3$  (see section A.5). In particular, we note that  $\operatorname{Im}[f_{\widetilde{\mathcal{D}}}^{(1)}] \supset (2\pi)^{-1} w^{\alpha} \rho_{\alpha}$ , so we could already identify the  $C_4$ -axions  $\rho_{\alpha}$  as candidate spectator axions whose couplings to gauge fields can be potentially be increased by wrapping the D7-brane stack multiple times.

A distinct candidate spectator axion can be identified in compactifications with  $h_-^{1,1} > 0$  by allowing magnetic flux in the D7-branes. This is done by turning on quantized field strength units of  $F_2^A$  on a 2-cycle of the extra dimensions [331–334]. This 2-cycle must be non-trivial in homology either with respect to the full CY (and thus exist as a pullback from  $\tilde{X}_3$  to  $\tilde{\mathcal{D}}$ ) or at least in relative homology with respect to the divisor wrapped by the D7-brane itself. Suppressing the gauge index, the quantization condition of  $F_2^A$ -flux reads

$$\int_{\Pi_{2}^{\mathscr{A}}} \frac{\ell_{s}^{2}}{2\pi} F_{2} + \frac{1}{2} \int_{\Pi_{2}^{\mathscr{A}}} c_{1}(\Pi^{\mathscr{A}}) = m^{\mathscr{A}} \in \mathbb{Z}.$$
 (6.6)

Here  $\ell_s = 2\pi\sqrt{\alpha'}$  is the string length and  $\mathscr A$  labels the set of 2-cycles on which gauge flux can be put, such that  $\mathscr A = \alpha, a, r_{\vee}$  splits into the orientifold-even pullback 2-cycles  $\alpha = 1...h_{+}^{1,1}$ , orientifold-odd pullback 2-cycles  $a = 1...h_{-}^{1,1}$  and the 4-cycle-local 2-cycles  $r_{\vee}$  which are trivial in the CY.<sup>3</sup> We can then expand such a  $F_2$ -flux in terms of the relevant 2-forms

$$\frac{\ell_s^2}{2\pi}F_2 = m^\alpha \omega_\alpha + m^a \omega_a + m^{r_\vee} \omega_{r_\vee}. \tag{6.7}$$

Such gauge flux induces couplings between the 2-form axions  $c^a$  and  $b^a$  and the 4d gauge field strength  $F_{\mu\nu}^A$ .

These additional couplings are captured by extending the gauge kinetic function beyond eq. (6.5) to

$$f_{\widetilde{D}}^{(2)} = \frac{w^{\alpha}}{2\pi} \left\{ T_{\alpha} + i\kappa_{\alpha bc} \left( G^{b} m^{c} + \frac{S}{2} m^{b} m^{c} \right) \right\}$$

$$= \frac{w^{\alpha}}{2\pi} \left\{ \tau_{\alpha} + e^{-\phi} \kappa_{\alpha bc} \left( b^{b} m^{c} - \frac{1}{2} b^{b} b^{c} - \frac{1}{2} m^{b} m^{c} \right) \right\}$$

$$+ i \frac{w^{\alpha}}{2\pi} \left( \rho_{\alpha} + \kappa_{\alpha bc} c^{b} (m^{c} - b^{c}) + C_{0} \kappa_{\alpha bc} \left( \frac{1}{2} b^{b} b^{c} + \frac{1}{2} m^{b} m^{c} - b^{b} m^{c} \right) \right),$$

$$(6.8)$$

where  $w^{\alpha} \in \mathbb{Z}$  are once again the wrapping numbers of the D7-brane stack. Here we have assumed that quantized flux is placed only on odd 2-cycles. Plugging this into eq. (6.3) we acquire additional CS couplings

$$S_{EFT} \supset \int_{M_4} d^4x \sqrt{-g_4} \left[ -\frac{1}{4} \left( \frac{w^{\alpha}}{2\pi} \kappa_{\alpha b c} m^c \right) c^b F_{\mu\nu} \widetilde{F}^{\mu\nu} \right] . \tag{6.9}$$

Thus we can increase the effective CS coupling of a  $C_2$ -axion to 4d gauge fields by turning on internal quantized  $F_2$  gauge flux on the D7-brane stack, as well as increasing the wrapping number of the stack.

From the discussion above, we see that type IIB orientifolds with D7-branes do indeed provide the particle content for spectator models. However, there is a restriction on these constructions that must be taken into account - the axions and massless gauge bosons

 $<sup>^{3}</sup>$ The half-integer shift of the 2nd term of the LHS is controlled by the 1st Chern class  $c_{1}$  of the 4-cycle in question, and it is zero unless the 4-cycle is not spin, in which case it accounts for the Freed-Witten quantization condition, see [335].

may gain large masses via the Stückelberg mechanism [336]. This can occur with both the  $C_2$ - and  $C_4$ -axions, but the nature of the mechanism is distinct between the two types of axions. To be concrete, let us imagine a stack of  $N_{\rm D7}$  D7-branes on  $\widetilde{\mathcal{D}}$  giving rise to a  $U(N_{\rm D7}) = SU(N_{\rm D7}) \times U(1)$  gauge theory in the EFT. From section A.5, the  $C_4$ - and  $C_2$ -axions associated with  $\widetilde{\mathcal{D}}$  will have kinetic terms determined by the covariant derivatives

$$\nabla c^{a} = dc^{a} - q^{a}A, \qquad q^{a} = \frac{N_{D7}}{2\pi}w^{a},$$

$$\nabla \rho_{\alpha} = d\rho_{\alpha} - iq_{\alpha}A, \qquad q_{\alpha} = -\frac{N_{D7}}{2\pi}\kappa_{\alpha bc}m^{b}w^{c}.$$
(6.10)

Where A is the 1-form gauge potential of the diagonal U(1) gauge interaction and we have again omitted some terms by forbidding flux on even 2-cycles. Appearing here is the magnetization on odd 2-cycles,  $m^b$ , as well as odd wrapping numbers  $w^a$  defined in eq. (A.18). From these expressions, we see that the  $C_4$ -axions have a flux-induced Stückelberg mechanism in that the gauging of the axion shift symmetry only occurs in the presence of non-zero magnetic flux. On the other hand,  $C_2$ -axions have a geometric Stückelberg mechanism that arises purely from the details of the orientifold  $\widetilde{X}_3$  in the form of the odd wrapping number  $w^a$ . In either case, the U(1) factor of the gauge group becomes massive by eating an axion.

For stringy spectator models with non-Abelian gauge fields, the Stückelberg mechanism is only dangerous insofar as a candidate spectator axion may be lost. For Abelian spectator sectors, the Stückelberg couplings above present a major obstacle that must be evaded to ensure that both axions and massless U(1)s exist in the spectrum of the EFT. This requirement furnishes our first restriction on spectator models in string theory. Thus we will focus on Abelian spectators here and classify potential models via different methods to realize U(1) gauge theories in the EFT. We also describe how to ensure a viable candidate spectator axion appears in the EFT. We do not claim that this list is exhaustive, but we merely outline schematic requirements.

From the form of eq. (6.10), we see that the general strategies to fulfill this task are to i). ensure that the odd wrapping numbers  $w^a$  vanish ii). require that certain intersection numbers  $\kappa_{\alpha bc}$  vanish and/or iii). assume a structure that leads to cancellation of Stückelberg couplings. To implement these strategies, we must refine our discussion of the divisor wrapped by the D7-branes. The divisor  $\widetilde{\mathcal{D}}$  of  $\widetilde{X}_3$  descends from a divisor  $\mathcal{D}$  of  $X_3$  and its image divisor  $\mathcal{D}'$  under the orientifold involution. Adopting the organization scheme of [337], the classes of spectator models depends on the precise relation between  $\mathcal{D}$  and  $\mathcal{D}'$  as we now describe.

#### • Class I Spectators:

The most naive approach to realizing an Abelian spectator model is to place a single D7-brane on a divisor  $\widetilde{\mathcal{D}}$  that does not lie on top of an orientifold plane. This yields a U(1) gauge theory in the 4d EFT and one can consider  $C_4$ - or  $C_2$ -axions as spectators. However, there is a danger that the Stückelberg mechanisms described above remove the Abelian gauge boson from the massless spectrum.

To avoid this,  $\widetilde{\mathcal{D}}$  must be chosen such that the divisors  $\mathcal{D}$  and  $\mathcal{D}'$  in  $X_3$  are in the same homology class of  $X_3$ , i.e.  $[\mathcal{D}] = [\mathcal{D}']$ . If this condition is fulfilled, then the odd wrapping numbers in eq. (6.10) vanish and the Stückelberg couplings are eliminated.

A generalization of this setup can be achieved by considering  $N_{U(1)}$  D7-branes, all wrapping distinct 4-cycles  $\Pi^{\alpha}$  of  $X_3$ , where  $\alpha=1,..,N_{U(1)}$ . Naively this gives  $N_{U(1)}$  Abelian gauge sectors, labelled as  $U(1)_{\alpha}$ , but some will become massive due to the Stückelberg mechanism. The linear combinations that do not become massive are those that mimic the mechanism just described: any linear combination  $\sum_{\alpha} p_{\alpha}U(1)_{\alpha}$  such that the corresponding homology element maps to itself under the orientifold involution [338]. Mathematically, the criterion is  $\sum_{\alpha} p_{\alpha}([\Pi^{\alpha}] - [\Pi^{\alpha'}]) = 0$ . In this class, we avoid both the geometric and flux Stückelberg mechanisms and both  $C_4$ -and  $C_2$ - are candidates spectator axions.

#### • Class II Spectators:

In Class I, the Stückelberg couplings are circumvented through a judicious choice of  $\widetilde{\mathcal{D}}$  such that  $[\mathcal{D}] = [\mathcal{D}']$ . An alternative scenario is a divisor  $\widetilde{\mathcal{D}}$  such that  $[\mathcal{D}] \neq [\mathcal{D}']$ . Branes on such divisors can interact with both  $C_4$ - and  $C_2$ -axions in the EFT, but the odd wrapping number is necessarily non-zero and the geometric Stückelberg mechanism is active. Thus in the absence of flux, a  $C_2$ -axion is eaten and the  $U(N_{\rm D7})$  gauge theory realized by the  $N_{\rm D7}$  D7-branes wrapping  $\widetilde{\mathcal{D}}$  loses its U(1) factor and becomes  $SU(N_{\rm D7})$ . In the case of  $N_{\rm D7} = 1$ , the gauge theory is replaced by a massive gauge boson.

To realize a U(1) gauge factor in the EFT for such scenarios, we consider two options. The first is by breaking the  $SU(N_{\rm D7})$  via flux to a subgroup containing a U(1) factor. However, care must be taken since flux may induce Stückelberg couplings that remove the new Abelian gauge bosons from the massless field content. Thus one may have to assume the vanishing of certain intersection numbers in eq. (6.10) or simply obtain a sufficiently large number of U(1) factors from the breaking of  $SU(N_{\rm D7})$ .

The second possibility depends on the topology of the orientifold space itself. We can consider a scenario where  $\widetilde{\mathcal{D}}$  corresponds to a solitary 4-cycle  $\widetilde{\Pi}$  in  $\widetilde{X}_3$  such that the homology class of  $\widetilde{\Pi}$  has additional volume-minimizing representatives. In other words, there exists two or more distinct  $\widetilde{\Pi}^{(i)} \in [\widetilde{\Pi}]$ . D7-branes can be wrapped on the various  $\widetilde{\Pi}^{(i)}$ , and each stack produces a U(1) factor in the EFT gauge group. One linear combination of the U(1)s eats the  $C_2$ -axion of  $[\widetilde{\Pi}]$  and becomes massive. If magnetic flux is turned on, another linear combination of U(1)s may gain a mass by eating the  $C_4$ -axion of  $[\widetilde{\Pi}]$ . This can be circumvented if certain intersection numbers vanish. Alternatively, one could consider scenarios with at least 3 homologous cycles, as was used to realize aligned natural inflation in [334].

We label the above possibilities as Class IIa and Class IIb, respectively.

As for the axionic state of the spectator sector, in the absence of flux, one could consider the  $C_4$ -axions as spectators. To have a  $C_2$ -axion as a spectator candidate requires a bit of care as the geometric Stückelberg coupling is present. For both sub-classes, we can consider a  $C_2$ -axion that is associated to some other divisor,  $\widetilde{\mathcal{D}}^{alt}$ , in  $\widetilde{X}_3$ . There are two obvious possibilities.

The first is that there exists a divisor and image-divisor pair in  $X_3$  such that the even combination  $\widetilde{\mathcal{D}}^{alt}$  is rigid and is stabilized by an ED3 instanton. If we assume that such a  $\widetilde{\mathcal{D}}^{alt}$  has certain trivial intersection numbers with divisors that support D7-branes, then the geometric Stückelberg mechanism can be avoided. For this

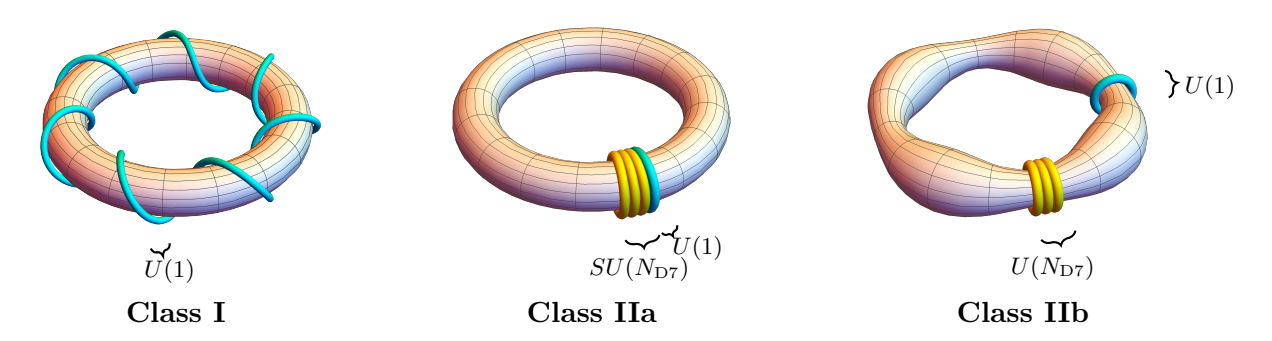


Figure 6.1: Pictorial representation of the D7-brane(s) configurations giving rise to spectator sector classes discussed in the text. Class III has a representation similar to Class IIa but with a different gauge group.

 $C_2$ -axion to couple to the worldvolume theory of  $\widetilde{\Pi}$ , we must also assume that appropriate intersection numbers between  $\widetilde{\mathcal{D}}$  and  $\widetilde{\mathcal{D}}^{alt}$  exist.

The second possibility is that  $\widetilde{\mathcal{D}}^{alt}$  arises from a cycle and image-cycle pair that are homologous in  $X_3$ , as in the Class I spectator theories. Then the  $C_2$ -axion could couple to the worldvolume theory of  $\widetilde{\Pi}$  assuming appropriate intersection numbers are non-trivial.

#### • Class III Spectators:

The final class corresponds to the case where  $\mathcal{D}$  is invariant under the orientifold involution so that  $\mathcal{D} = \mathcal{D}'$  pointwise. This class shares certain features with both of the previous classes. First, the odd wrapping numbers  $\boldsymbol{w}^a$  of  $\widetilde{\mathcal{D}}$  vanish, so both the geometric and flux Stückelberg mechanism are absent. However,  $\widetilde{\mathcal{D}}$  sits on top of an orientifold plane, and local D3-tadpole cancellation gives rise to orthogonal or symplectic gauge groups [339] and there is no diagonal U(1) factor. To obtain a U(1) factor in the EFT, we must implement flux to break the gauge group.

Once again  $C_4$ -axions are candidate spectators. To obtain  $C_2$ -axion spectators, one must assume the existence of a separate 4-cycle  $\widetilde{\mathcal{D}}^{alt}$  with the properties outlined in Class II above.

There is an important caveat to the above discussion - namely, the vevs of the  $b^a$  axions. Magnetization on the brane induces a D-term [333,340]

$$D_{\widetilde{D}} \propto \kappa_{\alpha b c} v^{\alpha} (b^c - m^c) w^b , \qquad (6.11)$$

where the  $v^{\alpha}$  determine 2-cycle volumes and the  $w^b$  are wrapping numbers on odd cycles, as explained in section A.5<sup>4</sup>. If these D-terms are non-zero, one can set  $\langle b^a \rangle = m^a$  to cancel them. In doing so, we see from eq. (6.8) that the CS coupling of the  $C_2$ -axion is set to zero. This is not an issue for Class I or Class III models as the odd wrapping numbers  $w^a$  automatically vanish. For Class II models, demanding a coupling of the  $C_2$ -axions to the gauge field may require vacua with some  $\langle b^a \rangle \neq m^a$  or manifolds that have certain intersection numbers set to zero. As a side note, typically, Kähler modulus stabilization enforces  $\langle b^a \rangle = 0$ . Cancellation of D-terms then becomes a construction-dependent question on the charged matter in the brane.

<sup>&</sup>lt;sup>4</sup>Here we have excluded contributions from charged matter fields.

From this section, we see that even demanding the existence of spectator sectors is non-trivial from the string theory viewpoint and many restrictions are already enforced. Our first restrictions arose from demanding the necessary field content and led to our discussion on the classes above. The second restriction here arises from demanding that a CS coupling exist between axions and gauge fields. There are also constraints from D3-tadpoles and control of the compactification, which we outline below.

#### 6.1.2 Axion Decay Constants

In this and the subsequent sub-section, we outline the origin of spectator model parameters in string constructions. The decay constants for the axion states described in the previous section are determined by their kinetic terms

$$S_{axions} \supset M_p^2 \int d^4x \sqrt{-g} \left( -K^{\alpha\beta} \partial_{\mu} \rho_{\alpha} \partial^{\mu} \rho_{\beta} - K_{ab} \partial_{\mu} c^a \partial^{\mu} c^b \right), \tag{6.12}$$

where again  $\alpha, \beta = 1, ..., h_+^{1,1}$  and  $a, b = 1, ..., h_-^{1,1}$ . For more explicit formulae for the Kähler metrics, see section A.5.

For simplicity, we consider an orientifold with  $h_-^{1,1}=1$  and/or  $h_+^{1,1}=1$ , then the kinetic terms of the even  $C_4$ -axion,  $-K^{11}(\partial\rho)^2$ , and only odd  $C_2$ -axion,  $-K_{11}(\partial c)^2$ , allows us to identify the axion decay constants

$$F_o = \langle 2K_{11} \rangle^{1/2} M_p , \qquad F_e = \langle 2K^{11} \rangle^{1/2} M_p , \qquad (6.13)$$

then the re-scaled axions

$$\vartheta_o = F_o c, \qquad \vartheta_e = F_e \rho,$$
(6.14)

have canonical kinetic terms.

The above steps can be generalized for orientifolds with  $h_{-}^{1,1} > 1$  and/or  $h_{+}^{1,1} > 1$ . The only complication is that one must implement orthogonal transformations to diagonalize the metrics  $K^{\alpha\beta}$  and  $K_{ab}$  before re-scaling the axions. The orthogonal transformation in principle affects the coupling of the axion to the spectator gauge fields, but without a specific compactification manifold we cannot determine their precise impact.

#### 6.1.3 Axion Masses

The shift symmetries of the  $C_4$ - and  $C_2$ -axions have their origins in the gauge symmetries of the corresponding 10d gauge potentials and are thereby protected at all orders in string perturbation theory. Thus, to give a mass to these potential spectator axions, which break the shift symmetries, we must introduce non-perturbative effects via either Euclidean or Lorenztian objects.

From Euclidean objects, axion potentials can be generated by Euclidean D3-branes (ED3s), Euclidean D1-branes (ED1s), or bound states thereof. An ED3 brane wrapping a 4-cycle of  $\widetilde{X}_3$  gives a contribution to the superpotential of the form

$$W_{ED3} \sim \mathcal{A}e^{-2\pi T} \,. \tag{6.15}$$

Here we neglect the typical dependence of the 1-loop Pfaffian factor  $\mathcal{A}$  on other fields of the theory, such as the complex structure moduli. Such a superpotential yields a periodic

potential for the  $C_4$ -axion  $\rho$  embedded in the T supermultiplet of the 4-cycle<sup>5</sup>:

$$\delta V_{ED3} \sim \mu^4 e^{-2\pi\tau} \cos(2\pi\rho) = \mu^4 e^{-2\pi\tau} \cos\left(2\pi\frac{\vartheta_e}{F_e}\right). \tag{6.16}$$

To obtain a mass for a  $C_2$  spectator axion, we turn to ED1-branes wrapping the orientifoldeven 2-cycles. As an illustration, consider a scenario with intersection numbers such that the volume of the wrapped 2-cycle v and the volume of its dual 4-cycle  $\tau$  are related as  $\tau = \frac{1}{2}\kappa_{+++}v^2$ . We also let the 2-cycle have a non-zero intersection number  $\kappa_{+--}$ with an orientifold-odd combination 2-cycle supporting the 2-form axion chiral multiplet G. Such an object contributes to the Kähler potential and schematically might take the form [44,341]

$$K = -3\ln\left[T + \bar{T} - \frac{3}{2(S - \bar{S})}\kappa_{+--}(G + \bar{G})^2 + e^{-2\pi\sqrt{\frac{T + \bar{T}}{\kappa_{+++}}}}\cos\left(2\pi\frac{G + \bar{G}}{2}\right)\right]. \quad (6.17)$$

If this ED1-brane instanton contributes to the scalar potential of G, its contribution from the path integral has to scale as

$$\delta V_{\text{ED1}} \sim \mu^4 \operatorname{Re} e^{-\mathcal{S}_{\text{ED1}}} = \mu^4 \operatorname{Re} e^{-2\pi v - 2\pi i c}$$
$$= \mu^4 e^{-2\pi v} \cos\left(2\pi \frac{\vartheta_o}{F_o}\right), \tag{6.18}$$

by direct evaluation of  $S_{\text{ED1}}$  (eq. (A.20) with  $\ell_s = 1$ ). In the second line, we have rewritten the argument in terms of the axion with canonically normalized kinetic term.

It is possible that a single instanton effect can give masses to both  $C_4$ - and  $C_2$ -axions. The full contribution of an ED3 instanton includes summing over all possible magnetic fluxes of the divisor wrapped by the ED3, which can be thought of as a sum over ED3-ED1 bound states. This requires a modification of eq. (6.15) to  $W_{ED3} \to W_{ED3/ED1} \simeq \Theta(G)e^{-2\pi T}$ , where  $\Theta(G)$  is a holomorphic theta function from the theory of modular forms [342,343]. In the presence of D7-branes such that axion shift symmetries are gauged due to the presence of a Stückelberg mechanism, the sum over fluxes defining  $\Theta(G)$  must be suitably restricted to include only gauge-invariant instantons [333]. Setting aside this subtlety, the ED3-ED1 bound states gives rise to terms with the schematic form  $W_{ED3/ED1} \sim e^{2\pi(G+T)}$ . Such a term contributes to mass-mixing between the even and odd axions. This mixing forces one to rotate into the mass eigenbasis, which introduces some coefficient in the Chern-Simons coupling. In the following, we will neglect this complication and consider  $C_2$ -axion masses arising only from ED1 contributions to the Kähler potential.

Alternatively, spectator axions could obtain potentials from Lorentzian branes via gaugino condensation. This requires that the spectator axion couples to both the spectator U(1) as well as a condensing hidden non-Abelian gauge sector. We will take this to be the case and assume that there is a stack of D7-branes wrapping a 4-cycle  $\widetilde{\Pi}^{\mathcal{G}}$  of  $\widetilde{X}_3$  realizing a non-Abelian gauge group  $\mathcal{G}$ . The gaugino condensate then contributes to the non-perturbative part of the superpotential as

$$W_{np} \sim \mathcal{A}e^{-\frac{(2\pi)^2}{c(\mathcal{G})}f_{\mathcal{G}}}, \tag{6.19}$$

<sup>&</sup>lt;sup>5</sup>Here and below we assume the superpotential has the standard type IIB flux compactification structure of  $W = W_0 + W_{np}$ , where  $W_0$  is a constant and  $W_{np}$  is the non-perturbative contribution.

Case	Axion(s)	Mass Mechanism
1	$C_4$	ED3 Instantons
2	$C_2$	ED1 Instantons
3	$C_4$	Gaugino Condensation
4	$C_2\&C_4$	Gaugino Condensation

Table 6.1: Spectator axions organized by mass generation mechanism.

where  $f_{\mathcal{G}}$  and  $c(\mathcal{G})$  are the gauge kinetic function and the dual Coxeter number of  $\mathcal{G}$ , respectively. For  $\mathcal{G} = SU(N_{\mathcal{G}})$ ,  $c(\mathcal{G}) = N_{\mathcal{G}}$ . If we are considering a scenario without worldvolume flux, then  $f_{\mathcal{G}} \propto T_{\widetilde{\Pi}^{\mathcal{G}}} = \tau_{\mathcal{G}} + i\rho_{\mathcal{G}} + \cdots$  and the  $C_4$ -axion in  $T_{\widetilde{\Pi}^{\mathcal{G}}}$  obtains a potential similar to that of eq. (6.16) but with an extra factor of  $c(\mathcal{G})^{-1}$  in the argument of the cosine.

If instead the D7-brane stack is magnetized and has a non-zero intersection number  $\kappa_{\mathcal{G}} \equiv \kappa_{\mathcal{G}--}$  with the odd cycle supporting an odd chiral supermultiplet G, then  $f_{\mathcal{G}}$  can take the form of  $f_{D7}^{(2)}$  in eq. (6.8). Then the scalar potential will have a contribution

$$\delta V_{cond} \simeq \mu^4 e^{-\frac{2\pi w_{\mathcal{G}}}{c(\mathcal{G})} \tau_{\mathcal{G}}} \cos \left( 2\pi \frac{w_{\mathcal{G}}}{c(\mathcal{G})} \left[ \rho_{\mathcal{G}} + \kappa_{\mathcal{G}} m_{\mathcal{G}} c \right] \right) 
= \mu^4 e^{-\frac{2\pi w_{\mathcal{G}}}{c(\mathcal{G})} \tau_{\mathcal{G}}} \cos \left( 2\pi \frac{w_{\mathcal{G}}}{c(\mathcal{G})} \left[ \frac{\vartheta_e}{F_e} + \kappa_{\mathcal{G}} m_{\mathcal{G}} \frac{\vartheta_o}{F_o} \right] \right).$$
(6.20)

where  $w_{\mathcal{G}}$  and  $m_{\mathcal{G}}$  are the wrapping number and magnetization on  $\Pi_{\mathcal{G}}$ . Such a potential introduces mass mixing between the two axions. The masses and eigenstates are

$$\vartheta_{1} = \frac{1}{\sqrt{1+\varepsilon^{2}}} \left( \vartheta_{0} - \varepsilon \vartheta_{e} \right) \qquad m_{1}^{2} = 0, 
\vartheta_{2} = \frac{1}{\sqrt{1+\varepsilon^{2}}} \left( \vartheta_{e} + \varepsilon \vartheta_{o} \right) \qquad m_{2}^{2} = \left( \frac{2\pi w_{\mathcal{G}}}{c(\mathcal{G})F_{e}} \right)^{2} (1+\varepsilon^{2}).$$
(6.21)

We have also defined the parameter  $\varepsilon = \kappa_{\mathcal{G}} m_{\mathcal{G}} F_e/F_o$ , which tracks the mixing between the axions. Below we will take  $\kappa_{\mathcal{G}} m_{\mathcal{G}} \simeq 1$  so that  $\varepsilon \simeq F_e/F_o$ , which is generally expected to be less than unity due to the natural hierarchy between the decay constants of even and odd axions – see section A.5 for more details. If we assume that both  $\vartheta_e$  and  $\vartheta_o$  couple to a U(1) gauge sector, then the mass eigenstates couple as

$$S \supset -\frac{1}{4} \int \left(\frac{\lambda_e}{F_e} \vartheta_e + \frac{\lambda_o}{F_o} \vartheta_o\right) F_{\mu\nu} \widetilde{F}^{\mu\nu}$$

$$= -\frac{1}{4} \int \left(\frac{F_e \lambda_o - \varepsilon F_o \lambda_e}{F_o F_e \sqrt{1 + \varepsilon^2}}\right) \vartheta_1 F_{\mu\nu} \widetilde{F}^{\mu\nu} - \frac{1}{4} \int \left(\frac{F_o \lambda_e + \varepsilon F_e \lambda_o}{F_e F_o \sqrt{1 + \varepsilon^2}}\right) \vartheta_2 F_{\mu\nu} \widetilde{F}^{\mu\nu} .$$

$$(6.22)$$

To classify the spectator axion(s) and their mass generation mechanism, we introduce the cases displayed in table 6.1.

Finally, we note that we have made several assumptions on the structure of  $\widetilde{X}_3$  in order to permit the above non-perturbative effects. For example, a 4-cycle must be rigid to support ED3 instantons [344], which places requirements on the sheaf cohomology of the divisor. More precisely, a sufficient (but not necessary) condition for generation of a superpotential by an ED3 instanton is that the 4-cycle D is rigid, and in addition  $D \neq D'$ 

pointwise but [D] = [D']. The Hodge numbers of the divisor determine the number of chiral fields charged under the worldvolume theory of a non-Abelian D7-branes stack, which in turn could affect the existence of a gaugino condensate. In the following we will assume the required structures whenever necessary and leave a detailed study of their abundance for our scenarios to future work.

#### 6.1.4 From Strings to Spectators

We now combine all of the above to make contact with the spectator Lagrangian eq. (5.1). First, let us consider a single  $C_4$ - or  $C_2$ -axion coupled to a hidden U(1) gauge theory. From the discussion of the previous sections, we have contributions to the EFT Lagrangian of the form

$$\mathcal{L}_{EFT} \supset \Lambda^4 \cos \left( 2\pi \mathcal{J} \frac{\vartheta}{F} \right) - \frac{g_{\widetilde{\mathcal{D}}}^2}{8\pi} \mathcal{M} \frac{\vartheta}{F} F_{\mu\nu} \widetilde{F}^{\mu\nu} \,. \tag{6.23}$$

Note that we have re-scaled the worldvolume gauge field from eq. (6.4) as  $A_{\mu} \to g_{\widetilde{D}} A_{\mu}$  to canonically normalize the gauge field kinetic term. We have also re-scaled the axion as per eq. (6.14) to obtain a canonically-normalized axion  $\vartheta$ . Here  $\mathcal{M}$  depending on the 10*d* origin of  $\vartheta$  and encodes either just the wrapping number w of the brane or combinations from eq. (6.9) such as  $w\kappa_{+--}m_1$ . The factor  $\mathcal{J}$  specifies extra information on the non-perturbative effect giving the axion a mass:

$$\mathcal{J} = \begin{cases}
1 & \text{ED1 or ED3 Instantons} \\
\frac{w}{c(\mathcal{G})} & \text{Gaugino Condensation (only } C_4).
\end{cases}$$
(6.24)

For the second line above, we assume that any  $C_2$ -axions in the EFT do not couple to the condensing gauge group  $\mathcal{G}$ . If  $C_2$ -axions do couple via magnetic flux, then  $\mathcal{J}$  becomes matrix-valued. We address this general case below.

For now, we define a re-scaled decay constant

$$f = \frac{F}{2\pi \mathcal{J}}, \tag{6.25}$$

such that the axion has the conventional periodicity  $\vartheta \to \vartheta + 2\pi f$ . The spectator parameters in eq. (5.47) and then given by

$$m = \frac{2\pi \mathcal{J}\Lambda^2}{F} = \frac{\Lambda^2}{f},$$

$$\lambda = \frac{g_{\tilde{\mathcal{D}}}^2}{4\pi^2 \mathcal{J}} \mathcal{M} = \frac{\alpha_{\tilde{\mathcal{D}}}}{\pi \mathcal{J}} \mathcal{M}.$$
(6.26)

The above can be generalized to cases with multiple spectators and more complicated gaugino condensation scenarios. We can consider the following subset of terms in the EFT Lagrangian

$$\mathcal{L}_{EFT} \supset -\sum_{a=1}^{N_{np}} \Lambda_a^4 \cos \left[ 2\pi \sum_{b=1}^{N_{ax}} \mathcal{J}_{ab} \frac{\vartheta_b}{F_b} \right] - \sum_{c=1}^{N_{U(1)}} \sum_{b=1}^{N_{ax}} \frac{\alpha_c}{\pi} \mathcal{M}_{cb} \left( \frac{\vartheta_b}{F_b} \right) F_{(c)} \wedge F_{(c)} . \tag{6.27}$$

where we have included  $N_{ax}$  axions that couple to  $N_{U(1)}$  Abelian gauge sectors via a coupling matrix  $\mathcal{M}_{cb}$ , and  $N_{np}$  non-perturbative effects giving cosine potentials that include

mass-mixing via the matrix  $\mathcal{J}_{ab}$ . The potential in eq. (6.27) defines a mass matrix for the axions

$$(M^2)_{ij} = \sum_a \Lambda_a^4 \left(\frac{4\pi^2}{F_i}\right) \mathcal{J}_{ai} \mathcal{J}_{aj}. \tag{6.28}$$

This can be diagonalized via an orthogonal matrix  $O_{jb}$  such that  $(O^T)_{ai}M_{ij}O_{jb} = m_a^2\delta_{ab}$  and so the axion mass eigenstates are given by

$$\vartheta_a' = \sum_i (O^T)_{ai} \vartheta_i \,. \tag{6.29}$$

These states have Chern-Simons couplings

$$\mathcal{L} \supset \sum_{c,b} \frac{\alpha_c}{\pi} \mathcal{M}_{cb} O_{bi} \frac{\vartheta_i'}{F_b} F_{(c)} \wedge F_{(c)}. \tag{6.30}$$

With this, all the parameters defined a spectator model has been identified from our D7-brane constructions. What remains to be shown is that the parameters necessary for an observable signal can be generated. First however, we must consider the inherent limitations of these setups.

### 6.2 Constraints on Spectator Models in String Theory

In the previous subsection, we discussed how to realize spectator model parameters in string theory, in particular how the large Chern-Simons coupling can potentially be realized by magnetizing D7-branes and/or a sufficiently high wrapping number. However, this enhancement comes at a price.

Focusing on  $C_2$  spectators, a boosted Chern-Simons coupling can be achieved by magnetized D7-branes. However, such a flux induces an effective D3-brane charge that contributes to the D3-brane tadpole cancellation condition. This is reviewed in section A.5, here we merely list the effective charge from the magnetized branes, which reads as<sup>6</sup>:

$$Q_{D3,ind} = w \kappa_{+--}(m_1)^2 N_{D7}, \qquad (6.31)$$

where we have made the simplifying assumptions of considering branes on particular 4-cycle and flux  $m_1$  on an odd 2-cycle that insects only with this wrapped 4-cycle. Other contributions to the D3-tadpole include the number of D3-branes as well as the spacetime curvature contributions from the D7-branes and O7-planes. The cancellation of the D3-tadpole is non-trivial and involves an interplay between the number of branes, their magnetizations, and the cycles they wrap. In the absence of a detailed compactification, we instead take an approximate approach and argue for an upper bound on the allowed D3-tadpole that a spectator model can induce. This is not a strict requirement, but nonetheless a spectator model that violates the bound would be hard pressed to find a home in the string landscape.

To get an estimate for the allowed amount of magnetization, we turn to F-theory compactified on an elliptically fibred Calabi-Yau 4-fold  $Y_4$ . In such scenarios, the D3-tadpole cancellation condition takes the form [345]

$$N_{\rm D3} + \int_{Y_4} G_4 \wedge G_4 = \frac{\vartheta(Y_4)}{24} \,.$$
 (6.32)

<sup>&</sup>lt;sup>6</sup>For simplicity we still assume work with a single pair of even and odd cycles.

On the left hand side of the above relation,  $N_{\rm D3}$  is the total number of D3-branes while the second term is a 4-form flux that contains eq. (6.31) in the type IIB limit. On the right hand side,  $\vartheta(Y_4)$  is the Euler characteristic of  $Y_4$ <sup>7</sup> and in the type IIB limit this encodes the curvature D3-charge from the D7-branes and O7-planes [346].

eq. (6.32) implies an absolute upper bound on the amount of magnetic flux allowed in a CY 4-fold  $Y_4$  as  $Q_{D3,ind} < \vartheta(Y_4)/24$ . Thus the size of CS couplings on a given 4-fold are inherently limited by the topology. However, this is too lax a constraint. For a working type IIB string compactification, we must also stabilize the complex structure moduli of the CY 3-fold and the axio-dilaton via the 3-form fluxes  $H_3$ ,  $F_3$ . These contribute to the D3-charge as well, taking the form

$$Q_{\mathrm{D3},H_3\&F_3} \sim \int_{X_3} F_3 \wedge H_3 \,.$$
 (6.33)

Therefore, to maintain a sufficient amount of tadpole to allow moduli stabilization, we take a conservative approach and estimate that the amount of flux that can be used to generate large CS couplings is  $\sim \mathcal{O}(0.1) \times \frac{\vartheta(X_4)}{24}$ . Thus we will enforce the following effective constraint

$$Q_{\text{D3},ind.} < Q_{eff}(Y_4) := 0.1 \times \frac{\vartheta(Y_4)}{24}.$$
 (6.34)

A related but distinct question to the one above is if there is a universal upper bound on the Euler characteristics of elliptically fibred CY 4-folds. Such a bound would provide a universal constraint on CS couplings. No such upper bound currently exists, but we can consider the 4-fold with the largest known characteristic. In terms of the Hodge numbers of a CY 4-fold, one has

$$\vartheta(Y_4) = 6(8 + h^{1,1} + h^{3,1} - h^{2,1}). \tag{6.35}$$

There exists a CY 4-fold  $\hat{Y}_4$  with Hodge numbers [347]

$$(h^{1,1}, h^{2,1}, h^{3,1}) = (303148, 0, 252), (6.36)$$

which gives  $\vartheta(\hat{Y}_4)/24 = 75852 \simeq 10^5$ . If we take this CY 4-fold as representing an estimate for the largest possible  $\vartheta(Y_4)$ , then in analogy with eq. (6.34) we can bound spectator models by the effective usable charge

$$\hat{Q}_{eff} := 0.1 \times \frac{\vartheta(\hat{Y}_4)}{24} \simeq 10^4 \,,$$
 (6.37)

as

Constraint I: 
$$Q_{\text{D3},ind} \leq \hat{Q}_{eff}$$
. (6.38)

We now consider the implications of the above arguments on attempts to embed non-Abelian spectator models into type IIB compactifications [206]. The authors consider two separate scenarios within the LVS framework – Kähler inflation [48] and fibre inflation. In both examples, the spectator sector is given by the EFT of a stack of magnetized, multiply-wound D7-branes, with the spectator axion given by one of the descendents of  $C_2$ . In particular, [206] give the required model parameters as a triplet  $(m, N_{D7}, w)$ .

$$(m, N_{\rm D7}, w) \sim \begin{cases} (10^4, 10^5, 25) & \text{K\"{a}hler Inflation} \\ (10^2, 10^3, 1) & \text{Fibre Inflation} \end{cases}$$
 (6.39)

<sup>&</sup>lt;sup>7</sup>In F-theory models with non-Abelian gauge groups,  $Y_4$  is singular and one must calculate the Euler characteristic of  $\bar{Y}_4$ , the resolution of  $Y_4$ .

With these parameters, one can utilize eq. (6.31) to get an estimate of the required tadpole for the models in [206]. However, there is a degeneracy in their parameter m and the product of intersection numbers and D7-brane magnetization,  $\kappa_{+--}m_1$  as described above.

Therefore, we must make some assumptions to estimate the tadpole. One can imagine two scenarios for the models of [206]. In the first scenario, the intersection numbers are  $\mathcal{O}(1)$  and  $m_1 \simeq m$ . Then we have

Scenario I: 
$$Q_{\mathrm{D3},ind} \simeq \begin{cases} 25(10^4)^2 10^5 \sim 10^{14} & \text{K\"{a}hler Inflation} \\ (10^2)^2 10^3 \sim 10^7 & \text{Fibre Inflation} \end{cases}$$
 (6.40)

Alternatively, one could consider a cycle with large intersection numbers so that  $\kappa_{+--} \simeq m$  and  $m_1 \simeq \mathcal{O}(1)$ ,

Scenario II: 
$$Q_{\text{D3},ind} \simeq \begin{cases} 25(10^4)10^5 \sim 10^{10} & \text{K\"{a}hler Inflation} \\ (10^2)10^3 \sim 10^5 & \text{Fibre Inflation} \end{cases}$$
 (6.41)

In both scenarios, Kähler inflation requires a tadpole orders of magnitude larger than  $\vartheta(\hat{Y}_4)/24 \simeq 10^5$ . This is also true for fibre inflation in Scenario I. In Scenario II, fibre inflation is borderline consistent with tadpole cancellation, but if we incorporate moduli stabilization and enforce  $Q_{\text{D3},ind} < \hat{Q}_{eff}$ , then even this case is problematic.

While the above not does constitute a proof that the SCNI models of [206] are inconsistent, it does provide a strong hint that such models may be impossible to realize given our current understanding of string models. One may therefore be tempted to place them in the string swampland as opposed to the landscape.

Turning back to MASA models, we also supplement eq. (6.38) with conditions to ensure control of the stringy MASA construction. First, we require that the various U(1) gauge factors are under perturbative control below the string scale. Since the gauge field theory loop expansion parameter is  $\alpha_{U(1)}/2\pi$ , we impose

Constraint II: 
$$\frac{\alpha_{U(1)}}{2\pi} \lesssim 1$$
 (6.42)

for each U(1) gauge theory factor. We must also demand that the expansions of non-perturbative effects giving the spectator axions masses remain under control, i.e. the higher-order terms are suppressed relative to the leading order one.

For spectator axion masses obtained via ED1 instantons, the scale of the non-perturbative effect is controlled by the wrapped 2-cycle volume as  $e^{-2\pi v}$ . To ensure that the next higher order instanton is sufficiently suppressed that it can be ignored, we demand  $2\pi v \gtrsim 2$ . Assuming a simple intersection structure such that  $\tau = \frac{1}{2}\kappa_{+++}v^2$ , this translates into a bound

Constraint III: 
$$\frac{\pi^2}{\kappa_{+++}w_1\alpha_1} \gtrsim 1$$
 (6.43)

where we have replaced  $\tau$  with the fine-structure constant of the U(1) gauge theory wrapped on the 4-cycle associated with  $\tau$ . For ED3 instantons, we place a similar constraint to the previous one except that the relevant exponential depends on 4-cycle volumes controlled by the Kähler moduli  $\tau$ . Thus we impose  $2\pi\tau \gtrsim 2$  for any 4-cycle

supporting an ED3 instanton, which translates to a bound

Constraint IV: 
$$\frac{\pi}{2w_1\alpha_1} \gtrsim 1$$
 (6.44)

Where we have again replaced  $\tau$  with the Abelian fine-structure constant of the world-volume theory of the D7-brane that is also wrapping the 4-cycle.

Finally, for cases that include gaugino condensation arising from a non-Abelian gauge group  $\mathcal{G}$  we impose

Constraint V: 
$$\frac{\pi}{2} \frac{1}{c(\mathcal{G})\alpha_{\mathcal{G}}} \gtrsim 1$$
 (6.45)

to suppress high-order gauge instanton effects.

Concerning the axion sector, we should raise a final issue which arises from boosting the CS coupling of these axions by increasing the wrapping number w of the relevant D7branes. This concerns specifically the even axions, as a large w could be the unique way in which the CS coupling could be boosted, but is valid also for the  $C_2$  CS couplings. The point is that a D7-brane which is wrapping a given 4-cycle  $\Pi$  several times, in a certain sense can be thought of as 'partitioning' the cycle volume  $\mathcal{V}_{\widetilde{\Pi}}$  among its wrappings. For an isotropically shaped 4-cycle with a single size  $L_{\Sigma} = R_{\widetilde{\Pi}}/\sqrt{\alpha'} \sim \mathcal{V}_{\widetilde{\Pi}}^{1/4}$  we can interpret this as an average distance between two adjacent wrapping loops  $d_w = (\mathcal{V}_{\widetilde{\Pi}}/w)^{1/4} \sim L_{\widetilde{\Pi}}/w^{1/4}$ . As long as SUSY is unbroken, a multi-wrapped D7-brane is still a BPS object and as such has no potential energy change associated with the wrapping number and its associated wrapping distance  $d_w$ . However, once SUSY is broken at high scales during inflation where our scenario takes place, the SUSY breaking will communicate at some level to the D7-brane in question as well. In that situation, stretching the single D7-brane over multiple wrappings costs energy, and thus we expect a potential energy which increases with w and shows a potential barrier as a function of the adjacent loop distance  $d_w$ . Hence, in this regime we expect a tunneling instability toward recombination of adjacent loops of the wrapped-up D7-brane. While the strength of this barrier is clearly dependent on the amount of SUSY breaking communicated to the D7-brane, a very first conservative guess may be that suppressing the tunneling instability requires separating the wrappings by more than a string length which implies a constraint  $d_w > 1$ . Imposing this, by the above scaling argument, implies an upper bound on the wrapping number

$$w < \mathscr{V}_{\widetilde{\Pi}} = \operatorname{Re} T = \mathscr{O}(10\dots 100).$$
 (6.46)

We can now insert this bound into the relation determining the D7-brane U(1) gauge coupling  $g^{-2} = w \operatorname{Re} T_{\widetilde{\Pi}}/2\pi = w \mathcal{V}_{\widetilde{\Pi}}/2\pi = w L_{\widetilde{\Pi}}^4/2\pi$ , which gives the following bound once inserted in eq. (6.46)

$$w < 1/\sqrt{2\alpha_1}. \tag{6.47}$$

For values of the gauge coupling  $\alpha_1 = \mathcal{O}(1...5)$  picked out by the constraint plots below, enforcing this constraint rigorously would restrict us to having only singly wrapped D7-branes. Consequently, this would eliminate the even axions from the spectrum of axions detectable by GW emission, presenting a qualitative argument against the viability of the  $C_4$  axions as potential spectators. However, as elaborated further below, even axions face elimination as candidates for observable GW signals already due to the detrimental impact of a strong CS coupling on control of the EFT. In the case of odd axions instead,

their viability remains more resilient. Since they do not depend solely on multiple winding to enhance their CS coupling and typically only require a wrapping factor  $w \sim \mathcal{O}(1)$  to PTA amplitudes, we do not view this constraint as overly stringent.

## 6.3 Type IIB MASA Models

We now examine possibilities to realize MASA models in compactifications of type IIB string theory. To this end, we will not consider a concrete compactification manifold, but instead examine potential scenarios by assembling the above ingredients. Effectively, this will provide us with a set of selection rules for the existence of viable MASA models in type IIB string theory on CY orientifolds.

The pairing of a specific class with a corresponding case establishes the essential ground-work, delineating the minimum set of physical parameters needed to formulate a viable spectator model. It is imperative, however, to ensure the compatibility of these pairings by addressing additional considerations. In the subsequent discussion we delve into these intricacies while also incorporating the constraints described of the previous subsection.

Intuitively from the QFT-centric arguments of [203, 204], one may expect that realizing spectator models with large signals in string theory would be quite challenging. Indeed it is. In fact, it is simple to show that visible spectator models utilizing  $C_4$ -axions are quite difficult to realize. The crucial point is that for a stack of D7-branes wrapping a 4-cycle  $\widetilde{\Pi}$ , the Chern-Simons coupling of the  $C_4$ -axion is entirely determined by the vev of the related Kähler modulus

$$\lambda_{C_4} \simeq \frac{1}{\langle \tau \rangle} \,. \tag{6.48}$$

In particular, the CS coupling is independent of both the wrapping and magnetization of the precise D7-brane configuration one is considering. To have a visible GW signal in the near-term future, we would need  $\lambda_{C_4} = \mathcal{O}(10)$ , which implies  $\langle \tau \rangle \simeq 0.1$ . If we assume that the  $C_4$ -axion gets a mass from an ED3 instanton, then control of the EFT is encapsulated by eq. (6.44). This requires  $\langle \tau \rangle \gtrsim 0.3$ , rendering visible GWs and EFT control mutually exclusive. An identical argument can be made for  $C_4$ -axions that obtain masses via gaugino condensation.

Of course the details of the above can be complicated by kinetic or mass mixing between axions. However, it seems unlikely that sufficient kinetic mixing can exist. Naively, if one has a two-axion model of the form

$$\mathcal{L} \supset \frac{1}{2} \left( (\partial a_1)^2 + (\partial a_2)^2 + 2\varepsilon \partial_{\mu} a_1 \partial^{\mu} a_2 \right) + \Lambda^4 \cos \left( \frac{a_2}{f_2} \right) - \frac{\lambda_1}{4f_1} a_1 F_{\mu\nu} \widetilde{F}^{\mu\nu} , \qquad (6.49)$$

up to  $\mathcal{O}(\varepsilon^2)$  corrections, the kinetic terms can be diagonalized by a shift  $a_1 \to a_1 - \varepsilon a_2$ , which induces a Chern-Simons coupling for the  $a_2$  axion as

$$\mathcal{L} \supset \frac{\varepsilon f_2}{f_1} \frac{\lambda_1}{4f_2} a_2 F_{\mu\nu} \widetilde{F}^{\mu\nu} \,. \tag{6.50}$$

If  $f_2/f_1 \gg \varepsilon^{-1}$ , then the  $a_1$  axion would have a CS coupling  $\lambda_2 = \varepsilon \lambda_1 f_2/f_1$  that would be boosted relative to  $\lambda_1$ .

Nevertheless, achieving a boosting effect in type IIB compactifications appears to be a challenging prospect. From the orientifold kinetic terms displayed in section A.5, we see

that  $C_4$ - and  $C_2$ -axions do not mix directly via the tree-level Kähler metric. Therefore, if our goal is to have a  $C_4$ - spectator axion realized via the kinetic mixing outlined in eq. (6.49), we might consider the kinetic mixing of two  $C_4$ -axions arising from a non-diagonal term in the Kähler metric. Broadly speaking,  $C_4$ -axions can be classified as either local or non-local, depending on whether they arise from blow-up cycles or cycles that determine the overall compactification volume, respectively. Typically, local axions have decay constants that scale as  $f \sim M_p \mathcal{V}^{-1/2}$  while the decay constants of non-local axions scale as either  $f \sim M_p \mathcal{V}^{-2/3}$  (isotropic compactifications) or  $f \sim M_p \mathcal{V}^{-1}$  (anisotropic compactifications) [17], where  $\mathcal{V}$  is the compactification volume in string units.

To get a handle on some possibilities, let us consider a Swiss cheese CY with volume form

$$\mathcal{V} = \alpha_0 \tau_b^{3/2} - \alpha_1 \tau_{s_1}^{3/2} - \alpha_2 \tau_{s_2}^{3/2} - \beta_1 \tau_{s_1} \tau_{s_2}^{1/2} - \beta_2 \tau_{s_2} \tau_{s_1}^{1/2}. \tag{6.51}$$

Here  $\tau_b$  controls the size of the CY volume  $\mathcal{V} \simeq \mathcal{V}_0 = \alpha_0 \langle \tau_b^{3/2} \rangle$  while  $\tau_1$  and  $\tau_2$  determine the size of blow-up cycles. This CY gives 3  $C_4$ -axions: two local axions  $\{\rho_{s_1}, \rho_{s_2}\}$  and a non-local axion  $\rho_b$ . The Kähler metric is determined by derivatives of  $K = -2\ln(\mathcal{V})$ . We have  $\alpha_1, \alpha_2 > 0$  and we need  $\langle \tau_{s_1} \rangle \gg \langle \tau_{s_2} \rangle$  for arbitrary  $|\beta_1| \lesssim \alpha_1$  and  $0 \leq \beta_2 \ll \alpha_2$  or  $\beta_2 < 0$  to retain positive kinetic terms for both axions from the two small blow-up cycles. There are three mixing scenarios one can consider from eq. (6.51).

- The first is a mixing between the non-local axion and one of the local ones. We set  $\beta_1 = \beta_2 = \alpha_2 = 0$  and discard the second blow-up cycle and associated axion. To allow for an enhancement factor, we wrap branes on a 4-cycle  $\widetilde{\Pi}_b$  of  $\widetilde{X}_3$  so that  $\rho_b$  has a CS coupling with the worldvolume gauge fields. If we assume that  $\rho_{s_1}$  obtains a mass from some non-perturbative effect, then we have an action of the form eq. (6.49) with  $\{\rho_b, \rho_{s_1}\}$  corresponding to  $\{a_1, a_2\}$ . The mixing parameter of eq. (6.49) is  $\varepsilon \sim \langle \tau_{s_1}/\tau_b \rangle^{3/4}$  so that after unmixing the axions,  $\rho_{s_1}$  couples to the gauge fields with CS coupling  $\lambda_{s_1} \propto \langle \tau_{s_1}/\tau_b \rangle^{1/2} \lambda_b$ . Since we must have the hierarchy  $\langle \tau_b \rangle \gg \langle \tau_{s_1} \rangle$ , the CS coupling of  $\rho_{s_1}$  is suppressed relative to that of  $\rho_b$ , not enhanced.
- We can also consider the mixing between the two local axions  $\rho_{s_1}$  and  $\rho_{s_2}$ . First we consider the "strong" Swiss-cheese scenario which corresponds to the volume form in eq. (6.51) with  $\beta_1 = \beta_2 = 0$ . Since the decay constants of the local axions are inversely proportional to the size of the cycle they are supported on, we can wrap branes on  $\tilde{\Pi}_{s_1}$  and assume a hierarchy  $\langle \tau_{s_1} \rangle \gg \langle \tau_{s_2} \rangle$  to obtain a setup akin to eq. (6.49) with  $\rho_{s_1}$  and  $\rho_{s_2}$  playing the roles of  $a_1$  and  $a_2$ , respectively. The mixing parameter is then  $\varepsilon \sim \langle \tau_{s_1} \tau_{s_2} \rangle^{3/4} / \mathcal{V}_0$  and diagonalization gives  $\rho_{s_2}$  a CS coupling  $\lambda_{s_2} \simeq \langle \tau_{s_1} \tau_{s_2}^{1/2} / \mathcal{V} \rangle \lambda_{s_1}$ . Since  $\langle \mathcal{V} \rangle \gg \langle \tau_{s_1} \rangle$ ,  $\langle \tau_{s_2} \rangle$ , we again have suppression as opposed to enhancement.
- Finally, we can consider the mixing of the two local axions but including the  $\beta_i$  terms in eq. (6.51). We again consider the hierarchy  $\langle \tau_{s_1} \rangle \gg \langle \tau_{s_2} \rangle$  and branes wrapping  $\widetilde{\Pi}_{s_1}$ . If  $\beta_1 \gtrsim \alpha_1$  we get for the kinetic mixing parameter  $\varepsilon \sim \langle \tau_{s_2}/\tau_{s_1} \rangle^{1/4} \ll 1$  and a CS coupling for  $\rho_{s_2}$  of strength  $\lambda_{s_2} \simeq \langle \tau_{s_1}/\tau_{s_2} \rangle^{1/2} \lambda_{s_1}$ . Thus with the assumed hierarchy in the sizes of the blow-up cycles, we do see an enhancement of the  $\rho_{s_2}$  CS coupling relative to that of  $\rho_{s_1}$ . However, there is an important caveat in that  $\lambda_{s_1} \propto \langle \tau_{s_1} \rangle^{-1}$  so that  $\lambda_{s_2} \propto \langle \tau_{s_1} \tau_{s_2} \rangle^{-1/2}$ . Thus attempting to increase the enhancement factor  $\varepsilon f_{s_2}/f_{s_1}$  by enlarging  $\langle \tau_{s_1} \rangle$  will in truth drive the gauge coupling down and spoil any attempts to realize a large CS coupling.

Note that this last case was considered by [315] in the context of the QCD axion and the authors found that an enhancement of axion coupling to QED may be possible. Their scenario works as discussed because they fix the fine structure constant to that of QED. In our scenario, the strength of the gauge coupling is determined by the size of the 4-cycles and the enhancement factor is rendered ineffectual. While the above arguments do not entirely forbid enhancement of  $C_4$ -axion CS couplings in the type IIB orientifold landscape, it suggests that achieving enhancement via kinetic mixing is not simple to realize.

We end this discussion on  $C_4$ -axions with some caveats. First, we have discussed very simple scenarios, and one could consider more complicated setups, such as more general divisors. This would involve multiple wrapping numbers and  $C_4$ -axions. However, it is not clear that this complication helps. The worldvolume gauge theory will couple to some linear combination of  $C_4$ -axions, and the gauge coupling will also be determined by a linear superposition of  $\tau_{\alpha}$  also determined by the wrapping numbers. Thus, an attempt to create a large CS coupling by boosting wrapping numbers will simply alter the dominant fields in the superpositions and cancel out when determining the CS coupling, similar to the discussion around eq. (6.48) above. Next, in arguing against  $C_4$ -axions as viable spectators, we are more specifically referring to the impossibility of observing GWs at near-term detectors as summarized in fig. 5.14. If  $\lambda_{C_4} \simeq 1$ , which is more reasonable from the standpoint of control of the EFT, then  $P_T = \mathcal{O}(10^{-22})$ . This is far below the reach of any proposed detector, but we do not exclude the possibility of extremely advanced detection methods that would be able to reach this level and see peaks arising from  $C_4$ axion spectators. We also note that the above argument only rules out visible  $C_4$ -axions due to demanding an approximation scheme that permits one to neglect higher-order non-perturbative effects. If one could reliably calculate an infinite number of instanton terms, then this constraint could be neglected and the possibility of more visible GWs from  $C_4$  spectators opens up. A caveat to these statements is that one still requires small values of  $\langle \tau \rangle$ , which could result in a tower of states becoming light and ruining the EFT, as predicted by the Swampland Distance and Emergent String conjectures [42,348]. The precise statement then is that visible GWs from  $C_4$  axions requires one to live near the center of Kähler moduli space and far from asymptotic regions.

A similar argument can be made to rule out  $C_2$ -axion spectators in certain compactifications. For simplicity, let us assume a construction with  $h_{-}^{1,1} = 1$  and where the vev of the sole  $B_2$ -axion vanishes in a particular vacuum. Then from eq. (6.8), we see that the gauge coupling constant is  $g^{-2} = \frac{w}{2\pi} \left( \langle \tau_{\widetilde{1}} \rangle - \frac{\kappa_{+--}}{2g_s} (m_1)^2 \right)$ , where we have used a shorthand for the relevant intersection number. As is evident from this expression, the sign of  $\kappa_{+--}$  plays an essential role in the viability of a controlled spectator model. If  $\kappa_{+--} < 0$ , then increasing magnetization leads to a decrease in the gauge coupling constant. Since  $\lambda \propto \alpha \simeq g^2$ , this increases the difficulty of realizing a large CS coupling. In fact, from eq. (6.9) the CS coupling has the form

$$\lambda_{C_2} = \frac{\kappa_{+--}}{\pi} \frac{g_s m_1}{(2g_s \langle \tau_{\widetilde{\Pi}} \rangle - \kappa_{+--} m_1^2)}. \tag{6.52}$$

For  $\kappa_{+--} < 0$  and fixed  $\langle \tau_{\widetilde{\Pi}} \rangle$ ,  $|\lambda_{C_2}|$  increases with the magnetization m as long as  $m < m_{max}$  and then starts to decrease with further increasing  $m_1$ . At the maximum  $m_{max} \sim \sqrt{-g_s \langle \tau_{\widetilde{\Pi}} \rangle / \kappa_{+--}}$  we find  $|\lambda_{C_2}|_{max} \sim 1/m_{max}$ . Hence, even by tuning  $g_s$  and  $\langle \tau_{\widetilde{\Pi}} \rangle$  to arrange for a long regime of  $|\lambda_{C_2}|$  growing linearly with  $m_1$ , its magnitude will be

driven deeper into the region  $|\lambda_{C_2}| \ll 1$ . In fact, since  $|\lambda_{C_2}|_{max}$  is inversely proportional to  $\langle \tau_{\widetilde{\Pi}} \rangle^{1/2}$ , satisfying the control constraints of the previous section drives one inexorably to small CS coupling, similar to the above discussion on  $C_4$ -axions. Thus the associated GW signal is far too small to be observed in the near future and we see there is a general tension between observable spectator axions and models with  $h_-^{1,1} = 1$  and  $\kappa_{+--} < 0$ . To avoid this issue, one has two obvious paths. The first is to consider compactifications with  $h_-^{1,1} > 1$ . In such cases, it may be possible to have intersection numbers such that one  $C_2$ -axion obtains a large CS coupling without introducing the quadratic flux terms if certain intersection numbers are zero or if opposing fluxes can be placed to cancel the quadratic terms. The second option is to consider compactifications with  $\kappa_{+--} > 0$ . For  $\kappa_{+--} > 0$ , the magnitude of eq. (6.52) can be increased significantly for fixed  $g_s$  and m assuming some tuning of  $\langle \tau_{\widetilde{\Pi}} \rangle$  is permitted. This may even occur in such a way that the control conditions discussed in the previous subsection are easily satisfied.

Having discussed the severe limitations on realizing spectator models in type IIB models, we now discuss two potentially viable scenarios.

#### • Class I Spectators: Case 2

This scenario contains a single U(1) gauge factor and a  $C_2$  axion. We allow the D7-brane to have multiple wrappings parametrized by  $w_1$  and magnetic flux  $m_1$  in its worldvolume<sup>8</sup>. The axion receives a mass via ED1 instantons wrapping a 2-cycle. The Chern-Simons coupling is given by eq. (6.26) with  $\mathcal{J} = 1$  and  $\mathcal{M} = w_1 \kappa_{+--} m_1$  so that  $\lambda = \frac{\alpha_{U(1)}}{\pi} w_1 \kappa_{+--} m_1$ .

We now want to consider observable GW signals in this setup while keeping in mind the induced D3-charge of the brane stack. To this end, we can fix the CS coupling to a value required to produce a specific GW peak, i.e.  $\lambda = \lambda_{\rm GW}$ . Then we can trade one microscopic parameter, say the flux  $m_1$ , for  $\lambda_{\rm GW}$ . We can use this to replace  $m_1$  in the expression for induced D3-brane charge, and arrive at a scaling relation for the D3-charge necessary to produce a desired GW peak amplitude. Choosing reference parameters

$$(\lambda_{\text{GW}}, \alpha_{D7}, \kappa_{+--}, w_1) = (22, 0.8, 1, 1),$$
 (6.53)

we obtain a D3-charge "Drake Equation"  $(DDE)^9$ :

$$Q_{\rm D3,ind.} \simeq 7.5 \times 10^3 \left(\frac{1}{w_1 \,\kappa_{+--}}\right) \left(\frac{0.8}{\alpha_{D7}}\right)^2 \left(\frac{\lambda_{\rm GW}}{22}\right)^2$$
. (6.54)

To motivate a string embedding of this scenario, we demand that eq. (6.54) satisfies eq. (6.38). We also enforce constraints on perturbativity eq. (6.42) and ED1 control eq. (6.43). An example parameter space including these bounds is displayed in fig. 6.2 below.

#### • Class IIb Spectators: Case 4

We now consider a scenario that involves both  $C_4$ - and  $C_2$ -axions. We consider homologous 4-cycles  $\widetilde{\Pi}^{(1)}$  and  $\widetilde{\Pi}^{(2)}$  in  $\widetilde{X}_3$  such that  $\widetilde{\Pi}^{(1)}$  supports a stack of  $N_{\rm D7}$  D7-branes and  $\widetilde{\Pi}^{(2)}$  has a single D7-brane wrapped on it. We also consider a third

<sup>&</sup>lt;sup>8</sup>Here we will neglect the term in the gauge kinetic function that is quadratic in the flux. As described in the preceding paragraphs, such a term will either completely invalidate this model, or greatly relax control restrictions.

<sup>&</sup>lt;sup>9</sup>Named in analogy with the Drake equation [349].

cycle  $\widetilde{\Pi}^{(3)} \in \widetilde{X}_3$  that is the even combination of cycles  $\Pi_4^{(3)}$  and  $\Pi_4^{(3)}$  in  $X_3$ . We assume that  $\widetilde{\Pi}^{(3)}$  supports an ED3 instanton that stabilizes its Kähler modulus and provides a mass for the associated  $C_4$ -axion. We will also assume there is a non-trivial even-odd-odd intersection number (called here  $\kappa_-$  for convenience) such that the  $C_2$ -axion from the odd cycle associated to  $\widetilde{\Pi}^{(3)}$  couples to the gauge theories on  $\widetilde{\Pi}^{(1)}$  and  $\widetilde{\Pi}^{(2)}$ . For ease of discussion, we also assume that certain intersection numbers of  $\widetilde{\Pi}^{(1)}$  vanish to avoid a flux-induced Stückelberg coupling.

The EFT of this configuration again contains an  $SU(N_{\rm D7}) \times U(1)_1 \times U(1)_2$  gauge sector. There are also three axions - a  $C_4$ - and a  $C_2$ -axion from  $[\widetilde{\Pi}^{(1)}]$ , and an additional  $C_2$ -axion from  $\widetilde{\Pi}^{(3)}$ . A linear combination of  $U(1)_1 \times U(1)_2$  will eat the  $C_2$  associated to  $[\widetilde{\Pi}^{(1)}]$ . The surviving U(1) boson couples to the  $[\widetilde{\Pi}^{(1)}]$   $C_4$ -axion as well as the  $C_2$ -axion c from  $\widetilde{\Pi}^{(3)}$ :

$$S_{EFT} \supset -\int \sqrt{-g} \ d^4x \left\{ \rho + \frac{\kappa_{-}(w_1 m_N + N_{D7}^2 w_N m_1)}{w_1 + N_{D7}^2 w_N} c \right\} \frac{2w_1 \alpha_1}{4} X_{\mu\nu}^{(2)} \widetilde{X}^{(2)\mu\nu} \,. \tag{6.55}$$

Here  $X_{\mu\nu}^{(2)}$  is the field strength of the surviving U(1) and its Chern-Simons couplings to the axions  $\rho \& c$  are obtained by rotating the original gauge fields. In the above we have allowed for a non-zero magnetization  $m_1$  of the  $\widetilde{\Pi}^{(2)}$  D7-brane, and we have also used the relation  $w_N\alpha_N=w_1\alpha_1$ . We assume that the D7-brane stack on  $\widetilde{\Pi}^{(1)}$  undergoes gaugino condensation. If we allow for magnetization  $m_N$  on this stack, then both axions appear in the potential as in eq. (6.20) with  $\{w_{\mathcal{G}}, m_{\mathcal{G},c(\mathcal{G})}\} = \{w_N, m_N, N_{\text{D7}}\}$ . Defining decay constants  $f_e = \frac{N_{\text{D7}}}{2\pi w_N} F_e$  and  $f_o = \frac{N_{\text{D7}}}{2\pi w_N} \frac{F_o}{\kappa m_N}$  the scalar potential reads:

$$V = -\Lambda_N^4 \cos \left[ \frac{\vartheta_e}{f_e} + \frac{\vartheta_o}{f_o} \right]. \tag{6.56}$$

The masses and eigenstates are those of eq. (6.21) with  $\varepsilon = \kappa_- m_N F_e/F_o = f_e/f_o$ . For the massive axion  $\vartheta_2$  we define a re-scaled axion decay constant

$$f_2 = \frac{f_e}{\sqrt{1 + \varepsilon^2}} \,. \tag{6.57}$$

Using  $f_e$  and  $f_o$  we can define Chern-Simons coupling parameters

$$\lambda_{e} = \frac{\alpha_{N} N_{D7}}{\pi}$$

$$\lambda_{o} = \frac{\alpha_{N} N_{D7}}{\pi} \left\{ \frac{(w_{1}/w_{N}) + N_{D7}^{2}(m_{1}/m_{N})}{w_{1} + N_{D7}^{2}w_{N}} \right\}.$$
(6.58)

The coupling of the massive axion  $\vartheta_2$  to the massless gauge field  $X^{(2)}$  in the form of eq. (5.47), with decay constant  $f_2$  will therefore read:

$$\lambda_2 = \frac{\lambda_e + \varepsilon^2 \lambda_o}{1 + \varepsilon^2} \,. \tag{6.59}$$

Since  $\lambda_o$  is proportional to the magnetization  $m_1$  of the brane wrapping  $\widetilde{\Pi}^{(2)}$ , we see that increasing  $m_1$  will boost the Chern-Simons coupling of the axion  $\vartheta_2$ . However, there is a hurdle to overcome – we expect  $\varepsilon < 1$ , and the magnetization must overcome this suppression in order to achieve the desired coupling strength. The  $\vartheta_1$  axion couples to  $X^{(2)}$ , with strength

$$\lambda_1 \simeq \lambda_o - \lambda_e$$
, (6.60)

6.4. Remarks 127

where we are approximating  $1 + \varepsilon^2 \simeq 1$  and  $f_1 \simeq f_o$ . Thus one can boost the Chern-Simons coupling of  $\vartheta_1$  without having to overcome suppression by  $\varepsilon$ . Unfortunately,  $\vartheta_1$  in the model above is massless and is not a viable spectator.

This can be remedied by the inclusion of an ED1 instanton that gives rise to a potential of the form eq. (6.18) for the  $C_2$ -axion c. In terms of  $\vartheta_1$  and  $\vartheta_2$ , we have a contribution to the potential of the form

$$V \supset -\Lambda_{ED1}^4 \cos \left[ \frac{N_{\rm D7}}{\kappa_- w_N m_N} \frac{\vartheta_1 + \varepsilon \vartheta_2}{f_o \sqrt{1 + \varepsilon^2}} \right].$$
 (6.61)

The ED1 introduces a mixing between  $\vartheta_1$  and  $\vartheta_2$ , but to lowest order in  $\varepsilon$  this potential simply provides a mass for  $\vartheta_1$ . If we also take  $\kappa_- w_N m_N \simeq 1$ , then indeed  $f_1 \simeq f_o$  defines the periodicity of  $\vartheta_1$ .

With the above ingredients, we see that we have two spectator axions coupled to the U(1) gauge field  $X^{(2)}$ . The induced D3 tadpole depends on the string parameters as

$$Q_{D3,ind} = \kappa_{-} w_1 m_1^2 + \kappa_{-} w_N m_N^2 N_{D7}.$$
 (6.62)

From here, one can replace  $m_1$ , derive a DDE equation in analogy with eq. (6.54), and look for a valid region in parameter space. We can then imagine that  $\vartheta_1$  is the spectator axion associated with an observable peak, while  $\vartheta_2$  produced a lower signal. While there is a valid parameter space for  $\lambda_1 = 22$ , it lies dangerously close to saturating our tadpole condition and can therefore be realized only in the most extreme of compactifications.

We note here an observation relevant for future GW experiments: given that the GW peak amplitude is exponentially sensitive to  $\lambda$ , the CS coupling reacts only logarithmically to increasing the sensitivity of future GW detection experiments. Compared to the peak amplitude corresponding to the recently reported evidence for a nanoGRAV/PTA stochastic GW signal, even the most futuristic GW detection experiment currently envisioned – DECIGO/BBO – would increase sensitivity only such, that the required value of  $\lambda$  for a matching axion-generated signal lowers only by a factor of two.

#### 6.4 Remarks

From the viewpoint of string theory, MASA models can provide a glimpse into the axionic content of a given compactification. However, this is not to say that observable MASA models are simple to realize. We have found that there are numerous restrictions that must be satisfied to have a viable spectator sector. One of the largest challenges is simply ensuring a suitable U(1) factor exists in the gauge group of the EFT. The primary difficulty here is avoiding Stückelberg couplings that would pair an axion and U(1) gauge boson into a massive vector boson. Ostensibly, type IIB compactifications have two natural spectator axion candidates from dimensional reduction of the 10d p-forms  $C_4$  and  $C_2$ . However, as argued above, it is quite difficult to generate sufficiently large CS couplings for the  $C_4$ -axions. This leaves  $C_2$ -axions as the sole viable spectator candidates.

On top of the difficulty in simply realizing the field content for spectator sectors, string constructions place further limitations on the parameters of the models. Boosting the CS coupling of  $C_2$ -axions requires non-zero magnetic flux in the worldvolume theory of D7-branes, which induces an effective D3-tadpole. This tadpole must be cancelled by

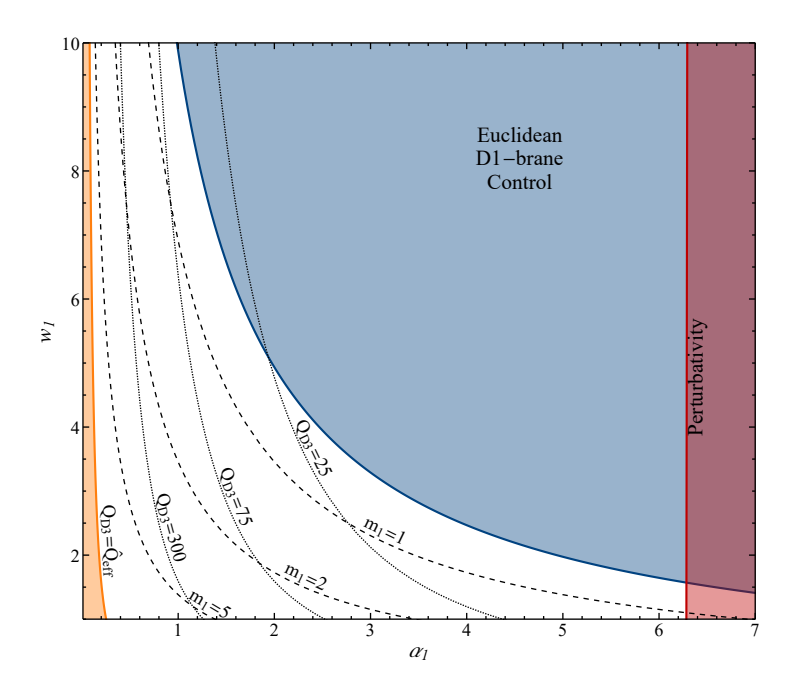


Figure 6.2: Example parameter space for Class I: Case 2 MASA models. The excluded shaded regions arise from constraints on control of the instanton expansion for ED1s (in blue), perturbativity of the U(1) gauge theory (in red), and the tadpole constraint eq. (6.38) (in orange). The dashed (dotted) contours correspond to parameter values with fixed magnetization  $m_1$  (D3-tadpole  $Q_{\rm D3}$ ). We chose parameters  $\lambda_{GW}=22$  and  $\kappa_{+--}=10$ .

other sources in the compactification manifold, such as orientifold planes, and is inherently limited. Furthermore, demanding perturbative and non-perturbative control of the construction places additional restrictions on the viable parameter space.

Despite all the above constraints, there still appears to be viable scenarios. By far the least constrained scenarios are Class I: Case 2 models, where the Stückelberg mechanism is sidestepped by appropriate features of the divisor wrapped by a D7-brane. An example of the parameter space of such models is presented in fig. 6.2. An interesting feature of this plot is that a viable spectator model can survive with relatively little magnetic flux - simply  $m \simeq \mathcal{O}(1)$  can suffice so long as the fine-structure constant is sufficiently large. The root of this feature lies in the fact that Abelian spectators are not required to have extremely small gauge couplings to be viable. On the other hand, non-Abelian spectator models do feature small gauge couplings, which brings them in tension with tadpole cancellation as discussed above.

So far, in the string context we have discussed only single-axion spectator models. To have multiple spectators, one needs several copies of the constructions that realize the Abelian gauge bosons and axions. Furthermore, one must heed the constraint of D3-tadpole cancellation. Since the parameter space in fig. 6.2 allows for  $\mathcal{O}(10)$  D3-tadpoles, it is not inconceivable that some compactifications may yield multiple visible spectator sectors. A distinct possibility is to stack a multitude of spectator sectors such that the collective signal is enhanced relative to that of a single constituent. This would require

6.4. Remarks 129

similar initial conditions for all axions involved, making it perhaps less generic. A precise distribution of initial conditions for the axions would be required to make this statement more precise.

One might interpret the above restrictions as an indication that visible spectator models are highly disfavored in string theory. An alternative viewpoint is that visible spectators serve as a powerful superselection rule in string vacua. If one is able to see a GW peak from a spectator axion, then one has learned valuable information regarding the topological structure of the manifold. For example, since  $C_4$ -axions are poor spectator candidates, a spectator GW peak is a direct probe of the odd moduli content of a type IIB compactification. Previous studies [17] considered the experimental signals of even axions. If we take the optimistic viewpoint that we will be able to probe some features of the string compactification underlying our Universe, then direct coupling experiments will most likely probe even axions. Thus our MASA models provide a means to go beyond this and probe odd axions, which would reveal new information on the string embedding of our Universe. For example, a very optimistic scenario would be the future detection of several PTA-strength peaked GW signals at different frequencies. In this situation, by the argument above, we need to attribute all of them to odd sector string axions with GW signals increased sufficiently by choosing large enough magnetizing D7-brane fluxes. However, this potentially runs into the D3-brane charge tadpole bound, because for each odd sector string axion the induced D3-brane charge contribution on coupled D7-branes increases quadratically in m. Hence, generating several strong GW peaks all by using odd sector string axions tends to use a significant fraction of the background D3-brane charge tadpole. This observational outcome would thus point us towards the F-theory compactifications on elliptic CY 4-folds with the largest Euler numbers, and may limit the number of strong GW wave peaks which we can explain using odd sector string axions. It is in this sense that a future "wideband spectroscopy" of GW signals may provide us with observational clues about the underlying topological structure and flux choices of the string compactification describing our Universe.

Another interesting aspect of MASA models is that the GW signal is not directly dependent on the decay constants of the spectator axions, but is encoded in other parameters, such as  $\delta$ . On one hand, for fixed  $\delta$  this removes the possibility of boosting the signal by lowering the decay constants. However, this feature is actually a boon from the string theory perspective. A persistent issue in probing string axions is that the axion decay constants are  $\mathcal{O}(10^{16})$  GeV or above, making direct detection via terrestrial experiments extremely difficult, even if they couple to the Standard Model. Some haloscope experiments [350–353] will probe this interesting parameter space, but only for axions that i). couple directly to the Standard Model, ii). have sub-eV masses, and iii). constitute some non-trivial fraction of the observed dark matter. In contrast, MASA models more naturally probe heavier axions that need not couple to the Standard Model nor be present in dark matter. Thus one should consider searching for spectator GW signals as complementary to probing lighter elements of the type IIB string axiverse that could be the QCD axion [17] or fuzzy dark matter [69].

# Chapter 7

# Post-Inflationary Dynamics

For every model of inflation embedded into string theory, it is essential to verify that the predicted cosmological observables are consistent with current data. Usually, one tries to construct the inflationary model such that the spectral index, the tensor-to-scalar ratio, and the non-Gaussianities, are consistent with current data. Beyond that, a viable reheating mechanism must be identified. In particular, one must ensure that perturbative reheating is available and efficient in transferring energy from the inflaton field to the matter content of the universe. Inflation ends once the inflaton begins its descent to the minimum of its potential leading to an epoch of damped oscillations. In simple models, these oscillations cease as the inflaton perturbatively decays into either standard model particles directly or dark sector states that eventually reheat the universe.

This scenario of perturbative reheating changes significantly upon the inclusion of a preheating era [354–358]. During this period, the inflaton can produce its own quanta and/or spectator<sup>1</sup> scalar particles via the non-perturbative phenomena of parametric resonance and tachyonic preheating. In this paper, we restrict ourselves to preheating via parametric resonance. This mechanism requires scalar particles whose masses vary with the inflaton oscillations. If active, parametric resonance leads to explosive growth of scalar particle modes that are in resonance with the inflaton oscillations. In many cosmological models, this behavior is captured by the Mathieu equation [359], whose secular dynamics are described via Floquet theory [360], or its generalization for expanding spacetimes.

The population of spectator particles produced during preheating can significantly alter the naive cosmology of an inflationary scenario. If this population becomes non-relativistic soon after its production, it can serve as a component of dark matter. Indeed this mechanism has been used as a production mechanism for axions [361–364] and ultralight dark photon dark matter [365–369]. Instead, if this population remains relativistic until today, it will contribute to current dark radiation. Both outcomes can lead to constraints on inflationary models — if too many non-relativistic particles are produced, parametric resonance can eventually overclose the universe. Conversely, if too much dark radiation is produced, one will run afoul of the current bound on  $\Delta N_{\rm eff}$ .

The dynamics of preheating have been well-studied in the cosmology literature, but it has not yet been as widely explored in string models of inflation. There are several mo-

<sup>&</sup>lt;sup>1</sup>Spectator here referring to scalar particles that do not appreciably contribute to inflationary background dynamics.

tivating reasons to amend this. First, string theory provides a natural setting to study inflation since one begins from a valid theory of quantum gravity and can therefore address fundamental issues of cosmic inflation directly. Among these are the role of protective symmetries for trans-Planckian field ranges tied to high-scale inflation with a detectable level of primordial direct tensor mode production and the structure and size of inflatondark sector cross couplings [22,370]. Furthermore, in contrast to simple QFT models, the masses of all states in a string compactification arise from the vacuum expectation values (vevs) of scalar fields. If some subset of these scalar fields participate in inflation, one expects that many fields have masses that vary as the inflaton oscillates at the end of inflation. A natural question then is to understand the prevalence of parametric resonance in the string landscape. The utility of this is twofold. First, models of string cosmology are known to suffer from issues of overproduction of dark radiation [96, 97, 371–374]. As mentioned above, parametric resonance can contribute to  $\Delta N_{\rm eff}$  and thereby exacerbate dark radiation issues for string models. Second, if parametric resonance produces a non-relativistic spectator, avoiding dark matter overproduction provides an additional constraint. In both cases, the resulting condition can be used to constrain the spaces of underlying microscopic parameters controlling the string theory constructions of inflation and spectator sectors. Studies of parametric resonance in the string cosmology literature include the self-production of the inflaton in blow-up inflation [375] and fibre inflation [376].

We will instead be focused on the non-perturbative production of axions during inflation in string cosmology. Axions are believed to be a general feature of string compactifications, an expectation enshrined in the notion of the String Axiverse [15, 17, 18]. As a generic prediction of string theory, the string axiverse is one of the most important tools to tie string theory to experiments, both through standard model couplings and through secondary primordial gravitational wave production [73,86,87] based on the mechanism first established in [165,167,377,378]. Preheating of axions in string-inspired models where the inflaton  $\varphi$  is coupled to the axion  $\vartheta$  via a quartic coupling  $\lambda \varphi^2 \vartheta^2$  to the axions was studied in [379]. Such a coupling is commonly considered in typical preheating models in cosmology. Naively, one might then consider that the usual treatment of parametric resonance in the literature is sufficient to understand the non-perturbative production of axions in string cosmology. However, in this paper we show that this to be insufficient due to the fact that string theory features non-perturbative effects that have no analogue in EFT models. Namely, the extended objects in string theory, such as Euclidean Dp-branes, can wrap sub-manifolds of the compactification manifold and rise to axion potentials not normally considered in the field theory context.

To motivate this statement, we note that closed string axions have distinguished properties that set them apart from their field-theoretic analogues. In particular, the perturbative shift symmetry of a closed string axion is preserved to all orders in string perturbation theory. Therefore, axion potentials can only be generated via non-perturbative effects. These can include field-theoretic effects, such as gauge instantons, but also wormholes and purely stringy effects such as worldsheet or Euclidean D-brane instantons. The strength of such stringy effects is controlled by the size of the sub-manifold wrapped by the Euclidean object, which in turn is governed by the vev of a modulus. This gives rise to the general leading-order potential for the axions:

$$\frac{\mathcal{L}}{\sqrt{-g}} \supset -\sum_{a} \Lambda_a^4 e^{-q_i^a \tau^i} \cos(q_i^a \theta^i). \tag{7.1}$$

Here the  $\{\theta^i\}$  are non-canonically normalized axions while the  $\{\tau^i\}$  are the moduli controlling the strength of the non-perturbative effects. The  $\{q_i^a\}$  denote the instanton charges, and the  $\{\Lambda_a\}$  are overall scales that will depend on the  $\tau^i$  and may additionally depend on other moduli via 1-loop determinants. In general there are higher-order instanton effects correcting eq. (7.1) which we have omitted.

In a viable compactification, the terms in eq. (7.1) will be supplemented in the total Lagrangian by a potential for the moduli  $\{\tau_i\}$  that will ensure that they obtain vevs. This in turn provides a mass for the axions via the potential in eq. (7.1). Therefore, if we identify a subset of the  $\{\tau_i\}$  with the fields responsible for inflation, it follows that the masses of at least some axions will vary with time as the inflaton(s) oscillate at the end of inflation. Hence all of the ingredients for parametric resonance can be present in string cosmology. However, the equation of motion that follows from eq. (7.1) is not the Mathieu equation, but rather a generalization of the Hill equation [380] (see also [381]) called the Whittaker-Hill equation. Hence, the standard approximations used to study parametric resonance are not sufficient to completely determine the behavior of preheating from string inflation once considering the expanding background.

# 7.1 The Mathematics of Preheating

In this section, we review the mathematics of parametric resonance and its application to cosmology via preheating. To motivate this study, we start by considering models described by the general Lagrangian

$$\frac{\mathcal{L}}{\sqrt{-g}} \supset g^{\mu\nu} K_{i\bar{\jmath}} \partial_{\mu} T^{i} \partial_{\nu} \bar{T}^{\bar{\jmath}} - V(T^{i}, \bar{T}^{\bar{\imath}})$$

$$= g^{\mu\nu} K_{i\bar{\jmath}} (\partial_{\mu} \tau^{i} \partial_{\nu} \tau^{\bar{\jmath}} + \partial_{\mu} \theta^{i} \partial_{\nu} \theta^{\bar{\jmath}}) - V(\tau^{i}, \theta^{i}), \tag{7.2}$$

where the  $\{T^i = \tau^i + i\theta^i\}$  are a collection of i = 1, ..., N complex scalar fields and the noncanonical kinetic terms depend on functions  $K_{i\bar{\jmath}}$  of the  $\{\tau^i\}$ . In subsequent sections we will consider  $\mathcal{N}=1$  supersymmetric theories obtained from Calabi-Yau orientifold compactifications of Type IIB string theory. In this context, the  $\{T^i\}$  will be the complexified Kähler moduli fields representing the scalar components of their associated chiral supermultiplets and  $K_{i\bar{\jmath}}$  the Kähler metric. Generally, the scalar potential V will have an expansion for the inflaton modulus  $\tau_{\varphi}$  of the form

$$V(T^{i}, \bar{T}^{\bar{i}}) \simeq V_{\inf}(\tau_{\varphi}, \langle \tau^{i} \rangle | i \neq 1) + V_{N}(\tau_{\varphi}, \tau^{i} - \langle \tau^{i} \rangle | i \neq 1) + \Delta V_{\text{non-pert}}(\tau_{\varphi}, \theta, \tau^{i}, \theta^{i} | i \neq 1),$$

$$(7.3)$$

where  $V_{\rm inf}(\tau_{\varphi}, \langle \tau^i \rangle | i \neq 1)$  is the inflation-driving potential of the inflaton Kähler modulus  $\tau_{\varphi}$ ,  $V_N(\tau_{\varphi}, \tau^i - \langle \tau^i \rangle | i \neq 1)$  the perturbative potential of all the remaining Kähler moduli, and  $\Delta V_{\rm non-pert}(\tau_{\varphi}, \theta, \tau^i, \theta^i | i \neq 1)$  denotes the whole instanton-generated non-perturbative contribution which couples the moduli  $\tau^i$  to the axions  $\theta^j$  which appear in the  $T^k \equiv \tau^k + i\theta^k$ .

From hereon,  $T \equiv T^1 = \tau_{\varphi} + i\theta$  denotes the complex scalar field containing the inflation  $\tau_{\varphi} \equiv \tau^1$  and its partner axion  $\theta \equiv \theta^1$ . As these fields will share a non-canonical  $\tau_{\varphi}$ -dependent kinetic term, we will call  $\varphi$  and  $\vartheta$  the canonically normalized fields corresponding to  $\tau_{\varphi}$  and  $\theta$ , respectively. We consider the generic case where, after the end

of inflation, the inflaton is oscillating around its minimum, so that the potential can be approximated as

$$V_{\rm inf}(\varphi) = \frac{1}{2} m_{\varphi}^2 \varphi^2 \,. \tag{7.4}$$

The equations of motion

$$\ddot{\varphi}(t) + 3H\dot{\varphi}(t) + V'(\varphi(t)) = 0$$
, with  $H^2(t) = \frac{1}{3M_{\rm Pl}^2} \left(\frac{\dot{\varphi}^2(t)}{2} + V(\varphi(t))\right)$ , (7.5)

are solved by

$$\varphi(t) = \varphi_0 + \Delta \varphi \frac{1}{t} \cos(m_{\varphi} t). \tag{7.6}$$

If there is an additional (pseudo)scalar field  $\theta$  coupled to  $\varphi$ , the inflaton field can decay non-perturbatively through parametric resonance in the time interval between the end of inflation and the beginning of reheating. The equation of motion for  $\theta$  reads

$$\frac{\partial \mathcal{L}}{\partial \theta} - \partial_{\mu} \frac{\partial \mathcal{L}}{\partial (\partial_{\mu} \theta)} = 0. \tag{7.7}$$

If the kinetic terms are diagonal, the equation becomes

$$\frac{\partial \mathcal{L}}{\partial \theta} = -\sqrt{-g} \frac{\partial V}{\partial \theta}, \qquad \partial_{\mu} \frac{\partial \mathcal{L}}{\partial (\partial_{\mu} \theta)} = \partial_{\mu} (\sqrt{-g} K_{T\bar{T}} \theta) \partial^{\mu} \theta + \sqrt{-g} K_{T\bar{T}} \partial_{\mu} \partial^{\mu} \theta . \tag{7.8}$$

Therefore, the equation of motion in a flat expanding universe where  $\sqrt{-g} = a^3$ , reads

$$K_{T\bar{T}}\left(\ddot{\theta} + 3H\dot{\theta} - \frac{\nabla^2 \theta}{a^2}\right) - \partial_{\mu}K_{T\bar{T}}\partial^{\mu}\theta + \frac{\partial V}{\partial \theta} = 0.$$
 (7.9)

It is convenient to decompose the axion field  $\theta$  into a spatially homogeneous background and fluctuations as  $\theta(t, \vec{x}) = \theta_0(t) + \delta\theta(t, \vec{x})$ . We can then write the coupled differential equations for the axion by expanding the potential up to linear term in the fluctuations  $V(\theta + \delta\theta) = V(\theta) + V'(\theta)\delta\theta + \mathcal{O}(\delta\theta^2)$ ,

$$\begin{cases}
\ddot{\theta}_0 + \left(3H - \frac{\partial_0 K_{T\bar{T}}}{K_{T\bar{T}}}\right)\dot{\theta}_0 + \frac{1}{K_{T\bar{T}}}V' = 0, \\
\ddot{\delta\theta} + \left(3H - \frac{\partial_0 K_{T\bar{T}}}{K_{T\bar{T}}}\right)\dot{\delta\theta} - \frac{\nabla^2 \delta\theta}{a^2} + \frac{1}{K_{T\bar{T}}}V''\delta\theta = 0.
\end{cases}$$
(7.10)

We retain terms only up to linear order in the fluctuations  $\delta\theta$  because they are sufficient to capture the quantum process of particle production, as reflected in the growth of the occupation numbers of the quantum fluctuations. We canonically normalize the axion as

$$\mathcal{L} \supset K_{T\bar{T}} \partial_{\mu} \theta \partial^{\mu} \theta = \frac{1}{2} \partial_{\mu} \vartheta \partial^{\mu} \vartheta , \qquad (7.11)$$

where  $\vartheta \equiv \theta \sqrt{2K_{T\bar{T}}}$ . We denote  $(\cdots)' = \frac{\partial}{\partial \theta}(\cdots) = \sqrt{2K_{T\bar{T}}} \frac{\partial}{\partial \vartheta}(\cdots)$ . By setting the initial homogeneous background field to  $\vartheta_0 \simeq 0$ , we can ignore the background equation of motion and focus on the second line in eq. (7.10), which now reads

$$\dot{\delta\vartheta} + \left(3H - \frac{\partial_0 K_{T\bar{T}}}{K_{T\bar{T}}}\right)\dot{\delta\vartheta} - \frac{\nabla^2 \delta\vartheta}{a^2} + \frac{1}{K_{T\bar{T}}}V''\delta\vartheta = 0.$$
 (7.12)

The fluctuation field can be expressed in terms of time dependent mode functions for the individual Fourier modes

$$\vartheta(t,\vec{x}) = \vartheta_0 + \delta\vartheta_k(t,\vec{x}), \quad \delta\vartheta_k(t,\vec{x}) = \int \frac{d^3k}{(2\pi)^3} \left[ \hat{a}_k \vartheta_k(t) e^{i\vec{k}\cdot\vec{x}} + \hat{a}_k^{\dagger} \vartheta_k^*(t) e^{-i\vec{k}\cdot\vec{x}} \right]. \quad (7.13)$$

Since the absolute direction of momenta is not important when assuming homogeneity and isotropy, we are interested only in the absolute values of  $\vec{k}$ , and in the following we will use  $k \equiv |\vec{k}|$ . eq. (7.12) finally becomes

$$\ddot{\vartheta}_k + \left(3H - \frac{\partial_0 K_{T\bar{T}}}{K_{T\bar{T}}}\right)\dot{\vartheta}_k + \left(\frac{k^2}{a^2} + 2\frac{\partial^2 V}{\partial \vartheta^2}\right)\vartheta_k = 0.$$
 (7.14)

## 7.1.1 The Mathieu Equation and Preheating

Let us first consider the simple example of parametric resonance where the kinetic term of the axion is canonical, and the inflaton is coupled to  $\vartheta$  via the operator

$$V_1(\varphi, \vartheta) = g\vartheta^2\varphi^2. \tag{7.15}$$

Neglecting the expansion of the universe (i.e. H=0), the inflaton oscillations are simply given by  $\varphi = \varphi_0 + \Delta \varphi \cos(m_{\varphi}t)$ . We can then plug this expression and eq. (7.15) into eq. (7.14). The resulting axion fluctuation dynamics can be analyzed via application of Floquet theory [360]. In this simple case, the fluctuation equation of motion can be rewritten as the Mathieu equation

$$\vartheta_k'' + (A_k - 2q\cos(2s))\vartheta_k = 0, \qquad (7.16)$$

where  $s = m_{\varphi}t/2$ ,  $q = 4g\Delta\varphi/m_{\varphi}^2$ , and  $A_k = 4k^2/m_{\varphi}^2$ . Solutions to this equation strongly depend on the parameters q and  $A_k$ , and exhibit an exponential instability  $\vartheta_k \sim e^{\mu_k s}$  when the modes enter a specific frequency band. The first and strongest of these bands is determined by  $\Delta k = \frac{m_{\varphi}}{2} \pm q$ . The  $\mu_k$  are called *Floquet exponents*: they determine the growth of the solution, and in the present case they can be found analytically. These instabilities correspond to exponential growth of the occupation numbers of quantum fluctuations  $n_k$ , which is computed as

$$n_k = \frac{\omega_k}{2} \left( \frac{|\dot{\vartheta}_k|^2}{\omega_k^2} + |\vartheta_k|^2 \right) - \frac{1}{2}. \tag{7.17}$$

It can be easily shown that the occupation number is exponentially sensitive to the Floquet exponents, as  $n_k \propto e^{2\mu_k s}$ . When  $\mu_k > H$ , the solution will have an exponential instability even when the expansion of the universe is taken into account, as we will see below.

# 7.1.2 The Hill Equation and Preheating

We can now generalize the previous section to more complicated potentials. One such example are the potentials discussed in section 7.2 describing the inflating saxion coupled to the axion with a string theory-inspired potential. In this case, one must use the *Hill equation* [380, 381]

$$\vartheta_k'' + (A_k + qF(t))\,\vartheta_k = 0\,, (7.18)$$

with F(t) a periodic function. This system can be treated again with Floquet theory: we can write the above differential equation as

$$\begin{cases} \vartheta_k' = \delta \pi_k ,\\ \delta \pi_k' = - (A_k + qF(t)) \vartheta_k . \end{cases}$$
 (7.19)

We will not exploit the details of the Floquet theory here, instead we will just outline the steps required to determine the Floquet indices. For further details, we refer the reader to e.g. [382].

First, we derive the period T of the zero mode, which can be found by energy conservation of a periodic oscillation, and computed numerically; then we solve the system  $\partial_t \mathcal{O}(t, t_0) = U(t)\mathcal{O}(t, t_0)$  from  $t_0$  to  $t_0 + T$  to obtain  $\mathcal{O}(t_0 + T, t_0)$ . We can now diagonalize  $\mathcal{O}(t_0 + T, t_0)$  to obtain the eigenvalues  $o_k^s = |o_k^s|e^{i\theta_k^s}$ , where s = 1, 2. Explicitly,

$$\mathcal{O}(t_0 + T, t_0) = \begin{pmatrix} \vartheta_k^{(1)}(t_0 + T) \vartheta_k^{(2)}(t_0 + T) \\ \delta \pi_k^{(1)}(t_0 + T) \delta \pi_k^{(2)}(t_0 + T) \end{pmatrix},$$
(7.20)

with the initial condition  $\mathcal{O}(t_0,t_0)=\mathbb{1}$ . This is equivalent to solving eq. (7.18) for the two sets of initial conditions  $\{\vartheta_k^1(t_0)=1,\,\delta\dot{\varphi}_k^1(t_0)=0\}$  and  $\{\vartheta_k^1(t_0)=0,\,\delta\dot{\varphi}_k^1(t_0)=1\}$  from  $t_0$  to  $t_0+T$ . The eigenvalues of eq. (7.20) are given by

$$o_k^{\pm} = \frac{\vartheta_k^{(1)} + \delta \pi_k^{(2)}}{2} \pm \frac{1}{2} \sqrt{\left(\vartheta_k^{(1)} - \delta \pi_k^{(2)}\right)^2 + 4\vartheta_k^{(2)} \delta \pi_k^{(1)}}, \tag{7.21}$$

with all quantities evaluated at  $t_0 + T$ . Since  $\mathcal{O}(t_0 + T, t_0) = \exp[T\mathcal{M}]$ , where  $\mathcal{M}$  is a time-independent matrix whose eigenvalues are the Floquet exponents

$$\mu_k^{\pm} = \frac{1}{T} \left[ \ln(|o_k^{\pm}|) + i\theta_k^{\pm} \right]. \tag{7.22}$$

We have exponentially growing solutions if

$$\operatorname{Re}(\mu_k^{\pm}) = \frac{1}{T} \ln(|o_k^{\pm}|) > 0.$$
 (7.23)

After finding the solutions, one can construct an adiabatic invariant, which has the interpretation of the comoving occupation number of particles  $n_k$  in the mode k in an expanding universe:

$$n_k = \frac{\omega_k}{2} \left( \frac{|\dot{\Theta}_k|^2}{\omega_k^2} + |\Theta_k|^2 \right) - \frac{1}{2}, \qquad (7.24)$$

where  $\Theta_k \equiv a^{3/2} \vartheta_k$ . The total number of particles created will then be given by

$$n_{\vartheta}(t) = \frac{1}{(2\pi a)^3} \int d^3k \, n_k(t) = \frac{1}{4\pi^2 a^3} \int dk k^2 n_k(t) \,, \tag{7.25}$$

while the energy density of the produced particles is

$$\rho_{\vartheta} = \frac{1}{(2\pi)^3 a^4} \int d^3k \, n_k(t) \omega_k = \frac{1}{4\pi^2 a^4} \int dk k^2 n_k(t) \omega_k \,. \tag{7.26}$$

Once the growth of the quantities  $n_{\vartheta}$  and  $\rho_{\vartheta}$  will come to halt once parametric resonance ceases, they will start redshifting, respectively like matter and radiation.

#### 7.1.3 Cosmological Impact of Preheating

The axions produced via parametric resonance do not necessarily couple to the standard model, and could reside in a hidden sector. Such particles can be so light that they remain relativistic until today, hence behaving as dark radiation and contributing to the effective number of relativistic species  $N_{\text{eff}}$ . If instead they become non-relativistic during the evolution of the universe, they contribute to the dark matter abundance  $\Omega_{\vartheta}$ .

In any case, if they become non-relativistic after reheating (their mass is lower than the reheating scale  $m_{\vartheta} < T_{reh}$ ), the energy transferred to the axions is given by the inflaton, which in turn loses its energy and hastens the onset of reheating.

Inflation ends once slow roll conditions are violated, and the inflaton starts oscillating around its minimum, around  $H_{\rm inf} \sim m_{\varphi}$ . We assume that the decay of the inflaton into SM particles occurs perturbatively through the two-body decay processes, such that we can take the decay rate  $\Gamma_{\varphi}$  to be constant in time. However, reheating does not start immediately, as the perturbative decay of the inflaton to SM particles becomes active only when  $3H \sim 2\Gamma_{\varphi}$ . We write the total inflaton decay rate as

$$\Gamma_{\varphi} = (c_{hid} + c_{vis}) \frac{\pi^2}{48} \frac{m_{\varphi}^3}{M_{\text{Pl}}^2} \equiv (c_{hid} + c_{vis}) \Gamma_0,$$
(7.27)

where  $c_{vis}$  and  $c_{hid}$  are the coefficients giving the visible and hidden sector decays, respectively. In this part of the work, we shall approximate  $\Gamma_{\varphi} \simeq \Gamma_0$ . Therefore, given  $m_{\varphi} < M_{\rm Pl}$ , then  $H_{\rm inf} \gg \Gamma_{\varphi}$ .

After inflation ends, the inflaton field starts to oscillate around its minimum and behaves as pressureless matter, so that the Hubble parameter falls off as  $H \propto a^{-3/2} = t^{-1}$ . When H reaches the order of the inflaton decay rate, it starts decaying perturbatively and reheating begins. We can then write

$$3H_{reh} = 2\Gamma_{\varphi} \,. \tag{7.28}$$

To find the reheating temperature, we can use the relation between the dominant contribution to the energy density and temperature:

$$\rho_{\varphi}^{reh} = g_{reh} \frac{\pi^2}{30} T_{reh}^4 \,. \tag{7.29}$$

Tracing the inflaton energy density from its value at the end of inflation  $\rho_{\varphi}^{end} \simeq 3H_{end}^2 M_{\rm Pl}^2$  all the way to reheating, if we assume that the inflaton only decays perturbatively, then  $\rho_{\varphi}^{reh} \simeq 3H_{reh}^2 M_{\rm Pl}^2 \simeq \frac{4}{3}\Gamma_0^2 M_{\rm Pl}^2$ . However, before the inflaton starts decaying perturbatively, when  $H > \Gamma_0$ , there is a period of preheating when parametric resonance takes place. This has to be taken into account when computing the inflaton energy density at reheating, as some energy has been taken up by the excited axion quanta. This can be encapsulated by

$$\rho_{\varphi}^{reh} = \rho_{\varphi}^{max} \left(\frac{a_{max}}{a_{reh}}\right)^{3} = \left(\rho_{\varphi}^{end} \left(\frac{a_{end}}{a_{max}}\right)^{3} - \rho_{\vartheta}^{max}\right) \left(\frac{a_{max}}{a_{reh}}\right)^{3}, \tag{7.30}$$

where  $\rho_{\vartheta}^{reh}$  is the axion energy density evaluated at reheating. Therefore, simplifying the above expression,

$$\rho_{\varphi}^{reh} = \rho_{\varphi}^{end} \left(\frac{a_{end}}{a_{reh}}\right)^3 - \rho_{\vartheta}^{max} \left(\frac{a_{max}}{a_{reh}}\right)^3 = \rho_{\varphi}^{end} (1 - r_{PR}) \left(\frac{a_{end}}{a_{reh}}\right)^3, \tag{7.31}$$

where 
$$r_{\rm PR} \equiv \frac{\rho_{\vartheta}^{max}}{\rho_{\varphi}^{end}} \left( \frac{a_{max}^3}{a_{end}^3} \right)$$
, and

$$\rho_{\varphi}^{reh} = \rho_{\varphi}^{end} (1 - r_{PR}) \left( \frac{a_{end}}{a_{reh}} \right)^3 = g_{reh} \frac{\pi^2}{30} T_{reh}^4 = \frac{4}{3} \Gamma_0^2 M_{Pl}^2. \tag{7.32}$$

The scale factor  $a_{reh}$  denotes the moment at which H reaches  $\Gamma_0$ . Prior to this moment, the scale factor goes as  $a \sim t^{2/3}$  like the inflaton (which we take to be the dominant contribution to the energy budget of the universe). Thus H scales as  $H \sim a^{-3/2}$ . From the value of H at the end of inflation, we can assess its value at the onset of reheating via

$$H_{reh}^2 = H_{inf}^2 (1 - r_{PR}) \left( \frac{a_{end}}{a_{reh}} \right)^3 \simeq \frac{4}{9} \Gamma_0^2.$$
 (7.33)

Thus,  $\frac{a_{reh}}{a_{end}} = (1 - r_{PR})^{1/3} \left(\frac{3H_{\text{inf}}}{2\Gamma_0}\right)^{2/3}$ . The reheating temperature can then be computed via

$$T_{reh} = (\rho_{\varphi}^{reh})^{\frac{1}{4}} \left(\frac{30}{\pi^{2} g_{reh}}\right)^{\frac{1}{4}} = \left(\frac{30}{\pi^{2} g_{reh}}\right)^{\frac{1}{4}} \left[\rho_{\varphi}^{end} (1 - r_{PR})\right]^{\frac{1}{4}} \left(\frac{a_{end}}{a_{reh}}\right)^{\frac{3}{4}}$$

$$= \left(\frac{30}{\pi^{2} g_{reh}}\right)^{\frac{1}{4}} \left[\rho_{\varphi}^{end}\right]^{\frac{1}{4}} \left(\frac{2\Gamma_{0}}{3H_{\text{inf}}}\right)^{\frac{1}{2}}.$$
(7.34)

Given that we are taking the Hubble rate as though the inflaton is dominating the energy budget of the universe,  $H_{reh}$  will not change, as it is determined by the decay rate of the inflaton field. What changes in the end will be the scale factor at reheating while, maybe a bit surprisingly, the reheat temperature stays unchanged: the scale factor decreases due to the loss of energy density of the inflaton just as to compensate for the lower inflaton energy density after preheating. This keeps the reheat temperature fixed at the value dictated by eq. (7.28).

#### Effective number of relativistic species

We now assume that the parametric resonance will produce axions that are light enough to remain as dark radiation up to the modern era. In such a scenario, the axions contribute to the number of relativistic degrees of freedom. We now estimate their contribution.

The total radiation energy density after electron-positron annihilation reads

$$\rho = \sum_{i} \rho_{i} = \frac{\pi^{2}}{30} \left[ \sum_{i=bosons} g_{i} T_{i}^{4} + \frac{7}{8} \sum_{i=fermions} g_{i} T_{i}^{4} \right] = \frac{\pi^{2}}{30} g_{*}(T) T^{4}, \qquad (7.35)$$

where 
$$g_*(T) = \sum_{bosons} g_i \left(\frac{T_i}{T}\right)^4 + \frac{7}{8} \sum_{fermions} g_i \left(\frac{T_i}{T}\right)^4$$
.

In the absence of particle states beyond the standard model, the total radiation energy density comes from photons and neutrinos. Neutrinos remain in thermal equilibrium with the CMB until their interaction rate with other SM particles drops below the expansion rate. After decoupling, the neutrino temperature  $T_{\nu}$  remains approximately equal to

the CMB temperature until electron-positron annihilation, which causes the CMB temperature to rise, while it leaves the neutrino temperature nearly unaffected. Assuming instantaneous neutrino decoupling,  $T_{\nu}/T = (4/11)^{1/3}$ . The radiation energy density can be written as

$$\rho_R = \frac{\pi^2}{15} \left[ 1 + \frac{7}{8} N_\nu \left( \frac{T_\nu}{T} \right)^4 \right] T^4 = \left[ 1 + \frac{7}{8} \left( \frac{4}{11} \right)^{4/3} N_{\text{eff}} \right] \rho_\gamma , \qquad (7.36)$$

where  $N_{\nu}$  the number of neutrinos species and

$$N_{\text{eff}} = \left(\frac{1}{4}\right)^{4/3} N_{\nu} \left(\frac{T_{\nu}}{T}\right)^4 \tag{7.37}$$

quantifies the effective number of relativistic degrees of freedom that are not the photon. With three active neutrino species,  $N_{\nu}$  is slightly larger than 3 if one accounts for relic interactions between electrons and neutrinos during the time of electron-positron annihilation. The resulting value is  $N_{\rm eff} \simeq 3.046$ , which also incorporates finite temperature QED corrections to the electromagnetic plasma and flavor oscillations effects [383]. Various factors constrain the number of effective species. These include the predictions of BBN, paired with observations of light elements abundances [384], CMB temperature and polarization anisotropies [385], and the large scale structure (LSS) of matter distribution [386]. Within current experimental bounds, all the aforementioned probes show agreement with the standard prediction of  $N_{\rm eff} = 3.046$ . On the other hand, current limits allow for deviations from the SM prediction (i.e. for a non-zero  $\Delta N_{\rm eff} \equiv N_{\rm eff} - 3.046$ ) which would signal new physics. Current bounds constraint  $\Delta N_{\rm eff} < 0.226$  [387]. Future observations are expected to greatly improve on the present bounds (see e.g. [388]).

Taking into account the presence of relativistic axions, the total amount of energy density of the universe reads

$$\rho_R = \left[ 1 + \frac{7}{8} \left( \frac{4}{11} \right)^{4/3} N_{\text{eff}} \right] \rho_\gamma + \rho_\vartheta \,. \tag{7.38}$$

By comparing it to

$$\rho_R = \left[ 1 + \frac{7}{8} \left( \frac{4}{11} \right)^{4/3} (N_{\text{eff}} + \Delta N_{\text{eff}}) \right] , \qquad (7.39)$$

we find

$$\Delta N_{\text{eff}} = \frac{8}{7} \left( \frac{T}{T_{\nu}} \right)^4 \frac{\rho_{\vartheta}}{\rho_{\gamma}} \,, \tag{7.40}$$

where  $\rho_{\gamma}$  is the energy density given by photons. We can then write the equation as [389]

$$\Delta N_{\text{eff}} = \frac{120}{7\pi^2} \left(\frac{11}{4}\right)^{4/3} \frac{\rho_{\vartheta}^{max}}{T^4} \left(\frac{a_{end}}{a_{reh}}\right)^4 \left(\frac{a_{reh}}{a}\right)^4 \left(\frac{a_{max}}{a_{end}}\right)^4.$$
 (7.41)

After inflation, when  $t_{end} < t < t_{reh}$ , the inflaton oscillations redshift approximately as pressureless matter,  $\rho_{\varphi}(t) \propto a(t)^{-3}$ . Furthermore, we can use adiabaticity in the expansion after reheating, so that  $a_{reh}T_{reh} = aT$ . Thus,

$$\Delta N_{\rm eff} = \frac{120}{7\pi^2} \left(\frac{11}{4}\right)^{4/3} \left(\frac{\rho_{\varphi}^{reh}}{\rho_{\varphi}^{end}}\right)^{4/3} \left(\frac{T}{T_{reh}}\right)^4 \left(\frac{a_{max}}{a_{end}}\right)^4 \frac{\rho_{\vartheta,max}}{T^4} \,. \tag{7.42}$$

The inflaton energy density during reheating is  $\rho_{\varphi}^{reh} = g \frac{\pi^2}{30} T_{reh}^4$ , which once substituted in the previous equation gives

$$\Delta N_{\text{eff}} = \frac{4}{7} \left[ g(T)^4 \left( \frac{11}{4} \right)^4 \frac{\pi^2}{30} \left( \frac{m_{\varphi}^4}{\rho_{\varphi}^{end}} \right) \left( \frac{T_{reh}}{m_{\varphi}} \right)^4 \right]^{1/3} \left( \frac{\rho_{\vartheta}^{max}}{\rho_{\varphi}^{end}} \right) \left( \frac{a_{max}}{a_{end}} \right)^4. \tag{7.43}$$

Note that our computation relies on the assumption that we are operating in a regime where the inflaton energy density dominates. A natural question arises when particle production reaches such significant levels that the primary contributor to the universe's energy content becomes the generated particles themselves. Yet, as previously discussed, once the energy density of these particles approaches that of the inflaton, effects like backreaction and inflaton fragmentation come into play and can no longer be overlooked [357,358]. These phenomena act to halt parametric resonance, slowing down the growth of the axion energy density. Therefore, eq. (7.43) is a valid approximation for the analysis of this work.

#### Dark matter

Parametric resonance gives rise to relativistic particles during preheating. However, they can be heavy enough that they become non-relativistic during the evolution of the universe, and therefore will not contribute to the effective number of relativistic species  $N_{\rm eff}$ . These axions will then constitute some portion of dark matter.

The relic abundance of dark matter today is given by

$$\Omega_{\vartheta} = \frac{m_{\vartheta} n_{\vartheta}(a_0)}{\rho_c} \,, \tag{7.44}$$

where  $\rho_c$  is the critical energy density at the present time. We can compute the number density via eq. (7.25); it grows until  $n_{\vartheta}^{max}$  and then redshifts as  $a^{-3}$ . Therefore, assuming entropy conservation after reheating, we find

$$n_{\vartheta}(a_0) = n_{\vartheta}^{max} \left(\frac{a_{max}}{a_0}\right)^3 = n_{\vartheta}^{max} \left(\frac{a_{max}}{a_{end}}\right)^3 \left(\frac{2\Gamma_{\varphi}}{3H_{\text{inf}}}\right)^2 \left(\frac{T_0}{T_{reh}}\right)^3 . \tag{7.45}$$

Using  $T_0 \simeq 10^{-31} M_{\rm Pl}$ , the number density evaluated today is

$$n_{\vartheta}(a_0) \simeq 10^{-93} n_{\vartheta}^{max} \left(\frac{a_{max}}{a_{end}}\right)^3 \left(\frac{\pi^2}{72}\right)^2 \left(\frac{m_{\varphi}}{M_{\rm Pl}}\right)^4 \left(\frac{M_{\rm Pl}}{T_{reh}}\right)^3.$$
 (7.46)

Hence

$$\Omega_{\vartheta}h^{2} \simeq 3.8 \times 10^{23} \left(\frac{a_{max}}{a_{end}}\right)^{3} \left(\frac{m_{\vartheta}}{M_{\rm Pl}}\right) \left(\frac{m_{\varphi}}{M_{\rm Pl}}\right)^{4} \left(\frac{M_{\rm Pl}}{T_{reh}}\right)^{3} \left(\frac{n_{\vartheta}^{max}}{M_{\rm Pl}^{3}}\right) . \tag{7.47}$$

If we take the inflaton mass to be  $m_{\varphi} \simeq 5 \times 10^{-5} M_{\rm Pl}$ , and taking into account that parametric resonance ends after the end of inflation so that  $a_{max} > a_{end}$ , we find a lower bound for the value of the dark matter abundance:

$$\Omega_{\vartheta}h^2 \gtrsim 10^7 \left(\frac{m_{\vartheta}}{M_{\rm Pl}}\right) \left(\frac{M_{\rm Pl}}{T_{reh}}\right)^3 \left(\frac{n_{\vartheta}^{max}}{M_{\rm Pl}^3}\right).$$
(7.48)

The above is valid only as long as the produced dark matter does not overcome radiation before matter-radiation equality. It can indeed happen that the amount of dark matter produced overcloses the universe: if the produced particles become non-relativistic soon after or around reheating, their energy density will redshift like  $\sim a^{-3}$ , whereas the radiation produced by reheating redshifts like  $\sim a^{-4}$ . At some point, the two will be comparable. If the ratio of the two energy densities  $\rho_{\vartheta}/\rho_r$  becomes comparable before matter-radiation equality, the evolution of the universe changes and the above estimate is no longer valid. Let us then evaluate when this will happen by taking the following equality, assuming it stays relativistic until  $a_{nr}$ :

$$\rho_{\vartheta}^{reh} \left(\frac{a_{reh}}{a_{nr}}\right)^{4} \left(\frac{a_{nr}}{a_{eq}}\right)^{3} = \rho_{r}^{reh} \left(\frac{a_{reh}}{a_{eq}}\right)^{4}$$

$$\Rightarrow \rho_{\vartheta}^{max} \left(\frac{a_{max}}{a_{end}}\right)^{4} \left(\frac{a_{end}}{a_{reh}}\right)^{4} \left(\frac{a_{nr}}{a_{eq}}\right)^{3} = \rho_{r}^{reh} \left(\frac{a_{reh}}{a_{eq}}\right)^{4}$$

$$\iff \rho_{\vartheta}^{max} \left(\frac{a_{max}}{a_{end}}\right)^{4} \left(\frac{a_{end}}{a_{reh}}\right)^{4} = \rho_{r}^{reh} \left(\frac{a_{nr}}{a_{eq}}\right).$$

$$(7.49)$$

Assuming all the remaining energy density of the inflaton goes into the radiation bath,  $\rho_{\omega}^{reh} = \rho_r^{reh}$ , then

$$\rho_{\vartheta}^{max} \left(\frac{a_{max}}{a_{end}}\right)^{4} \left(\frac{a_{end}}{a_{reh}}\right)^{4} = \rho_{\varphi}^{reh} \left(\frac{a_{nr}}{a_{reh}}\right) \left(\frac{a_{reh}}{a_{eq}}\right)$$

$$= \rho_{\varphi}^{max} \left(\frac{a_{max}}{a_{end}}\right)^{3} \left(\frac{a_{end}}{a_{reh}}\right)^{3} \left(\frac{a_{nr}}{a_{eq}}\right). \tag{7.50}$$

Therefore

$$a_{eq} = \frac{\rho_{\varphi}^{max}}{\rho_{\vartheta}^{max}} a_{nr} \frac{a_{end}}{a_{max}} \frac{a_{reh}}{a_{end}}.$$
 (7.51)

This formula encapsulates also the possibility that the produced axions become non-relativistic before the end of reheating by simply taking  $a_{nr}=a_{max}$  and  $a_{eq}=\frac{\rho_{\varphi}^{max}}{\rho_{\vartheta}^{max}}a_{reh}$ . We want to compare this with  $a_{eq}^{\Lambda \text{CDM}}=\frac{\rho_{r,0}}{\rho_{m,0}}a_0\simeq 3\times 10^{-4}a_0$ . Thus,

$$\alpha_0 \equiv \frac{a_{eq}}{a_{eq}^{\Lambda \text{CDM}}} \simeq \frac{\rho_{\varphi}^{max}}{\rho_{\vartheta}^{max}} \frac{1}{3} \times 10^4 \left(\frac{a_{nr}}{a_0}\right) \frac{a_{end}}{a_{max}} \frac{a_{reh}}{a_{end}}$$

$$\simeq 3.33 \times 10^3 \frac{\rho_{\varphi}^{max}}{\rho_{\vartheta}^{max}} \left(\frac{T_0}{T_{nr}}\right) \frac{a_{end}}{a_{max}} \left(\frac{72M_{\text{Pl}}^2}{\pi^2 m_{\varphi}^2}\right)^{2/3} . \tag{7.52}$$

If  $\alpha_0 \geq 1$  the history of the universe is in agreement with  $\Lambda \text{CDM}$ . If, instead,  $\alpha_0 \ll 1$  the produced axions are overclosing the universe, and changing its history with respect to Big Bang cosmology. There are three different possible scenarios, which we shortly delineate here

First, if the axions do not interact with other particles and remain stable, they contribute to the dark matter density of the universe. In this case, if their density is too high, it could lead to the overclosure of the universe, thus imposing stringent constraints on the model parameters to avoid such a scenario, as in the case above. We can use eq. (7.52) to find the maximum value of the axion mass such that we are not obtaining an early matter radiation equality by imposing  $a_{eq} < a_{eq}^{\Lambda \text{CDM}}$ .

The second case is when the axions can decay into other massive particles. The corresponding cosmological implications depend on whether these decay products are relativistic or non-relativistic at the time of decay. If the decay products are non-relativistic, they effectively behave like cold dark matter, similar to the stable axion scenario, and the universe may still face the risk of overclosure. On the other hand, if the decay products are relativistic, they will initially redshift as radiation. As they become non-relativistic, they transition to behaving like matter, modifying the redshift dynamics and slightly relaxing the constraints on the model since the energy density redshifts more rapidly when the particles are relativistic.

We can modify eq. (7.52) to bound the axion mass assuming instantaneous decay and assuming that all the energy density in the axion decays into the heavy fields  $\rho_{\lambda}^{dec} = \rho_{\vartheta}^{dec}$ . The new matter-radiation equality condition, distinguishing the case where the axion decays after reheating (and after becoming non-relativistic) or before reheating (being still relativistic),<sup>2</sup> reads

$$\begin{cases}
\rho_{\vartheta}^{max} \left(\frac{a_{max}}{a_{end}}\right)^{4} \left(\frac{a_{end}}{a_{reh}}\right)^{4} \left(\frac{a_{reh}}{a_{nr}}\right)^{4} \left(\frac{a_{nr}}{a_{dec}}\right)^{3} \left(\frac{a_{dec}}{a_{NR}}\right)^{4} \left(\frac{a_{NR}}{a_{eq}}\right)^{3} = \rho_{r}^{reh} \left(\frac{a_{reh}}{a_{eq}}\right)^{4} & \text{if } T_{reh} > T_{dec} \\
\rho_{\vartheta}^{max} \left(\frac{a_{max}}{a_{end}}\right)^{4} \left(\frac{a_{end}}{a_{nr}}\right)^{4} \left(\frac{a_{nr}}{a_{reh}}\right)^{3} \left(\frac{a_{dec}}{a_{dec}}\right)^{4} \left(\frac{a_{NR}}{a_{eq}}\right)^{3} = \rho_{r}^{reh} \left(\frac{a_{reh}}{a_{eq}}\right)^{4} & \text{if } T_{reh} < T_{dec},
\end{cases} (7.53)$$

where now  $a_{dec}$  defines the time at which the axion decays into the heavy bosons, and  $a_{NR}$  corresponds to when the latter become non-relativistic. The two cases are actually the same if we readjust the scale factors. We can then write:

$$\rho_{\vartheta}^{max} \left(\frac{a_{max}}{a_{end}}\right)^{4} \left(\frac{a_{end}}{a_{reh}}\right)^{4} \left(\frac{a_{reh}}{a_{nr}}\right)^{4} \left(\frac{a_{nr}}{a_{dec}}\right)^{3} \times \\ \times \left(\frac{a_{dec}}{a_{NR}}\right)^{4} \left(\frac{a_{NR}}{a_{eq}}\right)^{3} = \rho_{\varphi}^{max} \left(\frac{a_{max}}{a_{end}}\right)^{3} \left(\frac{a_{end}}{a_{reh}}\right)^{3} \left(\frac{a_{reh}}{a_{eq}}\right)^{4}$$

$$\iff \rho_{\vartheta}^{max} \left( \frac{a_{max}}{a_{end}} \right) \left( \frac{a_{end}}{a_{reh}} \right) \left( \frac{1}{a_{nr}} \right) \left( \frac{a_{dec}}{a_{NR}} \right) = \rho_{\varphi}^{max} \left( \frac{1}{a_{eq}} \right) . \tag{7.54}$$

Therefore we can find the matter-radiation equality scale factor via:

$$a_{eq} = \frac{\rho_{\varphi}^{max}}{\rho_{\vartheta}^{max}} \left(\frac{a_{end}}{a_{max}}\right) \left(\frac{a_{reh}}{a_{end}}\right) \left(\frac{a_{NR}}{a_{dec}}\right) a_{nr}. \tag{7.55}$$

This will place a bound on the mass of the axion, but it will be less constraining with respect to the case in which the axions do not decay at all. We can define, similarly to eq. (7.52),

$$\alpha_1 \equiv \frac{a_{eq,1}}{a_{eq}^{\Lambda \text{CDM}}} \simeq \frac{1}{3} \times 10^4 \frac{\rho_{\varphi}^{max}}{\rho_{\vartheta}^{max}} \frac{a_{end}}{a_{max}} \frac{a_{reh}}{a_{end}} \frac{a_{NR}}{a_{dec}} \frac{a_{nr}}{a_0}.$$
 (7.56)

<sup>&</sup>lt;sup>2</sup>We should also consider the cases where the axion decays remaining relativistic, but it can be encapsulated in the first case by choosing  $a_{nr} = a_{dec}$  and in the second  $a_{nr} = a_{reh}$ .

Comparing this with  $\alpha_0$  we find

$$\frac{\alpha_1}{\alpha_0} = \frac{a_{NR}}{a_{dec}} \,. \tag{7.57}$$

The ratio on the right hand side is always greater than one, and so  $\alpha_1 > \alpha_0$ .

The third case is when the decay products are so light that they remain relativistic. They will not contribute to the matter density but will increase the effective number of relativistic species,  $\Delta N_{\rm eff}$ . The contribution to  $\Delta N_{\rm eff}$  can be computed as before:

$$\Delta N_{\text{eff}} = \frac{8}{7} \left( \frac{T}{T_{\nu}} \right)^4 \frac{\rho_{\lambda}}{\rho_{\gamma}}, \tag{7.58}$$

where we identified  $\rho_{\lambda}$  with the energy density of the decay products of the axion. If the decay happens instantaneously, and all energy density is transferred to the latter,  $\rho_{\lambda}^{dec} = \rho_{\vartheta}^{dec}$ . Therefore,

$$\rho_{\lambda}^{dec} = \rho_{\vartheta}^{dec} = \rho_{\vartheta}^{max} \left(\frac{a_{max}}{a_{end}}\right)^4 \left(\frac{a_{end}}{a_{reh}}\right)^4 \left(\frac{a_{reh}}{a_{nr}}\right)^4 \left(\frac{a_{nr}}{a_{dec}}\right)^3, \tag{7.59}$$

such that

$$\Delta N_{\text{eff}} = \frac{120}{7\pi^2} \left(\frac{11}{4}\right)^{4/3} \frac{\rho_{\lambda}^{dec}}{T^4} \left(\frac{a_{dec}}{a}\right)^4$$

$$= \frac{120}{7\pi^2} \left(\frac{11}{4}\right)^{4/3} \frac{\rho_{\vartheta}^{max}}{T_{reh}^4} \left(\frac{a_{max}}{a_{end}}\right)^4 \left(\frac{a_{end}}{a_{reh}}\right)^4 \left(\frac{a_{dec}}{a_{nr}}\right) \left(\frac{s_2}{s_1}\right)^{1/3}.$$
(7.60)

In the above we used the fact that  $s^{1/3}aT = const$ , where s corresponds to the entropy density of the universe, defined as  $s \equiv \frac{\rho+p}{T}$ . In principle, the entropy density will change if the degrees of freedom present in the universe will change. However, we will not take that into account, and as a first approximation we consider it constant. All these possibilities depend on the axion decay rates through  $a_{dec}$ , and therefore on the coupling of the axions and on their mass, and in general are very model dependent.

If we compare this with the effective number of relativistic degrees of freedom one would obtain in the case where the axion remains relativistic and never decays  $\Delta N_{\rm eff}^{rel}$ , we have

$$\frac{\Delta N_{\text{eff}}}{\Delta N_{\text{eff}}^{rel}} = \frac{a_{dec}}{a_{nr}} \left(\frac{s_2}{s_1}\right)^{1/3}.$$
 (7.61)

# 7.2 String axions and preheating

In this section, we examine parametric resonance in string-inspired cosmological models. Our main focus will be on type IIB O3/O7 orientifold compactifications, which are defined by first compactifying type IIB on a 6-dimensional Calabi-Yau manifold  $X_6$  with Hodge numbers  $\{h^{1,1},h^{2,1}\}$ . To obtain a theory with  $\mathcal{N}=1$  SUSY, we must quotient by a combination of worldsheet parity and a holomorphic involution  $\sigma$  of  $X_6$ . The Hodge numbers of the quotient  $\widetilde{X}_6 \equiv X_6/\sigma$  are split into positive and negative subspaces as  $h^{1,1} = h^{1,1}_+ + h^{1,1}_-$  and  $h^{2,1} = h^{2,1}_+ + h^{2,1}_-$ . For simplicity, we will assume  $h^{1,1}_- = h^{2,1}_+ = 0$ . The resulting 4D  $\mathcal{N}=1$  EFT will consist of the graviton, axiodilaton,  $h^{2,1}_-$  complex

structure moduli,  $h_{+}^{1,1}$  Kähler moduli, and the supersymmetric partners of these fields. Gauge sectors then arise from the inclusion of spacetime filling D3- and D7-branes.

We will assume that fluxes fix the complex structure moduli and axiodilaton at a high scale [28] and so the moduli of the EFT consist of the Kähler moduli and their axionic superpartners, which form chiral supermultiplets with scalar components  $T^j = \tau^j + i\theta^j$ . The effective Lagrangian takes the general form of eq. (7.2) with  $N = h_+^{1,1}$  and the kinetic terms determined by the Kähler metric

$$K_{i\bar{\jmath}} = \partial_{T^i} \partial_{\bar{T}^{\bar{\jmath}}} K \,, \tag{7.62}$$

where K is the Kähler potential. The scalar potential in eq. (7.2) is then identified as the F-term scalar potential determined by K and the superpotential W as

$$V = e^K \left( K^{i\bar{\bar{\jmath}}} \mathcal{D}_i W \mathcal{D}_{\bar{\jmath}} \overline{W} - 3|W|^2 \right) , \qquad (7.63)$$

where  $K^{i\bar{j}}$  is the inverse of the Kähler metric and the Kähler covariant derivative is  $\mathcal{D}_i W \equiv \partial_i W + K_i W$ .

As discussed in the introduction, the axions  $\{\theta^i\}$  obtain potentials only via non-perturbative effects. These can enter either the superpotential or the Kähler potential. In the present work we focus non-perturbative contributions to the superpotential as these are currently better controlled. If  $\mathcal{D}$  is a divisor of  $\widetilde{X}_6$ , then non-perturbative effects can arise from a stack of D7-branes or from a Euclidean D3-brane wrapping  $\mathcal{D}$ . In either case, the superpotential takes the form

$$W = W_0 + A_D e^{-a_D T_D} \,, \tag{7.64}$$

where  $T_{\mathcal{D}}$  is the complex Kähler modulus where  $\operatorname{Re} T_{\mathcal{D}}$  is the volume of  $\mathcal{D}$  and  $a_{\mathcal{D}}$  is a constant.  $W_0$  and  $A_{\mathcal{D}}$  are constants after the axio-dilaton and complex structure moduli are fixed by fluxes.

Inserting this superpotential into eq. (7.63) one obtains a scalar potential for the axion  $\theta_{\mathcal{D}}$  of the form

$$V \supset \Lambda_{\mathcal{D}}^4 e^{-a_{\mathcal{D}}\tau_{\mathcal{D}}} \cos(a_{\mathcal{D}}\theta_{\mathcal{D}}) . \tag{7.65}$$

This potential has the general form displayed in eq. (7.1) of the Introduction if we choose  $q_{\mathcal{D}}^i = a_{\mathcal{D}} \delta_{\mathcal{D}}^i$ . To obtain the usual EFT Lagrangian, we must canonically normalize the axions. This is done by diagonalizing the Kähler metric and rescaling the axions. Approximating the Kähler metric to be diagonal with diagonal entry  $K_{\mathcal{D}\bar{\mathcal{D}}}$ , one has a canonically normalized axion

$$\vartheta_{\mathcal{D}} := a_{\mathcal{D}} f_{\mathcal{D}} \theta_{\mathcal{D}}, \tag{7.66}$$

where

$$f_{\mathcal{D}} = \frac{1}{a_{\mathcal{D}}} \sqrt{2K_{\mathcal{D}\bar{\mathcal{D}}}} \tag{7.67}$$

is the decay constant of the axion  $\vartheta_{\mathcal{D}}$  such that the axion has periodicity  $\vartheta_{\mathcal{D}} \cong \vartheta_{\mathcal{D}} + 2\pi f_{\mathcal{D}}$ . If one now takes  $\tau_{\mathcal{D}}$  to be the inflaton, then this setup has the necessary ingredients for parametric resonance.

The setup above realizes the general discussion in the Introduction and will serve as the working example in the subsequent subsections. However, that is not to say that it is the only example of parametric resonance in string compactifications. For example, axions

that are not the scalar superpartner of the inflaton may nonetheless obtain masses that vary with time during inflation. This can occur, for example, via kinetic mixing in  $K_{i\bar{\jmath}}$  or multi-instanton contributions to the superpotential that furnish the full instanton lattice. There can also be high-order mixing terms in the scalar potential. At larger  $h^{1,1}$  parametric resonance arising from such higher-order terms will necessarily be suppressed compared to the typically handful of axions with leading-order couplings to a given inflaton Kähler modulus furnished by the sparseness structure in the intersection matrices of CY compactifications [18,390]. Furthermore, it is not necessary that the non-perturbative effects must appear only in the superpotential. ED3 instantons may wrap non-rigid cycles and instead contribute to the Kähler potential.

Finally, these considerations can be applied to compactifications of the other perturbative string sectors. For example, in the Type I or Heterotic theories, axions descending from the 10D 2-forms obtain worldsheet instanton superpotentials from Euclidean F-strings. The strength of such effects are controlled by the volume of 2-cycles given by the vevs of the Kähler moduli. If the inflaton arises from the Kähler moduli, then once again parametric resonance can arise.

### 7.2.1 Structure & dynamics of the Hill equation for string axions

Building on the preceding discussion, we now focus on the chiral multiplet  $T \equiv \tau_{\varphi} + i\theta$  containing the inflaton  $\tau_{\varphi}$  (vis a vis its canonically normalized pendant  $\varphi$ ) and its partner axion  $\theta$  (whose canonical normalization is  $\vartheta$ ). Starting from eq. (7.65), after canonical normalization of the axion field, the string theory inspired axion potential can be written as:

$$V_{ax} = \Lambda^4(\tau_{\varphi})e^{-a_{\varphi}\tau_{\varphi}}\cos\left(\frac{\vartheta}{f_{\vartheta}}\right), \qquad (7.68)$$

the equation of motion eq. (7.14) can be written as:

$$\ddot{\vartheta}_k + \left(3H - \frac{\partial_0 K_{T\bar{T}}}{K_{T\bar{T}}}\right)\dot{\vartheta}_k + \left(\frac{k^2}{a^2} + \frac{\Lambda^4(\tau_\varphi)}{f_\vartheta^2}e^{-a_\varphi\tau_\varphi}\right)\vartheta_k = 0, \qquad (7.69)$$

where  $\varphi$  is associated to the inflaton direction. In general, at first order, the entry of the Kähler metric is  $K_{T\bar{T}} \propto \frac{1}{\langle \tau_{\varphi} \rangle^2}$  if the inflaton is associated to the "big" modulus (fibre inflation), while  $K_{T\bar{T}} \propto (\mathcal{V}\sqrt{\tau_{\varphi}})^{-1}$  if the inflaton is associated to the blow-up modulus (blow-up inflation). At first order, the entry of the Kähler metric associated to the inflaton field is  $K_{T\bar{T}} \propto \langle \tau_{\varphi} \rangle^{-2}$ . Therefore we can write  $\frac{\partial_0 K_{T\bar{T}}}{K_{T\bar{T}}} = \beta \frac{\dot{\tau}_{\varphi}}{\tau_{\varphi}}$ , where  $\beta = 2$  for fibre inflation.<sup>3</sup> Finally, the equations of motion become

$$\ddot{\vartheta}_k + \left(3H + \frac{\beta \dot{\tau}_{\varphi}}{\tau_{\varphi}}\right) \dot{\vartheta}_k + \left(\frac{k^2}{a^2} + m_{\vartheta, \text{eff}}(\tau_{\varphi})\right) \vartheta_k = 0, \qquad (7.70)$$

where

$$m_{\vartheta,\text{eff}}^2(\tau_{\varphi}) = \frac{\Lambda^4(\tau_{\varphi})}{f_{\vartheta}^2} e^{-a_{\varphi}\tau_{\varphi}} \,.$$
 (7.71)

Parametrizing the inflaton oscillations as  $\varphi(t) \simeq \langle \varphi \rangle + \Delta \varphi \frac{1}{t} \cos(m_{\varphi} t)$ , and defining  $\tilde{\tau}_{\varphi} \equiv a_{\varphi} \tau_{\varphi}$ , the mass of the axion field becomes

$$m_{\vartheta,\text{eff}}^2(\tau_{\varphi}) = m_{\vartheta}^2 e^{-\Delta \tilde{\tau}_{\varphi} \frac{1}{s} \cos(2s)}, \qquad (7.72)$$

<sup>&</sup>lt;sup>3</sup>We keep the generic factor implicit so that the analysis can be carried over to e.g. blow-up inflation by using  $\beta = \frac{1}{2}$ .

where  $m_{\vartheta}^2 = \frac{\Lambda^4(\tau_{\varphi})}{f_{\vartheta}^2} e^{-\langle \tilde{\tau}_{\varphi} \rangle}$ , and  $s = \frac{m_{\varphi}t}{2}$  is a new time variable that counts the number of oscillations of the inflaton field. We shift the field as

$$\Theta_k \equiv \vartheta_k \frac{t_0}{t} \,, \tag{7.73}$$

where  $t_0 = \frac{\pi}{4m}$  corresponds to a quarter of oscillation of the inflaton field.<sup>4</sup> Changing the time variable to s, the equations of motion become

$$\Theta_k'' + \beta \frac{\tilde{\tau}_{\varphi}'}{\tilde{\tau}_{\varphi}} \Theta_k' + \left( \frac{4k^2}{m_{\varphi}^2} \left( \frac{1}{a} \right)^2 - \beta \frac{\tilde{\tau}_{\varphi}'}{\tilde{\tau}_{\varphi}} \frac{\dot{a}}{a} + \frac{4m_{\vartheta,\text{eff}}^2}{m_{\varphi}^2} \right) \Theta_k = 0, \qquad (7.74)$$

with

$$\frac{\tilde{\tau}_{\varphi}'}{\tilde{\tau}_{\varphi}} = -\frac{s_0}{s} \frac{\Delta \tilde{\tau}_{\varphi}(\cos(2s)/s + 2\sin(2s))}{\langle \tilde{\tau}_{\varphi} \rangle + \Delta \tilde{\tau}_{\varphi}\cos(2s)}.$$
 (7.75)

The efficiency of parametric resonance is governed by the effective mass parameter, which is directly tied to the mass of the axion field. For extremely light axions, the oscillating term is suppressed by the small axion mass, rendering parametric resonance less effective. To contribute to the effective number of relativistic species today, axions must remain in the form of radiation, requiring their mass to satisfy  $m_{\vartheta} \lesssim \text{eV} \simeq 10^{-27} M_{\text{Pl}}$ . Consequently, the effective mass squared, as defined in eq. (7.72), is suppressed by approximately  $\mathcal{O}(10^{-54})$ .

This suppression arises from the exponential dependence on the vev of the inflaton field,  $e^{-\langle \tilde{\tau}_{\varphi} \rangle}$ . Initially, this suppression can be offset by the wide oscillations of the inflaton field. However, as the oscillations are damped and their amplitude decreases as  $t^{-1}$ , this compensating effect diminishes rapidly.

In an expanding universe, additional terms from the derivative of the Kähler metric become significant when performing a full analysis. As the inflaton oscillates with a decaying amplitude, the kinetic mixing term in the equation of motion eq. (7.74) initially dominates but weakens over time. When the axion is heavy, such that  $\frac{4m_{\vartheta,\text{eff}}^2}{m_{\varphi}^2} \gtrsim \beta \frac{\tilde{\tau}_{\varphi}'}{\tilde{\tau}_{\varphi}} H$ , the kinetic mixing term introduces only minor oscillations. Conversely, for a light axion with a small  $m_{\vartheta,\text{eff}}^2$ , this term grows in relative importance, eventually surpassing the mass term. In this regime, the kinetic mixing term becomes the primary driver of parametric resonance.

Thus, there exists a threshold below which the resonance effect becomes independent of the axion mass. For compactifications that result in extremely small axion masses — allowing axions to remain as radiation until today — parametric resonance can still occur even when the effective mass is negligible. However, the overall impact of this resonance in such cases is minor and not observationally significant.

#### Mathieu limit

Let us first ignore the expansion of the universe and set H = 0, a = 1. In order to have production of particles in the expanding universe, it is indeed a necessary, but not

 $<sup>^4</sup>$ We start our analysis from  $t_0$  in this section in order to trust the approximation of the oscillatory behavior of the inflaton field. Once a specific inflationary model is chosen, one should consider the whole trajectory of the inflaton field starting from the end of inflation, when the slow roll conditions are broken.

sufficient, condition that the exponential instability be present in the absence of the expansion.

$$\vartheta_k'' + \beta \frac{\tilde{\tau}_\varphi'}{\tilde{\tau}_\varphi} \vartheta_k' + \left( \frac{4k^2}{m_\varphi^2} + \frac{4}{m_\varphi^2} \frac{\Lambda^4(\tau_\varphi)}{f_\vartheta^2} e^{-\langle \tilde{\tau}_\varphi \rangle} e^{-\Delta \tilde{\tau}_\varphi \cos(2s)} \right) \vartheta_k = 0.$$
 (7.76)

The damping term  $\frac{\tilde{\tau}_{\varphi}'}{\tilde{\tau}_{\varphi}}\vartheta_k' = -2\frac{\Delta\tilde{\tau}_{\varphi}\sin(2s)}{\langle\tilde{\tau}_{\varphi}\rangle + \Delta\tilde{\tau}_{\varphi}\cos(2s)}$  at first order in  $\Delta\tilde{\tau}_{\varphi}/\langle\tilde{\tau}_{\varphi}\rangle$ , is a function oscillating between positive and negative values of  $\frac{\Delta\tilde{\tau}_{\varphi}}{\langle\tilde{\tau}_{\varphi}\rangle} < 1$ .

When the displacement is small,  $\Delta \tilde{\tau}_{\varphi} < 1$ , the equation of motion can be reduced to the Mathieu equation by truncating the exponential series and neglecting the damping term. Therefore, we can write eq. (7.76) as

$$\vartheta_k'' + (A_k - 2q\cos(2s))\vartheta_k = 0, \qquad (7.77)$$

with  $A_k = \frac{4}{m_\varphi^2} (k^2 + \frac{\Lambda^4(\tau_\varphi)}{f_\vartheta^2} e^{-\langle \tilde{\tau}_\varphi \rangle})$  and  $q = \frac{2}{m_\varphi^2} \frac{\Lambda^4(\tau_\varphi)}{f_\vartheta^2} \Delta \tilde{\tau}_\varphi e^{-\langle \tilde{\tau}_\varphi \rangle}$ . Since we are in the regime where  $\Delta \tilde{\tau}_\varphi < 1$ , then the resonance parameter q has to satisfy

$$q < \frac{2}{m_{\varphi}^2} \frac{\Lambda^4(\tau_{\varphi})}{f_{\vartheta}^2} e^{-\langle \tilde{\tau}_{\varphi} \rangle} \,. \tag{7.78}$$

As we mentioned before, an important feature of the solutions to the Mathieu equation is the existence of an exponential instability  $\vartheta_k \propto e^{\mu_k s}$  within the set of resonance bands of frequency  $\Delta k$ . This instability corresponds to an exponential growth of the occupation numbers of quantum fluctuations  $n_k(t) \propto e^{2\mu_k s}$  that can be interpreted as particle production. The parameter q determines the amount of parametric resonance, and, in agreement with the Mathieu analysis, when there is narrow resonance (q < 1) we find the most amount of growth for modes with  $k \simeq k_{max}$ , where  $k_{max}$  is the mode for which  $A_k = 1$  (this is the so-called stability band), for which  $\mu_{k,max} = \frac{q}{2}$ . However, given that during the expansion of the universe the momenta will redshift, the narrow bands that characterize the resonance in the q < 1 regime, will obstacle the production of particles. In the limit  $q \to 0$  instead there will be no resonance.

fig. 7.1 shows an example of a solution and number density of particles eq. (7.24) for this limit, where  $m_{\varphi} \simeq 5 \times 10^{-5} M_{\rm Pl}$ , and the mass of the axion in this case reads  $m_{\vartheta} \simeq 2.3 \times 10^{-10} M_{\rm Pl}$ . Lower masses heavily suppress the parameter q, and the displacement is not able to offset this suppression. Therefore, in the limit of extremely small displacement and narrow resonance, the production of quanta that will stay radiation until now is extremely suppressed.

# Hill limit

When the displacement of the inflaton field is  $\Delta \tilde{\tau}_{\varphi} > 1$ , the full equation of motion eq. (7.74) is needed in order to fully capture the complexity of the system. We can write the equation at first order in  $\frac{\Delta \tilde{\tau}_{\varphi}}{\langle \tilde{\tau}_{\varphi} \rangle}$  as

$$\vartheta_k'' - 2\beta \frac{\Delta \tilde{\tau}_{\varphi}}{\langle \tilde{\tau}_{\varphi} \rangle} \vartheta_k' \sin(2s) + \left( \frac{4k^2}{m_{\varphi}^2} + \frac{4}{m_{\varphi}^2} \frac{\Lambda^4(\tau_{\varphi})}{f_{\vartheta}^2} e^{-\langle \tilde{\tau}_{\varphi} \rangle} e^{-\Delta \tilde{\tau}_{\varphi} \cos(2s)} \right) \vartheta_k = 0.$$
 (7.79)

In the regime where the amplitude of the inflation oscillations is small, this equation

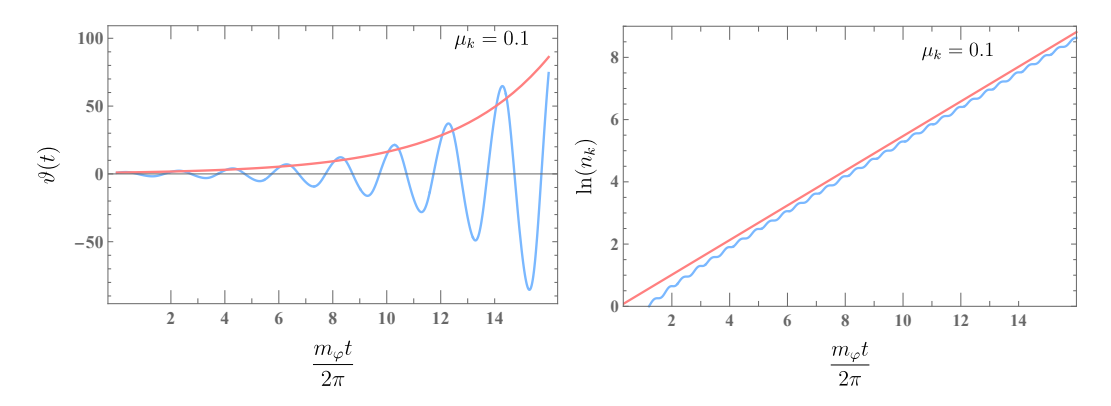


Figure 7.1: On the left: narrow parametric resonance for the field  $\vartheta$  in Minkowski space, for  $A_k=1$ , and  $q\simeq 0.19$ , for the momentum  $k_{max}$  that corresponds to the maximal speed of growth. The pink line corresponds to the solution  $\vartheta_k\simeq \exp\left(\frac{\mu_k}{2m_\varphi}t\right)$ , where  $\mu_k=q/2$ . On the right: the logarithm of the occupation number of particles  $n_k$  in this mode, see eq. (7.24). The number of particles grows exponentially, and the  $\ln n_k$  looks like a straight line with a constant slope. This slope, divided by  $2\pi$ , gives the Floquet exponent  $\mu_k$ , which in this case is  $\mu_k\simeq 0.1$ . The set of parameters used for these figures are  $\Delta \tilde{\tau}_\varphi \simeq \frac{1}{2}$ ,  $\tilde{\tau}_\varphi \simeq 5\pi$ ,  $\frac{\Lambda^4(\tau_\varphi)}{f_\vartheta^2} \simeq 10^{-4}$ .

resembles the Hill equation, and is known as the Whittaker-Hill equation:

$$\vartheta_k'' + 2p\sin(2s)\vartheta_k' + [B_k + 2qF(s)]\vartheta_k = 0, (7.80)$$

with, at first order in  $\frac{\Delta \tilde{\tau}_{\varphi}}{\langle \tilde{\tau}_{\varphi} \rangle}$ ,

$$p = -\beta \frac{\Delta \tilde{\tau}_{\varphi}}{\langle \tilde{\tau}_{\varphi} \rangle}, \quad B_k = \frac{4k^2}{m_{\varphi}^2}, \quad q = \frac{2}{m_{\varphi}^2} \frac{\Lambda^4(\tau_{\varphi})}{f_{\vartheta}^2} e^{-\langle \tilde{\tau}_{\varphi} \rangle}, \quad F(s) = e^{-\Delta \tilde{\tau}_{\varphi} \cos(2s)}.$$
 (7.81)

By defining the new function  $f(s) = e^{-p\cos(2s)/2}\vartheta_k$ , we can write the Whittaker-Hill equation as

$$f'' + \left[ B_k - \frac{p^2}{2} - 2p\cos(2s) + \frac{p^2}{2}\cos(4s) + 2qF(s) \right] f = 0.$$
 (7.82)

This equation is a second order differential equation with periodic coefficients, and therefore it has the form of the Hill equation. Therefore we can study it with a Floquet analysis. The solutions of this equation are

$$\vartheta_k(t) = \vartheta_{k+}(t)e^{\mu_k t} + \vartheta_{k-}(t)e^{-\mu_k t}, \qquad (7.83)$$

where  $\vartheta_{k\pm}$  are periodic functions in time and  $\mu_k$  are complex coefficients. A necessary, but not sufficient, condition for parametric resonance is  $\text{Re}[\mu_k] > 0$ : larger values of  $\text{Re}[\mu_k]$  indicate stronger parametric resonance.

fig. 7.2 shows an example of solutions in this limit for  $m_{\varphi} \simeq 5 \times 10^{-5} M_{\rm Pl}$  and a very light produced axion:  $m_{\vartheta} \sim 1.5 \times 10^{-31} M_{\rm Pl}$ . The axion therefore stays relativistic up to today, and contributes to  $\Delta N_{\rm eff}$ .

fig. 7.3 shows the momenta that get excited and their corresponding Floquet exponent. We can see that the peak of the excited momenta is around  $k \sim \frac{m_{\varphi}}{2}$ , as expected in the Mathieu case. However, in contrast to the Mathieu case, the other momenta in the

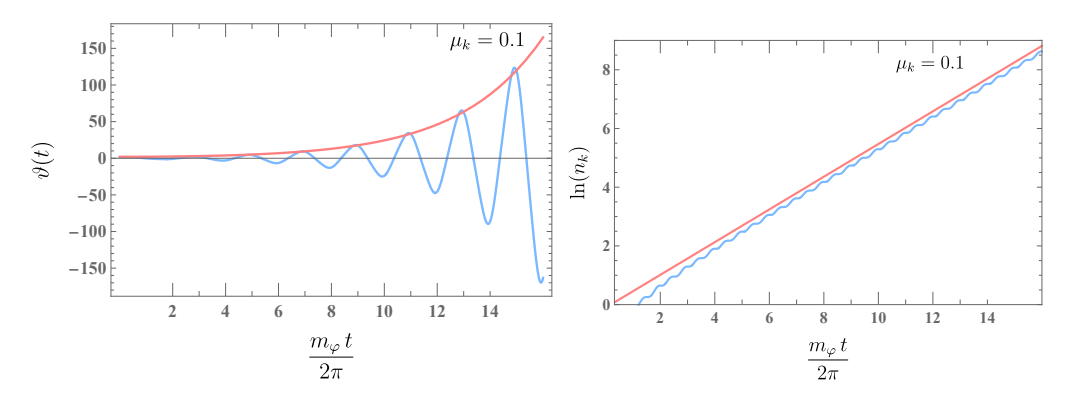


Figure 7.2: On the left: parametric resonance for the field  $\vartheta$  in Minkowski space, for  $B_k=1$ , for the momentum  $k_{max}$  that corresponds to the maximal speed of growth. The pink line corresponds to the solution  $\vartheta_k \simeq e^{\frac{\mu_k}{2m_\varphi}t}$ , where  $\mu_k$  is the Floquet exponent obtained via the Floquet theorem. Time is shown as  $\frac{s}{\pi} = \frac{m_\varphi t}{2\pi}$ , which is the number of oscillations of the inflaton field. On the right: the logarithm of the occupation number of particles  $n_k$  in this mode, see eq. (7.24). The number of particles grows exponentially, and the  $\ln n_k$  looks like a straight line with a constant slope. This slope, divided by  $2\pi$ , gives the Floquet exponent  $\mu_k$ , which in this case is  $\mu_k \simeq 0.106$ . The set of parameters used are  $\Delta \tilde{\tau}_\varphi \simeq 6\pi$  and  $\langle \tilde{\tau}_\varphi \rangle = 41\pi$ , and  $m_\vartheta^2 = \frac{\Lambda^4 \langle \tau_\varphi \rangle}{f_s^2} e^{-\langle \tilde{\tau}_\varphi \rangle} \simeq 2 \times 10^{-62} M_{\rm Pl}^2$ .

secondary bands are much less excited and therefore their contribution will be negligible.

In fig. 7.4 we show the stability charts of the Hill equation in eq. (7.82) for some choice of parameters, where the red points correspond to values of  $(\langle \tilde{\tau}_{\varphi} \rangle, \Delta \tilde{\tau}_{\varphi})$  whose solutions are exponentially unstable. We compute the instability only for  $k = k_{max}$ , as fig. 7.3 shows that this mode gives the main contribution. We require the initial displacement of the inflaton field to be lower than its vev — that is why there is a lack of unstable solutions below the line  $\Delta \tilde{\tau}_{\varphi} = \langle \tilde{\tau}_{\varphi} \rangle$ . The two different charts correspond to two separate sets of axion masses: the left panel shows the stability chart of heavy axions  $(m_{\vartheta} \in (10^{-11}, 10^{-5}) M_{\rm Pl})$ , while the one on the right shows the stability chart of light axions  $(m_{\vartheta} \in (10^{-38}, 10^{-27}) M_{\rm Pl})$ . For both charts there are regions of exponential instability, and we expect production of both light and heavy fields.

# Hill equation on expanding background

We now analyze how an expanding universe influences axion production. After inflation ends, the inflaton field behaves as a harmonic oscillator with a frequency approximately  $\omega \simeq m_{\varphi}$ . Assuming the scale factor evolves as  $a \sim t^{2/3}$ , the system can be approximated using eq. (7.74).

There are some caveats to this approach. First, we must account for the transition period between the end of inflation and the onset of the oscillatory regime, during which the inflaton does not behave like a harmonic oscillator. Therefore, we set  $t_0 = \frac{\pi}{2m_{\varphi}}$ , corresponding to the time after a quarter of one oscillation of the field  $\varphi$ . This provides sufficient time for the inflaton to enter the harmonic oscillatory regime. Second, the validity of this equation of motion breaks down when the backreaction of the axions and the fragmentation of the inflaton become significant. If the inflaton loses too much energy during the preheating process and the energy density of the axions becomes comparable to that of the inflaton, the problem is better addressed with a lattice simulation. However,

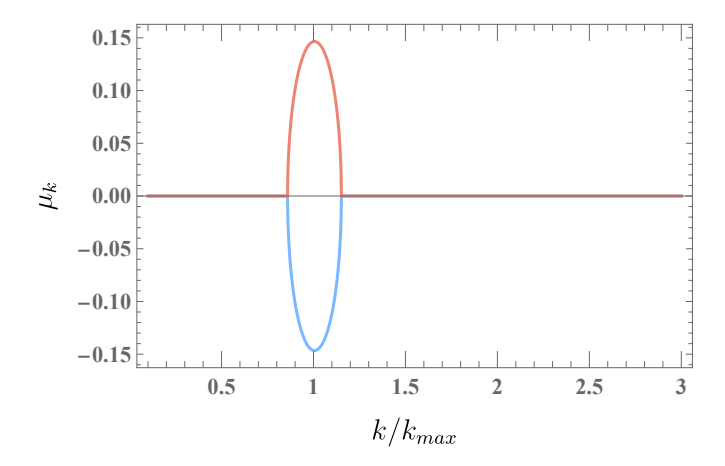


Figure 7.3: Floquet exponents as a function of the momentum k. In this case the exponential instability is only active in one band around the maximum  $k_{max}$ , for which  $B(k) \simeq 1$ .

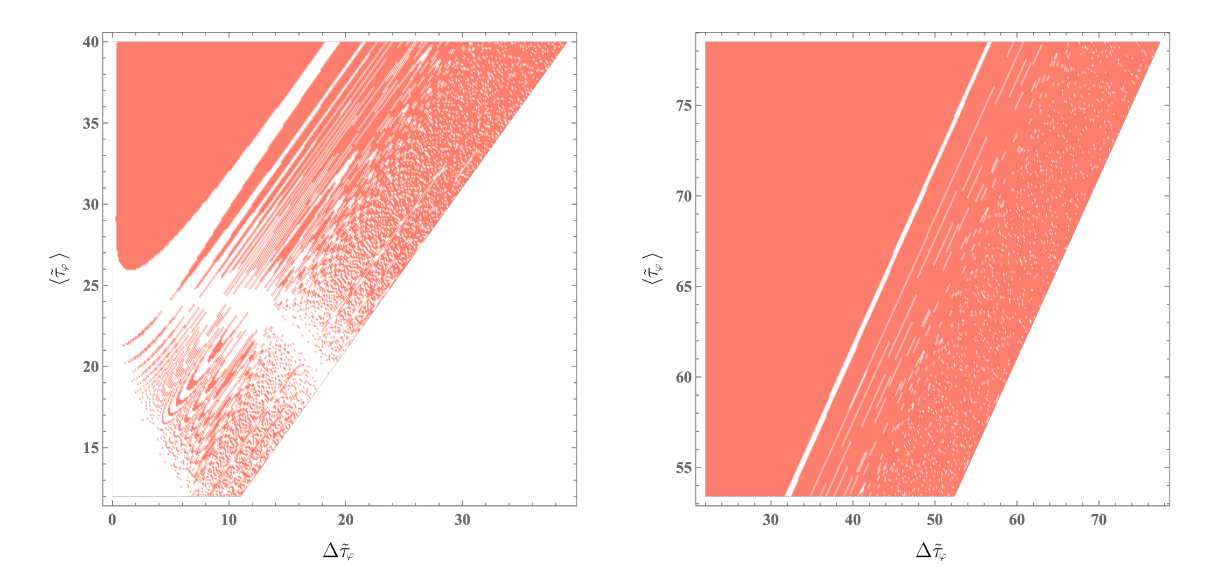


Figure 7.4: Stability charts for the Hill equation at  $k=k_{max}$ : the plot shows in red the points of  $\tilde{\tau}_{\varphi}$ ,  $\Delta \tilde{\tau}_{\varphi}$  for which the Floquet exponent  $\mu_k \geq 0.01$  for  $\frac{\Lambda^4(\tau_{\varphi})}{f_{\vartheta}^2} \simeq 4 \times 10^{-6}$ . The colored points represent the set of  $\Delta \tilde{\tau}_{\varphi}$  and  $\langle \tilde{\tau}_{\varphi} \rangle$  for which the Floquet exponent is  $\mu_k \geq 0.01$ , and therefore we have parametric resonance. The left plot shows the stability chart for those values of the inflaton vev that correspond to heavy axions  $-m_{\vartheta} \in (10^{-11}, 10^{-5}) M_{\rm Pl}$ —that would make up dark matter, while the plot on the right shows higher values of  $\langle \tilde{\tau}_{\varphi} \rangle$ , which corresponds to lighter axions  $-m_{\vartheta} \in (10^{-38}, 10^{-27}) M_{\rm Pl}$ —that stay relativistic until today.

backreaction and rescattering generally halt parametric resonance and the subsequent particle production. Thus, we stop our analysis once the energy density of the axions becomes comparable to that of the inflaton, i.e. when  $\rho_{\vartheta} \simeq \mathcal{O}(10^{-1})\rho_{\varphi}$ . Consequently, we expect that a lattice simulation will not significantly alter the overall results.

eq. (7.74) can be considered analogous to the equation of a damped harmonic oscillator with a time-dependent frequency

$$\omega^{2}(s) = \frac{4k^{2}}{m_{\varphi}^{2}} \left(\frac{1}{a}\right)^{2} - \beta \frac{\tilde{\tau}_{\varphi}'}{\tilde{\tau}_{\varphi}} \frac{s_{0}}{s^{2}} + 4 \frac{\Lambda^{4}(\tau_{\varphi})}{f_{\vartheta}^{2} m_{\varphi}^{2}} e^{-\langle \tilde{\tau}_{\varphi} \rangle} e^{-\Delta \tilde{\tau}_{\varphi} \cos(2s)}.$$
 (7.84)

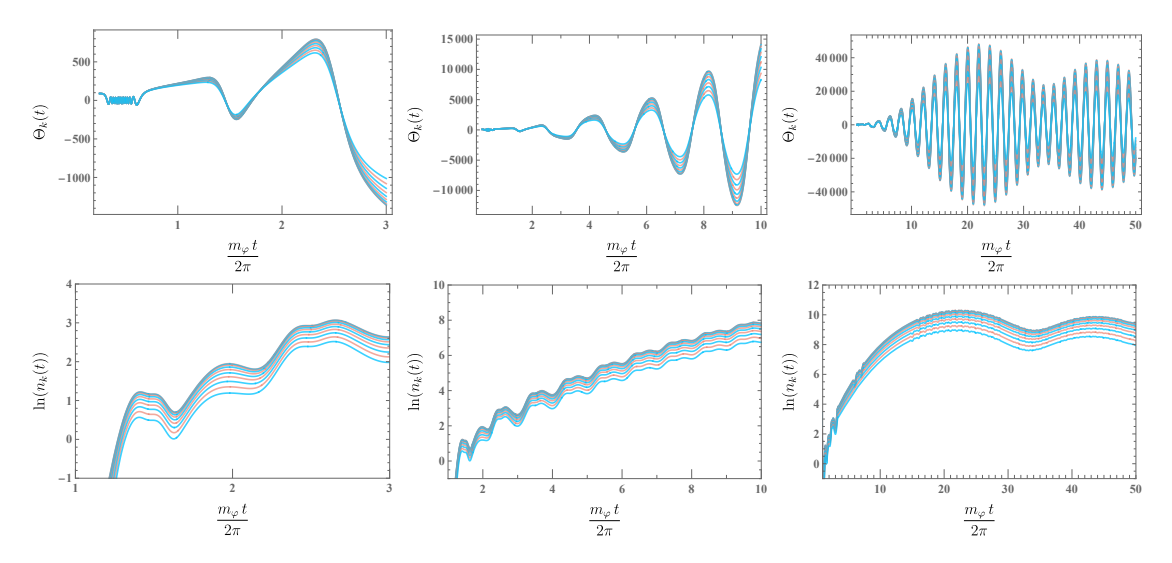


Figure 7.5: Different stages of parametric resonance for different modes k varying around  $k_{max} \simeq m_{\varphi}/2$ , in our theory in an expanding background with scale factor  $a \sim t^{2/3}$ . The values used in these plots are  $\Lambda^4(\tau_{\varphi}) \simeq 7 \times 10^{-4}$ ,  $m_{\varphi} \simeq 5 \times 10^{-5}$ ,  $\langle \tilde{\tau}_{\varphi} \rangle = 6.3\pi$  and  $\Delta \tilde{\tau}_{\varphi} = 5\pi$ , giving the axion mass  $m_{\vartheta} \simeq 2 \times 10^{-5} M_{\rm Pl}$ . From left to right we show longer periods of time. On the top, we plot the mode evolution, while on the bottom the number of particles  $n_k$ . The time is shown in units of  $2\pi/m_{\varphi}$ , which corresponds to the number of oscillations of the inflaton field. After around 20 oscillations, the resonance ceases, and the occupation number becomes constant.

As the inflaton oscillations dampen over time, the displacement  $\Delta \tilde{\tau}_{\varphi}(t)$  decreases as  $\Delta \tilde{\tau}_{\varphi}(t) = \Delta \tilde{\tau}_{\varphi}(t_0) \frac{t_0}{t}$ . Eventually,  $\Delta \tilde{\tau}_{\varphi} < 1$ , allowing the oscillatory exponential term to be expanded, simplifying the equation to the Mathieu equation. In this regime, parametric resonance becomes efficient when the computed Floquet exponents exceed the Hubble scale, i.e.,  $\mu_k > H$ . However, when  $\Delta \tilde{\tau}_{\varphi} > 1$ , higher-order terms in the oscillatory exponential must be included:

$$e^{-\langle \tilde{\tau}_{\varphi} \rangle} e^{-\Delta \tilde{\tau}_{\varphi} \frac{s_0}{s} \cos(2s)} = e^{-\langle \tilde{\tau}_{\varphi} \rangle} \left( 1 - \Delta \tilde{\tau}_{\varphi} \frac{s_0}{s} \cos(2s) + \frac{1}{2} \Delta \tilde{\tau}_{\varphi}^2 \left( \frac{s_0}{s} \right)^2 \cos^2(2s) + \dots \right). \tag{7.85}$$

When a=1, in a non-expanding background, the periodic sign change of  $\cos(2s)$  term temporarily offsets the suppression from  $\langle \tilde{\tau}_{\varphi} \rangle$ . In an expanding universe ( $a \neq \text{const.}$ ), the displacement  $\Delta \tilde{\tau}_{\varphi}$  decreases due to cosmic expansion, making the suppression from  $\langle \tilde{\tau}_{\varphi} \rangle$  increasingly significant over time.

To quantify resonance in an expanding background, even when  $\Delta \tilde{\tau}_{\varphi} > 1$ , we define a resonance parameter q:

$$q = 4 \frac{\Lambda^4(\tau_{\varphi})}{f_{\vartheta}^2 m_{\varphi}^2} \Delta \tilde{\tau}_{\varphi} e^{-\langle \tilde{\tau}_{\varphi} \rangle} = 4 \Delta \tilde{\tau}_{\varphi} \frac{m_{\vartheta}^2}{m_{\varphi}^2}.$$
 (7.86)

A larger q corresponds to stronger parametric resonance. While q scales linearly with  $\Lambda^4(\tau_{\varphi})$  and  $\Delta \tilde{\tau}_{\varphi}$ , it decreases quadratically with  $m_{\varphi}$ , implying that lower inflationary scales enhance resonance. The dependence of q on  $\langle \tilde{\tau}_{\varphi} \rangle$  is non-trivial: q initially increases but eventually drops sharply beyond a critical value.

fig. 7.5 illustrates the growth of the modes and its number density in an expanding background. Over time, the oscillations of  $\vartheta_k$  slow down, deviating from solutions derived

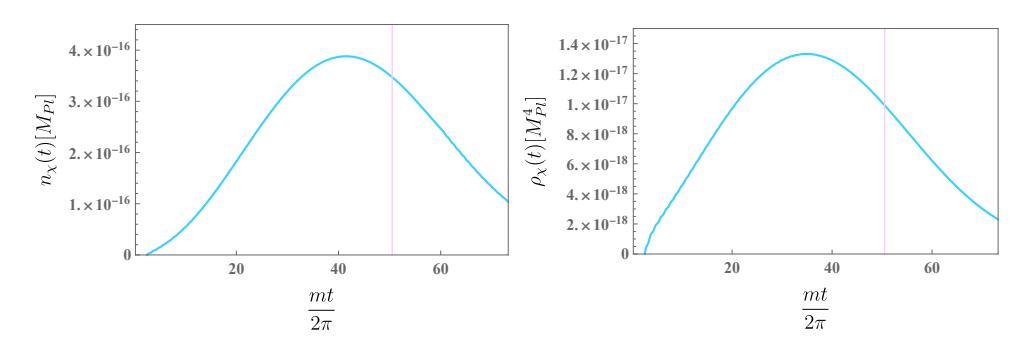


Figure 7.6: Number and energy density of particles created via parametric resonance for the model of fig. 7.5. We see that both quantities stop growing and start redshifting before the end of parametric resonance (shown by the pink vertical line).

from the Mathieu equation. Initially, axion production grows significantly, but resonance ceases after approximately 20 inflaton oscillations, as shown by the occupation number  $n_k$  plateauing in the bottom panels of fig. 7.5.

For the axion field to behave as radiation today, its mass must satisfy  $m_{\vartheta} \lesssim T_{\rm CMB} \simeq 10^{-31} M_{\rm Pl}$ . Under this condition, the resonance parameter q is constrained as:

$$q \lesssim 4 \times \frac{10^{-58}}{m_{\varphi}^2} \Delta \tilde{\tau}_{\varphi} \left( 1 - \frac{1}{\langle \tilde{\tau}_{\varphi} \rangle} \right) \simeq 10^{-48} \Delta \tilde{\tau}_{\varphi} \,.$$
 (7.87)

In this regime, q becomes extremely small, limiting the effectiveness of parametric resonance for low-mass axions. Thus, as discussed earlier, for very light axions the driving oscillations primarily arise from the kinetic mixing between the axion and the inflaton fields.

However, q grows exponentially when heavier axions are considered, allowing them to serve as viable dark matter candidates. The total number and the energy density of the created particles can be computed using eqs. (7.25) and (7.26), with the results shown in fig. 7.6. During the period of parametric resonance, both quantities increase significantly, but as preheating concludes, they begin to dilute as the expansion of the universe becomes non-negligible. The particle number redshifts as  $a^{-3}$ , while the energy density as  $a^{-4}$ . Interestingly, both quantities cease their growth slightly before the end of the parametric resonance, which is marked by the pink line in fig. 7.6. This subtle discrepancy amounts to roughly  $\sim 1\%$ :  $n_{\vartheta}(t_{22.7}) \simeq 5.2 \times 10^{-16} M_{\rm Pl}^3$ , while  $n_{\vartheta}(t_{17.7}) \simeq 6.8 \times 10^{-16} M_{\rm Pl}^3$ .

For this parameter set, the axion density parameter  $\Omega_{\vartheta}$  can also be computed using eq. (7.47), revealing a significant overproduction of DM. As detailed in the previous section, such an overproduction shifts the time of matter-radiation equality to an earlier epoch. To quantify this, the time of matter-radiation equality is calculated using eq. (7.52). Specifically, for the chosen parameters, the ratio of the scale factors is given by  $\frac{a_{eq}}{a_{eq}^{\Lambda \text{CDM}}} \simeq \mathcal{O}(10^{-14})$ , which is significantly less than unity. This result implies that matter-radiation equality occurs much earlier than in the standard  $\Lambda \text{CDM}$  cosmology, leading to a universe whose evolution diverges notably from our observed one. We can find the mass of the produced axions for which the axions saturate the DM bound and would make up of all DM  $(\Omega_{\vartheta}h^2 \simeq \Omega_{DM}h^2 \simeq 0.12)$ . We find that this condition is satisfied for  $m_{\vartheta} \simeq 8.2 \times 10^{-14} M_{\text{Pl}}$ . This result provides a constraint on the model parameters. By fixing the axion mass to this value, we can derive bounds on the remaining parameters of the model. These constraints are depicted in fig. 7.7, where we plot the values of

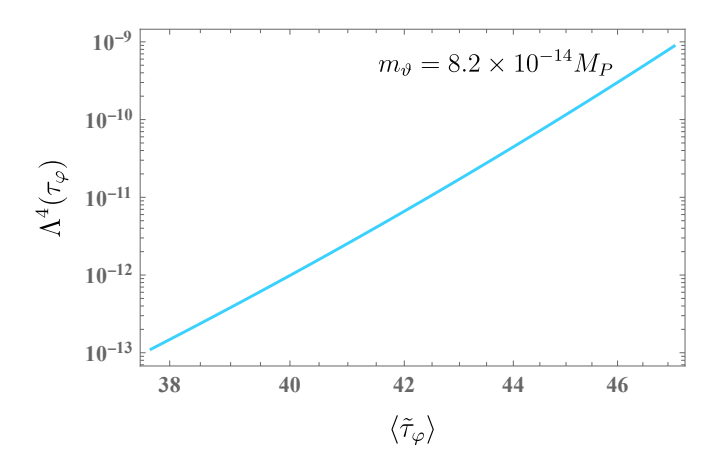


Figure 7.7:  $\Lambda^4(\tau_\varphi)$  vs  $\langle \tilde{\tau}_\varphi \rangle$  such that the mass of the axion satisfies the equality  $\Omega_\vartheta h^2 \simeq \Omega_{DM} h^2 \simeq 0.12$ , and makes up all of DM.

 $(\tilde{\tau}_{\varphi}, \Lambda^4)$  under the requirement that axions make up the entirety of the dark matter in the universe.

#### 7.2.2 The Fate of Preheated Axions

We now turn to the fate of axions produced via parametric resonance within string-inspired models. Addressing this requires examination of the possible axion decay channels into both visible and hidden sector states. This in turn depends critically on how the standard model (SM) and dark sectors are realized in the string construction. In Type IIB compactifications, for instance, the placement of the SM in extra dimensions—specifically its relation to the four-cycles whose volume moduli drive inflation—directly affects the coupling between the inflaton-partner axions and the SM. This, in turn, governs the axion decay rates into visible sector particles.

Without diving into the specifics of reheating channels, some general observations can be made, Firstly, axions sourced predominantly from kinetic mixing are ultralight. Irrespective of the reheating channel, their contribution to the effective number of relativistic degrees of freedom is negligible,  $\Delta N_{\rm eff} \lesssim 10^{-6}$ . For heavier axions, parametric resonance production is more efficient, but these massive axions cannot always persist through cosmic evolution without consequences. In the limit where  $m_{\vartheta} \sim m_{\varphi}$ , the axion becomes non-relativistic soon after production. During radiation domination, these axions redshift slower than radiation, potentially overtaking the universe's energy density and leading to overclosure. To prevent this, the axion decay must be efficient. If the axion decays to visible sectors particles, then it simply modifies the process of reheating. If instead the axions decay to hidden sector states, it could lead to an enhancement of  $\Delta N_{\rm eff}$ . We now enumerate the most obvious decay channels for the axions produced during preheating.

Axions couple to gauge fields via the usual Chern-Simons coupling

$$\mathcal{L} \supset -\frac{g_{\vartheta\gamma\gamma}}{4}\vartheta F\widetilde{F} \ . \tag{7.88}$$

where  $g_{\vartheta\gamma\gamma} \sim \frac{1}{f_{\vartheta}}$ . Therefore, the axion can decay into two gauge bosons with a decay rate

$$\Gamma_{\vartheta \to \gamma \gamma} = \frac{g_{\vartheta \gamma \gamma}^2 m_{\vartheta}^3}{64\pi} \,. \tag{7.89}$$

If the PR axions couple directly to the visible sector, the above allows a direct decay into visible sector gauge bosons. Alternatively, the gauge boson could be part of the hidden sector. In the context of type IIB, this can occur when a stack of D7-branes is supported on a blow-up cycle. In such a situation, the PR axions would eventually turn into a component of dark radiation. However, this is a difficult scenario to make consistent with reheating. Via  $\mathcal{N}=1$  supersymmetry, one expects that the scalar partner of the PR axion couples to the dark gauge bosons via an operator  $\varphi F^2$ . If this scalar field is the inflaton, then this operator yields a direct decay channel in dark radiation, disrupting the latter process of reheating. For fibred CY compactifications in fiber inflation models, this issue was first raised in [391]. Excessive dark radiation from these decays places significant constraints on such constructions. Current studies often avoid including this U(1) due to these challenges. More generally, it is difficult to construct scenarios where the axion interacts with a hidden sector while the corresponding saxion remains decoupled. In most cases, the inflaton decays perturbatively into the dark sector, saturating or exceeding the bounds on dark radiation.

A similar decay channel occurs via the gravitational Chern-Simons coupling of the axion. The relevant operator is

$$\mathcal{L} \supset \frac{g_{\vartheta hh}}{4} \vartheta R \widetilde{R} \,, \tag{7.90}$$

with  $g_{\vartheta hh} \sim 1/f_{\vartheta}$  which arises naturally in string theories [54, 106–108, 392–394], see chapter D. The Feynman diagram of this process is shown as the middle image of fig. 7.8. This interaction is characterized by the decay rate [395–398]

$$\Gamma_{\vartheta \to hh} = \frac{g_{\vartheta hh}^2 m_{\vartheta}^7}{512\pi M_{\rm Pl}^4} \,. \tag{7.91}$$

We can give an estimate of the order of magnitude by using the coupling as in eq. (D.13):

$$\Gamma_{\vartheta \to hh} = \left(\frac{N}{384\pi^2 f_{\vartheta}}\right)^2 \frac{m_{\vartheta}^7}{512\pi M_{\rm Pl}^4} \sim \mathcal{O}(10^{-11}) \frac{m_{\vartheta}^7}{f_{\vartheta}^2 M_{\rm Pl}^4} \sim \mathcal{O}(10^{-7}) \frac{m_{\vartheta}^7}{M_{\rm Pl}^6}, \tag{7.92}$$

where in the last equality we used  $f_{\vartheta} \sim 10^{-2} M_{\rm Pl}$ . While gravitons produced this way would constitute a contribution to  $\Delta N_{\rm eff}$ , the decay rate is so small as to be negligible. If the PR axions have no decay channel other than to gravitons, we can approximate them as stable for the purposes of their cosmological impact.

Most inflationary models in string compactifications are characterized by the presence of more than one axion. Via the kinetic mixing of the heavy and light axions (respectively  $\vartheta_h$  and  $\vartheta_l$ ), one obtains the following coupling

$$\mathcal{L} \supset \lambda \vartheta_h \vartheta_l^3 \,. \tag{7.93}$$

This represents the possibility of a three body decay (see the left Feynman diagram in fig. 7.8) that, in the limit  $m_{\vartheta_l} \to 0$ , has a decay rate

$$\Gamma_{\vartheta_h \to \vartheta_l \vartheta_l \vartheta_l} = \frac{9\lambda^2 m_{\vartheta_h}}{2(4\pi)^3} \,. \tag{7.94}$$

However, the coupling of the kinetic mixing between the axions depends on the mass of the light axion is  $\lambda \sim \frac{m_{\vartheta_l}^2}{f_{\vartheta}^2}$ . Indeed, when the mass of the light axion is very suppressed, the decay rate will be as well.

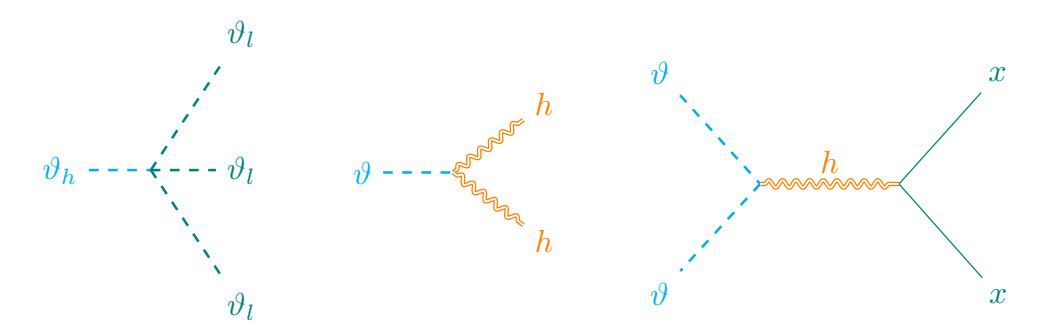


Figure 7.8: Feynman diagrams of the relevant processes for Case II-c where the produced axion is heavy and not stable. On the left, we depict the three body decay of the heavy axion into the light ones (green dashed lines). The middle diagram shows the heavy axion (blue dashed lines) decaying into gravitons (double squiggly orange lines). The right diagram instead shows the gravity-mediated scattering of the heavy axion into every other d.o.f. of the theory, which we label as x (continued green line).

The produced axions have a cross-section to produce all other particles of the theory via intermediary gravitons. We call these particles x, and they represent both the visible and the hidden sectors. The Feynman diagram of this interaction is shown as the right figure of fig. 7.8. Such an idea was also used for gravitational reheating in [399–401]. The scattering rate, in the case where  $m_x \to 0$  reads

$$\Gamma_{\vartheta\vartheta\to xx} \sim \frac{1}{1024\pi} \frac{n_\vartheta m_\vartheta^2}{M_{\rm Pl}^4} = \frac{1}{1024\pi} \frac{\rho_\vartheta m_\vartheta}{M_{\rm Pl}^4} \,. \tag{7.95}$$

To estimate this scattering rate, we can relate the axion properties to those of the inflaton field: in our analysis we stop the resonance when the energy density of the produced axions is at most  $\rho_{\vartheta} \sim 0.1 \, \rho_{\varphi} = 0.1 \times 3 H^2 M_{\rm Pl}^2$ , which at the end of inflation reads  $\rho_{\varphi} = 3 m_{\varphi}^2 M_{\rm Pl}^2$ . Furthermore, we are producing axions whose masses are not many orders of magnitudes away from that of the inflaton field. Having postulated this, the scattering rate can be roughly estimated as

$$\Gamma_{\vartheta\vartheta\to xx} \sim \mathcal{O}(10^{-5}) \, \frac{m_\vartheta^3}{M_{\rm Pl}^2} \,.$$
 (7.96)

We can therefore write the following set of equalities, relating the decay rates to that of the axion photon decay  $\Gamma_{\vartheta \to \gamma\gamma}$ :

$$\Gamma_{\vartheta \to hh} \simeq \mathcal{O}(10^{-2}) \, \Gamma_{\vartheta\vartheta \to xx} \frac{m_{\vartheta}^4}{M_{\rm Pl}^4} \sim \mathcal{O}(10^{-5}) \, \Gamma_{\vartheta \to \gamma\gamma} \frac{m_{\vartheta}^4}{M_{\rm Pl}^4} \frac{f_{\vartheta}^2}{M_{\rm Pl}^2} \,. \tag{7.97}$$

Taking  $f_{\vartheta} \sim 10^{-2} M_{\rm Pl}$ , and specifying the mass of the axion to be lower than H, then by taking  $H \sim 10^{-5} M_{\rm Pl}$ , the biggest values we obtain result in  $\Gamma_{\vartheta \to \gamma \gamma} \sim 10^{-13} M_{\rm Pl}$  and

$$\Gamma_{\vartheta \to hh} \sim \mathcal{O}(10^{-22}) \, \Gamma_{\vartheta\vartheta \to xx} \sim \mathcal{O}(10^{-29}) \, \Gamma_{\vartheta \to \gamma\gamma} \sim 10^{-42} M_{\rm Pl} \,.$$
 (7.98)

It is clear from this that the main decay channel, if it is present, will be the axion photon decay, as the gravitons-mediated interactions are very suppressed. However, if there is no axion-photon coupling, and the only possible interactions are the gravitational ones, the scattering of axions into x particles will be the predominant channel. Indeed, the gravitational axion scattering rate is greater than the axion-graviton decay rate. This happens because the scattering rate is enhanced by the number density of the axion

particles, which grows during preheating, and overcomes the suppression factor  $(\frac{1}{M_{\rm Pl}^4})$  common between the two rates.

We note that this hierarchy is valid at early times, when we can neglect the dilution of the energy densities due to expansion. At later times, the redshifting of the axion energy density will reverse the hierarchy.

# 7.3 Application: Fibre Inflation

We now specialize to a particular realization of string-inspired inflation models in the context of fibre inflation models embedded in the Large Volume Scenario (LVS) compactifications.

#### 7.3.1 Review of LVS & Fibre Inflation

We will consider a fibred CY 3-fold with volume

$$\mathcal{V} = \alpha \left( \sqrt{\tau_1} \tau_2 - \gamma \tau_3^{3/2} \right). \tag{7.99}$$

Crucially, the Kähler moduli and their axionic partners are stabilized by quantum corrections to K and W. The Kähler potential including perturbative corrections is given by

$$K = \mathcal{K}(g_s, \langle z_a \rangle) + K_0 + K_{\alpha'} + K_{g_s},$$

$$K_0 = -2\ln(\mathcal{V}),$$

$$K_{\alpha'} = -\hat{\xi}/\mathcal{V}.$$
(7.100)

where  $K_0$  is the tree-level Kähler potential that depends on the volume of  $X_6$ ,  $\mathcal{V}$ , while  $\mathcal{K}(g_s, \langle z_a \rangle)$  encloses the contributions from  $g_s$  and the stabilized complex structure moduli  $z_a$ , and contributes an overall factor to the potential. The corrections come from higher derivatives  $(K_{\alpha'})$  and string loops  $(K_{g_s})$ . The  $\alpha'$  correction depends on the Euler number of  $X_6$ ,  $\chi(X_6)$ , via the parameter  $\hat{\xi} := -\frac{\zeta(3)\chi(X_6)}{2(2\pi)^3g_s^{3/2}}$  [121] while loop corrections depend on the vacuum value of the complex structure moduli which are stabilized at tree-level by fluxes [402–404]. Additionally, one can also consider higher superspace-derivative corrections, which might be relevant for fibre inflation [405–407].

The non-perturbative contributions to W that we consider arise from D7-branes or ED3s wrapping 4-dimensional cycles in the CY. Those take the form

$$W = W_0 + \sum_i A_i e^{-a_i T_i} \,, \tag{7.101}$$

where  $A_i$  are the one-loop Pfaffian (that can depend on the complex structure moduli, the axiodilaton, and the brane moduli, which we take to be stabilized such that  $A_i$  is effectively a real constant), and  $a = 2\pi$  for ED3s or  $a = 2\pi/N$  for D7-branes, where N is the dual Coxeter number of the gauge group generated by the stack of branes.

For the purpose of computing an inflationary potential in the next sections, we focus on the large volume limit of the effective theory: in this way we can recast the potential

<sup>&</sup>lt;sup>5</sup>We omit a detailed treatment of both higher derivative and string loop corrections as their precise form will not affect the analysis in this work.

in inverse powers of  $\mathcal{V}$ . At first order, which corresponds to  $\mathcal{O}(\mathcal{V}^{-3})$ , we have the LVS potential [31]

$$V_{\text{LVS}} \cdot e^{-\mathcal{K}} = \frac{8a_3^2 A_3^2}{3\alpha\gamma} \frac{\sqrt{\tau_3} e^{-2a_3\tau_3}}{\mathcal{V}} + 4a_3 A_3 W_0 \frac{\tau_3 e^{-a_3\tau_3}}{\mathcal{V}^2} \cos(a_3\theta_3) + \frac{3\hat{\xi}W_0^2}{4\mathcal{V}^3} + \delta V_{\text{uplift}} . \quad (7.102)$$

At this order, the axion  $\theta_3$ , small cycle modulus and the overall volume are stabilized respectively at

$$\theta_3 = \frac{\pi}{a_3}, \quad \tau_3 = \left(\frac{2\alpha\gamma}{\hat{\xi}}\right)^{-2/3}, \quad \mathcal{V} = \frac{3\alpha\gamma\sqrt{\tau_3}W_0}{4a_3A_3}e^{a_3\tau_3},$$
 (7.103)

and the vacuum is a SUSY-breaking AdS minimum, which can be tuned to near-zero CC of either sign by the uplift term  $\delta V_{\text{uplift}}$  (for a discussion of the possible sources of uplifting see e.g. [408]). The fibre volume modulus  $\tau_1$  obtains a vev due to the Kähler potential string loop corrections  $K_{g_s}$ . The relevant terms in the potential arise at  $\mathcal{O}(\mathcal{V}^{-10/3})$  and are

$$V \supset \left(g_s^2 \frac{A}{\tau_1^2} - \frac{B}{V\sqrt{\tau_1}} + g_s^2 \frac{C\tau_1}{V^2}\right) \frac{W_0^2}{V^2}, \tag{7.104}$$

where we used  $\tau_2 \simeq \langle \mathcal{V} \rangle / \alpha \sqrt{\tau_1}$ . We can recast eq. (7.104) into the inflaton potential by defining the canonically normalized field [47]

$$\varphi \equiv \frac{\sqrt{3}}{2} \ln \tau_1 \,, \tag{7.105}$$

and considering its shift from the vacuum value,  $\varphi = \langle \varphi \rangle + \hat{\varphi}$ , such that  $V_{\inf}(\langle \varphi \rangle) = 0$ , the inflaton potential from fibre inflation reads

$$V_{\text{inf}} = V_{\text{LVS}} + \frac{W_0^2}{V^2} \left( g_s^2 A e^{-2\kappa \hat{\varphi}} - \frac{B}{V} e^{-\kappa \hat{\varphi}/2} + \frac{g_s^2 C}{V^2} e^{\kappa \hat{\varphi}} \right).$$
 (7.106)

Here, we defined  $A = A_{\text{loop}}e^{-2\kappa\langle\varphi\rangle}$ ,  $B = B_{\text{loop}}e^{-\kappa\langle\varphi\rangle/2}$  and  $C = C_{\text{loop}}e^{\kappa\langle\varphi\rangle}$  in terms of  $A_{\text{loop}}$ ,  $B_{\text{loop}}$ , and  $C_{\text{loop}}$  which contain the string 1-loop corrections to the Kähler potential of the Kähler moduli.

The  $\theta_1$  and  $\theta_2$  axions obtain their masses only at  $\mathcal{O}(\mathcal{V}^{-\frac{4}{3}}e^{-\mathcal{V}^{\frac{2}{3}}})$  from the terms

$$V \supset e^{K_0} \left( K_0^{\bar{T}_1 T_1} \bar{F}_1 F_1 + K_0^{\bar{T}_2 T_2} \bar{F}_2 F_2 \right) \tag{7.107}$$

$$\simeq \frac{4a_1 A_1 W_0}{V_0^2} \tau_1 e^{-a_1 \tau_1} \cos(a_1 \theta_1) + \frac{4a_2 A_2 W_0}{V_0^2} \tau_2 e^{-a_2 \tau_2} \cos(a_2 \theta_2). \tag{7.108}$$

Thus the axions have vanishing vevs  $\langle \theta_1 \rangle = \langle \theta_2 \rangle = 0$ . Akin to the inflaton, we will need the canonically normalized axions to study parametric resonance. Following the procedure discussion in section 7.2, the Kähler metric  $g_{ij} = 2 \frac{\partial^2 K}{\partial T^i \partial T^j}$  at leading order reads

$$g_{ij} \simeq 2 \begin{pmatrix} \frac{1}{4\tau_1^2} & 0 & 0\\ 0 & \frac{\alpha^2 \tau_1}{2\mathcal{V}^2} & 0\\ 0 & 0 & \frac{3\alpha\gamma}{8\sqrt{\tau_3}\mathcal{V}} \end{pmatrix}, \tag{7.109}$$

where we replaced the modulus  $\tau_2$  with its vev. Thus we find decay constants

$$f_1 = \frac{1}{\sqrt{2} a_1 \tau_1}$$
 and  $f_2 = \frac{\alpha}{a_2 \tau_2}$ , (7.110)

and  $a_i\theta_i = \vartheta_i/f_i$ . For the axionic partner of the inflaton, the canonically normalized potential is

$$-V_{\rm ax} \simeq \frac{8a_1|A_1W_0|\tau_1}{\mathcal{V}^2} e^{-a_1\tau_1} \cos(\theta_1/f_1). \tag{7.111}$$

# 7.3.2 The Visible Sector and Perturbative Reheating in Fibre Inflation

The above ingredients stabilize the compactification and realize inflationary physics. From here, we can study the preheating of axions in the model. Before doing so, we first review certain requirements for viable fibre inflation models. These requirements illuminate the visible and hidden sector content of the EFT, which is critical for predicting the eventual fate of preheated axions. This step is also essential for constructing a complete cosmological model, as the compactification must feature a sector that mimics the minimal supersymmetric standard model (MSSM) or an extension thereof, as well as a mechanism to reheat this MSSM-like sector.

The interplay between the SM-like sector, fibre inflation, and axion physics can lead to two main possible outcomes for the inflaton-partner axion:

- I- If the SM sector resides on one of the fibration four-cycles that drive inflation, this setup enforces the absence of stringy instantons on that cycle, leaving the partnered axion extremely light. Due to the shared four-cycle, this axion may interact with the SM gauge fields. In such a scenario, the axion could manifest as an ultra-light Cosmic Axion Background (CaB), contributing negligibly to dark radiation with a maximal  $\Delta N_{\rm eff} \lesssim 10^{-6}$ . If the axion decays into SM particles, such as photons, no observable axion relic would remain.
- II- If the SM is instead located on an additional, smaller blow-up four-cycle, the inflatonpartner axion becomes sequestered from the SM and forms part of the dark sector. This case leads to several sub-scenarios:
  - a. A super-sequestered axion scenario, where the axion decays solely within the dark sector. If the axion is sufficiently light, it behaves as a CaB; otherwise, it risks overproduction, contributing excessively to dark matter.
  - b. The axion decays into heavier dark sector states, such as those associated with a condensing gauge group. The outcome mirrors the super-sequestered case (II-a).
  - c. Couplings between axions and additional light sectors allow the axion to decay further. In the absence of such couplings, the only remaining interaction would be gravitational.

To better understand these scenarios, we now outline the necessary conditions for a consistent fibre inflation framework and reheating mechanisms in these setups. The MSSM-like sector can arise from either D7-branes wrapping 4-cycles of  $\widetilde{X}_6$  or D3-branes localized at singularities. The coexistence of a SM-like particle physics sector and successful fibre inflation within the same CY orientifold compactification places certain constraints on the total setup:

• Fibre inflation requires a certain set of string loop corrections to generate the inflationary scalar potential.

One generic way often studied in literature to ensure this condition consists of putting D7-brane stacks on the  $\tau_1$  and  $\tau_2$  fibration 4-cycles [409]. This condition

becomes significantly less constraining if some of the loop corrections arise from 10D bulk loops of closed strings as argued in [410].

• The LVS mechanism of Kähler moduli stabilization underlying a viable setup for fibre inflation requires the presence of a non-perturbative effect on the LVS blow-up 4-cycle responsible for the stabilization of the CY volume.

This condition can be satisfied by either wrapping a Euclidean D3-brane (producing an ED3 instanton) or a small D7-brane stack (producing gaugino condensation) on the LVS blowup 4-cycle. Using the ED3 variant is unfeasible as this results in LVS stabilization of the overall CY volume at a value which renders the scale of the fibre inflation scalar potential incompatible with CMB normalization [409]. Hence, the first possibility to implement this and the above condition unavoidably give rise to hidden sectors.

• A SM-like particle physics sector only works if the 4-cycle carrying the SM sector 7-branes carries no brane instantons and does not intersect with any other instanton-generating 4-cycle in the CY orientifold.

This condition in turn requires [411,412] a judicious choice of D7-brane gauge fluxes to avoid the unwanted intersections and/or to de-rigidify the fibre or base 4-cycle in case the SM sector 7-branes were wrapped on one of them. Finally, there is the phenomenological requirement [409] of putting the SM sector, when realized on 7-branes, on a small 4-cycle (typically this limits placement to one of the blow-ups) to avoid too weak SM sector gauge couplings.

Let us now briefly review the literature on reheating in fibre inflation models [47,96,97, 372,413–416]. Reheating mechanisms vary depending on whether the SM sector arises from D7-branes or D3-branes. If the MSSM-like sector arises from D7-branes on the fibre divisor, the inflaton directly couples to the visible sector. This leads to dominant inflaton decay modes into visible gauge bosons and Higgs degrees of freedom. On the other hand, for a visible sector realized by D3-branes at a singularity, reheating is more challenging due to the absence of direct couplings. Modifications to the Giudice-Masiero term in the Kähler potential have been proposed [416] to facilitate reheating while avoiding excessive dark radiation production. These terms read

$$\frac{K}{M_{\rm Pl}^{2}} \supset \frac{H_{u}\bar{H}_{u}}{\left(T_{1} + \bar{T}_{1}\right)^{y_{1}} \left(T_{2} + \bar{T}_{2}\right)^{y_{2}}} + \frac{H_{d}\bar{H}_{d}}{\left(T_{1} + \bar{T}_{1}\right)^{w_{1}} \left(T_{2} + \bar{T}_{2}\right)^{w_{2}}} + \frac{ZH_{u}H_{d} + \text{h.c.}}{\left(T_{1} + \bar{T}_{1}\right)^{k_{1}} \left(T_{2} + \bar{T}_{2}\right)^{k_{2}}},$$
(7.112)

where  $y_1+y_2=w_1+w_2=1$  and  $k_i=y_i+w_i/2$  for  $i=1,2, H_u$  and  $H_d$  are the MSSM Higgs doublets and Z represents a bilinear coupling of the Higgs fields. The Giudice-Masiero mechanism traditionally introduces terms that couple the moduli to visible-sector fields, enabling the generation of soft supersymmetry-breaking terms in supergravity. However, in this context, it serves an additional purpose: facilitating reheating by allowing the inflaton to decay into MSSM fields indirectly.

The Giudice-Masiero terms also affect the dynamics of axions. In cases where the SM sector is on D3-branes, the axion, being the imaginary part of the fibre Kähler modulus, does not directly couple to visible-sector fields. The introduction of the Giudice-Masiero terms provides an indirect decay channel for the inflaton as well as for its partner axion,

ensuring that the energy initially stored in the axion field can be transferred to MSSM particles, such as Higgs bosons or gauge fields. As we will see, this interaction is crucial if one wants to mitigate overclosure: in the absence of such terms, the axion could dominate the energy budget of the Universe, either as a component of dark radiation or dark matter.

## 7.3.3 Preheating in Fibre Inflation

We now turn to preheating in fibre inflation models. We will take the inflationary potential given in eq. (7.106) and consider the non-perturbative production of  $\vartheta \equiv \vartheta_1$  axions, whose potential is given in eq. (7.111). After Fourier transforming the  $\vartheta$  axion field, the relevant system of equations to be solved is as in eq. (7.13)

$$\begin{cases} \ddot{\hat{\varphi}} + 3H\dot{\hat{\varphi}} + \left(\frac{\partial V}{\partial \hat{\varphi}}\right) = 0, \\ \ddot{\vartheta}_k + \left(3H - 2\frac{\dot{\tau}_1}{\tau_1}\right)\dot{\vartheta}_k + \left(k^2 + \frac{\partial^2 V}{\partial \vartheta^2}\right)\vartheta_k = 0, \end{cases}$$
(7.113)

which can be rewritten in terms of  $\Theta_k = a^{3/2} \vartheta_k$ , with  $' = \frac{d}{ds}$  as

$$\begin{cases}
\hat{\varphi}'' + 3\frac{2}{m_{\varphi}}H\hat{\varphi}' + \frac{4}{m_{\varphi}^{2}}\left(\frac{\partial V}{\partial \hat{\varphi}}\right) = 0, \\
\Theta_{k}'' + 2\hat{\varphi}'\Theta_{k}' + \left(\frac{4}{m_{\varphi}^{2}}k^{2} - \frac{\hat{\varphi}'}{a^{3/2}} + 64\frac{|A_{1}W_{0}|}{m_{\varphi}^{2}\mathcal{V}^{2}}\langle \tilde{\tau}_{1}\rangle^{3}e^{\frac{2}{\sqrt{3}}\hat{\varphi}}e^{-\langle \tilde{\tau}_{1}\rangle e^{\frac{2}{\sqrt{3}}\hat{\varphi}}}\right)\Theta_{k} = 0,
\end{cases} (7.114)$$

Here, we again define as in (7.105) the canonically normalized inflaton as  $\varphi \equiv \frac{\sqrt{3}}{2} \ln \tau_1$  and split this as  $\varphi = \langle \varphi \rangle + \hat{\varphi}$  into the vacuum expectation value  $\langle \varphi \rangle = \frac{\sqrt{3}}{2} \ln \langle \tau_1 \rangle$  at the stabilized minimum and the displacement  $\hat{\varphi} = \frac{\sqrt{3}}{2} \ln \frac{\tau_1}{\langle \tau_1 \rangle}$ .

We plot in fig. 7.9 the mode functions and the evolution of the particle number density. We can again compute the reheating temperature, and the DM abundance. We find also here that  $\Omega_{\vartheta} > \Omega_{DM}$ . During the evolution of the universe, the produced axion particles overcome the radiation produced during reheating before  $a_{eq}^{\Lambda \text{CDM}}$ , and therefore would change the history of the universe.

We note that one should also consider the possible self-resonance from the inflaton field induced on itself. The equations one needs to solve will look fairly similar:

$$\begin{cases}
\hat{\varphi}'' + 3\frac{2}{m_{\varphi}}H\hat{\varphi}' + \frac{4}{m_{\varphi}^{2}}\left(\frac{\partial V}{\partial \hat{\varphi}}\right) = 0, \\
\hat{\varphi}_{k}'' + 2\hat{\varphi}'\hat{\varphi}_{k}' + \left[\frac{4}{m_{\varphi}^{2}}k^{2} - \frac{\hat{\varphi}'}{a^{3/2}} + \frac{4}{m_{\varphi}^{2}}\frac{\partial^{2}V_{\text{inf}}}{\partial \hat{\varphi}^{2}}\right] \\
+ 64\frac{|A_{1}W_{0}|}{m_{\varphi}^{2}V^{2}}\langle \tilde{\tau}_{1}\rangle^{2}\left(\langle \tilde{\tau}_{1}\rangle e^{\frac{2}{\sqrt{3}}\hat{\varphi}} - 2\right)e^{-\langle \tilde{\tau}_{1}\rangle e^{\frac{2}{\sqrt{3}}\hat{\varphi}}}\right]\hat{\varphi}_{k} = 0,
\end{cases} (7.115)$$

We check that this produces a negligible amount of parametric self-resonance. Let us consider the following parameters

By taking the second derivative of eq. (7.111) we see that the axion mass is

$$m_{\vartheta_i} \simeq \frac{8a_i |A_i W_0|}{\mathcal{V}^2 f_i^2} \tau_i e^{-a_i \tau_i} \,.$$
 (7.117)

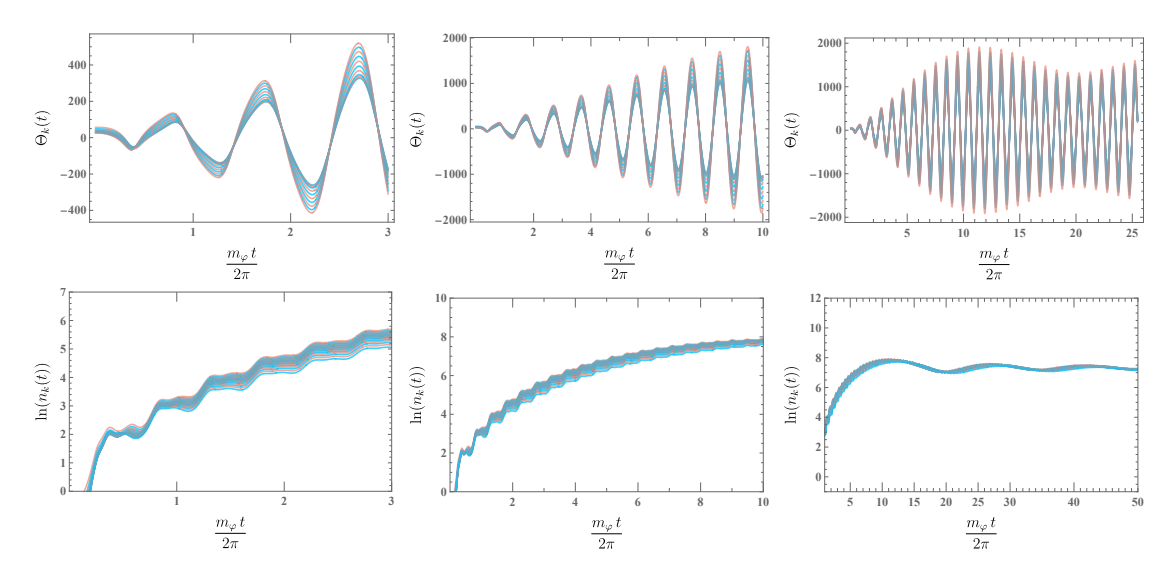


Figure 7.9: Different stages of parametric resonance in our theory in an expanding universe, for the values in eq. (7.116), inflaton mass  $m_{\varphi} \simeq 7.710^{-4} M_{\rm Pl}$ , and axion mass  $m_{\vartheta} \simeq 6.77 \times 10^{-5} M_{\rm Pl}$ . From left to right, we show longer periods of time. On the top, we display the mode evolution, while on the bottom the number of particles  $n_k$ . The time is shown in units of  $2\pi/m_{\varphi}$ , which corresponds to the number of oscillations of the inflaton field. After around 10 oscillations, resonance ceases and the occupation number becomes constant.

For concreteness, we take the approximated value for the vev of the fibre modulus  $\tau_1$ , stabilized as  $\langle \tau_1 \rangle \simeq g_s^{4/3} \left( \frac{4A}{B} \langle \mathcal{V} \rangle \right)^{2/3} \sim 6.28$ , then the base modulus  $\tau_2$  acquires a vev  $\langle \tau_2 \rangle = \frac{\langle \mathcal{V} \rangle}{\alpha \sqrt{\langle \tau_1 \rangle}} \sim \mathcal{O}(10^3)$ . The mass of the base axion will be exponentially suppressed by  $\tau_2$ , and therefore we can safely approximate  $m_{\vartheta_2} \to 0$ . We note that, if one of the axions is heavy, the other one has to be very light. This is because the volume modulus is fixed, and the fibre and base moduli vary accordingly.

In order to keep track of the complete evolution of the inflaton field from the end of inflation on, we keep the full potential. We note that the validity of this analysis is limited once backreaction of the axions and fragmentation of the inflaton become important. If the inflaton loses too much energy in the preheating process, and the energy density of the axions becomes comparable to that of the inflaton, a lattice simulation would be in place. However, the generic effects of backreaction and rescattering are to stop parametric resonance, and subsequently to stop particle production. Therefore, we stop our analysis once the energy density of the axions becomes comparable to that of the inflaton, i.e.  $\rho_{\theta} \simeq \rho_{\varphi}$ , and we expect that a lattice simulation will not change much the overall result. While this regime of strong backreaction is beyond the scope of our work, we note that a full treatment with lattice simulations may show further non-perturbative phenomena such as the formation of oscillons [417] or axion stars [418] (i.e. a Bose-Einstein condensate).

#### 7.3.4 Constraints on Fibre Inflation

There are two possible constructions of the SM compatible with fibre inflation. These correspond to Cases I and II discussed earlier. In Case I, the SM resides on a stack of D7-branes that wrap the same 4-cycle as the inflaton. This configuration leads to an unsequestered SM, where the soft terms are of the same order as the gravitino mass.

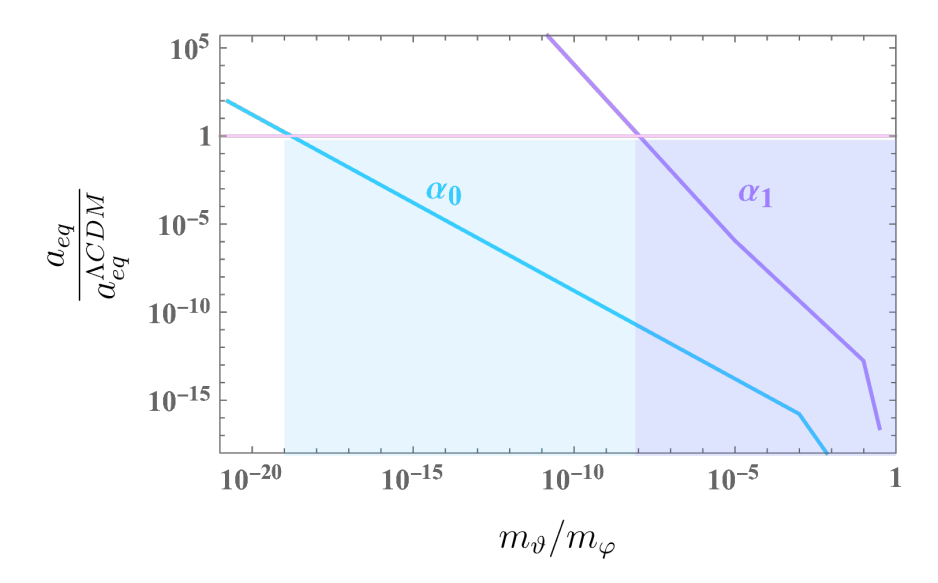


Figure 7.10: Blue: Case II-a, idealized case where the axion does not decay. Purple: Case II-c, axion decays to Higgses. Ratio of matter radiation equality scale factor  $a_{eq}$  over the one from  $\Lambda$ CDM vs. the ratio between the axion and the inflaton mass. Underneath the pink line, where the ratio is 1, the produced heavy axions are "overclosing" the universe. The parameters used for computing this plot are corresponding to eq. (7.116).

Since the inflaton instead is much lighter than the gravitino, its decay into supersymmetric particles is kinematically forbidden [372]. Consequently, the primary decay channels of the inflaton are into Higgs bosons, SM gauge bosons, and hidden sector axions. In this case, the branching ratio of inflaton perturbative decay into the two axions is small, significantly less than unity. Parametric resonance effects will non-perturbatively produce light axions, contributing to dark radiation, but the observational effect will remain in agreement with observational constraints ( $\Delta N_{\rm eff} \lesssim 10^{-6}$ ).

If, however, the produced axions are heavier, their interactions with the SM particles will cause them to decay into visible sector particles. This would accelerate the reheating process, leading to a higher reheating temperature.

In Case II, the SM is living on D3-branes at singularities, and it is sequestered from the bulk, resulting in an effective decoupling of the inflaton sector from the visible degrees of freedom. This case in its most simple realization has been ruled out in [372] because it produces too much dark radiation. A later construction [416] solves this problem by considering a more general moduli-dependence of the Giudice-Masiero term that allows to considerably reduce the production of dark radiation by introducing an additional coupling between the inflaton fields and the Higgses in the Kähler potential (cf. eq. (7.112)).

In Case II-a, if the produced axions are heavy and remain stable, they contribute to the universe's dark matter energy density. In this case, if their density is too high, they could lead to the overclosure of the universe, thus imposing stringent constraints on the model parameters to avoid such a scenario. The heavier the axion, the earlier the time of matter-radiation equality is reached. We can use eq. (7.52) to find the maximum value of the axion mass such that we do not obtain an early matter radiation equality: we want  $\alpha_0 = \frac{a_{eq}}{a_{eq}^{\Lambda \text{CDM}}} < 1$ . This provides an upper bound on  $m_{\vartheta}$ , depending on the model parameters. In fig. 7.10, we plot this ratio as the blue line. Since the produced axions remain as

non-relativistic particles and do not decay, values below the pink line in the shaded blue region ( $\alpha_0 = 1$ ) indicate overproduction of dark matter, leading to an overclosed universe. Therefore this leads to a bound on the axion mass  $m_{\vartheta} \lesssim 10^{-19} m_{\varphi} \sim 10^{-2}$  MeV. However, we stress that this is an idealized benchmark case, as in a realistic scenario the heavy fields will find some channel through which they decay.

Case II-b describes the case in which the axions decay products are massive. Here, we need to distinguish further between two cases: if they decay into massive non-relativistic fields or into massive but relativistic fields. In both cases, the universe still faces the risk of overclosure. In the first case we are in a similar situation as in the stable axion scenario II-a, and the expression for  $a_{eq}/a_{eq}^{\Lambda \text{CDM}}$  does not change from eq. (7.52). If the decay products are relativistic instead, they will initially redshift as radiation, and as they become non-relativistic, they transition to behaving like matter, modifying the redshift dynamics and slightly relaxing the constraints on the model since the energy density redshifts more rapidly when the particles are relativistic. The new  $a_{eq,1}$  comes from eq. (7.55) and we can use eq. (7.56) to constraint the axion mass via the new ratio  $\alpha_1$ . Case II-c instead corresponds to axions decaying into relativistic degrees of freedom, that will therefore contribute to  $\Delta N_{\text{eff}}$  as eq. (7.60).

The different possible decay channels are illustrated in the previous section; let us now expand on them. As discussed in section 7.2.2, a light dark sector arising from D7-branes wrapping a blow-up 4-cycle is disfavored. This is because perturbative decays of the inflation into such a sector tend to overproduce dark radiation. In the context of fiber inflation, the same reasoning applies directly, leading to a similar issue. Consequently, we exclude the possibility of a 7-brane dark sector associated with additional blow-ups in this setup.

We now estimate the decay of the fibre axion in the base axion via kinetic mixing (cf. the left diagram of fig. 7.8). Indeed, in fibre inflation, the vev of the fibre modulus defines the vev of the base modulus by keeping the overall volume fixed, and therefore the mass of the base axion is set by fixing the mass of the fibre axion: if one is heavy, the other will be very light. Therefore, the three body decay defined above will be extremely suppressed, as the decay rate  $\Gamma_{\vartheta_h \to \vartheta_l \vartheta_l \vartheta_l}$  depends on the mass of the light axion  $\vartheta_l$ , where now  $\vartheta_l = \vartheta_2$  and  $\vartheta_h = \vartheta_1$ . For the values we chose in eq. (7.116),  $m_{\vartheta_1} \simeq 8.6 \times 10^{-5} M_{\rm Pl}$ , and  $m_{\vartheta_2} \sim 10^{-370} M_{\rm Pl} \sim 0$ .

The two other interactions in fig. 7.8 do not require any direct coupling, but rely on gravitational interaction. First, the axion can decay to gravitons via a two body decay with decay rate

$$\Gamma_{\vartheta \to hh} = \frac{|g_{\vartheta hh}|^2 m_{\vartheta}^7}{M_{\text{Dl}}^4 512\pi} \,, \tag{7.118}$$

where  $g_{\vartheta hh} \sim \frac{1}{384\pi^2 f_{\vartheta}}$  is derived in eq. (D.13). The time for the axion to decay into the gravitons therefore reads

$$a_{dec} \sim \frac{1}{T_{dec}} \simeq \left(\frac{g_* 8\pi^3}{90}\right)^{1/4} \frac{1}{\Gamma^{1/2} M_{\rm Pl}^{1/2}} = \left(\frac{g_* 8\pi^3}{90}\right)^{1/4} \frac{512^{1/2} \pi^{1/2}}{m_{\vartheta}^{7/2} |g_{\vartheta hh}| M_{\rm Pl}^{-3/2}}, \tag{7.119}$$

contributing to  $\Delta N_{\rm eff}$  as

$$\Delta N_{\text{eff}} = \frac{120}{7\pi^2} \left(\frac{11}{4}\right)^{\frac{4}{3}} \frac{\rho_{\vartheta}^{max}}{T_{reh}^4} \left(\frac{a_{max}}{a_{end}}\right)^4 \left(\frac{a_{end}}{a_{reh}}\right)^4 \left(\frac{g_* 8\pi^3}{90}\right)^{\frac{1}{4}} \left(\frac{512\pi M_{\text{Pl}}^3}{m_{\vartheta}^5 |g_{\vartheta hh}|^2}\right)^{\frac{1}{2}} \left(\frac{s_2}{s_1}\right)^{\frac{1}{3}},$$
(7.120)

Another interesting possibility is the scattering  $\vartheta\vartheta \to xx$ , where with xx we mean both hidden sector and visible sector particles, as it is a gravitational interaction. The decay rate, independently of the decay products, can be approximated, as explained in the above section, by

$$\Gamma_{\vartheta\vartheta\to xx} \sim \frac{1}{1024\pi} \frac{m_{\varphi}^3}{M_{\rm Pl}^2} \,.$$
 (7.121)

This interaction will lead to a contribution to  $\Delta N_{\rm eff}$  when x is a dark sector or the light axion — even if a negligible one — while it will contribute and fasten the reheating process when x is a SM particle. There will therefore be a branching ratio that takes into account the amount of visible or hidden degrees of freedom if we want to compute these contributions in any given sufficiently concrete specific string model with an explicit SM-like sector.

Finally, we consider the terms in eq. (7.112) used to obtain a direct channel with the MSSM and achieve an efficient reheating. These introduce additional derivative couplings between the axion and the Higgs fields, that lead to a scattering  $\vartheta\vartheta \to HH$ , as we derive in section D.1. The decay rate (considering  $y_1 = 1$  and  $y_2 = 0$ ) reads

$$\Gamma_{\vartheta\vartheta\to HH} \sim \frac{1}{64\pi} \frac{\rho_{\vartheta}}{m_{\vartheta}} \frac{1}{m_{\vartheta}^2 + |\vec{p}_{\vartheta}|^2} \frac{f_{\vartheta}^2 |\vec{p}_{\vartheta}|^4}{M_{\rm Pl}^6} \,. \tag{7.122}$$

Since the resonance is most efficient when the momentum of the produced axion is  $|\vec{p}_{\vartheta}| \sim m_{\varphi}/2$ , we can estimate

$$\Gamma_{\vartheta\vartheta\to HH} \sim \frac{1}{4\times64\pi} \frac{\rho_{\vartheta}}{m_{\vartheta}} \frac{1}{1 + \frac{4m_{\vartheta}^2}{m_{\varphi}^2}} \frac{f_{\vartheta}^2 m_{\varphi}^2}{M_{\rm Pl}^6}.$$
 (7.123)

This decay will contribute to the reheating of the standard model, if efficient enough. However, before decaying, this axion behaves as matter, and will contribute to dark matter. Depending on its mass and its energy density, it might take over the energy budget of the universe before  $a_{eq}^{\Lambda \text{CDM}}$ , and therefore overclose the universe. To check this, we need to estimate  $\alpha_1 \equiv \frac{a_{eq,1}}{a_{\Lambda \text{CDM}}}$ . We can estimate the time of decay as:

$$T_{dec} = \left(\frac{90}{8\pi^3 q_*}\right)^{1/4} \Gamma^{1/2} M_{\rm Pl}^{1/2}. \tag{7.124}$$

Therefore,

$$a_{dec} \sim \frac{1}{T_{dec}} \simeq \left(\frac{g_* 8\pi^3}{90}\right)^{1/4} \frac{1}{\Gamma^{1/2} M_{\text{Pl}}^{1/2}}$$

$$= \left(\frac{g_* 256^2 8\pi^5}{90}\right)^{1/4} \left(\frac{m_{\vartheta}}{\rho_{\vartheta}} \left(1 + \frac{4m_{\vartheta}^2}{m_{\varphi}^2}\right)\right)^{1/2} \frac{M_{\text{Pl}}^{5/2}}{f_{\vartheta} m_{\varphi}}.$$
(7.125)

With eq. (7.56), we find

$$\alpha_{1} = \alpha_{0} \frac{a_{NR}}{a_{dec}} = \alpha_{0} \frac{T_{dec}}{m_{H}} =$$

$$= \alpha_{0} \left( \frac{90}{g_{*}256^{2}8\pi^{5}} \right)^{1/4} \left( 1 + \frac{4m_{\vartheta}^{2}}{m_{\varphi}^{2}} \right)^{-1/2} \frac{f_{\vartheta}m_{\varphi}}{M_{\text{Pl}}^{2}} \frac{\rho_{\vartheta}^{1/2}}{m_{\vartheta}^{1/2}M_{\text{Pl}}^{1/2}m_{H}},$$
(7.126)

7.4. Remarks 165

where we defined  $\alpha_0$  in eq. (7.52) as the ratio between the matter radiation equality in the  $\Lambda$ CDM model and in the idealized case where the axion does not decay. We plot the two curves  $\alpha_0$  and  $\alpha_1$  in fig. 7.10. This case is much less constraining, as we expected, with respect to the idealized case where the axion did not decay. The axion mass is now constrained to  $m_{\vartheta} \lesssim 10^{-8} m_{\varphi} \sim 100 \,\text{TeV}$ .

#### 7.3.5 Influence of axion initial conditions

Our approach relies on taking the initial condition of the axion for parametric resonance to be  $\langle \vartheta \rangle = 0$ . However, this may not be the state of the axion field after inflation. During inflation, the axion can undergo a random walk if its mass is below the Hubble scale  $H_{\rm inf}$  during inflation. If the axion walks, the initial condition for parametric resonance may be non-zero. As long as the displacement of the axion at the end of inflation is such that the effective axion mass is positive, one can modify the discussion above by keeping track of the axion zero mode. However, if  $m_{\vartheta, {\rm eff}}^2 < 0$  initially, there will be a tachyonic instability which will lead to a non-perturbative production of axions as well — we do not enter into details as this was already well studied in [419]. This issue is relevant only if the axion is sufficiently lighter than H. Above we have illustrated that parametric resonance for closed string axions is most efficient when the axion mass is roughly that of the inflaton. In this case, the axion will not undergo large displacements from random walks during inflation and instead finds its minimum rapidly.

#### 7.4 Remarks

Certain string compactifications give rise to axion potentials that depend on an exponential function of the Kähler moduli. Identifying one of these moduli with the inflaton results in an axion mass that varies with time as the inflaton oscillates about the minimum of its potential, which sets the stage for parametric resonance. However, this exponential coupling gives rise to different phenomenology compared to typical parametric resonance studies. Furthermore, the inflaton couples kinetically with the axion, and so the axion equation of motion is described by the Whittaker-Hill equation, a generalization of the typical Mathieu equation found in preheating literature.

In this framework, particle production occurs most effectively when the inflaton reaches its maximum negative displacement relative to its vacuum expectation value, where the produced particles remain light. As the inflaton oscillates to positive values, these particles become heavy. In an expanding universe, the oscillations of the inflaton field are dampened due to the Hubble expansion. This damping plays a key role because it gradually shifts the resonance from being broad, where particle production is very efficient, to narrow, where particle production becomes much less efficient, before eventually slowing it to a halt. In the case of string inflation, the damping is even more severe. The oscillations in the exponential coupling lead to exponential damping, which means that the conditions for resonance can change dramatically compared to standard QFT models. This drastic damping highlights an important point: it is not enough to simply compare the growth rate of resonance in a non-expanding universe to the expansion rate of the universe in order to predict resonance in an expanding universe. In fact, the exponential suppression due to damping must be carefully accounted for to understand when and if resonance occurs.

Moreover, the oscillation strength, and consequently the particle production rate, de-

pends on the axion mass, as this is determined by the same coupling that drives the oscillations. Parametric resonance produces a very light axions primarily through kinetic mixing, independent of the non-perturbative mass terms. In contrast, for a heavier axion, the instanton contribution to the superpotential dominates production via parametric resonance. This difference arises because the kinetic mixing produces effectively a bilinear coupling between inflaton and axion resulting in small amounts of production by parametric resonance. The coupling provided by the instanton, however, is highly non-linear and thus drives strong parametric resonance unless its overall scale is suppressed by dialing the axion mass to be small.

This results in two major classes of outcomes. Case I characterizes axions that are light enough to contribute to the effective number of relativistic degrees of freedom  $\Delta N_{\rm eff}$ . On the other hand, Case II describes the situation where the axion is heavy. From the time of its production onward, it can either stay heavy throughout the cosmic evolution (which we call Case II-a), or it can decay into massive stable fields (Case II-b), or lastly it can decay into massless or very light particles (Case II-c). In Cases II-a and II-b, the axion makes up a fraction of DM, depending on how much and how energetically they are produced. Bounding the amount of DM today with  $\Omega_{DM}h^2\simeq 0.12$  we can put a bound on the axion mass. Case II-c instead characterizes a universe filled with non-relativistic degrees of freedom — the decay products of the axions. These contribute to dark matter abundance, but the details depend on the decay rate, the mass of the final particles, and other details of the compactification and the inflationary model under consideration. We provide expressions for each Case, including final observable quantities and the associated limits. As an illustrative example, we examine fibre inflation, considering the evolution of both the inflaton and axion fields.

In order to simplify the study of parametric resonance, we considered scenarios where complicating factors such as self-resonance of the inflaton field, or tachyonic preheating from an imaginary effective axion mass, could be safely neglected. We achieved this by choosing to assign as initial condition of the classical mode of the axion field the minimum of the potential, such that  $m_{\vartheta,\text{eff}}^2>0$ . However, in models of inflation where  $H>m_{\vartheta}$ , the axion field value can undergo random walks. In the case where the axion field initially is displaced from its vev, one needs to take into account also the motion of the axion field towards the minimum of the potential. This can lead to a delay in the start of preheating, or to tachyonic reheating if  $m_{\vartheta,\text{eff}}^2<0$ . We note that parametric resonance in string inflation may also allow for a process akin to "instant reheating," where particles decay almost immediately after being produced, in the case where the axion decay is very rapid and is energetically allowed.

Finally, we wish to highlight that for fibre inflation there is no self resonance of the inflaton quanta, as was found instead for blow-up inflaton in [375]. The difference lies in the very sharp minimum of the blow-up modulus inflationary potential, such that [375] finds a periodic tachyonic instability where the effective mass of the inflaton field becomes imaginary. The scalar potential that characterizes fibre inflation does not have a sharp minimum, and therefore also the oscillations of the inflaton field around its minimum will not be that violent. The effective mass therefore can, but does not have to, become imaginary. The effect of parametric resonance as a non-perturbative mechanism to produce axions from preheating is most visible when it is the lone non-perturbative effect present, and therefore we assume to be in a situation where we can neglect these additional phenomena. We note that for a complete analysis, one should consider both

7.4. Remarks 167

of these types of preheating together, on a lattice. For our purposes, that is, to illustrate the role parametric resonance plays in a non-perturbative production of axions, staying below the limit of inflaton fragmentation and backreaction, separating the two effects is a reasonable assumption.

# Chapter 8

# Conclusions

There are questions that lie just beyond the reach of our best instruments, questions about the beginning of time, the structure of space, and the laws that shape the Universe. What happened in the earliest instants after the Big Bang? Why do the forces of nature look so different at low energies yet appear to unify in the ultraviolet? Is there a consistent quantum theory of gravity—and how could we ever test it?

Remarkably, the Universe itself may offer the answers. The largest structures, the cosmic microwave background (CMB), large-scale structure, and perhaps a stochastic gravitational-wave background are relics of extreme-energy epochs. Cosmology, once datastarved, is now a precision science, beginning to probe scales far beyond the reach of any collider.

New observational windows have opened. Pulsar timing arrays are sensitive to nanohertz gravitational waves and have reported evidence for a common-spectrum background. While astrophysical sources may dominate, a cosmological origin such as inflation is tantalizing. A confirmed background would provide our first direct glimpse of physics at energies where gravity is quantum and the fundamental forces converge.

This is the regime of string theory. As a consistent ultraviolet completion of gravity, it offers a framework in which spacetime geometry, gauge symmetries, and quantum fields emerge from a unified structure. The challenge is to connect this framework to the real world.

Axions provide one of the most promising bridges. Proposed originally to solve the strong-CP problem in QCD, axions arise generically in string compactifications. They are plentiful, often extremely light, and their masses and couplings are set by the topology and geometry of the extra dimensions. They can play many cosmological roles—from dark matter to inflationary relics to sources of gravitational waves.

In this thesis we explored the dynamics, phenomenology, and string-theoretic origins of axions in cosmology, with emphasis on observational signatures and embeddings in concrete compactifications. Our guiding question has been how the multitude of axions predicted by string theory—the axiverse—can leave imprints on early-Universe physics, and how such imprints can inform us about the compactification data, field content, and mechanisms of mass generation.

Taken together, these studies chart a map across several axes of the axiverse: from light

relics to heavy dark-matter candidates; from smooth backgrounds to sharply peaked, sourced perturbations; and from bottom-up phenomenology to top-down string constructions (and back again). They also reveal the challenges: realistic, observable models in string theory are strongly constrained. Nonetheless, we identified consistent regions where theory and observation can meet.

We have started the study of central aspects of the heterotic axiverse building on the foundations for axions in heterotic string theory and clarified when the strong-CP problem is solved or left unresolved. Several natural directions now suggest themselves. First, it would be valuable to construct an explicit compactification that simultaneously (i) yields a realistic Standard Model sector, (ii) solves strong CP with a QCD-aligned light axion, and (iii) hosts a hidden-sector multi-axion spectator (MASA) dynamics capable of sourcing a gravitational-wave signal. Concretely, this calls for a geometry-bundle-coupling pipeline. On the geometry side, one should pick a Calabi-Yau threefold with  $h^{1,1} \geq 2$ (to permit a nontrivial axion basis and kinetic mixings) and a polystable holomorphic vector bundle satisfying the DUY equations and the heterotic Bianchi identity. The visible bundle data must engineer a SM-like gauge sector with massless hypercharge (no Green-Schwarz Stückelberg mass) and a chiral spectrum. The hidden bundle/gauge factors provide the non-perturbative dynamics (e.g. gaugino condensation) that generate axion masses and, in the MASA setup, the gauge fields that couple to spectator axions. On the axion side, one should compute the kinetic matrix from the Kähler potential, the charge/Stökelberg matrix for anomalous U(1)'s to identify eaten directions, the anomaly coefficients governing Chern-Simons couplings, and the non-perturbative superpotential terms (gauge and worldsheet instantons) that lift axion combinations. Diagonalizing the kinetic and mass matrices then reveals whether a QCD-aligned light eigenstate exists with the required decay constant and domain-wall number, and how strongly the remaining spectators couple to hidden gauge fields. For the MASA phenomenology, the goal is a hidden Abelian or non-Abelian sector with effective couplings large enough during inflation to source scalar/tensor modes without violating isocurvature, backreaction, or  $\Delta N_{\rm eff}$ bounds. Multi-axion dynamics naturally lead to multi-peaked, correlated features ("GW forest"), so a key deliverable is a map from discrete heterotic data (intersection numbers, Chern classes, bundle fluxes, instanton numbers) to the effective parameters controlling the sourcing efficiency and to the predicted signal across CMB-to-PTA/LISA frequencies. Finally, consistency must be checked globally: moduli stabilization compatible with the axion sector, tadpole/Bianchi constraints, absence of a Stückelberg mass, control of worldsheet/gauge instanton expansions, and a viable thermal history. With such a model in hand, one can quantify the allowed Chern-Simons and gauge couplings, delineate the viable parameter space, and present sharp, multi-channel observational targets (GW, spectral distortions, isocurvature) that the heterotic constructions to data.

We quantified the conditions under which a spectator sector generates a correlated *GW* forest, together with its concomitant CMB spectral distortions. We also spelled out the compactification ingredients needed to embed a MASA spectator sector in Type IIB orientifold compactifications (e.g., adequate Chern–Simons couplings, absence of Stückelberg masses, and tadpole cancellation). Finally, we identified regions of parameter space consistent with all theoretical and observational constraints (including isocurvature and backreaction) that predict a gravitational-wave signal in the pulsar–timing–array (PTA) band. There are numerous directions that can be pursued from this work. First, an obvious direction is to attempt a bonafide embedding of Abelian MASA models into concrete string compactifications with specific orientifolds. Since the spectator mechanism hinges

on the existence of an inflationary sector, a natural place to start is extensions of models with fibre inflation, Kähler inflation, or monodromy inflation. Along a similar vein, it would be interesting to perform scans of the type IIB orientifold landscape to determine how common are the structures required to realize the field content of Abelian spectator models. We have focused entirely on models with O7-planes, but it would be worthwhile to explore other scenarios, such as compactifications with both O3- and O7-planes. Furthermore, we have only considered Chern-Simons couplings of axions to gauge fields, but one could also consider gravitational Chern-Simons couplings of the form  $\propto \lambda_{GR} \chi R \tilde{R}$ . We also note that we have entirely ignored any potential signals from axions with Stückelberg couplings, but an interesting direction would be the study of spectator models with massive vector bosons.

Furthermore, we quantified the effect of parametric resonance during preheating in string theoretic models of inflation. It provides a means to produce a Cosmic axion Background (CaB) of ultralight axions utilizing the kinetic coupling of the inflaton to axions. However, this population is small and lies far below upcoming experimental probes of  $\Delta N_{\rm eff}$ . Nonetheless, these CaB populations are unavoidable and may be observable in future experiments. On the other hand, heavy axions are much more efficiently produced. Thus parametric resonance in string inflation could be utilized as a means to produce dark matter or alternative routes of reheating. These results were largely couched in the framework of type IIB string theory, and it would be interesting to understand the situation in other perturbative frameworks, such as heterotic compactifications. Beyond these considerations, parametric resonance can produce compact objects such as oscillons or axion stars. This would require a lattice treatment, but would nonethless be a natural extension of the current work in order to completely categorize the observational consequences of parametric resonance of axions in string inflation. Finally, we expect parametric resonance to produce spectator axions via kinetic or instanton couplings also in setups where inflation is driven by a string axion as well. We leave this interesting issue for future work.

Spectator axions remain powerful diagnostics of hidden-sector structure, and their correlated signals across cosmological observables could serve as a practical "spectroscopy" of extra dimensions. If a common axion fingerprint were to emerge, i.e., coherent features in the CMB, spectral distortions, and a multi-band gravitational-wave background, it would not merely hint at new physics; it would amount to a measurement of the extra dimensions themselves, turning the sky into a laboratory for quantum gravity.

# Appendix A

# Geometry and String Conventions

This appendix summarizes the geometric and string-theoretic tools used throughout the thesis. We begin with a brief review of differential forms, cohomology, and characteristic classes on Calabi–Yau manifolds, and then describe conventions for Type IIB orientifold compactifications, axion kinetic terms, and gauge couplings arising from D7-branes.

# A.1 Geometry

#### Differential Forms and Exterior Calculus

On a d-dimensional oriented Riemannian manifold M, a p-form is a totally antisymmetric covariant tensor field of degree p:

$$\omega_{\mu_1...\mu_p}(x) = \omega_{[\mu_1...\mu_p]}(x), \qquad 0 \le p \le d.$$
 (A.1)

The space of smooth *p*-forms is  $\Omega^p(M) = \Gamma(\wedge^p T^*M)$ .

#### Basis and exterior derivative.

In local coordinates the natural basis is  $dx^{\mu_1} \wedge \ldots \wedge dx^{\mu_p}$  and

$$\omega_p = \frac{1}{p!} \,\omega_{\mu_1 \dots \mu_p} \, \mathrm{d}x^{\mu_1} \wedge \dots \wedge \mathrm{d}x^{\mu_p}. \tag{A.2}$$

The exterior derivative  $d: \Omega^p(M) \to \Omega^{p+1}(M)$  acts as

$$d\omega_p = \frac{1}{p!} \partial_\nu \omega_{\mu_1 \dots \mu_p} dx^\nu \wedge dx^{\mu_1} \wedge \dots \wedge dx^{\mu_p}, \tag{A.3}$$

and satisfies  $d^2 = 0$ . A form is *closed* if  $d\omega_p = 0$  and *exact* if  $\omega_p = d\eta_{p-1}$  for some (p-1)-form  $\eta_{p-1}$ . Exact  $\Rightarrow$  closed by nilpotency; the converse holds only locally (Poincaré lemma).

# Hodge theory.

Given the metric g on M we define the Hodge star  $\star : \Omega^p(M) \to \Omega^{d-p}(M)$ , the coderivative  $\delta = \star d\star$ , and the Laplacian  $\Delta = d\delta + \delta d$ . Forms obeying  $\Delta \omega_p = 0$  are called *harmonic*. They provide a particularly convenient basis for cohomology classes.

#### Stokes in one line.

For an oriented (p+1)-chain  $c_{p+1}$  with boundary  $\partial c_{p+1}$ ,

$$\int_{c_{p+1}} d\omega_p = \int_{\partial c_{p+1}} \omega_p. \tag{A.4}$$

Gauss', Stokes' and Green's theorems are all special cases of (A.4).

# A.2 Cohomology

The de Rham cohomology group is the quotient

$$H_{\mathrm{dR}}^p(M) = \frac{\ker \mathrm{d} \mid_{\Omega^p}}{\mathrm{im} \, \mathrm{d} \mid_{\Omega^{p-1}}}, \qquad \dim H_{\mathrm{dR}}^p(M) =: h^p. \tag{A.5}$$

Every cohomology class contains a unique harmonic representative.

# Homology and Poincaré duality.

Dually, the homology group  $H_p(M)$  is closed p-cycles mod boundaries. Poincaré duality identifies  $H^p(M) \simeq H_{d-p}(M)$  and allows us to rewrite integrals as  $\int_{c_p} \omega_p = \int_M PD(c_p) \wedge \omega_p$ .

## Complexes and exact sequences

A chain of vector spaces and linear maps  $\cdots \to A \xrightarrow{f_1} B \xrightarrow{f_2} C \to \cdots$  with  $f_{i+1} \circ f_i = 0$  is a complex; it is exact if im  $f_i = \ker f_{i+1}$ . The de Rham complex  $0 \to \Omega^0 \xrightarrow{d} \Omega^1 \xrightarrow{d} \Omega^2 \to \cdots$  fails to be exact precisely by the amount measured by  $H^p_{dR}(M)$ .

#### Dolbeault cohomology

On a complex manifold (M, J) the tangent bundle decomposes into holomorphic and antiholomorphic parts, and forms split into types (p, q). The exterior derivative decomposes as  $d = \partial + \bar{\partial}$  with  $\partial^2 = \bar{\partial}^2 = 0$ . Dolbeault cohomology is then

$$H^{p,q}_{\bar{\partial}}(M) = \frac{\ker \bar{\partial} \mid_{\Omega^{p,q}}}{\operatorname{im} \bar{\partial} \mid_{\Omega^{p,q-1}}}, \qquad \dim H^{p,q}_{\bar{\partial}} = h^{p,q}. \tag{A.6}$$

For Calabi–Yau threefolds the resulting Hodge diamond will be our main bookkeeping device.

### Vector-bundle cohomology

For a holomorphic vector bundle  $V \to M$  we denote by  $H^q(M,V)$  the sheaf (Čech or Dolbeault) cohomology groups. Serre duality gives  $H^q(M,V) \simeq H^{d-q}(M,V^* \otimes K_M)^*$ , and on Calabi–Yau manifolds  $(K_M \simeq \mathcal{O})$  this reduces to  $h^q(M,V) = h^{d-q}(M,V^*)$ . The chiral index  $\chi(M,V) = \sum_{q=0}^d (-1)^q h^q(M,V)$  is topological and often far easier to compute than each  $h^q$ .

# A.3 Topological invariants

#### Chern classes.

Given a connection  $\omega$  on a rank-r complex bundle  $\mathcal{V} \to M$  with curvature  $\Omega = d\omega + \omega \wedge \omega$ , the total Chern class is

$$c(\mathcal{V}) = \det\left(\mathbf{1} + \frac{i\Omega}{2\pi}\right) = 1 + c_1(\mathcal{V}) + c_2(\mathcal{V}) + \dots + c_r(\mathcal{V}). \tag{A.7}$$

For the tangent bundle TM the same formula with  $\Omega = R$  reproduces the usual curvature forms.

#### Chern character and Todd class.

They are defined by

$$\operatorname{ch}(\mathcal{V}) = \operatorname{tr} \exp\left(\frac{i\Omega}{2\pi}\right), \qquad \operatorname{Td}(\mathcal{V}) = \prod_{j=1}^{r} \frac{\lambda_j}{1 - e^{-\lambda_j}},$$
 (A.8)

where  $\lambda_j$  are the Chern roots. Expanding gives the familiar series used in index calculations.

#### Hirzebruch-Riemann-Roch.

For a holomorphic vector bundle  $\mathcal{V}$  on a d-complex-dimensional manifold

$$\chi(M, \mathcal{V}) = \sum_{q=0}^{d} (-1)^q h^q(M, \mathcal{V}) = \int_M \operatorname{ch}(\mathcal{V}) \operatorname{Td}(TM). \tag{A.9}$$

On a Calabi–Yau threefold  $(c_1(TM) = 0)$  this collapses to  $\chi(M, \mathcal{V}) = \frac{1}{2} \int_M c_3(\mathcal{V})$  for SU(N) bundles, and to the well-known cubic expression for line bundles.

### A.4 Divisors

## Divisors and Line Bundles

A divisor D on a complex threefold X is a formal  $\mathbb{Z}$ -linear combination of irreducible codimension-one subvarieties. Equivalently, it can be defined as the zero locus  $\{f=0\}$  of a global holomorphic section  $f \in H^0(X, \mathcal{O}_X(D))$ . Two divisors are said to be linearly equivalent if their difference is the divisor of a global meromorphic function. The set of equivalence classes forms the divisor class group  $\mathrm{Cl}(X)$ , which embeds into  $H^{1,1}(X,\mathbb{Z})$  via the first Chern class.poli

#### From divisors to line bundles.

To every divisor D we associate the holomorphic line bundle  $\mathcal{O}_X(D)$  whose transition functions keep track of how the local equations  $f_i = 0$  glue together. Conversely, the vanishing of  $H^1(X, \mathcal{O}_X)$  implies that line bundles are classified by their (divisor) first Chern class.

#### Intersection numbers and volumes.

Choosing a basis  $\{D_i\}$  of  $\mathrm{Cl}(X)$  the triple intersection numbers  $\kappa_{ijk} = \int_X D_i \wedge D_j \wedge D_k$  are topological invariants and determine the classical Kähler potential through  $\mathcal{V} = \frac{1}{6}\kappa_{ijk}\,t^it^jt^k$  with  $t^i = \int_{D_i}J$ . In Type IIB compactifications the  $D_i$  support wrapped D7-branes, Euclidean D3-instantons, and fluxes, so keeping track of their volumes and intersection form is indispensable.

## Effective, nef and ample.

A divisor is *effective* if it has a holomorphic representative, nef if  $D \cdot C \geq 0$  for every curve C, and ample if some positive multiple embeds X into projective space. Physically, ample (or at least nef) divisors guarantee positive volumes inside the Kähler cone, i.e. control over  $\alpha'$  corrections and a good supergravity limit.

# A.5 String Conventions

## A.5.1 Type IIB Orientifolds

In this subsection, we outline further details of 4d type IIB orientifold models. We will list only the essential details – for more in-depth discussion, see [17, 331, 332, 340].

We consider type IIB string theory on Calabi-Yau 3-fold  $X_3$  with cohomology groups  $H^{p,q}(X_3)$  and independent Hodge numbers  $(h^{1,1},h^{2,1})$ . The orientifold is defined by a projection operator composed of a holomorphic involution on  $X_3$  and a worldsheet partity operator. Under the involution, the cohomology groups split into positive and negative eigenspaces as  $H^{p,q} = H^{p,q}_+ \oplus H^{p,q}_-$  such that

$$h^{1,1} = h_{+}^{1,1} + h_{-}^{1,1} \qquad h^{2,1} = h_{+}^{2,1} + h_{-}^{2,1}.$$
 (A.10)

As in the main text, we will use lower case Latin (Greek) indices to enumerate elements of the positive (negative) cohomologies as  $\alpha, \beta, \gamma = 1, ..., h_+^{1,1}$  and  $a, b = 1, ..., h_-^{1,1}$ .

The particle content of the 4d,  $\mathcal{N}=1$  supergravity effective field theory includes  $h_+^{2,1}$  vector multiplets and chiral supermultiplets for the axiodilaton,  $h_+^{1,1}$  complexified Kähler moduli,  $h_-^{1,1}$  odd moduli, and  $h_-^{2,1}$  complex structure moduli. The vacuum expectation values of the  $h_+^{1,1}$  scalars  $\tau_\alpha$  control the size of 4-cycles in  $X_3$  and are related to 2-cycle volumes  $v^\alpha$  via the intersection numbers  $\kappa_{\alpha\beta\gamma}$  as  $\tau_\alpha = \frac{1}{2}k_{\alpha\beta\gamma}v^\beta v^\gamma$ . The axions of the model are  $C_0$ ,  $b^a$ ,  $\rho_\alpha$ , and  $c^a$ . The latter two sets have kinetic terms

$$S_{axions} \supset -e^{\Phi} G_{ab} \ dc^a \wedge \star dc^b + \frac{1}{16\mathcal{V}^2} G^{\alpha\beta} \ d\rho_{\alpha} \wedge \star d\rho_{\beta} \,. \tag{A.11}$$

Above we have introduced metrics on the space of harmonic 2-forms as

$$G_{ab} = -\frac{\mathcal{T}_{ab}}{4\mathcal{V}^2}$$

$$G_{\alpha\beta} = \frac{1}{4\mathcal{V}^2} \left(\frac{\tau_{\alpha}\tau_{\beta}}{\mathcal{V}^2} - \mathcal{T}_{\alpha\beta}\right),$$
(A.12)

with  $G^{\alpha\beta} = (G^{-1})^{\alpha\beta}$ . Here  $\mathcal{V} = \frac{1}{6} \kappa_{\alpha\beta\gamma} v^{\alpha} v^{\beta} v^{\gamma}$  is the volume of  $X_3$  and

$$\mathcal{T}_{\alpha\beta} = \kappa_{\alpha\beta\gamma} v^{\gamma}$$

$$\mathcal{T}_{ab} = \kappa_{ab\gamma} v^{\gamma} .$$
(A.13)

These define the metrics used in eq. (6.12). In the presence of D7-branes, the axions  $c^a$  and  $\rho_{\alpha}$  can become charged under gauge U(1) interactions. In the Calabi-Yau  $X_3$ , we consider two divisors  $\mathcal{D}$  and  $\mathcal{D}'$  that are mapped to each other under the involution. One can then define  $\mathcal{D}^+ = \mathcal{D} \cup \mathcal{D}'$  and  $\mathcal{D}^- = \mathcal{D} \cup (-\mathcal{D}')$ , where the negative sign refers to orientation reversal. Note that in the main text,  $\mathcal{D}^+$  is denoted as  $\widetilde{\mathcal{D}}$ . If we wrap one D7-brane on both  $\mathcal{D}$  and  $\mathcal{D}'$ , the exterior derivatives in eq. (A.11) are promoted to the covariant derivatives

$$\nabla c^a = dc^a - q^a A \tag{A.14}$$

$$\nabla \rho_{\alpha} = d\rho_{\alpha} - iq_{\alpha}A. \tag{A.15}$$

Where A is the 1-form of the worldvolume gauge theory and the axion charges are

$$q^{a} = \frac{1}{2\pi} N_{D7} w^{a} \tag{A.16}$$

$$q_{\alpha} = -\frac{N_{\rm D7}}{2\pi} (\kappa_{\alpha\beta\gamma}\tilde{m}^{\beta}w^{\gamma} + \kappa_{\alpha bc}m^{b}w^{c}), \qquad (A.17)$$

where  $\tilde{m}^{\alpha}$  ( $m^{c}$ ) is worldvolume flux supported on even (odd) 2-cycles<sup>1</sup>. The  $w^{\alpha}$  ( $w^{a}$ ) are wrapping numbers along the basis elements  $\tilde{\omega}^{\alpha}$  ( $\tilde{\omega}^{a}$ ) of  $H^{2,2}_{+}(X_{3},\mathbb{Z})$  ( $H^{2,2}_{-}(X_{3},\mathbb{Z})$ ):

$$w^{\alpha} = \int_{\mathcal{D}^{+}} \tilde{\omega}^{\alpha}, \qquad w^{a} = \int_{\mathcal{D}^{-}} \tilde{\omega}^{a}.$$
 (A.18)

Notably, the charge  $q^a$  is independent of flux and is determined by the odd wrapping number  $w^a$ . This motivates the description of  $C_2$ -axion Stückelberg couplings as being geometric in nature, as discussed in the main text. If  $[\mathcal{D}] = [\mathcal{D}']$ , so that the divisor and image divisor are homologous, then  $w^a$  vanishes and the Stückelberg mechanism can be avoided as discussed in ??.

# A.5.2 Worldvolume Theory of D7-branes and Induced Tadpoles

In this section, we briefly review the relation between 4d gauge theories and the worldvolume theory of D7-branes wrapped on 4-cycles. We will follow here the conventions used in [420] as well as in [331]. In string frame, the bosonic portion of the low-energy 10d type IIB action in the democratic formulation is

$$S_{IIB} \supset \frac{2\pi}{\ell_s^8} \left( \int e^{-2\phi} R \star_{10} 1 - \frac{1}{2} \int e^{-2\phi} \left( 8d\phi \wedge \star_{10} d\phi - H_3 \wedge \star_{10} H_3 \right) + \frac{1}{4} \int \sum_{p=1,3,5,7,9} G_p \wedge \star_{10} G_p \right)$$
(A.19)

Here  $\phi$  is the dilaton,  $H_3 = dB_2$ , and the various field strengths are defined is terms of the *p*-form gauge potentials  $C_p$  by  $G_1 = dC_0$  for p = 1 and  $G_p = dC_{p-1} - dB_2 \wedge C_{p-2}$  otherwise. Here we define the string length as  $\ell_s \equiv 2\pi\sqrt{\alpha'}$ . Dimensional reduction of eq. (A.19) on the 6*d* orientifold, and transition to the Einstein frame, yields the kinetic terms in eq. (A.15) addition to the kinetic terms of moduli.

<sup>&</sup>lt;sup>1</sup>Technically  $\tilde{m}^{\alpha}$  is a combined flux of the worldvolume gauge theory and the pullback of  $B_2$ .

Contributions to the 10d bosonic effective action from the various supersymmetric (BPS) Dp-branes take the form of the Dirac-Born-Infeld (DBI) action and the Chern-Simons action:

$$S_{Dp} = -\frac{2\pi}{\ell_s^{p+1}} \int d^{p+1}x \sqrt{-\det(\varphi^*[g_{10} + B_2] - \frac{\ell_s^2}{2\pi} F_2)} + \frac{2\pi}{\ell_s^{p+1}} \int e^{\frac{\ell_s^2}{2\pi} F_2 - \varphi^*[B_2]} \wedge \sqrt{\frac{\hat{A}[\ell_s^2 R_T]}{\hat{A}[\ell_s^2 R_N]}} \wedge \bigoplus_q \varphi^*[C_q].$$
(A.20)

Where  $\varphi^*[\cdots]$  denotes the pullback to the D7-brane worldvolume,  $\hat{A}[\cdots]$  is the A-roof genus, and  $R_T$  ( $R_N$ ) is the curvature 2-form of the tangent (normal) bundle of the brane worldvolume embedding. From here we set  $\ell_s = 1$  and restore proper mass dimensions in the usual manner.

We now consider the dimensional reduction of eq. (A.20) for the scenario of a D7-brane (p=7) filling 4D macroscopic space-time  $M_4$  and wrapping a properly chosen 4-cycle  $\widetilde{\Pi}$  of a suitable Calabi-Yau (CY) O7-orientifold compactification. Keeping only relevant terms, we look at the Kaluza-Klein (KK) zero mode of  $C_4$  on  $\Pi_4$  and set  $C_4 = c_4 \omega_{\Pi_4} + \cdots$  and  $F_2 = \frac{1}{2} F_{\mu\nu} dx^{\mu} dx^{\nu}$ . Using  $F_2 \wedge F_2 = \frac{1}{4} \varepsilon^{\mu\nu\rho\sigma} F_{\mu\nu} F_{\rho\sigma} d^4 x$  and  $F_2 \wedge \star_4 F_2 = \frac{1}{2} F_{\mu\nu} F^{\mu\nu} \sqrt{-g_4} d^4 x$  as well as

$$\int_{M_4 \times \widetilde{\Pi}} d^8 x \sqrt{-\varphi^*[g_{10}]} = \underbrace{\int_{\widetilde{\Pi}} d^4 y \sqrt{g(\widetilde{\Pi})}}_{=\tau} \cdot \int_{M_4} d^4 x \sqrt{-g_4}$$

$$\int \sum_{q} e^{\frac{1}{2\pi} F_2 - \varphi^*[B_2]} \wedge C_q \supset \underbrace{\int_{\Pi_4} C_4 \cdot \int_{M_4} \frac{1}{2} \frac{1}{4\pi^2} F_2 \wedge F_2}_{=c_4}, \tag{A.21}$$

the two-derivative part of the D7-brane action to be

$$S_{D7-gauge} = -2\pi \int \left[ \frac{1}{4\pi^2} \tau_2 \frac{1}{2} F_2 \wedge \star_4 F_2 + \frac{1}{4\pi^2} c_4 \frac{1}{2} F_2 \wedge F_2 \right]$$

$$= \int d^4 x \sqrt{-g_4} \left[ -\frac{1}{4} \left( \frac{1}{2\pi} \tau \right) F_{\mu\nu} F^{\mu\nu} - \frac{1}{8} \left( \frac{1}{2\pi} c_4 \right) \varepsilon^{\mu\nu\rho\sigma} F_{\mu\nu} F_{\rho\sigma} \right] . (A.22)$$

We can compare this to the standard form of a 4D  $\mathcal{N}=1$  supersymmetric U(1) gauge theory with holomorphic gauge kinetic function f(T) of a chiral superfield  $T=\tau+ic_4$ , given by

$$S_{U(1)} = \int_{M_4} d^4x \sqrt{-g_4} \left[ \frac{1}{4} \int d^2\theta f(T) W_{\beta} W^{\beta} + h.c. \right], \tag{A.23}$$

where the  $\theta^2$  component of the square of the super field strength  $W_{\alpha}$  evaluates to ( $\lambda$  denotes the gaugino superpartner of the gauge field)

$$W_{\beta}W^{\beta}\Big|_{\theta\theta} = -2i\lambda\sigma^{\mu}\partial_{\mu}\bar{\lambda} - \frac{1}{2}F_{\mu\nu}F^{\mu\nu} + D^{2} + \frac{i}{4}\varepsilon^{\mu\nu\rho\sigma}F_{\mu\nu}F_{\rho\sigma}. \tag{A.24}$$

Plugging this into eq. (A.22) we get, for unbroken SUSY (D=0), for the bosonic sector

$$S_{U(1),bos.} = \int_{M_4} d^4x \sqrt{-g_4} \left[ -\frac{1}{4} \operatorname{Re} f(T) F_{\mu\nu} F^{\mu\nu} - \frac{1}{8} \operatorname{Im} f(T) \varepsilon^{\mu\nu\rho\sigma} F_{\mu\nu} F_{\rho\sigma} \right]. \tag{A.25}$$

Direct comparison with eq. (A.22) reveals that we must choose

$$f(T) = \frac{1}{2\pi}T, \qquad (A.26)$$

to match the D7-brane effective action. Up to this point everything was done for a single D7-brane generating a single U(1) supersymmetric gauge field theory. If we replace this with a stack of  $N_{\rm D7}$  coincident D7-branes wrapping the same 4-cycle, this stack will generate a non-Abelian 4D super-Yang-Mills (SYM) gauge theory. What effectively changes in this case in the expressions above is that every occurrence of  $F_2 \wedge F_2$  and  $F_2 \wedge \star F_2$  gets replaced by tr  $F_2 \wedge F_2$  and tr $F_2 \wedge \star F_2$ , respectively, where the trace pertains to  $F_2 = F_2^a T^a$  (with  $T^a$  the generators of the Lie group in a given representation) now being Lie algebra valued in the SYM gauge group. The additional trace will thus evaluate to tr  $T^a T^b$  producing an additional factor 1/2 for the  $T^a$  in the fundamental representation. As explained in ??, we can introduce an additional CS coupling of the gauge field to  $C_2$ -axions if we allow for the presence of magnetic flux in the D7-branes. Inclusion of these magnetic fluxes modifies the D7-brane gauge kinetic function to the expression in eq. (6.8). However, there is one more effect of turning on gauge flux-the D7-branes contribute additional terms to the D3-brane tadpole. The relevant contribution can be determined from dimensional reduction of the CS term in eq. (A.20):

$$\mathcal{S}_{\mathrm{D7}}^{CS} \supset 2\pi \frac{1}{2} \left\{ \int_{\Pi_{4}} \frac{1}{4\pi^{2}} F_{2} \wedge F_{2} + \int_{\Pi_{4}} \frac{1}{4\pi^{2}24} (p_{1}[R_{N}^{\widetilde{\Pi}}] - p_{1}[R_{T}^{\widetilde{\Pi}}]) \right\} \underbrace{\int_{M_{4}} C_{4}}_{=\mathrm{D3-brane \ CS-term}}$$

$$= \pi \left\{ (m_{1})^{2} \int_{\Pi_{4}} \omega_{\Pi_{2}^{G}} \wedge \omega_{\mathrm{dual}(\Pi_{2}^{G})} + \int_{\Pi_{4}} \frac{1}{24} c_{2}[R_{T}^{\widetilde{\Pi}}] \right\} \cdot \int_{M_{4}} C_{4}$$

$$= \pi \left\{ \underbrace{(m_{1})^{2} \kappa_{+--} + \frac{1}{24} \chi(\widetilde{\Pi})}_{Q_{\mathrm{D3 \ ind}}} \right\} \cdot \int_{M_{4}} C_{4} .$$
(A.27)

Where we have used the definition of the A-roof genus  $\hat{A}[R] = 1 - \frac{1}{24}p_1[R] + ...$  expressed in terms of Pontryagin classes  $p_n$ , while  $c_2$  corresponds to the second Chern class [421]. The subscripts T, N denote the tangent and normal bundle of  $\Pi_4$ .

The whole prefactor of  $\int_{M_4} C_4$  thus constitutes a D3-brane charge induced on the D7-brane world volume.

$$Q_{\text{D3},ind.} = \kappa_{+--}(m_1)^2 + \frac{1}{24}\chi(\Pi_4)$$
 (A.28)

The first term comes from turning on quantized internal gauge flux, while the second corresponds to the intrinsic curvature-induced amount of D3-brane charge which any D7-brane or O7-plane wrapping a non-flat 4-cycle acquires. This induced D3-brane charge grows quadratically in the gauge flux quanta  $m^G$  and linearly in the wrapping number. D3-brane charge, like any localized charge sourcing a long-range gauge field strength, satisfies a Gauss' law constraint. Hence, in the compact 6 dimensions of the CY the field lines emanating from  $D_{\text{D3},ind}$  must end on equal in magnitude and sign-opposite D3-charge. In a consistent type IIB string theory compactification on CY orientifolds this balancing D3-charge is generated by higher-curvature couplings in the CS terms of single D7-branes wrapping all the 4-cycles of the CY. Any such consistent type IIB CY orientifold compactification has a lift to F-theory, where the orientifolded CY 3-fold of

type IIB string theory gets lifted into an elliptically fibred CY 4-fold  $X_4$ . The total D3-brane charge from curvature couplings on D7-branes wrapping 4-cycles in type IIB becomes in F-theory equal to  $Q_{\mathrm{D3,tot.}}(X_4) = \chi(X_4)/24$  and is thus completely fixed by the topology of  $X_4$ .

# Appendix B

# CY examples

In this appendix we'll review the geometric information needed for the examples of the heterotic axions.

## B.0.1 Quintic Calabi-Yau

Consider the simplest example of a Calabi–Yau threefold: the quintic hypersurface  $\mathbb{CP}^4[5]$ , defined by

$$\sum_{i=1}^{5} z_i^5 = 0 \tag{B.1}$$

in  $\mathbb{CP}^4$ , with homogeneous coordinates  $z_i$  and divisors  $D_i = \{z_i = 0\}$ . All  $D_i$  are linearly equivalent, so we may identify the hyperplane class  $H \equiv D_i$  for all i.

#### Geometry of the quintic

The geometric  $\tilde{F}$ -term encodes the hypersurface condition, while the  $\tilde{D}$ -term describes the Kähler quotient:

$$\tilde{F}: \quad z_1^5 + z_2^5 + z_3^5 + z_4^5 + z_5^5 = 0, \qquad \tilde{D}: \quad |z_1|^2 + \dots + |z_5|^2 = b,$$
 (B.2)

with  $b \ge 0$  for X to be in the Kähler cone.

Since all  $Z_a$  have the same gauge charge, the divisors  $D_i$  are equivalent and generate  $H^{1,1}(X)$ :

$$\mathcal{D} \equiv H, \quad h^{1,1}(X) = 1. \tag{B.3}$$

### Triple intersection number

To compute  $H^3$ , set  $z_1 = z_2 = z_3 = 0$ . The  $\tilde{F}$ -term reduces to

$$z_4^5 + z_5^5 = 0. (B.4)$$

This equation in  $\mathbb{CP}^1$  has 5 distinct solutions for the ratio  $z_4/z_5$ :

$$\frac{z_4}{z_5} = e^{i(2k+1)\pi/5}, \quad k = 0, 1, 2, 3, 4.$$
(B.5)

Thus, the three divisors intersect in five points, and we find

$$H^3 = 5. (B.6)$$

#### Tangent bundle Chern classes

The total Chern class of the tangent bundle is

$$c(T_X) = \frac{c(T_{\mathbb{CP}^4})}{c(N_X)} = \frac{(1+H)^5}{(1+5H)}.$$
 (B.7)

Expanding the denominator as  $(1+5H)^{-1} = 1-5H+25H^2+...$  and multiplying out, we find

$$c(T_X) = 1 + 10H^2 + \dots$$
 (B.8)

so that  $c_1(T_X) = 0$  (as required for a Calabi–Yau) and  $c_2(T_X) = 10H^2$ .

### B.0.2 Bi-cubic CICY

Consider the bi-cubic complete intersection Calabi-Yau defined as a degree-(3,3) hypersurface in  $\mathbb{P}^2_x \times \mathbb{P}^2_y$ , with Hodge numbers  $(h^{1,1},h^{2,1})=(2,83)$ :

$$\mathbb{P}^2 \begin{bmatrix} 3 \\ 3 \end{bmatrix} .$$
(B.9)

Let  $h_1$  and  $h_2$  denote the hyperplane classes of the two  $\mathbb{P}^2$  factors, pulled back to the ambient space  $A = \mathbb{P}^2_x \times \mathbb{P}^2_y$ , so that

$$h^3 = 0, \quad k^3 = 0, \quad \int_A h_1^2 h_2^2 = 1.$$
 (B.10)

The bicubic hypersurface X has class

$$[X] = 3h_1 + 3h_2. (B.11)$$

We take the basis of divisors on X to be  $H_1 = h_1|_X$  and  $H_2 = h_2|_X$ . The triple intersection numbers are then

$$\kappa_{111} = \int_{A} h_{1}^{3} \wedge (3h_{1} + 3h_{2}) = 0,$$

$$\kappa_{222} = \int_{A} h_{2}^{3} \wedge (3h_{1} + 3h_{2}) = 0,$$

$$\kappa_{112} = \int_{A} h_{1}^{2} k \wedge (3h_{1} + 3h_{2}) = 3 \int_{A} h_{1}^{2} h_{2}^{2} = 3,$$

$$\kappa_{122} = \int_{A} h_{1} h_{2}^{2} \wedge (3h_{1} + 3h_{2}) = 3 \int_{A} h_{1}^{2} h_{2}^{2} = 3.$$
(B.12)

By symmetry of  $\kappa_{abc}$ , we have  $\kappa_{121} = \kappa_{211} = 3$  and  $\kappa_{212} = \kappa_{221} = 3$ .

The intersection polynomial is therefore

$$\mathcal{J}(v_1, v_2) = \sum_{a,b,c} \kappa_{abc} \, v_a v_b v_c = 3 \, v_1^2 v_2 + 3 \, v_1 v_2^2 = 3 \, v_1 v_2 \, (v_1 + v_2) \,. \tag{B.13}$$

**Volume** With Kähler form  $J = v_1H_1 + v_2H_2$ , the Calabi-Yau volume is

$$\mathcal{V} = \frac{1}{6} \int_{V} J^{3} = \frac{1}{6} \left( 3 v_{1}^{2} v_{2} + 3 v_{1} v_{2}^{2} \right) = \frac{1}{2} \left( v_{1}^{2} v_{2} + v_{1} v_{2}^{2} \right). \tag{B.14}$$

**Chern classes** Let  $A = \mathbb{P}_x^2 \times \mathbb{P}_y^2$  with hyperplane classes  $h_1, h_2$  pulled back from the two factors. For A one has  $c(T_A) = c(T_{\mathbb{P}_x^2}) c(T_{\mathbb{P}_y^2}) = (1 + h_1)^3 (1 + h_2)^3$ . The bi-cubic hypersurface  $X \subset A$  has class  $[X] = 3h_1 + 3h_2$ . By adjunction,

$$c(T_X) = \frac{(1+h_1)^3(1+h_2)^3}{1+3h_1+3h_2} \bigg|_{Y} = \frac{(1+H_1)^3(1+H_2)^3}{1+3H_1+3H_2}.$$
 (B.15)

Expanding to second order, we find

$$c(T_X)1 + (3H_1^2 + 9H_1H_2 + 3H_2^2) + \cdots$$
 (B.16)

Hence

$$c_1(T_X) = 0$$
,  $c_2(T_X) = 3H_1^2 + 9H_1H_2 + 3H_2^2 = 3(H_1^2 + 3H_1H_2 + H_2^2)$ , (B.17)

# B.0.3 CS couplings

We report the  $\tilde{\lambda}_i$  defined in the text at eq. (4.144) for the  $\boxed{\text{noGC}}$  - anisotropic case:

$$\tilde{\lambda}_{\varphi_1,v} \sim \frac{f_1^4 n_2^3 (-f_a) + f_2 f_1^2 n_1 n_2^2 f_a (f_1 - n_1 f_a) + f_2^3 n_1^2 (2f_1 n_1 f_a - n_1^2 f_a^2 + f_1^2)}{2f_1^2 f_2 n_1 n_2 f_a \sqrt{f_2^2 n_1^2 + f_1^2 n_2^2}}, \quad (B.18)$$

$$\tilde{\lambda}_{\varphi_2,v} \sim \frac{f_1^4 n_2^3 f_a + f_2 f_1^2 n_1 n_2^2 f_a (f_1 - n_1 f_a) - f_2^3 n_1^2 (n_1^2 f_a^2 + f_1^2)}{2 f_1^2 f_2 n_1 n_2 f_a \sqrt{f_2^2 n_1^2 + f_1^2 n_2^2}},$$
(B.19)

$$\tilde{\lambda}_{\varphi_3,v} \sim \frac{f_2 n_1 f_a + f_1 (n_2 f_a + f_2)}{f_a \sqrt{f_2^2 n_1^2 + f_1^2 n_2^2}},\tag{B.20}$$

$$\tilde{\lambda}_{\varphi_1,h} \sim \frac{f_1^4 n_2^3 f_a - f_2 f_1^3 n_1 n_2^2 f_a + f_2 f_1^2 n_1^2 (f_2^2 - n_2^2 f_a^2) - 2 f_2^3 f_1 n_1^3 f_a - f_2^3 n_1^4 f_a^2}{2 f_1^2 f_2 n_1 n_2 f_a \sqrt{f_2^2 n_1^2 + f_1^2 n_2^2}}, \quad (B.21)$$

$$\tilde{\lambda}_{\varphi_2,h} \sim \frac{-f_1^4 n_2^3 f_a - f_2 f_1^3 n_1 n_2^2 f_a - f_2 f_1^2 n_1^2 (n_2^2 f_a^2 + f_2^2) - f_2^3 n_1^4 f_a^2}{2f_1^2 f_2 n_1 n_2 f_a \sqrt{f_2^2 n_1^2 + f_1^2 n_2^2}},$$
(B.22)

$$\tilde{\lambda}_{\varphi_3,h} \sim \frac{f_1(f_2 - n_2 f_a) - f_2 n_1 f_a}{f_a \sqrt{f_2^2 n_1^2 + f_1^2 n_2^2}}.$$
(B.23)

# Appendix C

# MASA Power Spectra Calculations

# C.1 Tensor Perturbations

The mode functions in eq. (5.57) satisfy the equation

$$A_{\pm}^{i\prime\prime} + \left(k^2 \mp k \frac{\lambda_i \vartheta_i'}{f_i}\right) A_{\pm}^i = 0. \tag{C.1}$$

with the helicity vectors obeying the following relations

$$\vec{k} \cdot \vec{\varepsilon}^{(\pm)} = 0$$
,  $i\vec{k} \times \vec{\varepsilon}^{(\pm)} = \pm k\vec{\varepsilon}^{(\pm)}$ ,  $\vec{\varepsilon}^{(\pm)} \cdot \vec{\varepsilon}^{(\mp)} = 1$ ,  $\vec{\varepsilon}^{(\pm)} \cdot \vec{\varepsilon}^{(\pm)} = 0$ . (C.2)

In a spatially flat, inflating Universe, the second term in parentheses reads  $k\lambda_i\vartheta_i'/f_i = -2k\xi_i/\tau$  and eq. (5.58) follows.

Plugging in the WKB solution in eq. (5.59) into eq. (5.57), we get the following expressions for the gauge fields

$$\hat{A}_{m}^{1}(\tau, \vec{k}) = \int \frac{d^{3}k}{(2\pi)^{3/2}} e^{i\vec{k}\cdot\vec{x}} \varepsilon_{m}^{(+)}(\hat{k}) A_{+}^{1}(\tau, k) \left[ \hat{a}_{+}(\vec{k}) + \hat{a}_{+}^{\dagger}(-\vec{k}) \right] ,$$

$$\hat{A}_{m}^{2}(\tau, \vec{k}) = \int \frac{d^{3}k}{(2\pi)^{3/2}} e^{i\vec{k}\cdot\vec{x}} \varepsilon_{m}^{(+)}(\hat{k}) A_{+}^{2}(\tau, k) \left[ \hat{b}_{+}(\vec{k}) + \hat{b}_{+}^{\dagger}(-\vec{k}) \right] .$$
(C.3)

Next, to tie the above to the tensor perturbations, we write the metric as:

$$ds^{2} = a^{2}(\tau)[-d\tau^{2} + \left(\delta_{mn} + \hat{h}_{mn}(\tau, \vec{x})\right)dx^{m}dx^{n}], \qquad (C.4)$$

where the  $\hat{h}_{ij}$  have the mode expansion in eq. (5.62). Expanding the Einstein-Hilbert and gauge field action to second order in  $\hat{h}_{ij}$ , including the first order interaction term with the gauge field, one obtains

$$S_{\text{GW}} = \int d^4x \left[ \frac{M_p^2 a^2}{8} \left( |\hat{h}'_{mn}|^2 - |\hat{h}_{mn,p}|^2 \right) - \frac{a^4}{2} \hat{h}_{mn} \left[ \left( \hat{E}_m \hat{E}_n + \hat{B}_m \hat{B}_n \right)_1 + \left( \hat{E}_m \hat{E}_n + \hat{B}_m \hat{B}_n \right)_2 \right] \right].$$
(C.5)

Here the electric and magnetic fields are defined in eq. (5.61) and the subscripts "1" and "2" correspond to the spectators' labels.

## C.2 Curvature Perturbations

Beginning with the action in eq. (5.70), one can derive the following equations of motion for the modes  $\hat{Q}_{\phi}$  and  $\hat{Q}_{\vartheta}$ 

$$\left(\frac{\partial^{2}}{\partial \tau^{2}} + k^{2} + \tilde{M}_{\phi\phi}^{2}\right) \hat{Q}_{\phi} + \tilde{M}_{\phi\vartheta_{1}}^{2} \hat{Q}_{\vartheta_{1}} + \tilde{M}_{\phi\vartheta_{2}}^{2} \hat{Q}_{\vartheta_{2}} = 0,$$

$$\left(\frac{\partial^{2}}{\partial \tau^{2}} + k^{2} + \tilde{M}_{\vartheta_{i}\vartheta_{i}}^{2}\right) \hat{Q}_{\vartheta_{i}} + \tilde{M}_{\vartheta_{i}\phi}^{2} \hat{Q}_{\phi} + \tilde{M}_{\vartheta_{i}\vartheta_{k}}^{2} \hat{Q}_{\vartheta_{k}} = \lambda_{i} \frac{a^{3}}{f_{i}} \int \frac{d^{3}x}{(2\pi)^{3/2}} e^{-i\vec{k}\cdot\vec{x}} \mathbf{E}_{i} \cdot \mathbf{B}_{i}. \quad (C.6)$$

Taking the slow-roll expansion of the mass matrix in eq. (5.71), one finds

$$\tilde{M}_{ii}^2 = -\frac{2}{\tau^2} + \frac{3}{\tau^2} \eta_i - \frac{6}{\tau^2} \varepsilon_i \,,$$
 (C.7)

$$\tilde{M}_{ij}^2 = -\frac{6}{\tau^2} \sqrt{\varepsilon_i \varepsilon_j} \,, \tag{C.8}$$

where slow-roll parameters have been introduced for each of the fields  $\phi_i$ ,  $(\phi_1, \phi_2, \phi_3) = (\phi, \vartheta_1, \vartheta_2)$ . To leading order terms in slow roll, the mass matrix reads

$$\tilde{M}_{ij}^{2} \simeq -\frac{1}{\tau^{2}} \begin{pmatrix} 2 & 6\sqrt{\varepsilon_{\phi}\varepsilon_{\vartheta_{1}}} & 6\sqrt{\varepsilon_{\phi}\varepsilon_{\vartheta_{2}}} \\ 6\sqrt{\varepsilon_{\vartheta_{1}}\varepsilon_{\phi}} & 2 & 6\sqrt{\varepsilon_{\vartheta_{1}}\varepsilon_{\vartheta_{2}}} \\ 6\sqrt{\varepsilon_{\vartheta_{2}}\varepsilon_{\phi}} & 6\sqrt{\varepsilon_{\vartheta_{2}}\varepsilon_{\vartheta_{1}}} & 2 \end{pmatrix} . \tag{C.9}$$

To solve the equations of motion, one can introduce the retarded Green's function

$$G_k(\tau, \tau') = \Theta(\tau - \tau') \frac{\pi}{2} \sqrt{\tau \tau'} \left[ J_{3/2}(-k\tau) Y_{3/2}(-k\tau') - Y_{3/2}(-k\tau) J_{3/2}(-k\tau') \right], \quad (C.10)$$

where J and Y denote the Bessel functions with real arguments. This yields the particular solution presented in eq. (5.78), which can be rewritten more explicitly by defining the new vector  $\vec{p} \equiv \frac{\vec{p}}{k}$  as:

$$\zeta^{\text{src}}(\tau, \vec{k}) = \sum_{i=1,2} \frac{3\pi^{3/2} H^2 \lambda_i \sqrt{\varepsilon_{\vec{y}_*^i}}}{8M_p f_i} \int \frac{d^3 \tilde{p}}{(2\pi)^{3/2}} \tilde{p}^{1/4} |\hat{k} - \tilde{p}|^{1/4} \left( \tilde{p}^{1/2} + |\hat{k} - \tilde{p}|^{1/2} \right) N_i \left[ \xi_*^i, \tilde{p} x_*^i, \delta_i \right] 
N_i \left[ \xi_*^i, |\hat{k} - \tilde{p}| x_*^i, \delta_i \right] \hat{W}_i [\vec{p}, \vec{k}] T_\zeta^i \left[ \xi_*^i, x_*^i, \delta_i, \sqrt{\tilde{p}} + \sqrt{|\hat{k} - \tilde{p}|} \right], \quad (C.11)$$

where we introduced the quantities  $x = -k\tau$  and  $x_* = -k\tau_*$  and denoted with  $\hat{k}$  the unit vector. The coefficients  $N_i$  appearing in Eq. (C.11) arise from the gauge field mode functions:

$$\tilde{A}_{i}(\tau, p)\tilde{A}_{i}(\tau, |\vec{k} - \vec{p}|) = N_{i}[\xi_{*}^{i}, -p\tau_{*}^{i}, \delta_{i}]N_{i}[\xi_{*}^{i}, -|\vec{k} - \vec{p}|\tau_{*}^{i}, \delta_{i}] 
\exp \left[ -\frac{4(\xi_{*}^{i})^{1/2}}{1 + \delta_{i}} \left( \frac{\tau}{\tau_{*}^{i}} \right)^{\delta_{i}/2} \left( \sqrt{-p\tau} + \sqrt{-|\vec{k} - \vec{p}|\tau} \right) \right].$$
(C.12)

In Eq. (C.11), we also introduced the function

$$T_{\zeta}^{i}\left[\xi_{*}, x_{*}, d, Q\right] \equiv \int_{0}^{\infty} \frac{dx'}{x'} J_{3/2}\left(x'\right) \sqrt{\frac{\varepsilon_{\vartheta_{i}}\left(x'\right)}{\varepsilon_{\vartheta_{*i}}}} \int_{x'}^{\infty} dx'' x''^{3/2} \exp\left[-\frac{4\xi_{*}^{1/2}}{1+\delta_{i}} \frac{x''^{(1+\delta_{i})/2}}{x_{*}^{\delta_{i}/2}} Q\right] \left[J_{3/2}\left(x'\right) Y_{3/2}\left(x''\right) - Y_{3/2}\left(x'\right) J_{3/2}\left(x''\right)\right] .$$
(C.13)

and defined the operators:

$$\hat{W}_{i}[\vec{p}, \vec{k}] \equiv \varepsilon_{j}^{(+)}(\vec{p})\varepsilon_{j}^{(+)}(\hat{k} - \vec{p}) \left[ \hat{a}_{+}(\vec{p}) + \hat{a}_{+}^{\dagger}(-\vec{p}) \right] \left[ \hat{a}_{+}(\vec{k} - \vec{p}) + \hat{a}_{+}^{\dagger}(-\vec{k} + \vec{p}) \right], \quad (C.14)$$

for which the following relation holds (to leading order in slow-roll):

$$\langle \hat{W}_1 \hat{W}_2 \rangle = 0. \tag{C.15}$$

As a result, the contributions from the different axions are decoupled from one another and one can compute the total power spectrum as the sum of two separate contributions.

# C.3 Backreaction and Perturbativity

Given a set of model parameters, such as those provided in Table 5.3, consistency with the working assumptions in the previous sections demands that one verifies that the backreaction of the spectator fields on the Friedmann equation and the backreaction on the evolution of the axion background remain negligible. In addition, a self-consistent analysis requires the implementation of perturbativity bounds <sup>1</sup>. The study of backreaction in the case of a single (Abelian) spectator sector was worked out in [161]. Perturbativity constraints were also derived in [161], following [422]. We will now generalise those bounds to our model.

Following [161], we begin by requiring that the energy density of the axion fields gives a negligible contribution to the total energy density of the universe, in other words:

$$\sum_{i=1}^{N} \rho_{\vartheta_i} \equiv \sum_{i=1}^{N} \left( \frac{\dot{\vartheta_i}^2}{2} + V_{S_i}(\vartheta_i) \right) \ll 3H^2 M_P^2,$$
 (C.16)

where N is the number of spectator sectors. For each spectator, the maximum value of the kinetic energy is

$$\frac{\dot{\vartheta_{i*}}^2}{2} = 3H^2 M_P^2 \frac{\varepsilon_{\vartheta_{i*}}}{3} \,. \tag{C.17}$$

The maximum of the potential,  $V_{S_i}^{\max}(\vartheta_i) = \Lambda_i^4$ , can also be written in terms of the slow-roll parameter  $\varepsilon_{\vartheta_{i*}}$  using the expression  $\dot{\vartheta}_{i*} = f_i H \delta_i$  from Eq. (5.54), in combination with the relation  $\delta_i = \Lambda_i^4/(6H^2f_i^2)$ :

$$V_{S_i}^{\text{max}}(\vartheta_i) = 3H^2 M_P^2 \frac{4\varepsilon_{\vartheta_{i*}}}{\delta_i}. \tag{C.18}$$

With Eqs. (C.17) and (C.18), one obtains

$$\sum_{i=1}^{N} \rho_{\vartheta_{i}}^{\max} = 3H^{2}M_{P}^{2} \sum_{i=1}^{N} \left( \frac{\varepsilon_{\vartheta_{i*}}}{3} + \frac{4\varepsilon_{\vartheta_{i*}}}{\delta_{i}} \right) \simeq 3H^{2}M_{P}^{2} \sum_{i=1}^{N} \frac{4\varepsilon_{\vartheta_{i*}}}{\delta_{i}} \ll 3H^{2}M_{P}^{2}$$

$$\iff \sum_{i=1}^{N} \frac{\varepsilon_{\vartheta_{i*}}}{\delta_{i}} \ll \frac{1}{4}.$$
(C.19)

<sup>&</sup>lt;sup>1</sup>Perturbativity bounds are, ultimately, conditions imposed on loop corrections (induced by the Chern-Simons coupling) to the tree-level propagators of axion and gauge fields (see e.g. Fig. 3 of [161]).

This condition can be rewritten as

$$\sum_{i=1}^{N} \delta_i f_i^2 \ll \frac{M_P^2}{2} \,. \tag{C.20}$$

where the relation  $\varepsilon_{\vartheta_{i*}} = \delta_i^2 f_i^2/(2M_P^2)$  was employed. As an example, for values of the axion decay constant of order  $10^{-3}M_P$  to  $0.1\,M_P$ , Eq. (C.20) provides the corresponding upper bounds on the total number of axions,  $N^{\max} \in [10^2, 10^6]$  (assuming  $\delta_i$  values of order 0.5, as in the main text, and the same value of f for all spectators).

The second backreaction constraint arises from requiring that the gauge fields amplification does not alter the motion of the axions. To this end, it was verified in [161] that it suffices to impose the condition  $\rho_A^{\text{max}} \ll \dot{\vartheta}_*^2/2$  ( $\rho_A$  being the gauge field energy density). Explicit expressions, and the corresponding inequalities, were derived for  $\rho_A^{\text{max}}$  in [161]. Those results straightforwardly apply to the case of multiple spectators, as the various sectors are only minimally coupled to one another. The same goes for the perturbativity constraints worked out in the same paper, these being inherent to each individual sector. These combined backreaction and perturbativity constraints lead to the following conditions [161]:

$$\delta = 0.2: \quad 2 \cdot 10^{-5} e^{2.74\xi_*} \sqrt{\varepsilon_{\phi}} \lesssim \frac{f}{M_p} \lesssim 0.71 ,$$

$$\delta = 0.5: \quad \text{Max} \left[ 1.4 \cdot 10^{-5} e^{2.42\xi_*} \sqrt{\varepsilon_{\phi}}, 5.1 \cdot 10^{-6} e^{2.60\xi_*} \sqrt{\varepsilon_{\phi}} \right] \lesssim \frac{f}{M_p} \lesssim 0.28 ,$$
(C.21)

where  $\delta = 0.2, 0.5$  are two of the sample values of  $\delta$  considered also in the present manuscript. In each case, the second inequality is automatically satisfied given that  $f \lesssim M_p$ .

In the main text, for the computation of the power spectra, we used the value  $\varepsilon_{\phi} \sim 10^{-3}$ . If we take as reference  $f \sim 0.3 M_p$ , the bounds in ?? can then be rewritten as:

$$\delta = 0.2: \quad 6.32 \cdot 10^{-7} e^{2.74\xi_*} \lesssim 0.3 \implies \xi_* \lesssim 4.8,$$

$$\delta = 0.5: \quad \text{Max} \left[ 4.4 \cdot 10^{-7} e^{2.42\xi_*}, 1.6 \cdot 10^{-7} e^{2.60\xi_*} \right] \lesssim 0.3 \implies \xi_* \lesssim 5.5,$$
(C.22)

These  $\xi_*^{\rm max}$  values are fairly close to the benchmark points in Table 5.3. A signal at the level of the stochastic background observed with PTA would therefore saturate both perturbativity and weak backreaction constraints. Similar conclusions can be drawn for the other cases we considered,  $\delta = 0.3$  and  $\delta = 0.6$ .

# Appendix D

# Gravitational Chern-Simons Couplings in Type IIB Orientifolds

In this appendix we derive the coupling of 4D  $C_4$  axions to  $R\widetilde{R}$  terms in Type IIB orientifolds. Following [331], we assume a product ansatz for spacetime of the form  $\mathbb{R}^{3,1} \times \widetilde{X}_6$ . Here  $\widetilde{X}_6 = X_6/\mathcal{P}$  is the orientifold, while  $X_6$  is a Calabi-Yau 3-fold and  $\mathcal{P}$  is an orientifold projection defined via an isomorphic and holomorphic involution  $\sigma$  of  $X_6$ . We assume a product metric:

$$g_{10} := g_{\mu\nu} \ dx^{\mu} \otimes dx^{\nu} + 2g_{i\bar{j}}(y) \ dy^{i} \otimes d\bar{y}^{\bar{j}} \ .$$
 (D.1)

The effective 4D action bulk terms can be obtained from dimensional reduction of the 10D type IIB fields. In particular, the  $C_4$  expansion is

$$C_4 = \rho_{\alpha}(x)\widetilde{\omega}^{\alpha}(y) + \dots,$$
 (D.2)

where the  $\{\widetilde{\omega}^{\alpha}\}$ ,  $\alpha=1,...,h_{2,2}^+$ , form a basis for  $H_{\bar{\partial},+}^{(2,2)}(X_6)$  We will assume that there is a D7-brane permeating spacetime and wrapping a 4-cycle  $S_+$  of  $\widetilde{X}_6$  such that the worldvolume of the brane is

$$\mathcal{W} := \mathbb{R}^{3,1} \times S_+ \,. \tag{D.3}$$

We will denote the embedding map of the worldvolume as  $\varphi : \mathcal{W} \hookrightarrow \mathbb{R}^{3,1} \times \widetilde{X}_6$ . Note also that  $S_+ \in H_4(X_6, \mathbb{Z})$  and is the union of two 4-cycles  $S_1$  and  $S_2$  in  $X_6$ . We will denote the embedding map as  $\iota : S_+ \hookrightarrow X_6$ . The pullback of eq. (D.1) is

$$\varphi^* g_{10} = g_{\mu\nu} dx^{\mu} \otimes dx^{\nu} + 2g_{i\bar{j}}(y) dy^i \otimes d\bar{y}^{\bar{j}} + 2g_{i\bar{j}}(y) \partial_{\mu} \xi^i \partial_{\nu} \bar{\xi}^{\bar{j}} dx^{\mu} \otimes dx^{\nu}, \qquad (D.4)$$

where the internal part is suitably restricted to the wrapped 4-cycle. For the moment, we will set the fluctuations  $\xi^i = 0$ . Then the worldvolume metric can be written as

$$\varphi^* g_{10} = \eta_{\alpha\beta} \theta^{\alpha} \otimes \theta^{\alpha} + 2\delta_{I\bar{J}} \widetilde{\theta}^I \wedge \widetilde{\theta}^J , \qquad (D.5)$$

where  $\theta^{\alpha} := e^{\alpha}_{\ \mu} dx^{\mu}$  and  $\widetilde{\theta}^{I} := e^{I}_{i} dy^{i}$  define a non-coordinate basis via the external and internal vielbeins. Since the internal and external vielbeins depend only on external and internal coordinates, respectively, the Cartan structure equations imply that the

connection 1-form splits into independent external and internal pieces. The curvature 2-form follows the same behavior. Therefore, the curvature 2-form of the tangent bundle is block-diagonal between the external and internal pieces.

The relevant parts of the D7-brane Chern-Simons action are

$$S_{D7} \supset \mu_7 \int_{\mathcal{W}} \frac{1}{2} (2\pi\alpha')^2 \varphi^*(C_4) \wedge \frac{N}{48} \left( \operatorname{tr}(R_T \wedge R_T) - \operatorname{tr}(R_N \wedge R_N) \right). \tag{D.6}$$

Where  $R_{T/N}$  are the curvature forms of the tangent/normal bundle of W. From the above, we know that

$$\operatorname{tr}(R_T \wedge R_T) = \operatorname{tr}(R_{ST} \wedge R_{ST}) + \operatorname{tr}(R_+ \wedge R_+). \tag{D.7}$$

Thus we find a 4D coupling

$$S_{4D} \supset \frac{N\mu_7}{48} \int_{M_4} \frac{1}{2} (2\pi\alpha')^2 \ell_S^4 \rho_+ \operatorname{tr}(R_{ST} \wedge R_{ST})$$

$$= \frac{N}{192\pi} \int_{M_4} \rho_+ \operatorname{tr}(R_{ST} \wedge R_{ST})$$

$$= \frac{2\pi N}{48} \int \rho_+ p_1(R_{ST}).$$
(D.8)

Where  $p_1(R_{ST})$  is the first Pontrjagin class. For a 4D spin manifold, the integral of Pontrjagin class is quantized as

$$\int_{X_4} p_1(R_2) = 48m \tag{D.9}$$

with  $m \in \mathbb{Z}$ . Thus  $e^{iS_{4D}}$  is invariant under  $\rho_+ \to \rho_+ + n$  with  $n \in \mathbb{Z}$ . We can define a canonically-normalized axion via

$$\rho_{+} = \frac{\vartheta}{2\pi f_{\vartheta}} \tag{D.10}$$

Then we have a coupling

$$S_{4D} \supset \frac{N}{1536\pi^2} \int_{M_4} \frac{\vartheta}{f_{\vartheta}} R^{\mu\nu}_{\rho\sigma} R_{\mu\nu\alpha\beta} \varepsilon^{\rho\sigma\alpha\beta} d^4x \tag{D.11}$$

We can now define the coupling  $g_{\theta hh}$  we use in the action:

$$\mathcal{L} \supset \frac{g_{\theta hh}}{4} \vartheta \varepsilon_{\mu\nu\rho\sigma} R^{\mu\nu}_{\alpha\beta} R^{\rho\sigma\alpha\beta} , \qquad (D.12)$$

$$g_{\theta hh} = \frac{N}{384\pi^2 f_{\vartheta}}.$$
 (D.13)

# D.1 Axion Higgs coupling

In this appendix we derive the contribution to the kinetic terms of the axion fields coming from the Giudice-Masiero terms in the Kähler potential (cf. eq. (7.112)), introduced in order to allow a reheating process.

Recall that the kinetic terms will be given by  $K_{i\bar{j}}\partial_{\mu}\theta^{i}\partial^{\mu}\theta^{\bar{j}}$  where the Kähler metric is given by

$$K_{i\bar{j}} = \partial_{T_i} \partial_{\bar{T}_i} K. \tag{D.14}$$

Let us then consider the Giudice-Masiero terms of the form:

$$K \supset \frac{H\bar{H}}{\left(T_1 + \bar{T}_1\right)^{y_1} \left(T_2 + \bar{T}_2\right)^{y_2}}.$$
 (D.15)

The contribution to the kinetic terms then reads:

$$\mathcal{L} \supset \frac{y_{1}(y_{1}+1)}{\left(T_{1}+\bar{T}_{1}\right)^{y_{1}+2}\left(T_{2}+\bar{T}_{2}\right)^{y_{2}}}H\bar{H}\partial_{\mu}\theta_{1}\partial^{\mu}\theta_{1} + \frac{y_{1}y_{2}}{\left(T_{1}+\bar{T}_{1}\right)^{y_{1}+1}\left(T_{2}+\bar{T}_{2}\right)^{y_{2}+1}}H\bar{H}\partial_{\mu}\theta_{1}\partial^{\mu}\theta_{2} + \frac{y_{2}(y_{2}+1)}{\left(T_{1}+\bar{T}_{1}\right)^{y_{1}}\left(T_{2}+\bar{T}_{2}\right)^{y_{2}+2}}H\bar{H}\partial_{\mu}\theta_{2}\partial^{\mu}\theta_{2}.$$
(D.16)

Canonically normalizing the axions with the decay constants derived from the tree level Kähler potential  $f_i \sim \frac{1}{(T_i + \bar{T}_i)}$  in units of  $M_{\rm Pl}$ , we can rewrite the equation above as

$$\mathcal{L} \supset H\bar{H}f_1^{y_1}f_2^{y_2}\left(y_1(y_1+1)\partial_\mu\vartheta_1\partial^\mu\vartheta_1 + y_1y_2\partial_\mu\vartheta_1\partial^\mu\vartheta_2 + y_2(y_2+1)\partial_\mu\vartheta_2\partial^\mu\vartheta_2\right). \tag{D.17}$$

If we now reduce to the simple case where  $y_1 = 1$  and  $y_2 = 0$ , the above reduces to the single term

$$\mathcal{L} \supset 2f_1 H \bar{H} \partial_\mu \vartheta_1 \partial^\mu \vartheta_1 \,. \tag{D.18}$$

This corresponds to a  $2 \to 2$  scattering for which we can simply compute the cross-section and the corresponding decay rate, knowing now that the vertex is  $\sim f_1|p_{\vartheta}|^2$  in units of  $M_{\rm Pl}$ . The differential cross section thus reads

$$\frac{d\sigma}{d\Omega_{CM}} = \frac{1}{64\pi^2 s} |\mathcal{M}|^2 \frac{|p_f|}{|p_i|}, \tag{D.19}$$

where the Feynman amplitude  $|\mathcal{M}| \sim \left| \frac{f_q p_{\vartheta}^2}{M_{\text{Pl}}} \right|$  and  $s = (p + p')^2 = 4(m_{\vartheta}^2 + |p_{\vartheta}|^2)$ . The scattering rate  $\Gamma_{\theta\theta\to HH} = n\sigma v$  therefore reads:

$$\Gamma_{\vartheta\vartheta\to HH} \sim \frac{1}{64\pi} \frac{\rho_{\vartheta}}{m_{\vartheta}} \frac{1}{m_{\vartheta}^2 + |\vec{p}_{\vartheta}|^2} f_{\vartheta}^2 |\vec{p}_{\vartheta}|^4 \frac{|\vec{p}_{\vartheta}|}{m_{\vartheta}} \sqrt{1 + \frac{m_{\vartheta}^2}{m_{\varphi}^2}}. \tag{D.20}$$

In the above we used the fact that  $n_{\vartheta} = \rho_{\vartheta}/m_{\vartheta}$  and  $v = \frac{p_{\vartheta}}{m_{\vartheta}}$ .

- [1] F. Englert and R. Brout. Broken Symmetry and the Mass of Gauge Vector Mesons. *Phys. Rev. Lett.*, 13:321–323, 1964.
- [2] Peter W. Higgs. Broken symmetries, massless particles and gauge fields. *Phys. Lett.*, 12:132–133, 1964.
- [3] Georges Aad et al. Observation of a new particle in the search for the Standard Model Higgs boson with the ATLAS detector at the LHC. *Phys. Lett. B*, 716:1–29, 2012.
- [4] Serguei Chatrchyan et al. Observation of a New Boson with Mass Near 125 GeV in pp Collisions at  $\sqrt{s} = 7$  and 8 TeV. *JHEP*, 06:081, 2013.
- [5] Alan H. Guth. The Inflationary Universe: A Possible Solution to the Horizon and Flatness Problems. *Phys. Rev. D*, 23:347–356, 1981.
- [6] Andrei D. Linde. A New Inflationary Universe Scenario: A Possible Solution of the Horizon, Flatness, Homogeneity, Isotropy and Primordial Monopole Problems. *Phys. Lett. B*, 108:389–393, 1982.
- [7] Andreas Albrecht and Paul J. Steinhardt. Cosmology for Grand Unified Theories with Radiatively Induced Symmetry Breaking. *Phys. Rev. Lett.*, 48:1220–1223, 1982.
- [8] Hans Peter Nilles. Supersymmetry, Supergravity and Particle Physics. *Phys. Rept.*, 110:1–162, 1984.
- [9] Rudolf Haag, Jan T. Lopuszanski, and Martin Sohnius. All Possible Generators of Supersymmetries of the s Matrix. *Nucl. Phys. B*, 88:257, 1975.
- [10] J. Wess and B. Zumino. Supergauge transformations in four dimensions. *Nuclear Physics B*, 70(1):39–50, 1974.
- [11] Daniel Z. Freedman, P. van Nieuwenhuizen, and S. Ferrara. Progress Toward a Theory of Supergravity. *Phys. Rev. D*, 13:3214–3218, 1976.
- [12] E. Bergshoeff, M. de Roo, B. de Wit, and P. van Nieuwenhuizen. Ten-Dimensional Maxwell-Einstein Supergravity, Its Currents, and the Issue of Its Auxiliary Fields. Nucl. Phys. B, 195:97–136, 1982.
- [13] R. D. Peccei and Helen R. Quinn. CP Conservation in the Presence of Instantons. Phys. Rev. Lett., 38:1440–1443, 1977.
- [14] Peter Syrcek and Edward Witten. Axions In String Theory. JHEP, 06:051, 2006.

[15] Asimina Arvanitaki, Savas Dimopoulos, Sergei Dubovsky, Nemanja Kaloper, and John March-Russell. String Axiverse. *Phys. Rev. D*, 81:123530, 2010.

- [16] Bobby Samir Acharya, Konstantin Bobkov, and Piyush Kumar. An M Theory Solution to the Strong CP Problem and Constraints on the Axiverse. *JHEP*, 11:105, 2010.
- [17] Michele Cicoli, Mark Goodsell, and Andreas Ringwald. The type IIB string axiverse and its low-energy phenomenology. *JHEP*, 10:146, 2012.
- [18] Mehmet Demirtas, Cody Long, Liam McAllister, and Mike Stillman. The Kreuzer-Skarke Axiverse. *JHEP*, 04:138, 2020.
- [19] Mehmet Demirtas, Naomi Gendler, Cody Long, Liam McAllister, and Jakob Moritz. PQ Axiverse. 12 2021.
- [20] Igor Broeckel, Michele Cicoli, Anshuman Maharana, Kajal Singh, and Kuver Sinha. Moduli Stabilisation and the Statistics of SUSY Breaking in the Landscape. JHEP, 10:015, 2020.
- [21] Y. Akra2021mi et al. Planck 2018 results. X. Constraints on inflation. *Astron. Astrophys.*, 641:A10, 2020.
- [22] Daniel Baumann and Liam McAllister. *Inflation and String Theory*. Cambridge Monographs on Mathematical Physics. Cambridge University Press, 5 2015.
- [23] David H. Lyth and Antonio Riotto. Particle physics models of inflation and the cosmological density perturbation. *Phys. Rept.*, 314:1–146, 1999.
- [24] P. A. R. Ade et al. Improved Constraints on Primordial Gravitational Waves using Planck, WMAP, and BICEP/Keck Observations through the 2018 Observing Season. *Phys. Rev. Lett.*, 127(15):151301, 2021.
- [25] Amit Giveon, Massimo Porrati, and Eliezer Rabinovici. Target space duality in string theory. *Physics Reports*, 244(2–3):77–202, August 1994.
- [26] Joseph Polchinski. Dirichlet Branes and Ramond-Ramond Charges. *Phys. Rev. Lett.*, 75:4724–4727, 1995.
- [27] Ralph Blumenhagen, Mirjam Cvetič, Paul Langacker, and Gary Shiu. Toward realistic intersecting d-brane models. *Annual Review of Nuclear and Particle Science*, 55(1):71–139, December 2005.
- [28] Steven B. Giddings, Shamit Kachru, and Joseph Polchinski. Hierarchies from fluxes in string compactifications. *Phys. Rev. D*, 66:106006, 2002.
- [29] Sergei Gukov, Cumrun Vafa, and Edward Witten. CFT's from Calabi-Yau four folds. Nucl. Phys. B, 584:69–108, 2000. [Erratum: Nucl.Phys.B 608, 477–478 (2001)].
- [30] Shamit Kachru, Renata Kallosh, Andrei D. Linde, and Sandip P. Trivedi. De Sitter vacua in string theory. *Phys. Rev. D*, 68:046005, 2003.
- [31] Vijay Balasubramanian, Per Berglund, Joseph P. Conlon, and Fernando Quevedo. Systematics of moduli stabilisation in Calabi-Yau flux compactifications. *JHEP*, 03:007, 2005.

[32] Iosif Bena, Mariana Grana, Stanislav Kuperstein, and Stefano Massai. Anti-D3 Branes: Singular to the bitter end. *Phys. Rev. D*, 87(10):106010, 2013.

- [33] Ben Michel, Eric Mintun, Joseph Polchinski, Andrea Puhm, and Philip Saad. Remarks on brane and antibrane dynamics. *JHEP*, 09:021, 2015.
- [34] Xin Gao, Pramod Shukla, and Rui Sun. On Missing Bianchi Identities in Cohomology Formulation. Eur. Phys. J. C, 79(9):781, 2019.
- [35] Michele Cicoli, Denis Klevers, Sven Krippendorf, Christoph Mayrhofer, Fernando Quevedo, and Roberto Valandro. Explicit de Sitter Flux Vacua for Global String Models with Chiral Matter. JHEP, 05:001, 2014.
- [36] Georges Obied, Hirosi Ooguri, Lev Spodyneiko, and Cumrun Vafa. De Sitter Space and the Swampland. 6 2018.
- [37] Hirosi Ooguri, Eran Palti, Gary Shiu, and Cumrun Vafa. Distance and de Sitter Conjectures on the Swampland. Phys. Lett. B, 788:180–184, 2019.
- [38] Sumit K. Garg and Chethan Krishnan. Bounds on Slow Roll and the de Sitter Swampland. *JHEP*, 11:075, 2019.
- [39] Renata Kallosh, Andrei Linde, Evan McDonough, and Marco Scalisi. dS Vacua and the Swampland. *JHEP*, 03:134, 2019.
- [40] David Andriot and Christoph Roupec. Further refining the de Sitter swampland conjecture. Fortsch. Phys., 67(1-2):1800105, 2019.
- [41] Niccolò Cribiori and Daniel Junghans. No classical (anti-)de Sitter solutions with O8-planes. *Phys. Lett. B*, 793:54–58, 2019.
- [42] Hirosi Ooguri and Cumrun Vafa. On the Geometry of the String Landscape and the Swampland. *Nucl. Phys. B*, 766:21–33, 2007.
- [43] Eva Silverstein and Alexander Westphal. Monodromy in the CMB: Gravity Waves and String Inflation. *Phys. Rev. D*, 78:106003, 2008.
- [44] Liam McAllister, Eva Silverstein, and Alexander Westphal. Gravity Waves and Linear Inflation from Axion Monodromy. *Phys. Rev. D*, 82:046003, 2010.
- [45] Nemanja Kaloper and Lorenzo Sorbo. A Natural Framework for Chaotic Inflation. *Phys. Rev. Lett.*, 102:121301, 2009.
- [46] Nemanja Kaloper, Albion Lawrence, and Lorenzo Sorbo. An Ignoble Approach to Large Field Inflation. JCAP, 03:023, 2011.
- [47] M. Cicoli, C. P. Burgess, and F. Quevedo. Fibre Inflation: Observable Gravity Waves from IIB String Compactifications. *JCAP*, 03:013, 2009.
- [48] Joseph P. Conlon and Fernando Quevedo. Kahler moduli inflation. *JHEP*, 01:146, 2006.
- [49] Sven Krippendorf and Fernando Quevedo. Metastable SUSY Breaking, de Sitter Moduli Stabilisation and Kahler Moduli Inflation. *JHEP*, 11:039, 2009.
- [50] S Dimopoulos, S Kachru, J McGreevy, and J G Wacker. N-flation. Journal of Cosmology and Astroparticle Physics, 2008(08):003, August 2008.

[51] Gia Dvali. Infrared hierarchy, thermal brane inflation and superstrings as superheavy dark matter. *Physics Letters B*, 459(4):489–496, July 1999.

[52] C. P. Burgess and F. Quevedo. Rg-induced modulus stabilization: perturbative de sitter vacua and improved d3-

 $\overline{d3}$ 

- inflation. Journal of High Energy Physics, 2022(6), June 2022.
- [53] Shamit Kachru, Renata Kallosh, Andrei D. Linde, Juan Martin Maldacena, Liam P. McAllister, and Sandip P. Trivedi. Towards inflation in string theory. JCAP, 10:013, 2003.
- [54] Edward Witten. Some Properties of O(32) Superstrings. *Phys. Lett. B*, 149:351–356, 1984.
- [55] Arthur Hebecker, Jakob Moritz, Alexander Westphal, and Lukas T. Witkowski. Axion Monodromy Inflation with Warped KK-Modes. *Phys. Lett. B*, 754:328–334, 2016. [Erratum: Phys.Lett.B 767, 493–493 (2017)].
- [56] Arthur Hebecker, Sascha Leonhardt, Jakob Moritz, and Alexander Westphal. Thraxions: Ultralight Throat Axions. *JHEP*, 04:158, 2019.
- [57] Federico Carta, Alessandro Mininno, Nicole Righi, and Alexander Westphal. Thraxions: towards full string models. JHEP, 01:082, 2022.
- [58] Michael R. Douglas and Shamit Kachru. Flux compactification. Rev. Mod. Phys., 79:733–796, 2007.
- [59] Thomas W. Grimm and Washington Taylor. Structure in 6D and 4D N=1 supergravity theories from F-theory. *JHEP*, 10:105, 2012.
- [60] C. Abel et al. Measurement of the Permanent Electric Dipole Moment of the Neutron. Phys. Rev. Lett., 124(8):081803, 2020.
- [61] Steven Weinberg. A New Light Boson? Phys. Rev. Lett., 40:223–226, 1978.
- [62] Frank Wilczek. Problem of Strong P and T Invariance in the Presence of Instantons. Phys. Rev. Lett., 40:279–282, 1978.
- [63] Jihn E. Kim. Weak Interaction Singlet and Strong CP Invariance. Phys. Rev. Lett., 43:103, 1979.
- [64] Mikhail A. Shifman, A. I. Vainshtein, and Valentin I. Zakharov. Can Confinement Ensure Natural CP Invariance of Strong Interactions? *Nucl. Phys. B*, 166:493–506, 1980.
- [65] A. R. Zhitnitsky. On Possible Suppression of the Axion Hadron Interactions. (In Russian). Sov. J. Nucl. Phys., 31:260, 1980.
- [66] Michael Dine, Willy Fischler, and Mark Srednicki. A Simple Solution to the Strong CP Problem with a Harmless Axion. *Phys. Lett. B*, 104:199–202, 1981.
- [67] Joseph P. Conlon. The QCD axion and moduli stabilisation. JHEP, 05:078, 2006.
- [68] Kang-Sin Choi, Ian-Woo Kim, and Jihn E. Kim. String compactification, QCD axion and axion-photon-photon coupling. JHEP, 03:116, 2007.

[69] Michele Cicoli, Veronica Guidetti, Nicole Righi, and Alexander Westphal. Fuzzy Dark Matter candidates from string theory. *JHEP*, 05:107, 2022.

- [70] Naomi Gendler, David J. E. Marsh, Liam McAllister, and Jakob Moritz. Glimmers from the Axiverse. 9 2023.
- [71] Elijah Sheridan, Federico Carta, Naomi Gendler, Mudit Jain, David J. E. Marsh, Liam McAllister, Nicole Righi, Keir K. Rogers, and Andreas Schachner. Fuzzy Axions and Associated Relics. 12 2024.
- [72] Junyi Cheng and Naomi Gendler. Universality in the Axiverse. 7 2025.
- [73] Ema Dimastrogiovanni, Matteo Fasiello, Jacob M. Leedom, Margherita Putti, and Alexander Westphal. Gravitational axiverse spectroscopy: seeing the forest for the axions. JHEP, 08:072, 2024.
- [74] Marc Kamionkowski and John March-Russell. Planck scale physics and the Peccei-Quinn mechanism. *Phys. Lett. B*, 282:137–141, 1992.
- [75] Richard Holman, Stephen D. H. Hsu, Thomas W. Kephart, Edward W. Kolb, Richard Watkins, and Lawrence M. Widrow. Solutions to the strong CP problem in a world with gravity. *Phys. Lett. B*, 282:132–136, 1992.
- [76] Stephen M. Barr and D. Seckel. Planck scale corrections to axion models. Phys. Rev. D, 46:539–549, 1992.
- [77] Maximilian Kreuzer and Harald Skarke. Complete classification of reflexive polyhedra in four-dimensions. Adv. Theor. Math. Phys., 4:1209–1230, 2000.
- [78] Mehmet Demirtas, Manki Kim, Liam McAllister, and Jakob Moritz. Conifold Vacua with Small Flux Superpotential. *Fortsch. Phys.*, 68:2000085, 2020.
- [79] Michele Cicoli, Andreas Schachner, and Pramod Shukla. Systematics of type IIB moduli stabilisation with odd axions. *JHEP*, 04:003, 2022.
- [80] Wayne Hu, Rennan Barkana, and Andrei Gruzinov. Cold and fuzzy dark matter. *Phys. Rev. Lett.*, 85:1158–1161, 2000.
- [81] Lam Hui, Jeremiah P. Ostriker, Scott Tremaine, and Edward Witten. Ultralight scalars as cosmological dark matter. *Phys. Rev. D*, 95(4):043541, 2017.
- [82] Peter W. Graham, Igor G. Irastorza, Steven K. Lamoreaux, Axel Lindner, and Karl A. van Bibber. Experimental Searches for the Axion and Axion-Like Particles. Ann. Rev. Nucl. Part. Sci., 65:485–514, 2015.
- [83] Igor G. Irastorza and Javier Redondo. New experimental approaches in the search for axion-like particles. *Prog. Part. Nucl. Phys.*, 102:89–159, 2018.
- [84] Katherine Freese, Joshua A. Frieman, and Angela V. Olinto. Natural inflation with pseudo Nambu-Goldstone bosons. *Phys. Rev. Lett.*, 65:3233–3236, 1990.
- [85] Danjie Wenren. Tilt and Tensor-to-Scalar Ratio in Multifield Monodromy Inflation. 5 2014.
- [86] Guido D'Amico, Nemanja Kaloper, and Alexander Westphal. General double monodromy inflation. *Phys. Rev. D*, 105(10):103527, 2022.

[87] Guido D'Amico, Nemanja Kaloper, and Alexander Westphal. Double Monodromy Inflation: A Gravity Waves Factory for CMB-S4, LiteBIRD and LISA. Phys. Rev. D, 104(8):L081302, 2021.

- [88] Jihn E. Kim, Hans Peter Nilles, and Marco Peloso. Completing natural inflation. JCAP, 01:005, 2005.
- [89] S. Dimopoulos, S. Kachru, J. McGreevy, and Jay G. Wacker. N-flation. JCAP, 08:003, 2008.
- [90] Sudhakar Panda, Yoske Sumitomo, and Sandip P. Trivedi. Axions as Quintessence in String Theory. *Phys. Rev. D*, 83:083506, 2011.
- [91] Michele Cicoli, Francisco G. Pedro, and Gianmassimo Tasinato. Natural Quintessence in String Theory. *JCAP*, 07:044, 2012.
- [92] Neil Barnaby, Enrico Pajer, and Marco Peloso. Gauge Field Production in Axion Inflation: Consequences for Monodromy, non-Gaussianity in the CMB, and Gravitational Waves at Interferometers. *Phys. Rev. D*, 85:023525, 2012.
- [93] Emanuela Dimastrogiovanni, Matteo Fasiello, and Tomohiro Fujita. Primordial Gravitational Waves from Axion-Gauge Fields Dynamics. *JCAP*, 01:019, 2017.
- [94] J. Chluba et al. New horizons in cosmology with spectral distortions of the cosmic microwave background. *Exper. Astron.*, 51(3):1515–1554, 2021.
- [95] Margherita Putti, Nicola Bartolo, Sukannya Bhattacharya, and Marco Peloso. CMB spectral distortions from enhanced primordial perturbations: the role of spectator axions. 3 2024.
- [96] Michele Cicoli, Joseph P. Conlon, and Fernando Quevedo. Dark radiation in LARGE volume models. *Phys. Rev. D*, 87(4):043520, 2013.
- [97] Stephen Angus. Dark Radiation in Anisotropic LARGE Volume Compactifications. JHEP, 10:184, 2014.
- [98] Tom Banks, Michael Dine, and Elie Gorbatov. Is there a string theory landscape? *JHEP*, 08:058, 2004.
- [99] Volker Braun, Yang-Hui He, Burt A. Ovrut, and Tony Pantev. The Exact MSSM spectrum from string theory. *JHEP*, 05:043, 2006.
- [100] Evgeny I. Buchbinder and Burt A. Ovrut. Vacuum stability in heterotic M theory. *Phys. Rev. D*, 69:086010, 2004.
- [101] Michael Dine and N. Seiberg. Nonrenormalization Theorems in Superstring Theory. Phys. Rev. Lett., 57:2625, 1986.
- [102] Ralph Blumenhagen, Mirjam Cvetic, Shamit Kachru, and Timo Weigand. D-Brane Instantons in Type II Orientifolds. *Ann. Rev. Nucl. Part. Sci.*, 59:269–296, 2009.
- [103] Melanie Becker, Gottfried Curio, and Axel Krause. De Sitter vacua from heterotic M theory. Nucl. Phys. B, 693:223–260, 2004.
- [104] Lara B. Anderson, James Gray, Andre Lukas, and Burt Ovrut. Stabilizing All Geometric Moduli in Heterotic Calabi-Yau Vacua. *Phys. Rev. D*, 83:106011, 2011.

[105] Jacob M. Leedom, Nicole Righi, and Alexander Westphal. Heterotic de Sitter beyond modular symmetry. *JHEP*, 02:209, 2023.

- [106] Kiwoon Choi and Jihn E. Kim. Harmful Axions in Superstring Models. *Phys. Lett.* B, 154:393, 1985. [Erratum: Phys.Lett.B 156, 452 (1985)].
- [107] Kiwoon Choi and Jihn E. Kim. Compactification and Axions in E(8) x E(8)-prime Superstring Models. *Phys. Lett. B*, 165:71–75, 1985.
- [108] Tom Banks and Michael Dine. Couplings and scales in strongly coupled heterotic string theory. *Nucl. Phys. B*, 479:173–196, 1996.
- [109] Mary K. Gaillard and Ben Kain. Is the universal string axion the QCD axion? *Nucl. Phys. B*, 734:116–137, 2006.
- [110] B. de Carlos, J. A. Casas, and C. Munoz. Supersymmetry breaking and determination of the unification gauge coupling constant in string theories. *Nucl. Phys. B*, 399:623–653, 1993.
- [111] Sergei Gukov, Shamit Kachru, Xiao Liu, and Liam McAllister. Heterotic moduli stabilization with fractional Chern-Simons invariants. *Phys. Rev. D*, 69:086008, 2004.
- [112] Mary K. Gaillard and Brent D. Nelson. Kahler stabilized, modular invariant heterotic string models. *Int. J. Mod. Phys. A*, 22:1451–1588, 2007.
- [113] Marco Serone and Alexander Westphal. Moduli Stabilization in Meta-Stable Heterotic Supergravity Vacua. *JHEP*, 08:080, 2007.
- [114] Lara B. Anderson, James Gray, Andre Lukas, and Burt Ovrut. Stabilizing the Complex Structure in Heterotic Calabi-Yau Vacua. *JHEP*, 02:088, 2011.
- [115] Ben Dundee, Stuart Raby, and Alexander Westphal. Moduli stabilization and SUSY breaking in heterotic orbifold string models. *Phys. Rev. D*, 82:126002, 2010.
- [116] Susha L. Parameswaran, Saul Ramos-Sanchez, and Ivonne Zavala. On Moduli Stabilisation and de Sitter Vacua in MSSM Heterotic Orbifolds. *JHEP*, 01:071, 2011.
- [117] Michele Cicoli, Senarath de Alwis, and Alexander Westphal. Heterotic Moduli Stabilisation. *JHEP*, 10:199, 2013.
- [118] Stephen H. Shenker. The Strength of nonperturbative effects in string theory. In Cargese Study Institute: Random Surfaces, Quantum Gravity and Strings, pages 809–819, 8 1990.
- [119] Philip Candelas, Xenia C. De La Ossa, Paul S. Green, and Linda Parkes. A Pair of Calabi-Yau manifolds as an exactly soluble superconformal theory. *Nucl. Phys. B*, 359:21–74, 1991.
- [120] T. Barreiro, B. de Carlos, and Edmund J. Copeland. On nonperturbative corrections to the Kahler potential. *Phys. Rev. D*, 57:7354–7360, 1998.
- [121] Katrin Becker, Melanie Becker, Michael Haack, and Jan Louis. Supersymmetry breaking and alpha-prime corrections to flux induced potentials. *JHEP*, 06:060, 2002.

[122] Lilia Anguelova, Callum Quigley, and Savdeep Sethi. The Leading Quantum Corrections to Stringy Kahler Potentials. *JHEP*, 10:065, 2010.

- [123] Prateek Agrawal, Michael Nee, and Mario Reig. Axion couplings in grand unified theories. *JHEP*, 10:141, 2022.
- [124] Prateek Agrawal, Michael Nee, and Mario Reig. Axion couplings in heterotic string theory. *JHEP*, 02:188, 2025.
- [125] Mario Reig and Timo Weigand. Testing the Heterotic String with the Axion-Photon Coupling. 9 2025.
- [126] Brett McInnes. The Semispin groups in string theory. J. Math. Phys., 40:4699–4712, 1999.
- [127] Brett McInnes. Gauge spinors and string duality. Nucl. Phys. B, 577:439–460, 2000.
- [128] David J. Gross, Jeffrey A. Harvey, Emil J. Martinec, and Ryan Rohm. The Heterotic String. *Phys. Rev. Lett.*, 54:502–505, 1985.
- [129] David J. Gross, Jeffrey A. Harvey, Emil J. Martinec, and Ryan Rohm. Heterotic String Theory. 2. The Interacting Heterotic String. *Nucl. Phys. B*, 267:75–124, 1986.
- [130] Volker Braun, Yang-Hui He, Burt A. Ovrut, and Tony Pantev. A Heterotic standard model. *Phys. Lett. B*, 618:252–258, 2005.
- [131] Wilfried Buchmuller, Koichi Hamaguchi, Oleg Lebedev, and Michael Ratz. Supersymmetric standard model from the heterotic string. *Phys. Rev. Lett.*, 96:121602, 2006.
- [132] Oleg Lebedev, Hans Peter Nilles, Stuart Raby, Saul Ramos-Sanchez, Michael Ratz, Patrick K. S. Vaudrevange, and Akin Wingerter. A Mini-landscape of exact MSSM spectra in heterotic orbifolds. *Phys. Lett. B*, 645:88–94, 2007.
- [133] Oleg Lebedev, Hans Peter Nilles, Stuart Raby, Saul Ramos-Sanchez, Michael Ratz, Patrick K. S. Vaudrevange, and Akin Wingerter. The Heterotic Road to the MSSM with R parity. *Phys. Rev. D*, 77:046013, 2008.
- [134] Lara B. Anderson, James Gray, Andre Lukas, and Eran Palti. Two Hundred Heterotic Standard Models on Smooth Calabi-Yau Threefolds. *Phys. Rev. D*, 84:106005, 2011.
- [135] S. K. Donaldson. ANTI SELF-DUAL YANG-MILLS CONNECTIONS OVER COMPLEX ALGEBRAIC SURFACES AND STABLE VECTOR BUNDLES. Proc. Lond. Math. Soc., 50:1–26, 1985.
- [136] K. Uhlenbeck and S. T. Yau. On the existence of hermitian-yang-mills connections in stable vector bundles. *Commun. Pure Appl. Math.*, 39(S1):S257–S293, 1986.
- [137] Edward Witten. Phases of N=2 theories in two-dimensions. *Nucl. Phys. B*, 403:159–222, 1993.
- [138] Ralph Blumenhagen, Boris Kors, Dieter Lust, and Stephan Stieberger. Four-dimensional String Compactifications with D-Branes, Orientifolds and Fluxes. Phys. Rept., 445:1–193, 2007.

[139] Lara B. Anderson, Yang-Hui He, and Andre Lukas. Monad Bundles in Heterotic String Compactifications. *JHEP*, 07:104, 2008.

- [140] Michael B. Green and John H. Schwarz. Anomaly Cancellation in Supersymmetric D=10 Gauge Theory and Superstring Theory. *Phys. Lett. B*, 149:117–122, 1984.
- [141] Arthur Hebecker and M. Trapletti. Gauge unification in highly anisotropic string compactifications. *Nucl. Phys. B*, 713:173–203, 2005.
- [142] Michael Dine, N. Seiberg, and Edward Witten. Fayet-Iliopoulos Terms in String Theory. *Nucl. Phys. B*, 289:589–598, 1987.
- [143] Vadim Kaplunovsky and Jan Louis. Field dependent gauge couplings in locally supersymmetric effective quantum field theories. *Nucl. Phys. B*, 422:57–124, 1994.
- [144] Lance J. Dixon, Vadim Kaplunovsky, and Jan Louis. Moduli dependence of string loop corrections to gauge coupling constants. *Nucl. Phys. B*, 355:649–688, 1991.
- [145] Michele Cicoli, Maximilian Kreuzer, and Christoph Mayrhofer. Toric K3-Fibred Calabi-Yau Manifolds with del Pezzo Divisors for String Compactifications. *JHEP*, 02:002, 2012.
- [146] Joseph P. Conlon, Fernando Quevedo, and Kerim Suruliz. Large-volume flux compactifications: Moduli spectrum and D3/D7 soft supersymmetry breaking. *JHEP*, 08:007, 2005.
- [147] Michele Cicoli, Joseph P Conlon, and Fernando Quevedo. Systematics of string loop corrections in type iib calabi-yau flux compactifications. *Journal of High Energy Physics*, 2008(01):052–052, January 2008.
- [148] Lara B. Anderson, James Gray, Andre Lukas, and Burt Ovrut. The Atiyah Class and Complex Structure Stabilization in Heterotic Calabi-Yau Compactifications. JHEP, 10:032, 2011.
- [149] Edward Witten. New Issues in Manifolds of SU(3) Holonomy. Nucl. Phys. B, 268:79, 1986.
- [150] G. Veneziano and S. Yankielowicz. An Effective Lagrangian for the Pure N=1 Supersymmetric Yang-Mills Theory. *Phys. Lett. B*, 113:231, 1982.
- [151] S. Ferrara, L. Girardello, and Hans Peter Nilles. Breakdown of Local Supersymmetry Through Gauge Fermion Condensates. *Phys. Lett. B*, 125:457, 1983.
- [152] A. Font, Luis E. Ibanez, D. Lust, and F. Quevedo. Supersymmetry Breaking From Duality Invariant Gaugino Condensation. *Phys. Lett. B*, 245:401–408, 1990.
- [153] Hans Peter Nilles and M. Olechowski. Gaugino Condensation and Duality Invariance. *Phys. Lett. B*, 248:268–272, 1990.
- [154] P. Binetruy and E. Dudas. Gaugino condensation and the anomalous U(1). *Phys. Lett. B*, 389:503–509, 1996.
- [155] Jihn E. Kim and Gianpaolo Carosi. Axions and the Strong CP Problem. Rev. Mod. Phys., 82:557–602, 2010. [Erratum: Rev.Mod.Phys. 91, 049902 (2019)].
- [156] Ralph Blumenhagen, Gabriele Honecker, and Timo Weigand. Loop-corrected compactifications of the heterotic string with line bundles. *JHEP*, 06:020, 2005.

[157] Lara B. Anderson, James Gray, Yang-Hui He, and Andre Lukas. Exploring Positive Monad Bundles And A New Heterotic Standard Model. *JHEP*, 02:054, 2010.

- [158] Lara B. Anderson, Antonella Grassi, James Gray, and Paul-Konstantin Oehlmann. F-theory on Quotient Threefolds with (2,0) Discrete Superconformal Matter. JHEP, 06:098, 2018.
- [159] Lara B. Anderson, James Gray, and Paul-Konstantin Oehlmann. F-Theory on Quotients of Elliptic Calabi-Yau Threefolds. *JHEP*, 12:131, 2019.
- [160] James Gray and Juntao Wang. Free quotients of favorable Calabi-Yau manifolds. *JHEP*, 07:116, 2022.
- [161] Marco Peloso, Lorenzo Sorbo, and Caner Unal. Rolling axions during inflation: perturbativity and signatures. *JCAP*, 09:001, 2016.
- [162] Ryo Namba, Marco Peloso, Maresuke Shiraishi, Lorenzo Sorbo, and Caner Unal. Scale-dependent gravitational waves from a rolling axion. *JCAP*, 01:041, 2016.
- [163] Ippei Obata and Jiro Soda. Chiral primordial Chiral primordial gravitational waves from dilaton induced delayed chromonatural inflation. *Phys. Rev. D*, 93(12):123502, 2016. [Addendum: Phys.Rev.D 95, 109903 (2017)].
- [164] Fred C. Adams, J. Richard Bond, Katherine Freese, Joshua A. Frieman, and Angela V. Olinto. Natural inflation: Particle physics models, power law spectra for large scale structure, and constraints from COBE. *Phys. Rev. D*, 47:426–455, 1993.
- [165] Mohamed M. Anber and Lorenzo Sorbo. Phys. Rev. D, 81:043534, 2010.
- [166] Neil Barnaby and Marco Peloso. Large Nongaussianity in Axion Inflation. Phys. Rev. Lett., 106:181301, 2011.
- [167] Jessica L. Cook and Lorenzo Sorbo. Particle production during inflation and gravitational waves detectable by ground-based interferometers. *Phys. Rev. D*, 85:023534, 2012. [Erratum: Phys.Rev.D 86, 069901 (2012)].
- [168] A. Maleknejad and M. M. Sheikh-Jabbari. Gauge-flation: Inflation From Non-Abelian Gauge Fields. Phys. Lett. B, 723:224–228, 2013.
- [169] Neil Barnaby, Ryo Namba, and Marco Peloso. Phenomenology of a Pseudo-Scalar Inflaton: Naturally Large Nongaussianity. JCAP, 04:009, 2011.
- [170] Peter Adshead and Mark Wyman. Chromo-Natural Inflation: Natural inflation on a steep potential with classical non-Abelian gauge fields. *Phys. Rev. Lett.*, 108:261302, 2012.
- [171] Emanuela Dimastrogiovanni, Matteo Fasiello, and Andrew J. Tolley. Low-Energy Effective Field Theory for Chromo-Natural Inflation. *JCAP*, 02:046, 2013.
- [172] Yuki Watanabe and Eiichiro Komatsu. Gravitational Wave from Axion-SU(2) Gauge Fields: Effective Field Theory for Kinetically Driven Inflation. 4 2020.
- [173] Ema Dimastrogiovanni, Matteo Fasiello, Martino Michelotti, and Lucas Pinol. Primordial Gravitational Waves in non-Minimally Coupled Chromo-Natural Inflation. 3 2023.

[174] Guido D'Amico and Nemanja Kaloper. Rollercoaster cosmology. *JCAP*, 08:058, 2021.

- [175] Naoya Kitajima, Jiro Soda, and Yuko Urakawa. Gravitational wave forest from string axiverse. *JCAP*, 10:008, 2018.
- [176] Vera Gluscevic and Marc Kamionkowski. Testing Parity-Violating Mechanisms with Cosmic Microwave Background Experiments. *Phys. Rev. D*, 81:123529, 2010.
- [177] Ben Thorne, Tomohiro Fujita, Masashi Hazumi, Nobuhiko Katayama, Eiichiro Komatsu, and Maresuke Shiraishi. Finding the chiral gravitational wave background of an axion-SU(2) inflationary model using CMB observations and laser interferometers. *Phys. Rev. D*, 97(4):043506, 2018.
- [178] Naoki Seto and Atsushi Taruya. Measuring a Parity Violation Signature in the Early Universe via Ground-based Laser Interferometers. *Phys. Rev. Lett.*, 99:121101, 2007.
- [179] Tristan L. Smith and Robert Caldwell. Sensitivity to a Frequency-Dependent Circular Polarization in an Isotropic Stochastic Gravitational Wave Background. *Phys. Rev. D*, 95(4):044036, 2017.
- [180] Valerie Domcke, Juan Garcia-Bellido, Marco Peloso, Mauro Pieroni, Angelo Ricciardone, Lorenzo Sorbo, and Gianmassimo Tasinato. Measuring the net circular polarization of the stochastic gravitational wave background with interferometers. *JCAP*, 05:028, 2020.
- [181] Nicola Bartolo and Giorgio Orlando. Parity breaking signatures from a Chern-Simons coupling during inflation: the case of non-Gaussian gravitational waves. JCAP, 07:034, 2017.
- [182] Nicola Bartolo, Giorgio Orlando, and Maresuke Shiraishi. Measuring chiral gravitational waves in Chern-Simons gravity with CMB bispectra. *JCAP*, 01:050, 2019.
- [183] Leila Mirzagholi, Eiichiro Komatsu, Kaloian D. Lozanov, and Yuki Watanabe. Effects of Gravitational Chern-Simons during Axion-SU(2) Inflation. JCAP, 06:024, 2020.
- [184] Aniket Agrawal, Tomohiro Fujita, and Eiichiro Komatsu. Large tensor non-Gaussianity from axion-gauge field dynamics. *Phys. Rev. D*, 97(10):103526, 2018.
- [185] Aniket Agrawal, Tomohiro Fujita, and Eiichiro Komatsu. Tensor Non-Gaussianity from Axion-Gauge-Fields Dynamics: Parameter Search. *JCAP*, 06:027, 2018.
- [186] Emanuela Dimastrogiovanni, Matteo Fasiello, Robert J. Hardwick, Hooshyar Assadullahi, Kazuya Koyama, and David Wands. Non-Gaussianity from Axion-Gauge Fields Interactions during Inflation. *JCAP*, 11:029, 2018.
- [187] Ogan Özsoy. Parity violating non-Gaussianity from axion-gauge field dynamics. *Phys. Rev. D*, 104(12):123523, 2021.
- [188] Juan Garcia-Bellido, Marco Peloso, and Caner Unal. Gravitational Wave signatures of inflationary models from Primordial Black Hole Dark Matter. JCAP, 09:013, 2017.
- [189] Ogan Özsoy and Zygmunt Lalak. Primordial black holes as dark matter and gravitational waves from bumpy axion inflation. *JCAP*, 01:040, 2021.

[190] C. P. Burgess, Gongjun Choi, and F. Quevedo. UV and IR Effects in Axion Quality Control. 1 2023.

- [191] Gongjun Choi and Jacob Leedom. Implications of Protecting the QCD Axion in the Dual Description. 7 2023.
- [192] David J. E. Marsh, Daniel Grin, Renée Hlozek, and Pedro G. Ferreira. Axiverse cosmology and the energy scale of inflation. *Phys. Rev. D*, 87:121701, 2013.
- [193] Hiroyuki Tashiro, Joseph Silk, and David J. E. Marsh. Constraints on primordial magnetic fields from CMB distortions in the axiverse. *Phys. Rev. D*, 88(12):125024, 2013.
- [194] Hirotaka Yoshino and Hideo Kodama. Probing the string axiverse by gravitational waves from Cygnus X-1. *PTEP*, 2015(6):061E01, 2015.
- [195] Marc Kamionkowski, Josef Pradler, and Devin G. E. Walker. Dark energy from the string axiverse. *Phys. Rev. Lett.*, 113(25):251302, 2014.
- [196] Bobby Samir Acharya and Chakrit Pongkitivanichkul. The Axiverse induced Dark Radiation Problem. *JHEP*, 04:009, 2016.
- [197] Ryuji Daido, Naoya Kitajima, and Fuminobu Takahashi. Domain Wall Formation from Level Crossing in the Axiverse. *Phys. Rev. D*, 92(6):063512, 2015.
- [198] Hirotaka Yoshino and Hideo Kodama. The bosenova and axiverse. *Class. Quant. Grav.*, 32(21):214001, 2015.
- [199] Razieh Emami, Daniel Grin, Josef Pradler, Alvise Raccanelli, and Marc Kamionkowski. Cosmological tests of an axiverse-inspired quintessence field. *Phys. Rev. D*, 93(12):123005, 2016.
- [200] Tanvi Karwal and Marc Kamionkowski. Dark energy at early times, the Hubble parameter, and the string axiverse. *Phys. Rev. D*, 94(10):103523, 2016.
- [201] Dmitry Gorbunov and Anna Tokareva. On the dark radiation problem in the axiverse. *JCAP*, 06:016, 2017.
- [202] Luca Visinelli and Sunny Vagnozzi. Cosmological window onto the string axiverse and the supersymmetry breaking scale. *Phys. Rev. D*, 99(6):063517, 2019.
- [203] Prateek Agrawal, Jiji Fan, and Matthew Reece. Clockwork Axions in Cosmology: Is Chromonatural Inflation Chrononatural? *JHEP*, 10:193, 2018.
- [204] Hengameh Bagherian, Matthew Reece, and Weishuang Linda Xu. The inflated Chern-Simons number in spectator chromo-natural inflation. *JHEP*, 01:099, 2023.
- [205] Evan McDonough and Stephon Alexander. Observable Chiral Gravitational Waves from Inflation in String Theory. *JCAP*, 11:030, 2018.
- [206] Jonathan Holland, Ivonne Zavala, and Gianmassimo Tasinato. On chromonatural inflation in string theory. *JCAP*, 12:026, 2020.
- [207] Tom Banks, Michael Dine, Patrick J. Fox, and Elie Gorbatov. On the possibility of large axion decay constants. *JCAP*, 06:001, 2003.

[208] Neil Barnaby, Jordan Moxon, Ryo Namba, Marco Peloso, Gary Shiu, and Peng Zhou. Gravity waves and non-Gaussian features from particle production in a sector gravitationally coupled to the inflaton. *Phys. Rev. D*, 86:103508, 2012.

- [209] Shinji Mukohyama, Ryo Namba, Marco Peloso, and Gary Shiu. Blue Tensor Spectrum from Particle Production during Inflation. *JCAP*, 08:036, 2014.
- [210] Kaloian D. Lozanov, Azadeh Maleknejad, and Eiichiro Komatsu. Schwinger Effect by an SU(2) Gauge Field during Inflation. JHEP, 02:041, 2019.
- [211] A. Maleknejad and E. Komatsu. Production and Backreaction of Spin-2 Particles of SU(2) Gauge Field during Inflation. *JHEP*, 05:174, 2019.
- [212] Tomohiro Fujita, Ryo Namba, and Ippei Obata. Mixed Non-Gaussianity from Axion-Gauge Field Dynamics. *JCAP*, 04:044, 2019.
- [213] Jeff Crowder and Neil J. Cornish. Beyond LISA: Exploring future gravitational wave missions. *Phys. Rev. D*, 72:083005, 2005.
- [214] Emanuela Dimastrogiovanni and Marco Peloso. Stability analysis of chromo-natural inflation and possible evasion of Lyth's bound. *Phys. Rev. D*, 87(10):103501, 2013.
- [215] Peter Adshead, Emil Martinec, and Mark Wyman. Perturbations in Chromo-Natural Inflation. *JHEP*, 09:087, 2013.
- [216] Peter Adshead, Emil Martinec, Evangelos I. Sfakianakis, and Mark Wyman. Higgsed Chromo-Natural Inflation. *JHEP*, 12:137, 2016.
- [217] Oksana Iarygina, Evangelos I. Sfakianakis, Ramkishor Sharma, and Axel Brandenburg. Backreaction of axion-SU(2) dynamics during inflation. 11 2023.
- [218] Gianguido Dall'Agata, Sergio González-Martín, Alexandros Papageorgiou, and Marco Peloso. Warm dark energy. *JCAP*, 08:032, 2020.
- [219] Valerie Domcke, Veronica Guidetti, Yvette Welling, and Alexander Westphal. Resonant backreaction in axion inflation. *JCAP*, 09:009, 2020.
- [220] Angelo Caravano, Eiichiro Komatsu, Kaloian D. Lozanov, and Jochen Weller. Lattice simulations of axion-U(1) inflation. *Phys. Rev. D*, 108(4):043504, 2023.
- [221] Marco Peloso and Lorenzo Sorbo. Instability in axion inflation with strong backreaction from gauge modes. *JCAP*, 01:038, 2023.
- [222] Richard von Eckardstein, Marco Peloso, Kai Schmitz, Oleksandr Sobol, and Lorenzo Sorbo. Axion inflation in the strong-backreaction regime: decay of the Anber-Sorbo solution. *JHEP*, 11:183, 2023.
- [223] Juan Garcia-Bellido, Alexandros Papageorgiou, Marco Peloso, and Lorenzo Sorbo. A flashing beacon in axion inflation: recurring bursts of gravitational waves in the strong backreaction regime. 3 2023.
- [224] Daniel G. Figueroa, Joanes Lizarraga, Ander Urio, and Jon Urrestilla. Strong Backreaction Regime in Axion Inflation. *Phys. Rev. Lett.*, 131(15):151003, 2023.
- [225] David H. Lyth and David Wands. Generating the curvature perturbation without an inflaton. *Phys. Lett. B*, 524:5–14, 2002.

[226] N. Aghanim et al. Planck 2018 results. VI. Cosmological parameters. *Astron. Astrophys.*, 641:A6, 2020. [Erratum: Astron. Astrophys. 652, C4 (2021)].

- [227] M. Tristram et al. Improved limits on the tensor-to-scalar ratio using BICEP and Planck data. *Phys. Rev. D*, 105(8):083524, 2022.
- [228] Giacomo Galloni, Nicola Bartolo, Sabino Matarrese, Marina Migliaccio, Angelo Ricciardone, and Nicola Vittorio. Updated constraints on amplitude and tilt of the tensor primordial spectrum. *JCAP*, 04:062, 2023.
- [229] Enrico Pajer and Marco Peloso. A review of Axion Inflation in the era of Planck. *Class. Quant. Grav.*, 30:214002, 2013.
- [230] Tomohiro Fujita, Kai Murai, and Ryo Namba. Universality of linear perturbations in SU(N) natural inflation. *Phys. Rev. D*, 105(10):103518, 2022.
- [231] A. Maleknejad and M. M. Sheikh-Jabbari. Non-Abelian Gauge Field Inflation. Phys. Rev. D, 84:043515, 2011.
- [232] Ira Wolfson, Azadeh Maleknejad, and Eiichiro Komatsu. How attractive is the isotropic attractor solution of axion-SU(2) inflation? *JCAP*, 09:047, 2020.
- [233] Tomohiro Fujita, Ryo Namba, and Yuichiro Tada. Does the detection of primordial gravitational waves exclude low energy inflation? *Phys. Lett. B*, 778:17–21, 2018.
- [234] Christian T. Byrnes, Philippa S. Cole, and Subodh P. Patil. Steepest growth of the power spectrum and primordial black holes. *JCAP*, 06:028, 2019.
- [235] John C. Mather et al. Measurement of the Cosmic Microwave Background spectrum by the COBE FIRAS instrument. *Astrophys. J.*, 420:439–444, 1994.
- [236] D. J. Fixsen. The Temperature of the Cosmic Microwave Background. *Astrophys. J.*, 707:916–920, 2009.
- [237] Joseph Silk. Cosmic black body radiation and galaxy formation. *Astrophys. J.*, 151:459–471, 1968.
- [238] Jens Chluba, Rishi Khatri, and Rashid A. Sunyaev. CMB at 2x2 order: The dissipation of primordial acoustic waves and the observable part of the associated energy release. *Mon. Not. Roy. Astron. Soc.*, 425:1129–1169, 2012.
- [239] Wayne Hu and Joseph Silk. Thermalization and spectral distortions of the cosmic background radiation. *Phys. Rev. D*, 48:485–502, 1993.
- [240] Karsten Jedamzik and Andrey Saveliev. Stringent Limit on Primordial Magnetic Fields from the Cosmic Microwave Background Radiation. Phys. Rev. Lett., 123(2):021301, 2019.
- [241] J. P. Ostriker and C. Thompson. Distortion of the Cosmic Background Radiation by Superconducting Strings. *apjl*, 323:L97, December 1987.
- [242] C. Burigana et al. Exploring cosmic origins with CORE: effects of observer peculiar motion. *JCAP*, 04:021, 2018.
- [243] Enrico Pajer and Matias Zaldarriaga. A New Window on Primordial non-Gaussianity. *Phys. Rev. Lett.*, 109:021302, 2012.

[244] Jonathan Ganc and Eiichiro Komatsu. Scale-dependent bias of galaxies and mu-type distortion of the cosmic microwave background spectrum from single-field inflation with a modified initial state. *Phys. Rev. D*, 86:023518, 2012.

- [245] Razieh Emami, Emanuela Dimastrogiovanni, Jens Chluba, and Marc Kamionkowski. Probing the scale dependence of non-Gaussianity with spectral distortions of the cosmic microwave background. *Phys. Rev. D*, 91(12):123531, 2015.
- [246] Jens Chluba, Emanuela Dimastrogiovanni, Mustafa A. Amin, and Marc Kamionkowski. Evolution of CMB spectral distortion anisotropies and tests of primordial non-Gaussianity. Mon. Not. Roy. Astron. Soc., 466(2):2390–2401, 2017.
- [247] Andrea Ravenni, Michele Liguori, Nicola Bartolo, and Maresuke Shiraishi. Primordial non-Gaussianity with  $\mu$ -type and y-type spectral distortions: exploiting Cosmic Microwave Background polarization and dealing with secondary sources. JCAP, 09:042, 2017.
- [248] Nicola Bartolo, Michele Liguori, and Maresuke Shiraishi. Primordial trispectra and CMB spectral distortions. *JCAP*, 03:029, 2016.
- [249] Maresuke Shiraishi, Nicola Bartolo, and Michele Liguori. Angular dependence of primordial trispectra and CMB spectral distortions. *JCAP*, 10:015, 2016.
- [250] Mathieu Remazeilles, Andrea Ravenni, and Jens Chluba. Leverage on small-scale primordial non-Gaussianity through cross-correlations between CMB E-mode and μ-distortion anisotropies. Mon. Not. Roy. Astron. Soc., 512(1):455–470, 2022.
- [251] Aditya Rotti, Andrea Ravenni, and Jens Chluba. Non-Gaussianity constraints with anisotropic  $\mu$  distortion measurements from Planck. *Mon. Not. Roy. Astron. Soc.*, 515(4):5847–5868, 2022.
- [252] Jens Chluba, Andrea Ravenni, and Thomas Kite. Spectro-spatial evolution of the CMB. Part II. Generalised Boltzmann hierarchy. *JCAP*, 11:027, 2023.
- [253] Thomas Kite, Andrea Ravenni, and Jens Chluba. Spectro-spatial evolution of the CMB. Part III. Transfer functions, power spectra and Fisher forecasts. *JCAP*, 11:028, 2023.
- [254] Enrico Pajer and Matias Zaldarriaga. A hydrodynamical approach to CMB  $\mu$ -distortion from primordial perturbations. *JCAP*, 02:036, 2013.
- [255] D. J. Fixsen, E. S. Cheng, J. M. Gales, John C. Mather, R. A. Shafer, and E. L. Wright. The Cosmic Microwave Background spectrum from the full COBE FIRAS data set. Astrophys. J., 473:576, 1996.
- [256] Federico Bianchini and Giulio Fabbian. CMB spectral distortions revisited: A new take on  $\mu$  distortions and primordial non-Gaussianities from FIRAS data. *Phys. Rev. D*, 106(6):063527, 2022.
- [257] Alan J. Kogut et al. The Primordial Inflation Explorer (PIXIE) Mission. *Proc. SPIE Int. Soc. Opt. Eng.*, 7731:77311S, 2010.
- [258] Philippe André et al. PRISM (Polarized Radiation Imaging and Spectroscopy Mission): An Extended White Paper. *JCAP*, 02:006, 2014.

[259] S. Masi et al. The COSmic Monopole Observer (COSMO). In 16th Marcel Grossmann Meeting on Recent Developments in Theoretical and Experimental General Relativity, Astrophysics and Relativistic Field Theories, 10 2021.

- [260] B. Maffei et al. BISOU: A balloon project to measure the CMB spectral distortions. In 16th Marcel Grossmann Meeting on Recent Developments in Theoretical and Experimental General Relativity, Astrophysics and Relativistic Field Theories, 10 2021.
- [261] J. Chluba et al. Spectral Distortions of the CMB as a Probe of Inflation, Recombination, Structure Formation and Particle Physics: Astro2020 Science White Paper. Bull. Am. Astron. Soc., 51(3):184, 2019.
- [262] J. Aasi et al. Advanced LIGO. Class. Quant. Grav., 32:074001, 2015.
- [263] F. Acernese et al. Advanced Virgo: a second-generation interferometric gravitational wave detector. Class. Quant. Grav., 32(2):024001, 2015.
- [264] T. Akutsu et al. Overview of KAGRA: Detector design and construction history. PTEP, 2021(5):05A101, 2021.
- [265] J. Antoniadis et al. The second data release from the European Pulsar Timing Array III. Search for gravitational wave signals. 6 2023.
- [266] Gabriella Agazie et al. The NANOGrav 15 yr Data Set: Evidence for a Gravitational-wave Background. Astrophys. J. Lett., 951(1):L8, 2023.
- [267] Christopher J. Moore, Deyan P. Mihaylov, Anthony Lasenby, and Gerard Gilmore. Astrometric Search Method for Individually Resolvable Gravitational Wave Sources with Gaia. *Phys. Rev. Lett.*, 119(26):261102, 2017.
- [268] Pau Amaro-Seoane et al. Laser Interferometer Space Antenna. 2 2017.
- [269] M. Punturo et al. The Einstein Telescope: A third-generation gravitational wave observatory. Class. Quant. Grav., 27:194002, 2010.
- [270] Matthew Evans et al. A Horizon Study for Cosmic Explorer: Science, Observatories, and Community. 9 2021.
- [271] Jens Chluba, Liang Dai, Daniel Grin, Mustafa Amin, and Marc Kamionkowski. Spectral distortions from the dissipation of tensor perturbations. *Mon. Not. Roy. Astron. Soc.*, 446:2871–2886, 2015.
- [272] Thomas Kite, Andrea Ravenni, Subodh P. Patil, and Jens Chluba. Bridging the gap: spectral distortions meet gravitational waves. *Mon. Not. Roy. Astron. Soc.*, 505(3):4396–4405, 2021.
- [273] Nicklas Ramberg, Wolfram Ratzinger, and Pedro Schwaller. One  $\mu$  to rule them all: CMB spectral distortions can probe domain walls, cosmic strings and low scale phase transitions. JCAP, 02:039, 2023.
- [274] Matteo Biagetti, Emanuela Dimastrogiovanni, Matteo Fasiello, and Marco Peloso. Gravitational Waves and Scalar Perturbations from Spectator Fields. JCAP, 04:011, 2015.

[275] Alba Kalaja, Nicola Bellomo, Nicola Bartolo, Daniele Bertacca, Sabino Matarrese, Ilia Musco, Alvise Raccanelli, and Licia Verde. From Primordial Black Holes Abundance to Primordial Curvature Power Spectrum (and back). *JCAP*, 10:031, 2019.

- [276] Kazunori Kohri, Tomohiro Nakama, and Teruaki Suyama. Testing scenarios of primordial black holes being the seeds of supermassive black holes by ultracompact minihalos and CMB  $\mu$ -distortions. *Phys. Rev. D*, 90(8):083514, 2014.
- [277] Ya. B. Zeldovich and R. A. Sunyaev. The Interaction of Matter and Radiation in a Hot-Model Universe. *Astrophys. Space Sci.*, 4:301–316, 1969.
- [278] R. A. Sunyaev and Ya. B. Zeldovich. The Interaction of matter and radiation in the hot model of the universe. *Astrophys. Space Sci.*, 7:20–30, 1970.
- [279] Carlo Burigana, L. Danese, and G. De Zotti. Formation and evolution of early distortions of the microwave background spectrum A numerical study. *Astron. Astrophys.*, 246(1):49–58, 1991.
- [280] Matteo Lucca, Nils Schöneberg, Deanna C. Hooper, Julien Lesgourgues, and Jens Chluba. The synergy between CMB spectral distortions and anisotropies. *JCAP*, 02:026, 2020.
- [281] J. Chluba and R. A. Sunyaev. The evolution of CMB spectral distortions in the early Universe. *Mon. Not. Roy. Astron. Soc.*, 419:1294–1314, 2012.
- [282] Rishi Khatri and Rashid A. Sunyaev. Beyond y and \mu: the shape of the CMB spectral distortions in the intermediate epoch,  $1.5 \times 10^4 < z < 2 \times 10^5$ . JCAP, 09:016, 2012.
- [283] Jens Chluba. Green's function of the cosmological thermalization problem. *Mon. Not. Roy. Astron. Soc.*, 434:352, 2013.
- [284] Jens Chluba. Green's function of the cosmological thermalization problem II. Effect of photon injection and constraints. *Mon. Not. Roy. Astron. Soc.*, 454(4):4182–4196, 2015.
- [285] Jens Chluba, Jan Hamann, and Subodh P. Patil. Features and New Physical Scales in Primordial Observables: Theory and Observation. *Int. J. Mod. Phys.* D, 24(10):1530023, 2015.
- [286] Jens Chluba. Which spectral distortions does  $\Lambda$ CDM actually predict? Mon. Not. Roy. Astron. Soc., 460(1):227–239, 2016.
- [287] L. Danese and G. De Zotti. Double Compton process and the spectrum of the microwave background. *Astron. Astrophys.*, 107(1):39–42, 1982.
- [288] R. A. Sunyaev and Ya. B. Zeldovich. Small scale entropy and adiabatic density perturbations? Antimatter in the Universe. *Astrophys. Space Sci.*, 9(3):368–382, 1970.
- [289] R. A. Daly. Spectral distortions of the microwave background radiation resulting from the damping of pressure waves. *Astrophys. J.*, 371, 1991.
- [290] John D Barrow and Peter Coles. Primordial density fluctuations and the microwave background spectrum. *Monthly Notices of the Royal Astronomical Society*, 248(1):52–57, 1991.

[291] Wayne Hu, Douglas Scott, and Joseph Silk. Power spectrum constraints from spectral distortions in the cosmic microwave background. *Astrophys. J. Lett.*, 430:L5–L8, 1994.

- [292] Arthur Kosowsky and Michael S. Turner. CBR anisotropy and the running of the scalar spectral index. *Phys. Rev. D*, 52:R1739–R1743, 1995.
- [293] Jens Chluba and Daniel Grin. CMB spectral distortions from small-scale isocurvature fluctuations. *Mon. Not. Roy. Astron. Soc.*, 434:1619–1635, 2013.
- [294] Jens Chluba, Adrienne L. Erickcek, and Ido Ben-Dayan. Probing the inflaton: Small-scale power spectrum constraints from measurements of the CMB energy spectrum. *Astrophys. J.*, 758:76, 2012.
- [295] Atsuhisa Ota, Tomo Takahashi, Hiroyuki Tashiro, and Masahide Yamaguchi. CMB  $\mu$  distortion from primordial gravitational waves. JCAP, 10:029, 2014.
- [296] Duane A. Dicus and Wayne W. Repko. Comment on damping of tensor modes in cosmology. Phys. Rev. D, 72:088302, 2005.
- [297] Steven Weinberg. Damping of tensor modes in cosmology. *Phys. Rev. D*, 69:023503, 2004.
- [298] Yuki Watanabe and Eiichiro Komatsu. Improved Calculation of the Primordial Gravitational Wave Spectrum in the Standard Model. Phys. Rev. D, 73:123515, 2006.
- [299] Alexandros Papageorgiou, Marco Peloso, and Caner Unal. Nonlinear perturbations from axion-gauge fields dynamics during inflation. *JCAP*, 07:004, 2019.
- [300] Renata Kallosh, Andrei Linde, and Diederik Roest. Superconformal Inflationary  $\alpha$ -Attractors. *JHEP*, 11:198, 2013.
- [301] Ippei Obata, Takashi Miura, and Jiro Soda. Chromo-Natural Inflation in the Axiverse. Phys. Rev. D, 92(6):063516, 2015. [Addendum: Phys.Rev.D 95, 109902 (2017)].
- [302] Liam McAllister, Sebastien Renaux-Petel, and Gang Xu. A Statistical Approach to Multifield Inflation: Many-field Perturbations Beyond Slow Roll. JCAP, 10:046, 2012.
- [303] Ogan Özsoy. Synthetic Gravitational Waves from a Rolling Axion Monodromy. JCAP, 04:040, 2021.
- [304] Shi Pi and Misao Sasaki. Gravitational Waves Induced by Scalar Perturbations with a Lognormal Peak. *JCAP*, 09:037, 2020.
- [305] J. Antoniadis et al. The second data release from the European Pulsar Timing Array III. Search for gravitational wave signals. *Astron. Astrophys.*, 678:A50, 2023.
- [306] Daniel J. Reardon et al. Search for an Isotropic Gravitational-wave Background with the Parkes Pulsar Timing Array. *Astrophys. J. Lett.*, 951(1):L6, 2023.
- [307] Pau Amaro-Seoane, Heather Audley, et al. Laser interferometer space antenna, 2017.

[308] Gemma Janssen et al. Gravitational wave astronomy with the SKA. *PoS*, AASKA14:037, 2015.

- [309] Céline Boehm et al. Theia: Faint objects in motion or the new astrometry frontier. 7 2017.
- [310] Vincent Corbin and Neil J. Cornish. Detecting the cosmic gravitational wave background with the big bang observer. *Class. Quant. Grav.*, 23:2435–2446, 2006.
- [311] Naoki Seto, Seiji Kawamura, and Takashi Nakamura. Possibility of direct measurement of the acceleration of the universe using 0.1-Hz band laser interferometer gravitational wave antenna in space. *Phys. Rev. Lett.*, 87:221103, 2001.
- [312] Arthur Hebecker, Joerg Jaeckel, and Ruben Kuespert. Small Kinetic Mixing in String Theory. 11 2023.
- [313] Caner Unal, Alexandros Papageorgiou, and Ippei Obata. Axion-Gauge Dynamics During Inflation as the Origin of Pulsar Timing Array Signals and Primordial Black Holes. 7 2023.
- [314] Gianguido Dall'Agata. Chromo-Natural inflation in Supergravity. *Phys. Lett. B*, 782:139–142, 2018.
- [315] Prateek Agrawal, JiJi Fan, Matthew Reece, and Lian-Tao Wang. Experimental Targets for Photon Couplings of the QCD Axion. *JHEP*, 02:006, 2018.
- [316] Marco Farina, Duccio Pappadopulo, Fabrizio Rompineve, and Andrea Tesi. The photo-philic QCD axion. *JHEP*, 01:095, 2017.
- [317] Luca Di Luzio, Belen Gavela, Pablo Quilez, and Andreas Ringwald. An even lighter QCD axion. *JHEP*, 05:184, 2021.
- [318] Luca Di Luzio, Belen Gavela, Pablo Quilez, and Andreas Ringwald. Dark matter from an even lighter QCD axion: trapped misalignment. *JCAP*, 10:001, 2021.
- [319] Jeff A. Dror and Jacob M. Leedom. Cosmological Tension of Ultralight Axion Dark Matter and its Solutions. *Phys. Rev. D*, 102(11):115030, 2020.
- [320] K. S. Babu, Stephen M. Barr, and D. Seckel. Axion dissipation through the mixing of Goldstone bosons. *Phys. Lett. B*, 336:213–220, 1994.
- [321] Kiwoon Choi, Hyungjin Kim, and Seokhoon Yun. Natural inflation with multiple sub-Planckian axions. *Phys. Rev. D*, 90:023545, 2014.
- [322] Kiwoon Choi and Sang Hui Im. Realizing the relaxion from multiple axions and its UV completion with high scale supersymmetry. *JHEP*, 01:149, 2016.
- [323] David E. Kaplan and Riccardo Rattazzi. Large field excursions and approximate discrete symmetries from a clockwork axion. *Phys. Rev. D*, 93(8):085007, 2016.
- [324] Anson Hook. Solving the Hierarchy Problem Discretely. *Phys. Rev. Lett.*, 120(26):261802, 2018.
- [325] T. Daniel Brennan, Federico Carta, and Cumrun Vafa. The String Landscape, the Swampland, and the Missing Corner. *PoS*, TASI2017:015, 2017.
- [326] Eran Palti. The Swampland: Introduction and Review. Fortsch. Phys., 67(6):1900037, 2019.

[327] Marieke van Beest, José Calderón-Infante, Delaram Mirfendereski, and Irene Valenzuela. Lectures on the Swampland Program in String Compactifications. Phys. Rept., 989:1–50, 2022.

- [328] Nathan Benjamin Agmon, Alek Bedroya, Monica Jinwoo Kang, and Cumrun Vafa. Lectures on the string landscape and the Swampland. 12 2022.
- [329] Fernando Marchesano, Bert Schellekens, and Timo Weigand. D-brane and F-theory Model Building. In *Handbook of Quantum Gravity*, 12 2022.
- [330] Thomas W. Grimm and Jan Louis. The Effective action of N=1 Calabi-Yau orientifolds. *Nucl. Phys. B*, 699:387–426, 2004.
- [331] Hans Jockers and Jan Louis. The Effective action of D7-branes in N = 1 Calabi-Yau orientifolds. *Nucl. Phys. B*, 705:167–211, 2005.
- [332] Hans Jockers and Jan Louis. D-terms and F-terms from D7-brane fluxes. *Nucl. Phys. B*, 718:203–246, 2005.
- [333] Thomas W. Grimm, Max Kerstan, Eran Palti, and Timo Weigand. On Fluxed Instantons and Moduli Stabilisation in IIB Orientifolds and F-theory. *Phys. Rev.* D, 84:066001, 2011.
- [334] Cody Long, Liam McAllister, and Paul McGuirk. Aligned Natural Inflation in String Theory. *Phys. Rev. D*, 90:023501, 2014.
- [335] Ralph Blumenhagen, Volker Braun, Thomas W. Grimm, and Timo Weigand. GUTs in Type IIB Orientifold Compactifications. *Nucl. Phys. B*, 815:1–94, 2009.
- [336] Erik Plauschinn. The Generalized Green-Schwarz Mechanism for Type IIB Orientifolds with D3- and D7-Branes. *JHEP*, 05:062, 2009.
- [337] Thomas W. Grimm, Max Kerstan, Eran Palti, and Timo Weigand. Massive Abelian Gauge Symmetries and Fluxes in F-theory. *JHEP*, 12:004, 2011.
- [338] Thomas W. Grimm and Timo Weigand. On Abelian Gauge Symmetries and Proton Decay in Global F-theory GUTs. *Phys. Rev. D*, 82:086009, 2010.
- [339] Eric G. Gimon and Joseph Polchinski. Consistency conditions for orientifolds and D-manifolds. *Phys. Rev. D*, 54:1667–1676, 1996.
- [340] Hans Jockers. The Effective Action of D-branes in Calabi-Yau Orientifold Compactifications. Fortsch. Phys., 53:1087–1175, 2005.
- [341] Pablo G. Camara and Emilian Dudas. Multi-instanton and string loop corrections in toroidal orbifold models. *JHEP*, 08:069, 2008.
- [342] Thomas W. Grimm. Axion inflation in type II string theory. *Phys. Rev. D*, 77:126007, 2008.
- [343] Thomas W. Grimm. Non-Perturbative Corrections and Modularity in N=1 Type IIB Compactifications. *JHEP*, 10:004, 2007.
- [344] Edward Witten. Nonperturbative superpotentials in string theory. *Nucl. Phys. B*, 474:343–360, 1996.
- [345] S. Sethi, C. Vafa, and Edward Witten. Constraints on low dimensional string compactifications. *Nucl. Phys. B*, 480:213–224, 1996.

[346] Andres Collinucci, Frederik Denef, and Mboyo Esole. D-brane Deconstructions in IIB Orientifolds. *JHEP*, 02:005, 2009.

- [347] Philip Candelas, Eugene Perevalov, and Govindan Rajesh. Toric geometry and enhanced gauge symmetry of F theory / heterotic vacua. *Nucl. Phys. B*, 507:445–474, 1997.
- [348] Seung-Joo Lee, Wolfgang Lerche, and Timo Weigand. Emergent strings from infinite distance limits. *JHEP*, 02:190, 2022.
- [349] F. D. Drake. Project Ozma. Physics Today, 14(4):40–46, April 1961.
- [350] I. Stern. ADMX Status. PoS, ICHEP2016:198, 2016.
- [351] Asher Berlin, Raffaele Tito D'Agnolo, Sebastian A. R. Ellis, and Kevin Zhou. Heterodyne broadband detection of axion dark matter. *Phys. Rev. D*, 104(11):L111701, 2021.
- [352] L. Brouwer et al. Projected sensitivity of DMRadio-m3: A search for the QCD axion below 1  $\mu$ eV. *Phys. Rev. D*, 106(10):103008, 2022.
- [353] S. Ahyoune et al. A proposal for a low-frequency axion search in the 1-2  $\mu eV$  range and below with the BabyIAXO magnet. 6 2023.
- [354] A. D. Dolgov and D. P. Kirilova. ON PARTICLE CREATION BY A TIME DE-PENDENT SCALAR FIELD. Sov. J. Nucl. Phys., 51:172–177, 1990.
- [355] Jennie H. Traschen and Robert H. Brandenberger. Particle Production During Out-of-equilibrium Phase Transitions. *Phys. Rev. D*, 42:2491–2504, 1990.
- [356] Y. Shtanov, Jennie H. Traschen, and Robert H. Brandenberger. Universe reheating after inflation. *Phys. Rev. D*, 51:5438–5455, 1995.
- [357] Lev Kofman, Andrei Linde, and Alexei A. Starobinsky. Reheating after inflation. *Physical Review Letters*, 73(24):3195–3198, dec 1994.
- [358] Lev Kofman, Andrei Linde, and Alexei A. Starobinsky. Towards the theory of reheating after inflation. *Physical Review D*, 56(6):3258–3295, sep 1997.
- [359] Émile Mathieu. Mémoire sur le mouvement vibratoire d'une membrane de forme elliptique. Journal de Mathématiques Pures et Appliquées, 13:137–203, 1868.
- [360] G. Floquet. Sur les équations différentielles linéaires à coefficients périodiques. Annales scientifiques de l'École Normale Supérieure, 2e série, 12:47–88, 1883.
- [361] Raymond T. Co, Lawrence J. Hall, and Keisuke Harigaya. QCD Axion Dark Matter with a Small Decay Constant. *Phys. Rev. Lett.*, 120(21):211602, 2018.
- [362] Keisuke Harigaya and Jacob M. Leedom. QCD Axion Dark Matter from a Late Time Phase Transition. *JHEP*, 06:034, 2020.
- [363] Sabir Ramazanov and Rome Samanta. Heating up Peccei-Quinn scale. 10 2022.
- [364] Aleksandr Chatrchyan, Cem Eröncel, Matthias Koschnitzke, and Géraldine Servant. ALP dark matter with non-periodic potentials: parametric resonance, halo formation and gravitational signatures. *JCAP*, 10:068, 2023.

[365] Prateek Agrawal, Naoya Kitajima, Matthew Reece, Toyokazu Sekiguchi, and Fuminobu Takahashi. Relic Abundance of Dark Photon Dark Matter. Phys. Lett. B, 801:135136, 2020.

- [366] Raymond T. Co, Aaron Pierce, Zhengkang Zhang, and Yue Zhao. Dark Photon Dark Matter Produced by Axion Oscillations. *Phys. Rev. D*, 99(7):075002, 2019.
- [367] Mar Bastero-Gil, Jose Santiago, Lorenzo Ubaldi, and Roberto Vega-Morales. Vector dark matter production at the end of inflation. *JCAP*, 04:015, 2019.
- [368] Jeff A. Dror, Keisuke Harigaya, and Vijay Narayan. Parametric Resonance Production of Ultralight Vector Dark Matter. *Phys. Rev. D*, 99(3):035036, 2019.
- [369] Peter Adshead, Kaloian D. Lozanov, and Zachary J. Weiner. Dark photon dark matter from an oscillating dilaton. *Phys. Rev. D*, 107(8):083519, 2023.
- [370] Michele Cicoli, Joseph P. Conlon, Anshuman Maharana, Susha Parameswaran, Fernando Quevedo, and Ivonne Zavala. String Cosmology: from the Early Universe to Today. 3 2023.
- [371] Joseph P. Conlon and M. C. David Marsh. The Cosmophenomenology of Axionic Dark Radiation. *JHEP*, 10:214, 2013.
- [372] Michele Cicoli and Gabriel A. Piovano. Reheating and Dark Radiation after Fibre Inflation. JCAP, 02:048, 2019.
- [373] Michele Cicoli, Arthur Hebecker, Joerg Jaeckel, and Manuel Wittner. Axions in string theory slaying the Hydra of dark radiation. *JHEP*, 09:198, 2022.
- [374] Arthur Hebecker, Patrick Mangat, Fabrizio Rompineve, and Lukas T. Witkowski. Dark Radiation predictions from general Large Volume Scenarios. JHEP, 09:140, 2014.
- [375] Neil Barnaby, J. Richard Bond, Zhiqi Huang, and Lev Kofman. Preheating After Modular Inflation. JCAP, 12:021, 2009.
- [376] Bao-Min Gu and Robert Brandenberger. Reheating and Entropy Perturbations in Fibre Inflation. *Chin. Phys. C*, 44(1):015103, 2020.
- [377] Bruce A. Campbell, Nemanja Kaloper, Richard Madden, and Keith A. Olive. Physical properties of four-dimensional superstring gravity black hole solutions. *Nucl. Phys. B*, 399:137–168, 1993.
- [378] Leonardo Senatore, Eva Silverstein, and Matias Zaldarriaga. New Sources of Gravitational Waves during Inflation. *JCAP*, 08:016, 2014.
- [379] Islam Khan, Aaron C. Vincent, and Guy Worthey. Preheating and reheating effects of the Kähler moduli inflation I model. *Phys. Rev. D*, 108(10):103546, 2023.
- [380] G. W. Hill. On the part of the motion of the lunar perigee which is a function of the mean motions of the sun and moon. *Acta Mathematica*, 8(none):1 36, 1900.
- [381] R. Reissig. Magnus, w. und s. winkler, hill's equation (interscience tracts in pure and applied mathematics, number 20). viii + 127 s. new york/london/sydney 1966. interscience publishers. preis geb. 68 s.net. ZAMM Journal of Applied Mathematics and Mechanics / Zeitschrift für Angewandte Mathematik und Mechanik, 48(2):138–139, 1968.

[382] Mustafa A. Amin, Mark P. Hertzberg, David I. Kaiser, and Johanna Karouby. Nonperturbative dynamics of reheating after inflation: A review. *International Journal of Modern Physics D*, 24(01):1530003, dec 2014.

- [383] N. Fornengo, C. W. Kim, and J. Song. Finite temperature effects on the neutrino decoupling in the early universe. *Phys. Rev. D*, 56:5123–5134, Oct 1997.
- [384] Subir Sarkar. Big bang nucleosynthesis and physics beyond the standard model. *Rept. Prog. Phys.*, 59:1493–1610, 1996.
- [385] Robert E. Lopez, Scott Dodelson, Andrew Heckler, and Michael S. Turner. Precision detection of the cosmic neutrino background. *Phys. Rev. Lett.*, 82:3952–3955, 1999.
- [386] Patrick Crotty, Julien Lesgourgues, and Sergio Pastor. Current cosmological bounds on neutrino masses and relativistic relics. *Phys. Rev. D*, 69:123007, 2004.
- [387] Tsung-Han Yeh, Jessie Shelton, Keith A. Olive, and Brian D. Fields. Probing physics beyond the standard model: limits from BBN and the CMB independently and combined. *JCAP*, 10:046, 2022.
- [388] Kevork N. Abazajian et al. CMB-S4 Science Book, First Edition. 10 2016.
- [389] Marcos A. G. Garcia, Mathias Pierre, and Sarunas Verner. Scalar dark matter production from preheating and structure formation constraints. *Phys. Rev. D*, 107(4):043530, 2023.
- [390] James Halverson, Cody Long, Brent Nelson, and Gustavo Salinas. Axion reheating in the string landscape. *Phys. Rev. D*, 99(8):086014, 2019.
- [391] Lilia Anguelova, Vincenzo Calo, and Michele Cicoli. LARGE Volume String Compactifications at Finite Temperature. *JCAP*, 10:025, 2009.
- [392] Ignatios Antoniadis, J. Rizos, and K. Tamvakis. Singularity free cosmological solutions of the superstring effective action. *Nucl. Phys. B*, 415:497–514, 1994.
- [393] Kiwoon Choi. Axions and the strong CP problem in M theory. *Phys. Rev. D*, 56:6588–6600, 1997.
- [394] Kiwoon Choi, Jai-chan Hwang, and Kyu Wan Hwang. String theoretic axion coupling and the evolution of cosmic structures. *Phys. Rev. D*, 61:084026, 2000.
- [395] Robert Delbourgo and Dong-sheng Liu. Electromagnetic and gravitational decay of the Higgs boson. Austral. J. Phys., 53:647–651, 2001.
- [396] Allan Alonzo-Artiles, Ana Avilez-López, J. Lorenzo Díaz-Cruz, and Bryan O. Larios-López. The Higgs-Graviton Couplings: from Amplitudes to the Action. 5 2021.
- [397] Yohei Ema, Kyohei Mukaida, and Kazunori Nakayama. Scalar field couplings to quadratic curvature and decay into gravitons. *JHEP*, 05:087, 2022.
- [398] Jing Yang and Fa Peng Huang. Gravitational waves from axions annihilation through quantum field theory. *Phys. Rev. D*, 108(10):103002, 2023.
- [399] Yann Mambrini and Keith A. Olive. Gravitational Production of Dark Matter during Reheating. *Phys. Rev. D*, 103(11):115009, 2021.
- [400] Basabendu Barman and Nicolás Bernal. Gravitational SIMPs. JCAP, 06:011, 2021.

[401] Md Riajul Haque and Debaprasad Maity. Gravitational reheating. *Phys. Rev. D*, 107(4):043531, 2023.

- [402] Gero von Gersdorff and Arthur Hebecker. Kahler corrections for the volume modulus of flux compactifications. *Phys. Lett. B*, 624:270–274, 2005.
- [403] Marcus Berg, Michael Haack, and Boris Kors. String loop corrections to Kahler potentials in orientifolds. *JHEP*, 11:030, 2005.
- [404] Michele Cicoli, Joseph P. Conlon, and Fernando Quevedo. Systematics of String Loop Corrections in Type IIB Calabi-Yau Flux Compactifications. *JHEP*, 01:052, 2008.
- [405] David Ciupke, Jan Louis, and Alexander Westphal. Higher-Derivative Supergravity and Moduli Stabilization. *JHEP*, 10:094, 2015.
- [406] Benedict J. Broy, David Ciupke, Francisco G. Pedro, and Alexander Westphal. Starobinsky-Type Inflation from  $\alpha'$ -Corrections. JCAP, 01:001, 2016.
- [407] Renata Kallosh, Andrei Linde, Diederik Roest, Alexander Westphal, and Yusuke Yamada. Fibre Inflation and  $\alpha$ -attractors. *JHEP*, 02:117, 2018.
- [408] Liam McAllister and Fernando Quevedo. Moduli Stabilization in String Theory. 10 2023.
- [409] Michele Cicoli and Anupam Mazumdar. Reheating for Closed String Inflation. JCAP, 09:025, 2010.
- [410] Xin Gao, Arthur Hebecker, Simon Schreyer, and Gerben Venken. Loops, local corrections and warping in the LVS and other type IIB models. *JHEP*, 09:091, 2022.
- [411] Ralph Blumenhagen, Sebastian Moster, and Erik Plauschinn. Moduli Stabilisation versus Chirality for MSSM like Type IIB Orientifolds. *JHEP*, 01:058, 2008.
- [412] Michele Cicoli, David Ciupke, Victor A. Diaz, Veronica Guidetti, Francesco Muia, and Pramod Shukla. Chiral Global Embedding of Fibre Inflation Models. *JHEP*, 11:207, 2017.
- [413] Michele Cicoli and Anupam Mazumdar. Inflation in string theory: A Graceful exit to the real world. *Phys. Rev. D*, 83:063527, 2011.
- [414] Tetsutaro Higaki and Fuminobu Takahashi. Dark Radiation and Dark Matter in Large Volume Compactifications. *JHEP*, 11:125, 2012.
- [415] Rouzbeh Allahverdi, Michele Cicoli, Bhaskar Dutta, and Kuver Sinha. Correlation between Dark Matter and Dark Radiation in String Compactifications. JCAP, 10:002, 2014.
- [416] Michele Cicoli, Kuver Sinha, and Robert Wiley Deal. The dark universe after reheating in string inflation. *JHEP*, 12:068, 2022.
- [417] Gyula Fodor. A review on radiation of oscillons and oscillatons. PhD thesis, Wigner RCP, Budapest, 2019.
- [418] Hong Zhang. Axion Stars. Symmetry, 12(1):25, 2019.

[419] Lev Kofman. Tachyonic preheating. In 8th International Symposium on Particles Strings and Cosmology, pages 167–182, 2001.

- [420] J. Polchinski. String theory. Vol. 2: Superstring theory and beyond. Cambridge Monographs on Mathematical Physics. Cambridge University Press, 12 2007.
- [421] Daniel Junghans and Gary Shiu. Brane curvature corrections to the  $\mathcal{N}=1$  type II/F-theory effective action. *JHEP*, 03:107, 2015.
- [422] Ricardo Z. Ferreira, Jonathan Ganc, Jorge Noreña, and Martin S. Sloth. On the validity of the perturbative description of axions during inflation. *JCAP*, 04:039, 2016. [Erratum: JCAP 10, E01 (2016)].